Effect of Catalysts on Kinetics of Hydrothermal Processing of Biomass

Andrés Chacón Parra

M. Eng. (Chem)

Thesis submitted for the degree of Doctor of Philosophy

School of Chemical Engineering and Advanced Materials

The University of Adelaide, Adelaide, Australia

July 2022

Table of Contents

List of Tables

List of Figures

Abstract

Hydrothermal liquefaction (HTL) of biomass and bio-waste is a promising waste management technology that might produce renewable bio-crude and other valuable aqueous and solid organic products from non-conventional, non-edible biomass and waste sources. The yields and properties of the product phases depend mostly on the biomass composition, reaction temperature, and residence time. However, the current renewable bio-crude is not close enough to the fuel oil properties. Issues such as high acidity, high nitrogen content, and high solid product yields limit the industrial application of HTL.

A complete renewable co-solvent and homogeneous catalyst system is investigated as a hydrogen donor co-solvent, alkylation, and esterification agent to reduce the effect of the renewable bio-crude issues, whereas the reaction mechanisms and kinetics models are established and coupled with multiple analytical techniques to understand the synergetic effect of the co-liquefaction conditions.

The HTL of the model lipids produced up to 90% renewable bio-crude yield, composed mainly of free fatty acids (FFA). While co-liquefaction produced up to 38% fatty acid ethyl ester (FAEE) known as bio-diesel, with reduced acidity levels. The hydrolysis, transesterification, and esterification are modelled in a loop of forward and reverse reactions to clarify the degrees of equilibrium at the different conditions. Additionally, the activation energies obtained are contrasted with the scientific literature.

The HTL of rich in protein biomass produces nearly a quarter mass yield of a high in nitrogen bio-crude and up to 60% nitrogen recovery in the aqueous phase. NOx are environmental pollutant gases from the combustion of rich in nitrogen feedstock, while nitrogen in water is potentially harmful to the aquatic ecosystem and can be complex to treat with biological nutrient removal (BNR). A complete elemental nitrogen balance and kinetic model are developed to understand the migration and transformations of nitrogen under HTL conditions, and a hydrogen

donor co-solvent system is tested to enhance renewable bio-crude yields and properties. However, the complexity of protein structure and reactions requires a more in-depth understanding.

The HTL of carbohydrates does not produce water-insoluble bio-crude and almost 50% of product yield is char. Solids are undesirable products from the HTL of biomass, as they reduce bio-crude yield and might increase the complexity of the bio-crude recovery due to oil trapping. However, valuable intermediate products such as 5-hydroxymethyl furfural and levulinic acid were found as substantial products in a detailed reaction mechanism and kinetic model from the HTL of glucose, fructose, and cellulose. Additionally, ethanol as a hydrogen donor co-solvent promoted the formation of ethyl levulinate and 5-ethoxymethyl furfural, structures with potential applications as fuel additives and tunable monomers.

The interactions between protein and carbohydrate, known as Maillard reactions, are investigated as the second most important pathway contributing to the renewable bio-crude phase. Previous studies with proteins and carbohydrates contribute to the design of experiment and response variables. Where GC-MS of aqueous phases plays a crucial role in providing a new understanding of the Maillard reaction transformation. Proline, as an isomer from glutamic acid and a potential product from the Strecker degradation and Amadori rearrangement of levulinic acid, is the primary candidate to produce pyrrolo-pyrazinedione and piperazinedione intermediates before further degradation into pyrazines and other final products.

Declaration

I certify that this work contains no material which has been accepted for the award of any other degree or diploma in my name, in any university or other tertiary institution and, to the best of my knowledge and belief, contains no material previously published or written by another person, except where due reference has been made in the text. In addition, I certify that no part of this work will, in the future, be used in a submission in my name, for any other degree or diploma in any university or other tertiary institution without the prior approval of the University of Adelaide and where applicable, any partner institution responsible for the joint-award of this degree.

I acknowledge that copyright of published works contained within this thesis resides with the copyright holder(s) of those works.

I also give permission for the digital version of my thesis to be made available on the web, via the University's digital research repository, the Library Search and also through web search engines, unless permission has been granted by the University to restrict access for a period of time.

I acknowledge the support I have received for my research through the provision of an Australian Government Research Training Program Scholarship.

_____ 09/12/21

Andrés Chacón-Parra Date

Acknowledgements

The present thesis would not have been possible without the support and guidance of many people.

I am grateful to the Adelaide Graduate Centre (AGC) for the tuition fee waiver and full scholarship (Adelaide Graduate Research Scholarship) granted. As an international student, it would have been impossible without these. I also acknowledge the funding of the Australian Research Council Linkage Project grant (LP150101241) and our industry partner, Southern Oil Refining Pty Ltd.

I would like to thank my supervision panel, Dr. Philip van Eyk, Professor David Lewis, and Professor Rachel Burton. I thank Philip for his constant professional and personal support, guidance, and patience. I thank David for his valuable contribution and his optimistic support, especially during the unprecedented CoVID-19 times.

I would like to acknowledge the help of Dr Tony Hall from the Faculty of Sciences at The University of Adelaide, and Professor Marianne Glasius from the Department of Chemistry at Aarhus University, their knowledge and chemical analysis guidance has helped me to develop the methods used over the last half of my PhD, which allowed me to gather some crucial and novel results. I also thank the members of the Faculty of Engineering, Computer and Mathematical Sciences (ECMS) Technical Services and Infrastructure Team, especially the Chemical Operations Team Leader Dr Qiuhong Hu, for her trust and patience with my long and demanding physical and chemical analysis work, and Senior Technician Mr Jason Peak, for his help with the countless issues I had in the laboratory with my experimental work.

I would also like to thank my fellow researchers in the hydrothermal processing research group, Dr. Benjamin Keiller, Dr. Sylvia Edifor, Dr. Jasim Al-Juboori, Md. Arafat Hossein, Thomas Scott, Robran Cock, Chye Yi Leow, and especially Dr. Reem Obeid, for her support at the early stage of my Ph.D.

Finally, I would like to thank my family, in particular my mom Marta, my siblings Angie and Tomas, and my wife Catalina for a life-time of support and love-full encouragement.

Preface

All the work presented in this thesis was conducted at the University of Adelaide between 2019 and 2021. This thesis is submitted as a series of publications and manuscripts under review, according to the ‘Specifications for Thesis 2022’ of the University of Adelaide. The journals in which the publications were published are given in the following table.

Journal	2021 Impact Factor
Chemical Engineering Journal	13.273
Fuel	6.609

The following four journal papers contain the main body of work of this thesis.

1. **Chacón-Parra, A.**, D. Lewis, and P. van Eyk, The effect of ethanol as a homogeneous catalyst on the reaction kinetics of hydrothermal liquefaction of lipids. Chemical Engineering Journal, 2021. 414: p. 128832. Copyright of this paper belongs to Elsevier.
2. **Chacón-Parra, A.**, D. Lewis, and P. van Eyk, Elemental nitrogen balance, reaction kinetics and the effect of ethanol on the hydrothermal liquefaction of soy protein. Chemical Engineering Journal, 2021. 425: p. 130576. Copyright of this paper belongs to Elsevier.
3. **Chacón-Parra, A.**, D. Lewis, M. Glasius, and P. van Eyk, A multi-component reaction kinetics model for the hydrothermal liquefaction of carbohydrates and co-liquefaction to produce 5-ethoxymethyl furfural. Fuel, 2021. 311: p. 122499. Copyright of this paper belongs to Elsevier.
4. **Chacón-Parra, A.,** T. Hall, D. Lewis, M, Glasius, and P. van Eyk, Elucidating the Maillard reaction mechanism in the hydrothermal liquefaction of binary model compound mixtures and spirulina. Manuscript submitted to ACS Sustainable Chemistry & Engineering.

Chapter 1

Introduction

1.1 Background

The growing demand for sustainable energy sources, coupled with the depletion of fossil fuels, has turned the world's attention to multiple renewable energy solutions. Biomass, as a renewable resource, has been used for heating and firing since the early beginning of human history. However, the lower energy density and high humidity, among other issues, made biomass an unfeasible solution for current technologies and demands. Hydrothermal liquefaction (HTL) is a thermochemical conversion method that can convert non-edible, non-conventional biomass sources into high energy-density renewable bio-crude and other valuable products (Biller & Ross, 2016; Gollakota, Kishore, & Gu, 2018; A. Kruse, Funke, & Titirici, 2013).

Hydrothermal conversion takes advantage of the exceptional water properties near the critical point. At subcritical conditions water ions break the structure of biomass, hydrolysing and releasing free fatty acids and glycerol from lipids, as well as basic amino acids from proteins, and monosaccharides from carbohydrates, among many other smaller and simpler water-soluble organic structures (Hayes, 2013; A. Kruse et al., 2013; Teri, Luo, & Savage, 2014). Then, as a reaction medium, water allows intermediates to interact and re-condense into different products and phases (Biller & Ross, 2016; Fan, Hornung, Dahmen, & Kruse, 2018; A. Kruse & Dinjus, 2007; Peterson et al., 2008; W. Yang, Li, Li, Tong, & Feng, 2015). The composition and distribution of the products heavily depend on the composition of the feedstock, the reaction temperature, and the residence time (Biller & Ross, 2011, 2016; Hayes, 2013; Toor, Rosendahl, & Rudolf, 2011).

The body of knowledge on the HTL of biomass requires a better understanding of the renewable bio-crude yield, properties, and composition (Biller & Ross, 2011, 2016; Hayes, 2013). The complexity and variability in biomass composition make the reported data and models restricted to specific real biomass sources and some modelling compounds (Hayes, 2013; Obeid, Lewis, Smith, & van Eyk, 2019; Teri et al., 2014). Furthermore, issues such as bio-crude acidity,

heteroatom content (nitrogen and sulphur) and undesirable solid yields limit the viability and industrial application of HTL as a promising technology to produce fuels and chemical commodities from biomass and bio-waste (Biller & Ross, 2011; Leng et al., 2020; Y. Zhang & Chen, 2018).

Heterogeneous catalysts have been tested to enhance the renewable bio-crude (Duan & Savage, 2011; Galadima & Muraza, 2018). However, the rapid decline in catalyst' surface area, due to phosphorus, sulphur, and nitrogen poisoning, limited the activity of the catalysts. Some homogeneous catalysts have been used as co-solvent and hydrogen donors have presented a substantial and consistent effect on product yields, properties, and composition (Isa, Abdullah, & Ali, 2018; Ross et al., 2010; Yin & Tan, 2012). However, the impact of the co-solvents and homogeneous catalysts has not been completely understood, and the reaction mechanisms and kinetic models up-to-date are limited to bulk product phases, ignoring the related chemical reactions and equilibrium degrees. Additionally, interactions like the Maillard reactions, require a more in-depth understanding (Hietala & Savage, 2021; Luo, Sheehan, Dai, & Savage, 2016; Obeid, Lewis, Smith, Hall, & van Eyk, 2020b; Obeid, Smith, Lewis, Hall, & van Eyk, 2022; P. J. Valdez, Tocco, & Savage, 2014).

The primary aim of this work is to characterise the products from the HTL of biomass model compounds and develop reaction mechanisms and kinetic models which integrate the relevant reactions with the main application drawbacks while evaluating the effect of ethanol under acidic conditions as a co-solvent, homogeneous catalyst, and hydrogen donor, to enhance the renewable bio-crude yield and properties. Followed by the understanding of the Maillard reaction as the most important interaction between protein and carbohydrate intermediates.

1.2 Scope and Structure of Thesis

Chapter 2 provides a critical review of the scientific literature on current HTL technology and its limitations. The emphasis of the review is on model

compounds for lipids, proteins, and carbohydrates as the top three key components of non-conventional biomass sources, as well as the reaction mechanisms, kinetic models, and analytical methods used to characterise the HTL products. The review also highlights the application gaps of the renewable bio-crude produced through HTL and the approaches previously defined to solve those problems.

Chapter 3 presents the HTL of sunflower oil as a model compound of lipids with and without a co-solvent and homogeneous catalyst system. The characterisation and quantification of triglycerides, FFA and FAEE, is accomplished with FT-IR and contrasted with TAN. The reaction mechanism and kinetic models are developed in a loop of forward and reverse reactions to capture the equilibrium degrees at the different conditions. The activation energies for the hydrolysis and transesterification of triglycerides are contrasted with the scientific literature with a remarkable agreement, the effect of ethanol in reducing the acidity levels as one of the key disadvantages of the HTL renewable bio-crude are discussed with positive results even at lower ethanol concentrations.

Chapter 4 comprises the HTL of soy protein as a model compound with the development of an elemental nitrogen balance to clarify the migrations and transformations of nitrogen as a critical organic heteroatom, a potential pollutant from post-combustion of rich in nitrogen bio-crude, and as a challenge for biological nutrient removal (BNR) of the post-HTL aqueous phase. Then, ethanol under low acidic conditions is tested as a hydrogen donor co-solvent to promote higher bio-crude yields and enhanced properties, while encouraging the removal of nitrogen from the bio-crude. The complexity of protein interactions limited the understanding of the co-solvent effect. However, the elemental balance provided a new comprehension of the nitrogenous migrations and transformations over the liquefaction and co-liquefaction of rich in protein biomass.

Chapter 5 involves the study of monosaccharides and polysaccharides under hydrothermal conditions. GC-MS and HPLC are used to identify and quantify the

most significant organics in the aqueous phase, which, once integrated with the other product phases into a reaction mechanism model, produce the detailed reaction kinetics for monosaccharides. Then, thermogravimetric analysis (TGA) and derivative TG are used to semi-quantify the unreacted cellulose within the solid products, which is indispensable to complete the polysaccharide reaction kinetics and a shrinking core model (based on particle size distribution). Finally, the addition of ethanol promoted the formation of 5-ethoxymethyl furfural and ethyl levulinate, two potential fuel additives and tunable monomers.

Chapter 6 incorporates the study of protein and carbohydrate model compound mixtures to clarify Maillard reactions, a well-known interaction over the food industry but not widely studied in the hydrothermal conversion of biomass. A central composite design (CCD) is used to incorporate a third variable and elucidate the primary effect of reaction temperature, residence time, and protein/carbohydrate mass ratio. The response variables included product yields, boiling point distribution and elemental composition of the renewable bio-crude. The tentative identification and semi-quantification of the ethanol-soluble bio-crude and the aqueous phases. Finally, a reaction mechanism suggests that levulinic acid as the most prominent carbohydrate intermediate from carbohydrate degradation is potentially converted into proline via Strecker degradation and Amadori rearrangement, as the principal Maillard intermediate. The results are then contrasted with HTL experiments with spirulina under similar conditions.

Chapter 7 presents the independent and systematic conclusions of the presented study, as well as recommendations for future work.

Finally, references are provided for Chapters 1, 2 and 7, while the references for Chapters 3 to 6 are provided in their respective publication papers and manuscript formats.

Chapter 2

Literature Review

2.1 Introduction

This chapter provides a critical review of the available scientific literature on the HTL of key biomass components, the reaction mechanism, and kinetic models presented, as well as the current application limitations. The following areas are addressed in the review:

- Hydrothermal conversion of modelling compounds for lipids, proteins, and carbohydrates, and considerations for key biomass components.
- The Maillard reactions (interactions) between protein and carbohydrate intermediates under hydrothermal conversion conditions.
- Analytical techniques used to characterise the renewable bio-crude and other product phases, advantages, and limitations.
- Reaction mechanisms and kinetic models for the product phases and chemical groups and how to integrate analytical data into the reaction models.
- Catalysts, co-solvents and additives tested to increase the bio-crude yield and the implications for the other product phases.

Special attention has been given to studies that present detailed reaction mechanisms and kinetic models based on biomass key compounds, compositional and elemental analysis, and co-liquefaction to enhance the renewable crude yield and properties.

2.2 Hydrothermal processing of biomass

Hydrothermal conversion comprises heating of aqueous biomass slurries at high pressures to generate high-energy-density products with potential applications as energy sources and in the chemical industry (Biller & Ross, 2016). Hydrothermal processing is classified into three main conversion processes based on temperature and product selectivity: hydrothermal carbonisation (HTC) aimed to produce solid products in a low temperature range (180 to 250°C) at the correspondent water saturation pressure. Hydrothermal liquefaction (HTL) aimed

to generate viscous renewable bio-crude products (potential substitute for petroleum fuel-oil after upgrading) in the mid-temperature range (250 to 375°C). Finally, hydrothermal gasification (HTG) of supercritical water gasification (SCWG) aims to produce syngas products at temperatures above 375°C, which is the critical temperature for water. As shown in Figure.1 (Biller & Ross, 2016; A. Kruse et al., 2013).

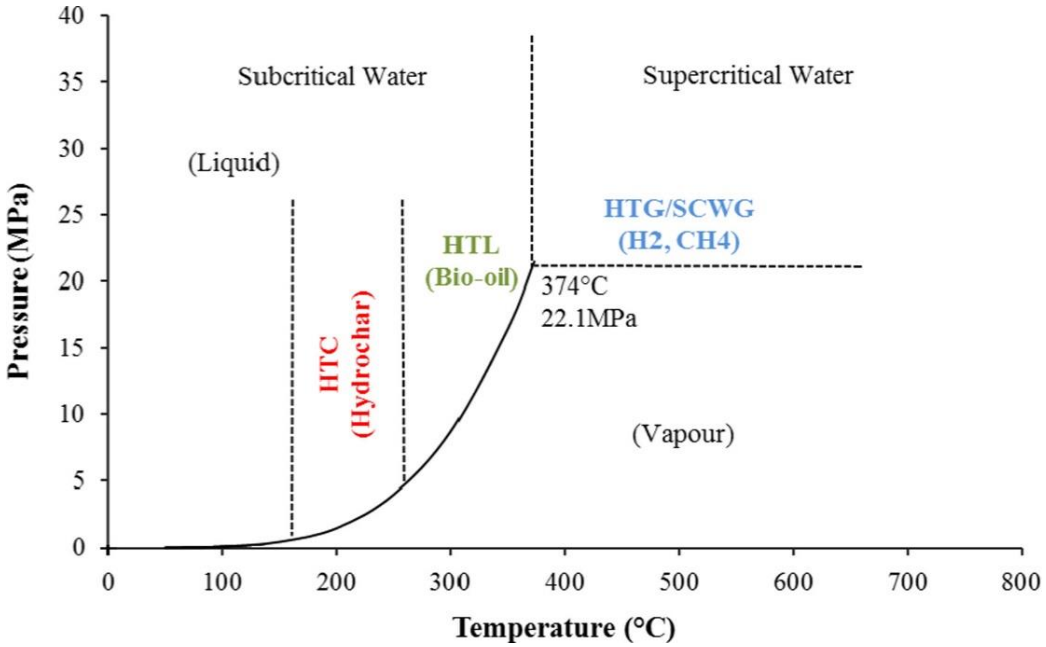

Figure 1. Temperature and pressure diagram for the hydrothermal conversion of biomass (Kambo & Dutta, 2015).

The primary advantage of hydrothermal processing over other thermochemical conversion methods is the ability to process wet-feed, as the pre-drying process could account for up to a quarter of the potential energy of biomass (Biller & Ross, 2016). Hydrothermal conversion could also process biomass sources with high moisture and high ash content, making it ideal for non-conventional wet biomass sources such as algae, municipal sewage sludge and bio-wastes (Biller & Ross, 2016; Kambo & Dutta, 2015; A. Kruse et al., 2013). Hydrothermal conversion takes advantage of the exceptional properties of water near the critical point to break bio-macromolecules in biomass and, as a reaction medium, allows the intermediates to react and re-condense into different products, which are heavily

influenced by the feedstock composition and process conditions (Arturi, Kucheryavskiy, & Søgaard, 2016; A. Kruse & Dinjus, 2007; Peterson et al., 2008).

2.3 Biomass feedstock and model compounds

Biomass is a term to denote all plant and animal materials used for energy. There are multiple classifications for biomass feedstocks, but the most commonly used is by generation. The first generation includes edible sources such as biodiesel via transesterification of lipids and bio-ethanol. The second generation is based on non-edible sources, among which energy crops, agricultural and forestry residues, and general bio-waste (including municipal waste and sludge) are the foremost. The third generation includes algae microorganisms, which have gained a lot of attention in recent years (Alalwan, Alminshid, & Aljaafari, 2019; A. Kruse et al., 2013). All biomass sources are composed of different portions of the same key components, and the principals are lipids, proteins, carbohydrates, and ash (lignocellulosic biomass also contains lignin) (Vassilev, Baxter, Andersen, & Vassileva, 2010). Each of these chemical structures has particular decomposition pathways that must be understood from a fundamental point of view before considering interactions in real biomass sources (Arturi et al., 2016; Biller & Ross, 2016; Hayes, 2013).

2.3.1 Lipids

Lipids are the most valued biomass components from an energy perspective, and the diesel engine was initially designed to run with vegetal oils. However, high viscosity and high surface tension generate poor atomization, incomplete combustion, carbonisation, and deposits (Go et al., 2016; Van Gerpen & Knothe, 2010). Among current methods for reducing the viscosity and surface tension of vegetal oils, transesterification is the most common. It generates three mono-alkyl esters molecules (also known as biodiesel) from one molecule of triglycerides through the substitution of the glycerol bond with monohydroxy alcohols, illustrated in Figure.2 (da Silva & Sousa, 2013; Van Gerpen & Knothe, 2010). Biomass sources of the first and second generation have been used to

produce biodiesel. However, energy intensive extraction and refining processes are required prior to transesterification, increasing the complexity and cost of the production process, plus the dilemma of using edible sources (first generation) for energy production (da Silva & Sousa, 2013; Go et al., 2016).

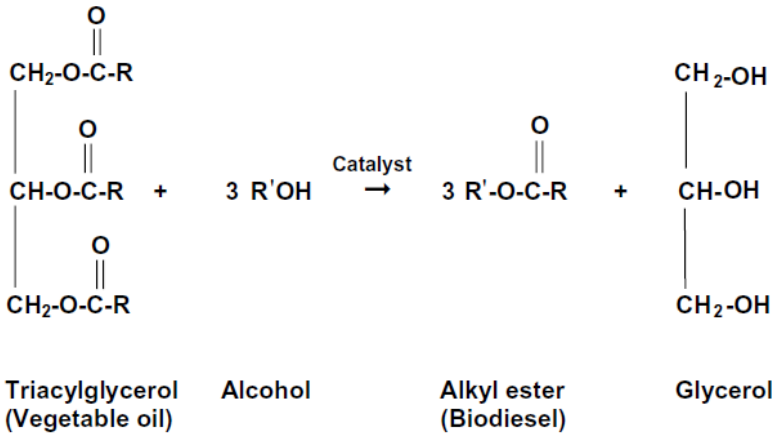

Figure 2. Schematic reaction for the transesterification of lipids (Van Gerpen & Knothe, 2010).

Biodiesel can be produced via alkaline, acid, or enzyme catalysed transesterification. In all cases, the water must be fully removed, as minor residual water could produce free fatty acids (in acidic conditions) or soap (in presence of alkali salts) (Go et al., 2016). Supercritical transesterification was proposed by Saka in 2001, in which supercritical ethanol self-catalysed the reaction (no catalyst required). However, the refining and drying steps that may account for almost 70% of the cost of biodiesel production are still necessary (Go et al., 2016). in-situ transesterification, which could be dated to 1966 by Dugan, involved the direct alcoholysis of lipids in biomass without lipid extraction, presenting economic advantages. However, the process is limited to acid-catalysed esterification conditions, producing a large amount of FFA from triglyceride hydrolysis, which requires more reaction mechanism and equilibrium research (Biller & Ross, 2011; da Silva & Sousa, 2013; Go et al., 2016; Moquin & Temelli, 2008).

2.3.1.1 Sunflower oil and oleic acid

Sunflower oil has been used as a lipid model compound under hydrothermal conditions by various prominent authors (Alenezi, Leeke, Santos, & Khan, 2009; Biller & Ross, 2011; Teri et al., 2014; Velez, Soto, Hegel, Mabe, & Pereda, 2012). Teri et al. (2014) have reported renewable bio-crude yields above 90% at 300°C and 350°C, with a major composition of free fatty acids (oleic and palmitic acid) and 4-octadecanolide via GC-MS (Teri et al., 2014). Alenezi et al. (2009) have reported the hydrolysis of sunflower oil as a series of reactions from triglyceride to diglyceride and monoglyceride, releasing a molecule of FFA at each step (Alenezi et al., 2009). However, acidity is one of the key drawbacks of the renewable bio-crude produced through the HTL of lipids. The HTL hydrolysis produces FFA with a total acid number (TAN) as high as 250 mgKOH/g-oil (Van Gerpen & Knothe, 2010). Acid bio-crude can cause corrosion problems and unstable viscosity. Therefore, a reduction in the acidity levels of bio-crude is essential for promoting the hydrothermal process of biomass, a sustainable solution for biodiesel and fuel oil (Go et al., 2016). Berrios et al. (2007) study the reaction kinetic for the acid esterification of FFA in sunflower oil in acid media (Berrios, Siles, Martin, & Martin, 2007). Furthermore, Velez et al. (2012) have reported the production of FAEE via supercritical transesterification of sunflower oil with high fractions of FFA formed (Velez et al., 2012) and Pinnarat and Savage (2010) have reported the non-catalytic esterification of oleic acid with different equilibrium degrees depending on temperature and the amount of residual humidity (Lascaray, 1949; Pinnarat & Savage, 2010). However, a complete reaction mechanism and kinetic model for hydrolysis, transesterification, and esterification of lipids under co-liquefaction conditions have not been completed.

2.3.2 Proteins

Proteins are the most significant components of non-conventional biomass sources, such as algae and bio-waste. Proteins are the source of most organic heteroatoms in biomass, primarily nitrogen, as they are composed of polypeptides, peptides, and amino acids in complex configurations (Chen, 2017;

Y. Zhang & Chen, 2018). HTL of rich in protein biomasses produces approximately a quarter mass yield of a tarry and viscous renewable bio-crude with an unpleasant smell (Luo et al., 2016; Sheehan & Savage, 2016). The bio-crude phase contains up to 10% elemental nitrogen, depending on the feedstock composition and process conditions. Nitrogen is a well-known post-combustion pollutant, as it would produce NOx gases (Leng et al., 2020; Lu, Li, Zhang, & Liu, 2018; Y. Zhang & Chen, 2018). Fuel-oil has a nitrogen content between 0.1 to 1.5% by mass, and heteroatoms are complex and expensive to remove via hydrogenation, limiting the potential application of HTL renewable bio-crude from rich protein biomass (Leng et al., 2020; Van Gerpen & Knothe, 2010).

Table 1. Summary composition of non-conventional biomass sources, conversion conditions, bio-crude yield, nitrogen content and recovery (Leng et al., 2020).

	Lipid [%]	Protein [%]	Carbo-hydrate [%]	Biomass N content [%]	Temp [°C]	Time [min]	Bio-oil yield [%]	Bio-oil N content [%]	Bio-oil N recovery [%]
Macroalgae									
Average	4.4	14.3	41.8	3.0	315	7	21.9	4.6	33.6
Max	11.2	33.5	91.4	7.0	350	10	41.0	7.1	41.6
Microalgae									
Average	15.2	45.3	24.3	7.6	307	46	35.7	5.8	27.2
Max	58.7	74.7	91.1	11.6	340	60	62.7	10.4	56.2
Manure									
Average	9.2	22.3	51.6	3.5	298	60	25.9	4.2	31.1
Max	22.0	34.7	74.8	6.1	340	120	39.0	5.9	37.7
Bio-waste (food waste)									
Average	26.4	26.2	40.6	3.6	329	41	33.6	3.1	28.9
Max	74.8	91.4	86.9	12.6	360	60	76.0	8.7	52.5
Municipal sewage sludge									
Average	7.2	42.5	35.8	6.4	323	28	30.5	5.5	26.2
Max	16.4	68.6	54.0	10.4	360	30	52.0	7.5	37.5
Lignocellulose									
Average	3.9	3.1	52.6	0.6	368	40	17.0	1.3	36.8
Max	8.2	8.8	91.5	2.8	420	60	45.6	5.3	86.3

As shown in Table.1, nitrogen recovery in the renewable bio-crude is on average 30.6 ± 3.7% with approximately 27.4 ± 6.5% renewable bio-crude yield (average). The denitrification of the renewable bio-crude is a crucial issue that must be solved by complex and expensive upgrading methods such as hydrogenation (Chen, 2017; Leng et al., 2020; Lu et al., 2018; Y. Zhang & Chen, 2018). Understanding and reducing nitrogen heteroatoms during hydrothermal processing not only reduces the potential cost of a narrow economically viable process, but it also makes the HTL of non-conventional biomass sources (such as bio-waste) more attractive (Leng et al., 2020; Lu et al., 2018). Besides the high nitrogen content of the renewable bio-crude, up to 60% of the nitrogen in the biomass is recovered within the aqueous phase as soluble total organic nitrogen (TON), ammonia, and nitrogen oxides (including nitrate and nitrite). Organic nitrogen and ammonia in water are considered potential pollutants for aquatic bodies of water, requiring a further treatment process of the aqueous products before integration into wastewater treatment plants (Burton et al., 2013).

The renewable bio-crude separation process and solvent extraction after HTL conversion affect nitrogen recovery according to the solubility and efficiency of the extraction process and solvent used (Leng et al., 2020; Lu et al., 2018; Martinez-Fernandez & Chen, 2017). Water, as a reaction medium, usually lowers the nitrogen content of the renewable bio-crude, because of the hydrolysis of nitrogen into ammonia and other inorganic nitrogen species (Martinez-Fernandez & Chen, 2017). However, the polarity and solubility of some organic solvents used to recover renewable bio-crude could increase the reported bio-crude yields as well as the nitrogen content (Lu, Liu, Zhang, & Savage, 2019). The synergetic effect of some organic solvents mixed with water in co-liquefaction conditions have shown to reduce heterocycles, amides, and other nitrogenous structures due to the alkylation and hydrogen donation ability of some co-solvents (Cheng, D'cruz, Wang, Leitch, & Xu, 2010; Leng et al., 2020). However, the potential in-situ HTL nitrogen reduction requires in-depth investigation to promote the application of HTL from non-conventional reach in protein biomass.

Table 2. Amino acid composition (wt.%) profile of high protein biomass (Becker, 1994; Sheehan & Savage, 2016)

Amino acid	Soy protein [%]	Spirulina maxima [%]	Chlorella vulgaris [%]	Chlorella pyrenoidosa [%]	Scenedesmus obliquus [%]	Dunaliella bardawil [%]
Glu	19	13.9	15.1	10.2	11.8	14
Asp	11.5	9.5	10.2	6.5	9.2	11.4
Leu	8.1	8.8	10.5	4.4	8	12.1
Arg	7.6	7.2	7.6	6.2	7.8	8
Lys	6.2	5.1	7	8.7	6.2	7.7
Phe	5.2	5.4	6.1	5	5.3	6.4
Ser	5.2	4.6	6.4	2.4	4.2	5.1
Pro	5.1	4.3	5.5	4.4	4.3	3.6
Val	5	7.2	7.7	5.6	6.6	6.4
Ile	4.8	6.6	3.5	3.7	4	4.6
Ala	4.3	7.5	10.3	6.5	9.9	8
Gly	4.2	5.3	6.9	5.3	7.8	6.1
Thr	3.7	5.1	5.8	3.5	5.6	5.9
Tyr	3.7	4.3	3.1	3	3.5	4.1
His	2.6	2	2.2	1.5	2.3	2
Met	1.4	1.5	1.4	2	1.7	2.5
Try	1.4	1.5	0	1.5	0.3	0.8
Cys	1.2	0.4	0	0	0.7	1.3

2.3.2.1 Soy protein isolate and rich protein biomass

The soybean protein isolate, used as a model compound, is a complex protein that may represent several vegetal and algae proteins (as illustrated in the compositional Table. 2). Soy protein is rich in glutamic and aspartic acid, the two electrically negative side chains, and arginine, a positively charged side chain amino acid (Becker, 1994). Luo et al. (2016) have investigated the hydrothermal conversion of a soy protein concentrate at 200, 250, 300, and 350°C, with a basic reaction network presented in Figure 3 (Luo et al., 2016). Sheehan and Savage (2016) have reported the fast hydrothermal liquefaction of soy protein at a temperature up to 500°C, with a nitrogen recovery in water of up to 80% with a

high fraction of ammonia (Sheehan & Savage, 2016). While Lu et al. (2019) studied the effect of different solvents for renewable bio-crude recovery with model compounds, including soybean oil and soy protein (Lu et al., 2019). However, the migration and transformation of nitrogen within the aqueous phase remain fairly unknown (Leng et al., 2020; Lu et al., 2018). The nitrogenous transformation under HTL conditions requires more understanding before defining ways to reduce the nitrogen content in the renewable bio-crude and the treatment of water-soluble nitrogen recovered.

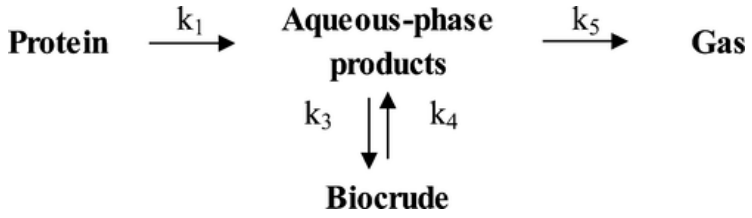

Figure 3. Reaction mechanism for the HTL of a soy protein isolate (Luo et al., 2016).

2.3.3 Carbohydrates

The hydrothermal conversion of carbohydrates and lignocellulosic biomass has a long history. Friedrich Bergius is known to be the first to expose hydrothermal conversion of cellulose in 1913, and later he received a Nobel Prize (shared with Carl Bosch) “in recognition of his contribution to the innovation and development of chemical high pressure methods” (Bergius, 1913; Gollakota et al., 2018; Kambo & Dutta, 2015). However, as the initial Bergius study suggests, the hydrothermal conversion of carbohydrates produces hydrochar (or just char), a high in carbon solid product used as a carbon substitute, and low yields of hydrogen in the gaseous phase, no bio-crude was described (Bergius, 1913).

The scientific literature for the hydrothermal conversion of mono-and-poly-saccharides is vast. Most of it is based on hydrothermal carbonisation with the primary goal of producing functional hydrochar products with potential applications as catalyst support, absorbent, and energy storage (Baccile, Weber, Falco, & Titirici, 2013; Falco, Baccile, & Titirici, 2011; Sevilla & Fuertes, 2009a,

2009b; Titirici, Antonietti, & Baccile, 2008; Titirici, White, Falco, & Sevilla, 2012). Carbohydrates do not produce water-insoluble renewable bio-crude. However, some studies have reported low bio-crude yields via solvent-extraction methods. Additionally, the formation of approximately 50% hydrochar yield limits the production of water-soluble organics which may be extracted from the aqueous phase (Baccile et al., 2009; Baccile et al., 2013; Falco et al., 2011; Sevilla & Fuertes, 2009a, 2009b; Titirici et al., 2008; Titirici et al., 2012).

The hydrothermal conversion of monosaccharides to produce char has no potential from an energy perspective, as processes such fermentation might produce alcohol (more attractive than hydrochar) out of simple sugars (Hayes, 2013; Rasmussen, Sorensen, & Meyer, 2014; Titirici et al., 2008; van Zandvoort et al., 2013). However, the decomposition of glucose, fructose, and others has been studied to understand the reaction mechanism and potential applications for functional carbonaceous material. The conversion of cellulosic biomass has been appealing due to the high resistance of the crystalline structure, which seems to be broken by subcritical water, releasing oligo and monosaccharides, among other organic compounds with many potential applications (Baccile et al., 2009; Rasmussen et al., 2014).

2.3.3.1 Cellulose

Considered the most abundant natural polymer on earth, cellulose has the potential of being a carbon neutral source for energy production (Alalwan et al., 2019; Biller & Ross, 2016; Khan et al., 2019; A. Kruse et al., 2013; Toor et al., 2011). Cellulose is composed of a long and relatively homogeneous (crystalline) chain of D-glucose monomers, via β(1-4) glycosidic bonds (Burnham, Zhou, & Broadbelt, 2015; Hayes, 2013; A. Kruse et al., 2013). Some studies have proposed hydrothermal conversion as a pre-treatment to release monosaccharides from cellulose and hemicellulose before fermentation to produce ethanol (Rasmussen et al., 2014). Among the large scientific literature investigating the decomposition (hydrolysis) of cellulose microcrystalline structures, Peterson et al. (2008), have synthesised the kinetics with a first-order

reaction model in a broad temperature range (210 to 370°C), computing an activation energy of 215kJ/mol (Peterson et al., 2008). However, morphological differences in hydrochar (solid products) from the HTL of glucose and cellulose have suggested that a secondary reaction occurs under hydrothermal conditions (Falco et al., 2011; Sevilla & Fuertes, 2009a, 2009b; Titirici et al., 2012). The reaction has been linked to the dry thermochemical decomposition of cellulose or pyrolysis (also known as primary char) due to the effect of temperature (Chacón-Parra & van Eyk, 2022; Dinjus, Kruse, & Tröger, 2011; Falco et al., 2011; M. S. Jatzwauck, 2015; Andrea Kruse, Krupka, Schwarzkopf, Gamard, & Henningsen, 2005). Some studies have also suggested hydrolysis as a shrinking core reaction model (Galgano & Blasi, 2003; Jayathilake, Rudra, & Rosendahl, 2020; Sasaki, Adschiri, & Arai, 2004). However, hydrochar formation has not been included in those core models.

Reza et al. (2013) have proposed a reaction kinetic model for the hydrothermal carbonisation of loblolly pine by considering the cellulose, hemicellulose and lignin composition in a series of first-order reactions (Reza et al., 2013). This has been recognised as one of the prominent kinetic studies considering the complex composition of a lignocellulosic biomass and served as a base for more studies. Álvarez-Murillo et al. (2016) have studied the hydrothermal conversion of microcrystalline cellulose in a pseudo-first-order reaction mechanism and kinetic model, including heat transport phenomena. However, the very different approach adopted difficult the comparison with Arrhenius kinetic modelling (Álvarez-Murillo, Sabio, Ledesma, Román, & González-García, 2016). Jatzwauck and Schumpe (2015) presented a reaction kinetic model for the hydrothermal carbonisation of soft rush, considering the cellulose composition and the hydrolysis into glucose as a step for hydrochar formation. The cellulose model was fully developed in the dissertation “Kinetik der Hydrothermalen Karbonisierung von Modellsubstanzen und Biomassen” by Jatzwauck. However, the dry pathway for char formation is not incorporated (M. Jatzwauck & Schumpe, 2015; M. S. Jatzwauck, 2015).

Karayildirim et al. (2008) investigated the mechanism and kinetics involving the formation of solid hydrochar directly from cellulose as a side reaction under hydrothermal conversion of cellulose (Karayıldırım, Sınağ, & Kruse, 2008). Dinjus et al. (2011) reference it as just char, and later on it was recalled as primary char (Dinjus et al., 2011). Lucian et al. (2019) and Paksung et al. (2020) studied the reaction kinetics for the direct transformation of cellulose and called pyrochar (Lucian, Volpe, & Fiori, 2019; Paksung, Pfersich, Arauzo, Jung, & Kruse, 2020). Finally, Chacón-Parra and van Eyk (2022) investigated the hydrothermal carbonisation of glucose and cellulose, and presented a reaction kinetic model in good agreement with a compilation of activation energy values from the scientific literature (Chacón-Parra & van Eyk, 2022).

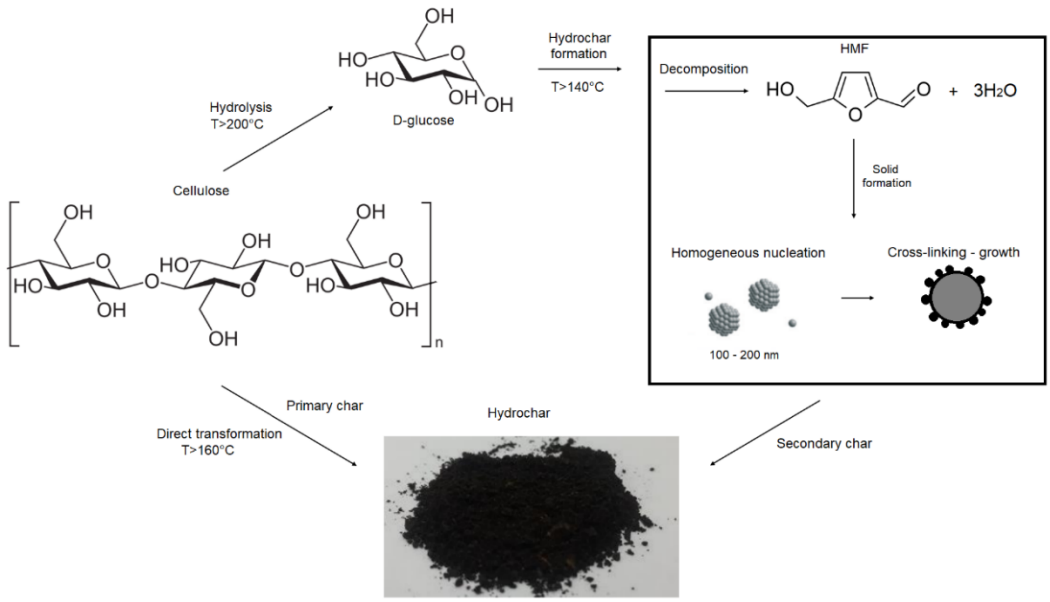

Figure 4. Reaction mechanism for the hydrothermal conversion of cellulose (Chacón-Parra & van Eyk, 2022).

2.3.3.2 Glucose and fructose

Glucose is widely recognised as the major product of the hydrolysis of cellulose. For this reason, it has been used as the model (monomer) compound for hydrothermal processing (Bobleter & Pape, 1968; Chacón-Parra & van Eyk, 2022; Chuntanapum & Matsumura, 2010; He, Yu, Wang, Suo, & Liu, 2021;

Knežević, van Swaaij, & Kersten, 2009; Minowa, Inoue, Hanaoka, & Matsumura, 2004; Patil, Heltzel, & Lund, 2012; Promdej & Matsumura, 2011; Qi et al., 2014; Rasmussen et al., 2014). The hydrothermal conversion of mono and polysaccharides produces some water-soluble intermediate such as 5-hydroxymethyl furfural (5-HMF) and levulinic acid (LA) among other monosaccharide degraded products, which re-condense into the solid phase via aldol condensation (Chuntanapum & Matsumura, 2010; Matsumura, Yanachi, & Yoshida, 2006; Paksung et al., 2020; Promdej & Matsumura, 2011; Sasaki et al., 2004). No water insoluble bio-crude has been produced over the hydrothermal conversion of carbohydrates. However, solvent extraction of products from the HTL of glucose with DCM (dichloromethane) has reported renewable bio-crude yields of up to 5% and organic composition via GC-MS (Obeid et al., 2019; Obeid, Lewis, Smith, Hall, & van Eyk, 2020a; Teri et al., 2014).

The first reaction kinetic study for the hydrothermal conversion of carbohydrates can be traced to Bobleter and Pape (1968), in which an activation energy of 120.9 kJ/mol was presented for the decomposition of glucose (Bobleter & Pape, 1968). Matsumura et al. (2006) presented a similar value with a much larger temperature range up to 400°C (hydrothermal gasification) (Matsumura et al., 2006). Knežević et al. (2009) and Chuntanapum and Matsumura (2010) reported 114 and 127kJ/mol respectively (Chuntanapum & Matsumura, 2010; Knežević et al., 2009). Additionally, Chuntanapum and Matsumura (2019) reported a reaction order of 1.21 and 4.29 for the formation of solid particles from TOC and 5-HMF, respectively (Chuntanapum & Matsumura, 2009). And Jatzwauck (2015) reported a fixed reaction order of 2.25 for hydrochar formation from glucose intermediates over the HTC of cellulose (M. Jatzwauck & Schumpe, 2015; M. S. Jatzwauck, 2015). Some studies have investigated the properties of humins, the solid products formed from monosaccharides. Patil et al. (2012) compared humins formed from glucose, fructose, and 5-HMF, van Zandvoort et al. (2013) studied the influence of processing conditions on formation, morphology, and structure of humins, while Tsilomelekis et al. (2016) reported some morphological and

structural properties of humins formed from 5-HMF (Patil et al., 2012; Patil & Lund, 2011; Tsilomelekis et al., 2016; van Zandvoort et al., 2013).

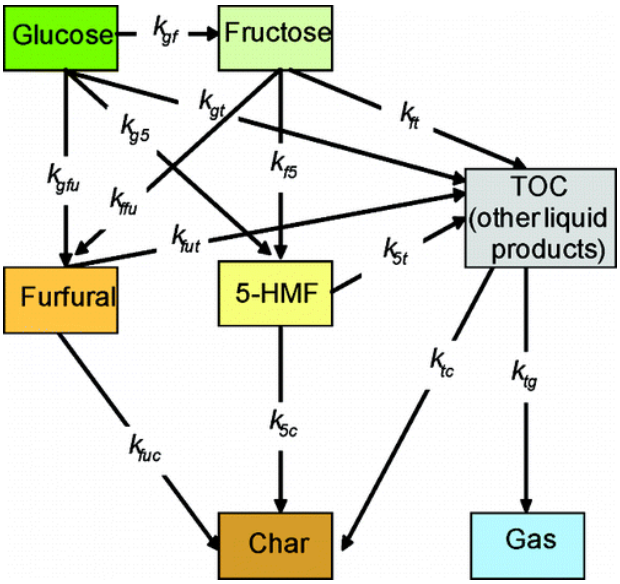

Figure 5. Reaction pathways for the hydrothermal conversion of glucose (Chuntanapum & Matsumura, 2010; Promdej & Matsumura, 2011).

As illustrated in Figure.5, fructose the initial product of the glucose isomerisation reaction, which produces a pyranose structure presented in 5-HMF and furfural, before the dehydration reaction (Antal, Mok, & Richards, 1990; Jung, Zimmermann, & Kruse, 2018; Körner, Jung, & Kruse, 2018; Luijkx, van Rantwijk, & van Bekkum, 1993; Poerschmann, Weiner, Koehler, & Kopinke, 2017). Jung et al. (2018) reported a growth reaction mechanism and kinetic model for the HTC of fructose by testing four salt additives as a factor to control the particle size (Jung et al., 2018). Finally, 5-HMF and some of its derivates have potential applications as an alternative, sustainable valuable chemicals to the chemical industry to produce medicines, polymers, and fuels with a theoretical calorific value of 22.06 kJ/kg (M. Zhang et al., 2012; Zhu et al., 2020). Despite the long and exhaustive literature on the hydrothermal conversion of cellulose and glucose as the most common carbohydrates, the reaction mechanisms, and kinetic models, including the effect of the multiple-product phase with aqueous characterisation and quantification, require more systemic understanding.

2.3.4 Maillard reactions

Under hydrothermal conversion conditions, intermediates from the degradation of carbohydrates and proteins interact, forming products known as Maillard reactions. These reactions pathway could contribute with 5 to 25% higher renewable bio-crude yield than lipid content (Biller, Riley, & Ross, 2011; Biller & Ross, 2011). For this reason, Maillard interactions could be considered the second most important pathway contributing to the renewable bio-crude yield phase. However, these reactions have received less attention than other mechanisms and variables during the hydrothermal conversion. Kruse et al. (2005), have disclosed that the Maillard reactions involve the formation of free radicals, which have a scavenging effect on free radical chain reactions involved in gas formation (Andrea Kruse et al., 2005). Therefore, Maillard interactions reduce the gaseous phase formation while increasing the renewable bio-crude.

Maillard reactions have been extensively studied in the food industry. In 1912, undesirable discolouration and loss of nutritional value has seized the attention of Louis-Camille Maillard, who has studied the reactions that take his name (Amaya-Farfan & Rodriguez-Amaya, 2021). For a long time, scientists believed these reactions were restricted to foods when heated or stored for long time. However, in the 1960s, it was revealed that these reactions also occurred in diluted aqueous systems, such as hydrothermal conversion conditions (Amaya-Farfan & Rodriguez-Amaya, 2021; Ashoor & Zent, 1984).

Maillard interactions comprise a highly complex arrangement of sequential, parallel, and interaction reactions, occurring simultaneously, producing multiple chemical structures of volatile low-mass and non-volatile high-mass compounds (Amaya-Farfan & Rodriguez-Amaya, 2021). The Hodge scheme define the Maillard reactions in three main stages: (1) sugar-amine condensation and the Amadori rearrangement (AR), (2) Sugar dehydration, sugar fragmentation, and Strecker degradation (SD), and (3) aldol condensation, aldehyde-amine polymerization, and formation of heterocyclic nitrogen compounds. The progression of these stages also follows the increase in colour intensity from

colourless to pale yellow and finally brown (Amaya-Farfan & Rodriguez-Amaya, 2021).

Peterson et al. (2010) have studied the mechanism and kinetics of the Maillard reactions under hydrothermal conversion conditions, using glucose and glycine mixtures, and have found that glucose presence resulted in severe destruction of glycine (Peterson, Lachance, & Tester, 2010). Different concentrations of glycine affected glucose conversion differently (Peterson et al., 2010). Madsen et al. (2016) and Qiu et al. (2019) have studied the Maillard reaction by analysing the products of HTL from model compound mixtures with gas chromatography-mass spectroscopy (René B. Madsen et al., 2016; Qiu et al., 2019). The Maillard reaction mechanisms for amino acids and sugars are summarised in Figure. 6. Therefore, the study of Maillard reactions is crucial to understand the reaction mechanism that takes place under the HTL of biomass and the implication on nitrogen migrations and transformation and the composition of renewable bio-crude (Lu et al., 2018).

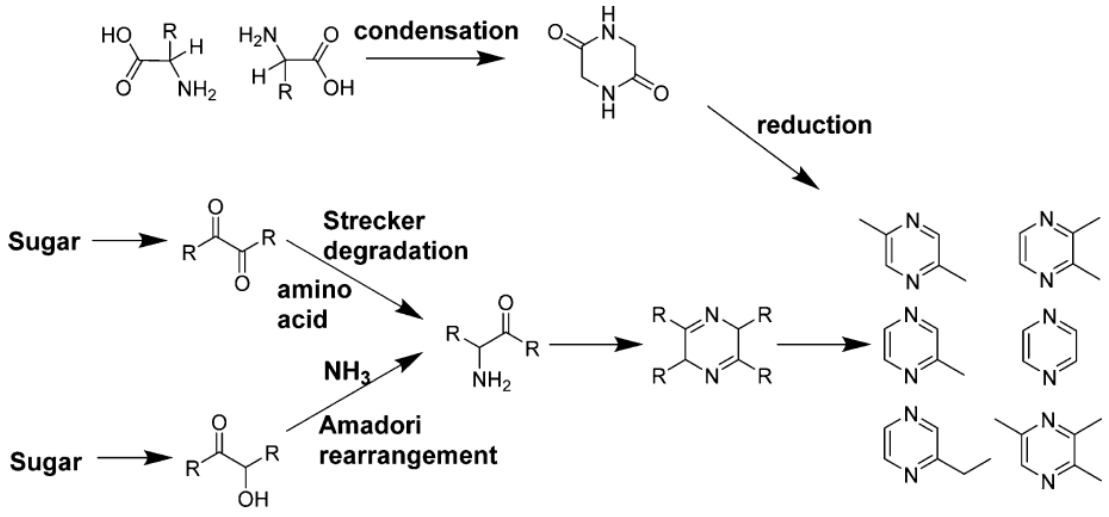

Figure 6. Schematic mechanisms involved in the Maillard reaction (René B. Madsen et al., 2016).

2.3.5 Ash and other components.

One of the key advantages of the hydrothermal conversion is its flexibility. High humidity and high ash biomass sources such as bio-waste and seawater algae are attractive non-conventional biomass sources to be transformed into energy dense products. However, the high ash content of some biomass sources has been shown to decrease the renewable bio-crude formation rates and negatively affect the heating value and low boiling point fractions of the bio-crude (Chen et al., 2017). Calcium carbonate is recognised as the major component of the inorganic fraction in biomass (ash). For the present thesis, Ash is considered inert and other minor components negligible (Chen et al., 2017; Liu et al., 2020; Vassilev et al., 2010).

2.4 Analytical methods

To fully understand the effect of the hydrothermal conversion conditions, multiple analytical techniques have been used to characterise, separate, and quantified HTL feedstock and product phases. Each method has pros and cons. In the present review of the scientific literature, some of the most used analytical methods are discussed and some key features are highlighted.

2.4.1 Thermogravimetric analysis

Thermogravimetric analysis (TGA) is a bulk analysis commonly conducted with the renewable bio-crude and solid phases to estimate the potential fractions based on boiling point temperature distribution (Obeid et al., 2019; Riazi, 2005; D. R. Vardon et al., 2011). The boiling point fractions are simulated by the proportional weight loss of the sample analysed at a constant heating rate under a nitrogen atmosphere within defined temperature ranges. The ranges are then contrasted with the distillation fractions of petroleum (Obeid et al., 2019; Teri et al., 2014). Some prominent authors have discussed the boiling point fraction of the renewable bio-crude and the implications of biomass feedstock composition as well as the hydrothermal conversion conditions (Biller & Ross, 2011; Chen et

al., 2017; Obeid et al., 2019; Ross, Anastasakis, Kubacki, & Jones, 2009; D. R. Vardon et al., 2011). The desirable ranges are gasoline and diesel, because of their potential application as fuel-oil substitute. However, because the analysis does not perform separation or characterisation, the comparison is limited to the similarity in boiling temperature.

This method has been criticised due to the lack of consideration of the chemical, structural, and elemental composition of the sample. It is known that, over the course of the TGA, the breaking of some structures should predict incorrect reading of the boiling point fraction due to thermal decomposition or pyrolysis (Ross et al., 2009). For this reason, thermogravimetric analysis should be considered as a comparative change in volatile and non-volatile fractions. Other methods, such as simulated distillation using gas-chromatography (GC), which could separate and potentially identify the organic compounds by using various detector types (Ross et al., 2009). Furthermore, thermogravimetric analysis coupled with mass spectrometry (TG-MS) might identify the mass-to-ratio (m/z) of the volatilise matter (Ross et al., 2009). However, GC and TG-MS are limited to the maximum temperature of the column system for the GC and the transfer line and detector for the TG-MS (Aeppli, Berg, Hofstetter, Kipfer, & Schwarzenbach, 2008; Coleman, 1996; R. B. Madsen et al., 2016; Torri, Garcia Alba, Samorì, Fabbri, & Brilman, 2012).

2.4.2 FT-IR and NMR

Fourier transform infrared spectroscopy (FT-IR) is another commonly used and unexpansive bulk analysis method which aims to identify the fundamental vibrations and rotational–vibrational characteristic of the functionality of some chemical structures in a sample (Mackie, Jahnke, Benyamin, & Sumner, 2016; Socrates, 2004). Attenuated total reflection (ATR) has revolutionised IR analysis as it is a non-destructive test, requires no sample preparation and can provide a wide spectrum (4000-400cm-1) with a sample depth of 2.5 to 25µm, ideal for liquids in close contact with the ATR crystal, as illustrated in Figure. 7 (Socrates, 2004). However, this method should not be used in isolation. The information

obtained with FT-IR is limited to the qualitative presence and quantitative abundance of particular functional groups and organic bonds in a bulk sample without separation prior to analysis (Cheng et al., 2010; Luo et al., 2016; Poiana et al., 2015; Socrates, 2004).

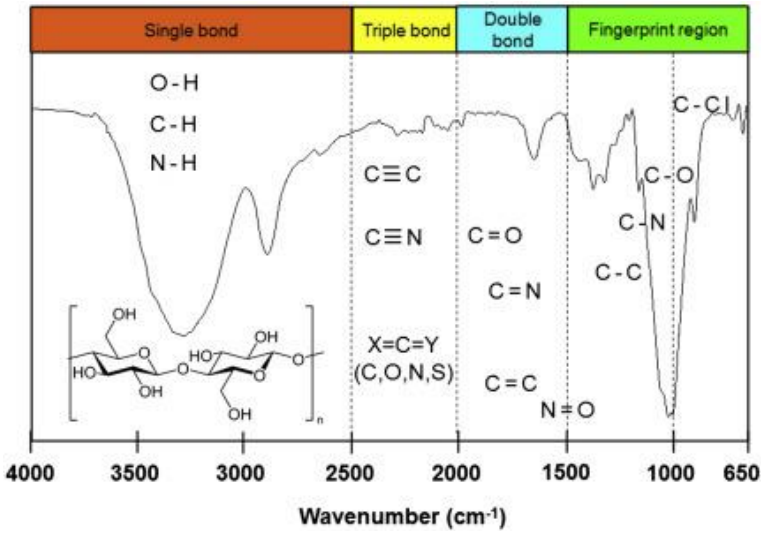

Figure 7. Cellulose (regenerated membrane) FT-IR spectra and absorption band regions for various types of organic bonds (Mohamed, Jaafar, Ismail, Othman, & Rahman, 2017).

For solids, irregular dispersions (space between the sample and the ATR) may be observed due to poorly adjusted attenuated total reflectance samplers (Socrates, 2004). as a result, deviations are more likely than with liquids. For this reason, nuclear magnetic resonances of hydrogen-1 and carbon-13 (^{1}H-NMR and ^{13}C-NMR) have been used to determine the functionalities of complex solid products from HTL of biomass (Baccile et al., 2009; Falco et al., 2011; Luo et al., 2016). Indeed, this method has been used to identify key differences between mono-and-polysaccharides char (solid) products, suggesting that two different reaction mechanisms occur during the conversion of cellulose (Baccile et al., 2009; Chacón-Parra & van Eyk, 2022; Falco et al., 2011; Sevilla & Fuertes, 2009a, 2009b).

2.4.3 Elemental analysis

Elemental analysis CHN/CHNS is commonly used to characterise the elemental composition of dry solids and renewable bio-crude products. The elemental composition is crucial for determining the compositional change over the hydrothermal process and the effect of the conversion conditions (Kambo & Dutta, 2015; A. Kruse et al., 2013). It also serves to estimate the potential calorific value (high heating value or HHV) via Dulong approximation and the changes in elements like nitrogen, sulphur, and oxygen (illustrated in table 1). The deoxygenation via decarboxylation is a desirable pathway from the hydrothermal conversion. However, dehydrogenation via hydrolysis, re-condensation, and polymerisation reduces the potential energy density of the products (Biller & Ross, 2016; Hayes, 2013; A. Kruse et al., 2013). The elemental composition is the preferred method for estimating the biomass transformations based on the O/C and H/C ratios, which are easily comparable in a van Krevelen diagram as shown in Figure. 8 (Kim, Kramer, & Hatcher, 2003). However, the elemental composition should be interpreted in conjunction with other analytical methods, such as tentative identification by GC-MS, proximate analysis, or volatile fractions of the boiling point distribution through TGA (Luo et al., 2016; Madsen & Glasius, 2019; Teri et al., 2014; Wu, Rodgers, & Marshall, 2004).

$$CHO_{Index} = \frac{2x[O]-[H]}{[C]} \qquad \textbf{Equation 1.}$$

$$HHV_{[MJ/kg]} = 33.86 \times [C] + 144.4 \times \left(\frac{[H]\text{-}[O]}{8}\right) + 9.428 \times [S] \qquad \textbf{Equation 2.}$$

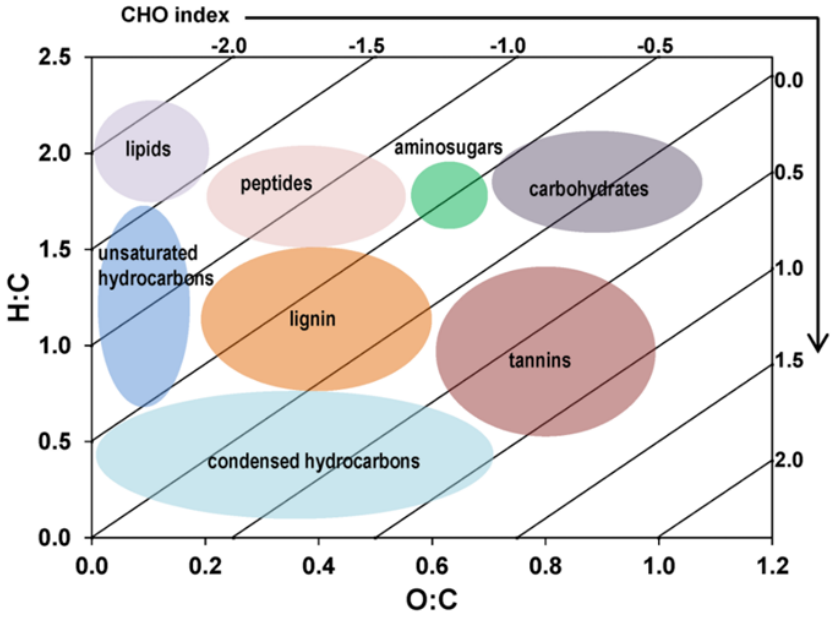

Figure 8. van Krevelen diagram with regions for various biological structures (O/C vs. H/C elemental ratios and the CHO index) (Kim et al., 2003; Mann et al., 2015).

2.4.4 Aqueous tests and wastewater

Some colorimetric tests for organics in water and wastewater have been incorporated into the HTL of biomass to elucidate the amount of total carbon and nitrogen recovered within the aqueous phase (Luo et al., 2016; Martinez-Fernandez & Chen, 2017). However, as the desirable product of HTL is the renewable bio-crude, the scientific literature on aqueous phase is limited to some sequential recovery of nutrients and carbon balance influential studies (Leng et al., 2020; Luo et al., 2016; Martinez-Fernandez & Chen, 2017). The study of aqueous transformation and migration of key elements and functionalities is essential to achieve a better understanding of the HTL reactions, as water is the major component (solvent), reaction medium, and catalyst (Biller & Ross, 2016; A. Kruse & Dinjus, 2007; Peterson et al., 2008). The natural cycle of nitrogen (shown in Figure. 9) is crucial to understand the migration and transformations of nitrogen during hydrothermal conversion. It has been reported up to 60% nitrogen recovery within the aqueous phase as organic nitrogen and ammonia, from total

nitrogen in water and total ammonia tests. However, the migrations and transformations of the denitrification reaction, desirable to produce a fuel-oil-like bio-crude, are not completely understood (Leng et al., 2020; Lu et al., 2018; Martinez-Fernandez & Chen, 2017; Soler-Jofra, Perez, & van Loosdrecht, 2020; Y. Zhang & Chen, 2018).

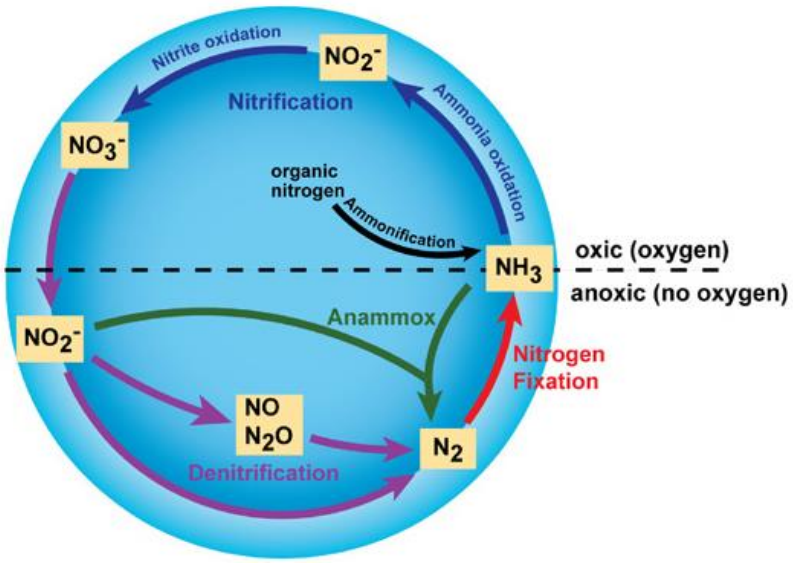

Figure 9. The primary transformation in the nitrogen cycle (Leng et al., 2020; Soler-Jofra et al., 2020; Yakubu, Gto, & Daniel, 2019).

2.4.5 Separation, identification, and quantification

Among the preferred methods to characterise the chemical composition of the renewable bio-crude, gas chromatography-mass spectrometry (GC-MS) is one of the most sophisticated and frequently used. However, the volatilisation temperature limit of the GC system and the molecular weight fraction of the MS, limit the spectrum of the HTL products (Luo et al., 2016; Obeid et al., 2019; Teri et al., 2014; Derek R. Vardon et al., 2011). Additionally, solvent extraction, derivatization, and differences in chromatography methods make it difficult the comparison among different studies. Madsen et al. (2016) have defined a thorough separation and derivatization method to analyse and quantify the organic species produced from HTL from various biomass sources (René B.

Madsen et al., 2016; Madsen & Glasius, 2019; R. B. Madsen et al., 2016). Teri et al. (2014) have disclosed some tentatively identified organic compounds from corn-starch, soy protein, and sunflower oil by itself, in binary and ternary mixtures, using dichloromethane (DCM) as extraction solvent (Teri et al., 2014). Obeid et al. (2019) used a similar method to characterise the main organic components of the polymeric and monomeric structures of carbohydrates, proteins and lipids of the model compound, presenting complete chromatograms and tentatively identifying the organic species in the supplementary material (Obeid et al., 2019; Obeid et al., 2020a). However, the complexity in the biomass composition, the differences in GC method, and the data curation (probability, match factor and reverse match factor) make it extremely difficult to contrast the different compounds (Aeppli et al., 2008; Cheng et al., 2010; Madsen & Glasius, 2019; R. B. Madsen et al., 2016).

GC-MS analysis of the aqueous phase has received less attention than renewable bio-crude, although water is the principal component, catalyst, and reaction medium under hydrothermal conditions (Aeppli et al., 2008; Maddi et al., 2016; René B. Madsen et al., 2016; Yu, Song, Yu, Han, & Liu, 2014). Additionally, the temperature and mass-to-ratio (m/z) ranges might fit better the water-soluble organic structures than the tarry viscous structures in solvent-extracted bio-crude (Aeppli et al., 2008; Lu et al., 2019). However, the differences in polarity and the potential fluctuation in vacuum pressure could affect the reproducibility of the GC-MS analysis. Nonetheless, the characterisation and quantification of the organics in the aqueous phase require further investigation.

2.5 Reaction Mechanism and Kinetic Models

Various biomass types have been considered as HTL feedstocks. Some studies in the scientific literature have developed reaction mechanism and kinetic models for specific biomass feedstocks. However, these models fit only the corresponding experiments due to the complexity of biomass composition and reaction conditions. Different feedstocks have different compositions of lipids, proteins, carbohydrates, lignin, and other components. Biller and Ross (2011),

Valdez et al. (2013) and Li et al. (2017) discussed the variations in algal biomass composition and linked the different product phase yields to the fractions of the main bio-molecules and the conversion conditions (Biller & Ross, 2011; Li et al., 2017; Peter J. Valdez & Savage, 2013). Yang et al. (2018) have synthesised the pathways of individual components in biomass, as well as the probable interaction of products, which improves the different phases of the product (J. Yang, He, Niu, Corscadden, & Astatkie, 2018). However, the complexity in composition and interaction difficult the synthesis of the reaction mechanism and prediction models, as illustrated in Figure. 10 (Hietala & Savage, 2021; Obeid et al., 2020b; Obeid et al., 2022; J. Yang et al., 2018).

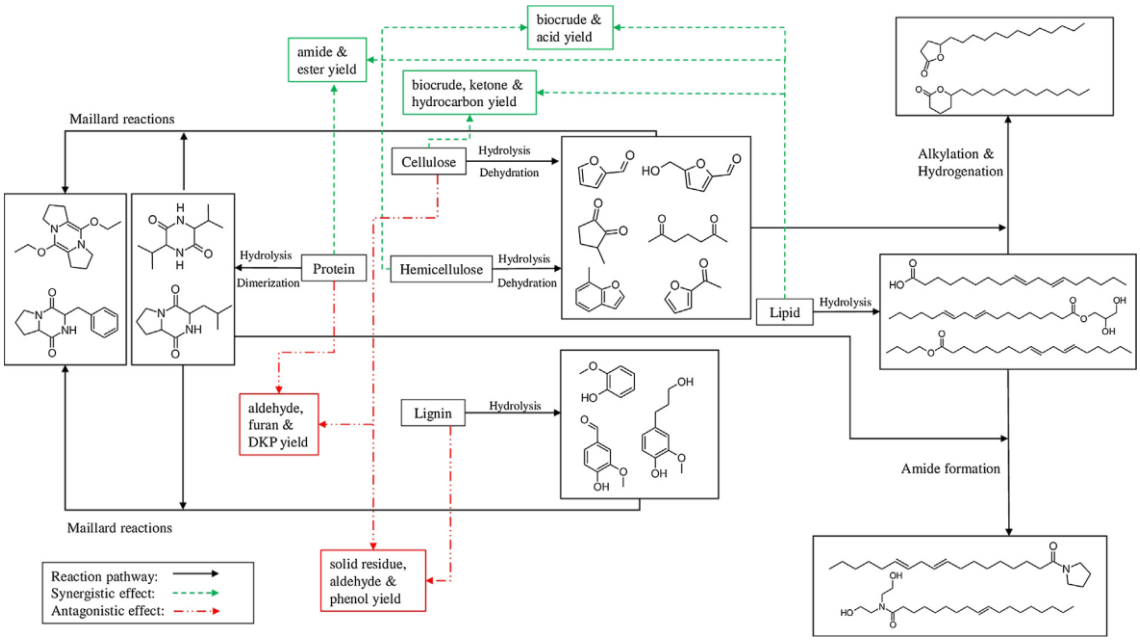

Figure 10. Reaction pathways and interactions for the hydrothermal conversion of individual components in biomass (J. Yang et al., 2018).

2.5.1 Bulk phase kinetic models

The most common approach to define the reaction kinetics from the hydrothermal conversion of biomass is the bulk product phases. Valdez et al. (2013) presented a reaction network and kinetic model for the HTL of Nannochloropsis sp (Peter J. Valdez & Savage, 2013). Then Valdez et al. (2014) synthesise a model for Chlorella protothecoides, Scenedesmus sp. and Nannochloropsis sp, shown in

Figure. 11 (P. J. Valdez et al., 2014). In this model, the decomposition of lipids, proteins and carbohydrates are modelled as independent components contributing to the product phases including the aqueous and bio-crude phases, from which the gaseous phase is likely to be formed, as a close loop of first order reaction with forward and reverse pathways only for the aqueous and bio-crude phases (P. J. Valdez et al., 2014). A similar reaction model (illustrated in Figure 3) has been used by Luo et al. (2016) to fit experimental data from soy protein to bulk product phase yields (Luo et al., 2016).

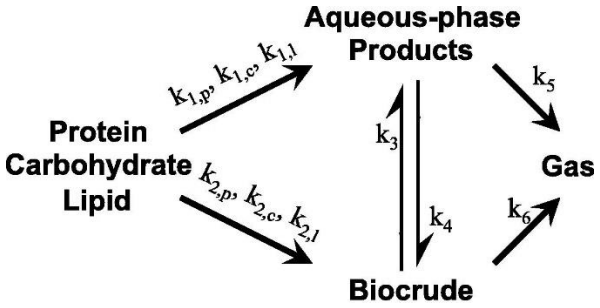

Figure 11. Reaction mechanism for the HTL of algae biomass based on bio-chemical composition (Peter J. Valdez & Savage, 2013; P. J. Valdez et al., 2014).

Reem et al. (2019) have adopted a comparable approach for bio-macromolecules and monomeric model structures of lipids, carbohydrates, proteins, and lignin, illustrated in Figure. 12 (Obeid et al., 2019; Obeid et al., 2020a). To produce a composite model that combines interactions from mixtures of model compound and contrasts the prediction of yield with real biomass feedstocks in a temperature range of 250°C to 350°C (Obeid et al., 2020b; Obeid et al., 2022). However, these models consider only the product phase yields, not the actual composition or the transformations within the phases. For instance, lipids are water-insoluble oils (bio-crude phase) before the conversion begins, and the transformations within the oily phase are not considered. Similarly, monosaccharides and proteins are partially to completely soluble in water (solubility increases with the increase in temperature), and polysaccharides are completely insoluble. The HTL product phases should be differentiated from the

feedstock components. However, the current approach does not make this clear distinction.

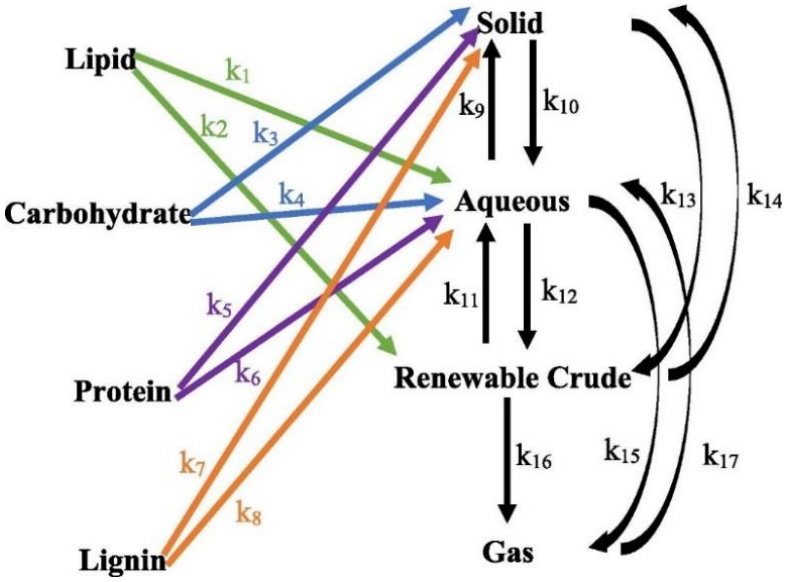

Figure 12. A bulk reaction mechanism for the HTL of any biomass, based on bio-chemical composition (Obeid et al., 2020b; Obeid et al., 2022).

2.5.2 Chemical based reaction mechanism and kinetic models.

Some attempts to capture the HTL transformation of biomass components in a complete reaction model have been completed. Hietala and Savage (2021) have presented a complex reaction mechanism and kinetic models for the hydrothermal conversion of micro-algae (Hietala & Savage, 2021). The model includes the main hydrothermal reactions (hydrolysis, re-polymerization, cyclo-dehydration, retro-aldol condensation, Maillard reactions, deamination, and decarboxylation) in an arrangement with 16 first-order reactions and 22 lumped-product components, as shown in Figure. 13 (Hietala & Savage, 2021). The model aimed to include the effect of the Maillard reaction, carbon, and ammonia recovery, and it fit to the collection of a large empirical database from the documented scientific literature. However, this highly complex model is restricted to algae biomass and model compounds within the specific composition ranges of algae, and it is based on a statistic approach from a compilation of experimental data.

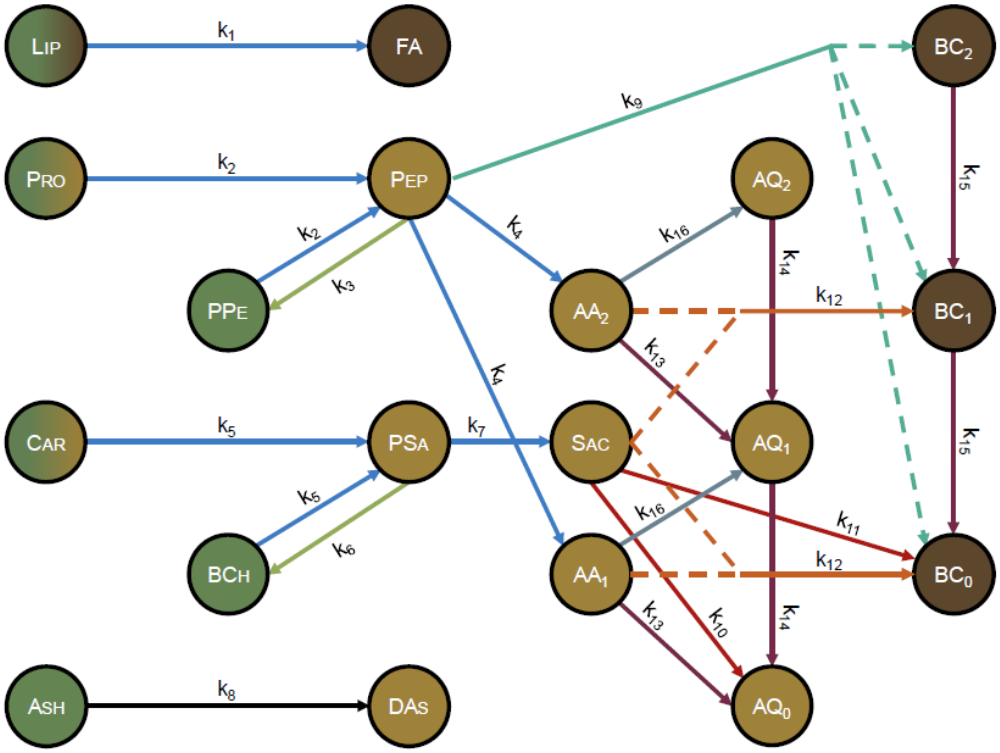

Figure 13. A complete reaction network for the kinetic model for the HTL of micro-algae (Hietala & Savage, 2021).

Despite the complexity of the model, it considers that the renewable bio-crude is only formed by peptides from proteins and the interaction of saccharides and amino acids, hydrolysed from carbohydrates and proteins, respectively (Ashoor & Zent, 1984; Peterson et al., 2010; C. Zhang, Tang, Sheng, & Yang, 2016). The hydrolysis of lipids into free fatty acids is considered independent and ash as inners. In summary, the model only reflects the Maillard reactions and does not contemplate de composition or elemental distribution of the phases (Biller et al., 2011; Chen et al., 2017; Hietala & Savage, 2021). Understanding the key migrations and transformations of the different key biomass components, before elucidating the interaction, could provide a more systematic and fundamental view of the hydrothermal conversion processes (Hietala & Savage, 2021; Leng et al., 2020; Li et al., 2017).

2.6 Catalysts and in-situ additives

Some studies have included, tested, and screened heterogeneous catalysts and in situ additives (homogeneous catalysts) to enhance process efficiency by promoting the renewable bio-crude yield while reducing char formation, as summarised in Table. 3 (Duan & Savage, 2011; Galadima & Muraza, 2018; Kumar, Olajire Oyedun, & Kumar, 2018). Homogeneous catalysts include mostly acids and alkaline salts, while heterogeneous catalysts include some active surface rare metals, and metallic oxides (Kumar et al., 2018).

Table 3. Screening of the effect of catalysts on renewable bio-crude yield (Galadima & Muraza, 2018).

Heterogeneous Catalysts				
Biomass	Catalyst	HTL Conditions	Bio-crude yield	Ref.
Nannochloropsis sp.	No-catalyst	350°C, 1 h, 0.384 g of catalyst, 95% water volume	35	(Duan & Savage, 2011)
	Pd/C		57	
	Pt/C		49	
	Ru/C		50	
	Ni/SiO_2-Al_2O_3		50	
	$CoMo/Al_2O_3$		55	
	Zeolite		48	
Homogeneous Catalysts				
Biomass	Catalyst	HTL Conditions	Bio-crude yield	Ref.
Spirulina	HCOOH	350°C, 1h 3 g algae + 27 ml of catalyst	14.2	(Ross et al., 2010)
	CH_3COOH		16.6	
	KOH		15.2	
	Na_2CO_3		20	
Chlorella vulgaris	HCOOH	350°C, 1h 3 g algae + 27 ml of catalyst	19.1	(Ross et al., 2010)
	CH_3COOH		20.4	
	KOH		22.4	
	Na_2CO_3		27.3	

The primary goal of including catalysts and additives has been to increase the overall renewable bio-crude yield. However, with homogeneous catalysts, the quality of the bio-crude has dropped as the catalysts reduces the level of

hydrolysis and decomposition of the biomass components, limiting the deoxygenation and the increase in energy density, and with the heterogeneous, the active surface of the catalysts and the cost are two significant drawbacks (Galadima & Muraza, 2018).

2.6.1 Heterogeneous catalysts

Heterogeneous catalysts include new reductive metals such as platinum and palladium, and nickel as pure metals and the Raney-Nickel complex, among many metallic oxides (MnO, MgO, NiO, ZnO, CeO_2, La_2O_3) and transition metals (Biller et al., 2011; Duan & Savage, 2011; Galadima & Muraza, 2018; Kumar et al., 2018; Morales et al., 2014). Nickel has shown a positive impact in increasing the bio-crude yields at lower temperature, which is desirable for industrial application (Saber, Golzary, Hosseinpour, Takahashi, & Yoshikawa, 2016). And transition metals have improved the quality of the renewable crude (Duan & Savage, 2011). However, the catalyst surface area gets deactivated and poisoned by the solid nano particles (hydrochar formation) reducing the efficiency, as a solution, carbon nano-tubes (CNT) have been tested as a support of the catalyst increasing the surface area and recyclability (Kumar et al., 2018). However, heterogeneous catalysts have been primarily used for post-HTL upgrading processes (Galadima & Muraza, 2018; Kumar et al., 2018).

2.6.2 Homogeneous catalysts and hydrogen donors

Additives such as co-solvents and homogeneous substances have been tested in situ (during the HTL) and after conversion as extraction solvents (Cheng et al., 2010; Isa et al., 2018; Lu et al., 2019; J. Zhang & Zhang, 2014). One of the most common approaches to define the effect of co-solvents is pH. Some studies have defined the differences in reaction mechanisms based on acidic and alkaline initial conditions of the hydrothermal conversion (García-Bordejé, Pires, & Fraile, 2017; Yin & Tan, 2012). pH has a significant effect on the hydrolysis of lipids and the formation of carbohydrate intermediates (dos Santos, Hamerski, Pedersen

Voll, & Corazza, 2018; Go et al., 2016; Reyero, Arzamendi, Zabala, & Gandía, 2015; Yin & Tan, 2012).

Karagöz et al. (2004) have tested four alkaline solutions as homogeneous catalysts at 280°C for 15 minutes, and found that potassium salts are the most active (K_2CO_3 > KOH > Na_2CO_3 > NaOH) (Karagöz et al., 2005). The advantages of homogeneous catalysts include an increase in the renewable bio-crude yield and properties, while reducing char formation. However, alkali salts increase the pH of the aqueous medium, decreasing the hydrolysis and dehydration rates, leading to higher shares of unsaturated structures of medium molecular weight (Kumar et al., 2018). Under alkaline conditions, the OH^- groups neutralise the hydrolysed ions, preventing re-polymerisation and re-condensation into solid products (Kumar et al., 2018; Ross et al., 2010; Yin & Tan, 2012).

Cheng et al. (2010) investigated the synergetic effect of subcritical water and supercritical alcohols (methanol and ethanol) on the HTL of pine sawdust at 300°C (Cheng et al., 2010). While the hydrothermal liquefaction produced a renewable bio-crude yield of 40%, the supercritical liquefaction produced 23 and 26% bio-crude yields with methanol and ethanol, respectively. Co-liquefaction with 50/50 ethanol and water mixtures generated bio-crude yields as high as 65% by mass, with a 95% conversion (Cheng et al., 2010). Isa et al. (2018) reviewed the effect of some common hydrogen donor solvents and their effect on the hydrothermal liquefaction of biomass (Isa et al., 2018). Alcohols have the potential to produce bio-diesel from lipids from the acid transesterification and esterification of lipids and FFA. The alkylation ability of alcohols might reduce the heteroatoms in the renewable bio-crude of proteins, while esterification of acids and etherification of hydroxy groups in 5-HMF, reducing solid yields and forming water-soluble organics with potential application in energy and polymer industries. The hydrogen donation mechanisms of ethanol are described in Figure. 14. Additionally, ethanol is a completely renewable co-solvent.

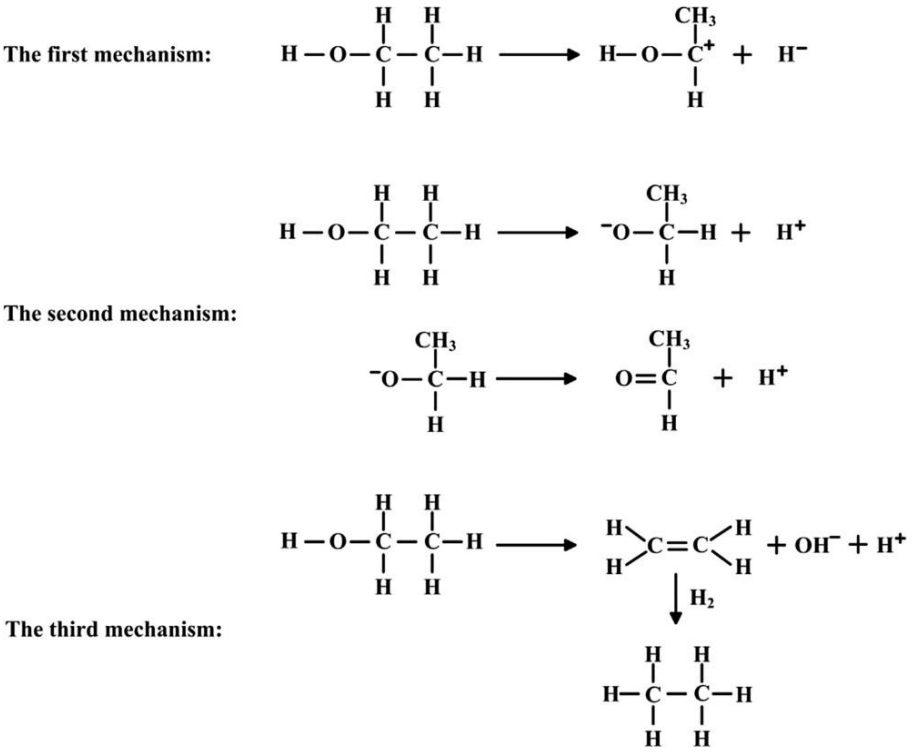

Figure 14. Reaction mechanisms of ethanol as a hydrogen donor (Huang & Yuan, 2015; Isa et al., 2018).

2.7 Current literature gaps

There have been important advances in the hydrothermal liquefaction of algae, bio-waste, and lignocellulosic biomass sources, as discussed in the scientific literature above. The most common research scope has been to determine the optimal conditions for reaction temperature and residence time among other conversion conditions, as well as ways to increase the renewable bio-crude yield, knowing the difference and variability in biomass composition.

Some biomass sources and model compounds have been used to fit and define reaction mechanisms and bulk kinetic models that aimed to predict the renewable bio-crude yield. However, the renewable bio-crude quality, based on the desirable fuel-oil product characteristics, requires more attention. Problems such as oil acidity, which causes corrosion, high viscosity and instability, high nitrogen content, which can cause NOx gases from post-combustion, and the undesirable

solid (char) products reduce the bio-crude yields and increase the complexity of separation processes.

Further drawbacks of the conducted literature review include the limited understanding of the interactions between the different biomass components, mostly from the Maillard reactions, which are claimed to be the second most important pathway contributing to the renewable bio-crude phase. Additionally, the use of highly toxic and flammable solvents for the extraction of the oily phases and the discrepancies in the conversion conditions.

Alcohols such as ethanol and methanol have been tested as supercritical solvents and co-solvents to increase the bio-crude yields. However, the reactions and products are not completely clarified. The synergetic effect of subcritical water and supercritical ethanol requires a better understanding to promote the industrial application of HTL and co-liquefaction with a fully renewable and sustainable co-solvent.

2.8 Objectives of thesis

The aim of the present study is to address the main application drawbacks of the up-to-date renewable bio-crude from the HTL of biomass by testing a hydrogen donor co-solvent and homogeneous catalyst system, while develop a reaction mechanism and kinetic models based on the biomass key components and interactions to clarify the effect of co-liquefaction conditions, by completing the following specific objectives:

1. Investigating the effect of ethanol as a homogeneous catalyst on the hydrothermal conversion of lipids, the reduction in total acid number (TAN) and boiling point fractions, the degrees of equilibrium of a loop reaction mechanism and the effect of ethanol/lipid mass ratio.
2. Elucidating the nitrogen migrations and transformations of a model soy protein under HTL conditions via an elemental nitrogen balance, the elemental composition and boiling point distribution of the renewable bio-

crude, the nitrogenous transformation in the aqueous phase and the fate of nitrogen in a reaction mechanism and kinetic model.

3. Understanding the aqueous transformation of carbohydrates via a multi-component reaction mechanism and kinetic model, the integrations of solid transformation in a shrinking core model for the HTL of cellulose and the co-liquefaction of saccharides with ethanol to produce 5-ethoxymethyl furfural and ethyl levulinate.
4. Clarifying the Maillard reactions under hydrothermal conditions by performing experiments using glucose and soy protein with a central composite design of experiments (CCD), the structure of the organic species in the aqueous and renewable bio-crude phase, and proline as a crucial Maillard intermediate before amino-acid condensation.

Chapter 3

The effect of ethanol as a homogeneous catalyst on the reaction kinetics of hydrothermal liquefaction of lipids

Andres Chacon-Parra, David Lewis, Philip van Eyk

School of Chemical Engineering and Advanced Materials, The University of Adelaide, Adelaide, SA 5005, Australia

Chemical Engineering Journal, **414,** (2021) 128832.

Statement of Authorship

Title of Paper	The effect of ethanol as a homogeneous catalyst on the reaction kinetics of hydrothermal liquefaction of lipids
Publication Status	☑ Published ☐ Accepted for Publication ☐ Submitted for Publication ☐ Unpublished and Unsubmitted w ork w ritten in manuscript style
Publication Details	Chacón-Parra, A., D. Lewis, and P. van Eyk, The effect of ethanol as a homogeneous catalyst on the reaction kinetics of hydrothermal liquefaction of lipids. Chemical Engineering Journal, 2021. 414: p. 128832.

Principal Author

Name of Principal Author (Candidate)	Andres Danilo Chacon Parra
Contribution to the Paper	Design and execution of experiments and analysis. Design and optimisation of the reaction models Data interpretation Drafting of the manuscript
Overall percentage (%)	90%
Certification:	This paper reports on original research I conducted during the period of my Higher Degree by Research candidature and is not subject to any obligations or contractual agreements with a third party that would constrain its inclusion in this thesis. I am the primary author of this paper.
Signature	Date 9/12/21

Co-Author Contributions

By signing the Statement of Authorship, each author certifies that:

i. the candidate's stated contribution to the publication is accurate (as detailed above);
ii. permission is granted for the candidate in include the publication in the thesis; and
iii. the sum of all co-author contributions is equal to 100% less the candidate's stated contribution.

Name of Co-Author	David Milton Lewis
Contribution to the Paper	Concept development Co-supervision Manuscript revision and editing.
Signature	Date 9/12/2021

Name of Co-Author	Philip Joseph van Eyk
Contribution to the Paper	Supervision Result interpretation Manuscript revision
Signature	Date 9/12/2021

Please cut and paste additional co-auth

Chapter 3 - The effect of ethanol as a homogeneous catalyst on the reaction kinetics of hydrothermal liquefaction of lipids

Chemical Engineering Journal 414 (2021) 128832

Contents lists available at ScienceDirect

Chemical Engineering Journal

journal homepage: www.elsevier.com/locate/cej

The effect of ethanol as a homogeneous catalyst on the reaction kinetics of hydrothermal liquefaction of lipids

Andrés Chacón-Parra *, David Lewis, Philip van Eyk

School of Chemical Engineering and Advanced Materials, The University of Adelaide, Adelaide, SA 5005, Australia

ARTICLE INFO

Keywords:
Hydrothermal liquefaction
Kinetics
Lipids
Sunflower oil
Free fatty acids (FFA)
Fatty acid ethyl ester (FAEE)

ABSTRACT

Promoting renewable sources of energy and waste management is essential to face environmental challenges such as global warming, and to ensure long-term fuel security also crucial for sustainable development. Hydrothermal liquefaction (HTL) of wet biomass is an emergent and promising waste management technology that can produce renewable crude from wet biomass and bio-waste. However, HTL crude properties are not close enough to fuel-oil like products. Issues such as high viscosity, instability, high acidity, nitrogen content, low energy density, and low crude yields limit its application. Lipids as a key component of biomass contribute with a high percentage of low boiling point fractions in the crude phase. However, lipids increase acidity because of the hydrolysis into free fatty acids (FFA), which cause considerable issues to the oil industry. In the present study, the functional groups' reaction kinetics for the HTL conversion of lipids is elucidated using FT-IR. Furthermore, ethanol under acid pH is integrated as a co-solvent and homogeneous catalyst to promote the alcoholysis of lipids and FFA, to reduce crude oil acidity. Reaction kinetics are used to define composition and equilibrium differences while boiling point distribution and total acid number (TAN) validate conversion and quality improvement of the renewable crude. The reported experiments were conducted in a batch reactor with 20% mass feedstock at 250 °C, 300 °C and 350 °C, using sunflower oil as a model lipid. The activation energy for the hydrolysis of sunflower oil into FFA under HTL conditions is 107.8 kJ/mol. When ethanol and acetic acid were included, the hydrolysis, transesterification, and esterification activation energies are 134.2, 74.1, and 9.1 kJ/mol, with a degree of alcoholysis of around 30% near-equilibrium conditions.

1. Introduction

Hydrothermal liquefaction (HTL) is a simple and promising thermochemical conversion method to process biomass and bio-waste in sub-critical water (250 °C to 375 °C at the corresponding saturation pressure). Biomass with up to 90% water and high ash content is suitable for HTL conversion because of the process flexibility. Therefore, feedstocks such as sewage sludge, food, and municipal wastes are attractive sources for energy production and waste management [1]. The most conspicuous advantage of HTL over other conversion technologies is that it is a wet feed process. Negating the need for drying is why considerable attention is being placed in the HTL of non-conventional biomass sources like microalgae, in which drying may account for up to 25% of the contained energy [1–3]. The benefits of using subcritical water include changes in pH, dielectric constant, and polarity. Water ions break the linkages of macromolecules in biomass, releasing oligomers and monomers which then interact and re-condensate in different compounds [1,4]. HTL products include renewable crude oil, water-soluble compounds, gases, and solid char. The yields of these phases heavily depend on feedstock type and composition, and reaction conditions such as pH, reaction temperature, and residence time [1,5]. Biomass composition is classified in lipids, proteins, carbohydrates, and lignin, each of them follows a particular decomposition pathway [1,5–7]. Lipids hydrolyse into free fatty acids, which then self-catalyse the reaction because of pH reduction. However, acidic crude oils present crucial risks to process equipment due to corrosion and instability [5,8–11].

The hydrolysis of triglycerides into free fatty acids as the most prominent reaction under HTL conditions (subcritical water) has been investigated for more than half a century. In 1949, Lascaray defined the hydrolysis of fats as a mass transfer phenomenon [12]. Most recent studies show that the hydrolysis of lipid compounds under subcritical water generate renewable crude oil yields of at least 90% by mass, with a negligible change in elemental composition and high heating values

* Corresponding author.
E-mail address: andres.chaconparra@adelaide.edu.au (A. Chacón-Parra).

https://doi.org/10.1016/j.cej.2021.128832
Received 10 October 2020; Received in revised form 24 January 2021; Accepted 31 January 2021
Available online 6 February 2021
1385-8947/

Chapter 3 - The effect of ethanol as a homogeneous catalyst on the reaction kinetics of hydrothermal liquefaction of lipids

(HHV) [6,13]. Boiling point distribution via thermogravimetric analysis may enlighten the hydrolysis and fractionating of triglycerides by the increase in lower boiling point fractions in the renewable crude over the reaction [6,7]. *Terri, Luo, and Savage (2014)* have also disclosed a tentative composition of the lipid HTL renewable crude, which includes oleic acid, palmitic acid, and 4-octadecanolide based on the largest GC–MS chromatogram peaks [6]. However, few of the current HTL studies have considered the compositional change of the glycerolipid throughout the HTL conversion and its effects, which is essential for CFD (Computer fluid dynamics) modelling and optimization.

Among the various lipid-containing oil upgrading techniques, transesterification seems to be the most cost-effective to solve viscosity, instability, and oil acidity issues. This reaction may be achieved through acidic, alkaline, or enzyme-catalysed transesterification. However, each of these methods has limitations such as long reaction times, low impurities tolerance and saponification [8–10]. Supercritical alcoholysis a non-heterogeneous catalytic reaction in which high temperature and pressure promote miscibility and reaction phenomena was initially considered by Saka in 2001 [10,14]. However, all current transesterification technologies require lipid extraction (refining and drying steps), which may account for up to 70% of the total cost of biodiesel production [8,10,15,16]. The addition of ethanol as a co-solvent and homogeneous catalyst under acid pH appears to be a humble but propitious solution to produce a renewable crude with lower acidity levels from wet biomass rich in triglycerides [1,10].

In this study, the reaction kinetics for the hydrothermal conversion of triglycerides is investigated using FT-IR as a quantitative method to estimate the concentration of the FFA and ester bonds (glycolipids and FAEE) present in the renewable crude. Then, a homogeneous catalyst system with ethanol and acetic acid is incorporated to reduce the acidity of the crude by promoting the in-situ alcoholysis of glycerolipids and FFA [10]. The results of non-catalytic HTL are the baseline to define kinetics, composition, conversion, and equilibrium differences with the in-situ homogeneous catalyst HTL. Boiling point fractions and TAN, validate the conversion and quality improvement of the renewable crude [8]. Additionally, the effect of ethanol concentration was investigated at 300 °C. The present study aims to elucidate the lipids functional groups' HTL conversion with reaction kinetics modelling, while incorporates homogeneous catalysts intended to enhance renewable crude oil yield and quality. The significance stands in the functional group approach for the reaction kinetics and the undesirable effects of HTL. Additionally, the homogeneous catalyst system proposed is fully renewable.

2. Materials and method

2.1. Materials and standards

Sunflower oil (food grade) was used as a lipid modelling compound. This commodity oil has 9.5% saturated, 26% monounsaturated, and 63.5% polyunsaturated fats. Oleic acid LR from Chem-Supply (Australia) used as a standard FFA is composed of at least 75% oleic acid (C18:1) and up to 13% linoleic acid (C18:2), with an acid number in the range 195 to 203 mg KOH/g.

Ethanol 100% (undenatured) used as a solvent and homogeneous catalyst and acetic acid glacial AR used as an additive were provided from Chem-Supply. 2-propanol (anhydrous), potassium hydroxide pellets AR crystals and solid phenolphthalein AR for Total Acid Number (TAN) colour titration were also obtained from the same supplier. Fatty acid ethyl ester (FAEE) used as the ideal final product from alcoholysis, was produced via alkaline transesterification of sunflower oil with ethanol (6:1 M ratio) and potassium hydroxide as a catalyst (1% by mass). The reaction took place in an Erlenmeyer for 60 min at 60 °C. The product phase was washed with water to remove glycerol and catalyst, then separated in a funnel and dried at 50 °C for 48 h [8].

2.2. Batch reactor and heating system

The reactor is made of a 20 cm long 316 stainless steel Swagelok® tube with a 12.7 mm external diameter and 1.65 mm wall thickness to produce a nominal volume of 15 ml. It is extended and equipped with a thermocouple, pressure transducer, pressure relief valve and ball valve to purge, charge and release gases. A schematic diagram of the reactor system is provided in *Obeid et al. (2019)* [7]. Heating was accomplished with a Techne SBL-2D alumina sand fluidized bed system, equipped with a Techne TC-9D temperature and airflow controller. A heating time window (approximately 2 to 3 min) to achieve 98% of the desired temperature was allowed, and the reaction was stopped in a two-step process, initially by blowing the reactor tube with compressed air until reaching 100 °C (around 3 min) and finally by quenching it in water (2 min).

2.3. Hydrothermal liquefaction experiments and product separation

The reactor was filled to 50% of its volume capacity at room temperature, with a feedstock slurry of 20% by mass in all cases. When ethanol and acetic acid are included, the volume of water was replaced by the homogeneous catalyst system. Before each experiment, the reactor was purged three times with nitrogen gas (50 bars) to minimize oxygen presence. Then the reactor was charged with nitrogen gas to water saturation pressure (at standard conditions) calculated using the Antoine equation. The pre-pressure values used were 25, 50 and 80 bars, at considered temperatures. Additionally, due to heat transfer phenomena, a difference between the temperature of the fluidized bed and controller is acknowledged and corrected (by setting bed temperature 3 °C above the reaction temperature). The residence time distribution was defined based on *Obeid et al. (2019)* reactor system observations and the literature on the effect of temperature in the HTL of lipid, to get enough useful data to complete the kinetic model. The longest reaction times were set to 90, 60, and 30 min respectively to 250, 300, and 350 °C, with further points distributed within the range [7,15,16].

Gaseous phase yields were measured by difference weighting the reactor before and after charge and release gases [7]. Liquid products were collected by pouring the reactor content into test tubes, centrifuged for 10 min at 5000 RPM to isolate the oil phases, then separated in a funnel and dried for 48 h at 50 °C to evaporate ethanol, water, and other volatile matter. For non-catalytic experiments, 10 ml of ethanol were used to rinse the reactor and remove trapped crude oil. The mixture was dried at 50 °C for 48 h and oil recovered was counted in total renewable crude yield. Last, the aqueous phase was calculated by mass balance (difference).

2.4. Product analysis

IR spectroscopy of the feedstock and products was conducted with a Nicolet 6700 FT-IR spectrophotometer (Thermo Fisher Scientific Inc.) Using a diamond ATR (Attenuate Total Reflectance) Smart Orbit accessory, equipped with a DTGS/KBr detector and a KBr Beam-splitter with IR source. Scanned 40 times with a resolution of 4 cm^{-1} in the range 4000–400 cm^{-1}. Compositional quantitative analysis (QA) of oleic acid, sunflower oil, FAEE, and mixtures was accomplished with single peak absorbance Beer-Lambert law, based on the carbonyl bond region where peaks are strong and relatively narrow [17,18].

The acidity of the renewable crude was measured by the total acid number (TAN) colour-indicator titration following the ASTM standard test method D974-12 [19]. 48hr dry crude samples were dissolved in 40 ml of anhydrous isopropanol with 5 drops of an indicator solution (0.1% in mass of phenolphthalein in a 1:1 vol mixture of water and ethanol). Titration was done with a 0.1 M solution of potassium hydroxide (KOH) in isopropanol (previously standardised with potassium acid phthalate in water). The sample size was 0.2 g with a sensibility of 0.001 g because of the high acidity range (25 to 250 mgKOH/g). All samples were tested

by duplicate.

Boiling point distribution tested via thermogravimetric analysis (TGA) was performed in a Mettler Toledo TGA-DSC 2. The method includes an isothermal segment at 80 °C for 20 min to remove humidity and dissolved water, followed by a dynamic ramp from 80 to 600 °C, with a 5 °C/min heating rate under nitrogen gas 50 ml/min flow at atmospheric conditions. The boiling point fractions are defined by the weight loss percentages within the following temperature ranges: 80–190 °C, 190–250 °C, 250–300 °C, 300–350 °C and 350–600 °C [7,20,21].

2.5. Kinetic modelling

Reaction kinetics were modelled with a set of first-order ordinary differential equations (ODE) system, solved using Matlab function *ODE45*. The reaction constants (k) were obtained via multivariable optimization using *lsqcurvefit* function by fitting the experimental concentration values (average) to the set of reaction constants at each temperature over the residence time range. Initial guess for all k values was 0,1 with lower and higher limits from 0 to 1, and Matlab has calculated the optimal *k* values by minimizing the squared norm of the residual function between experimental and modelled yields [22]. The maximum standard deviation values of each set of experiments are plotted as error bars in each case. Last, activation energies and pre-exponential factors were calculated with the Arrhenius equation using *nlparci* function to compute the regression within 95% confidence intervals [7,22,23].

3. Results and discussion

3.1. FT-IR and carbonyl bond quantification

FT-IR spectroscopy is relatively quick and requires no sample preparation to test solids and liquids. Infrared spectra have various absorbance wavelengths and not all of them are easy to analyze. Carbonyl bond (C═O) stretching has strong peaks in the region 1850 to 1550 cm^{-1} (5.41–6.45 μm), which enables the quantification of ketones, aldehydes, acids and ester groups present in a sample [17,18]. From the spectrograms of sunflower oil and oleic acid, remarkable differences were observed in the absorption bands of the carbonyl bonds of the FFA and glycerolipids. As illustrated in Fig. 1, stretching of the acid group in the FFA has a maximum absorbance peak in the region 1700 to 1715 cm^{-1}, whereas stretching of the ester group in the glycerolipid has its maximum peak in the range 1740 to 1750 cm^{-1} [17]. This relatively interference-free region makes possible the quantification of acid and ester functional groups present in the renewable crude by using peak height Beer-Lambert's law [18].

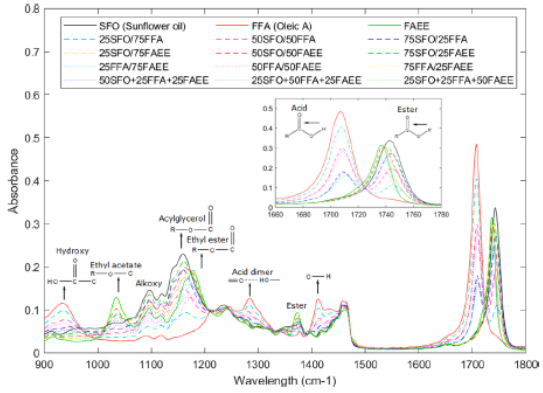

Fig. 1. FT-IR spectrograms of standards and mixtures.

For in-situ homogeneous catalyst, the quantification of FAEE is more complex as ester bonds present in the FAEE are essentially equal to the carbonyl bond linkage in the feedstock's glycerolipid. Consequently, overlapping occurs in the spectrograms. However, a clear variation (displacement) on one tail of the ester IR spectra at 1753 cm^{-1} (5.41 μm) where FFA, FAEE, binary and ternary mixtures reach common heights, allowing lipid ester estimation. The quantitative model for the three-component is made of fifteen points, including pure substance, binary, and ternary mixtures, shown in Fig. 1 legend [18]. The compositional model for the non-catalytic HTL includes the Beer-Lambert law linearisation using the *nlparci* function for the acid and glycerolipid ester peaks with R^2 values of 0.993 for the FFA and 0.997 for the triglyceride. When the homogeneous catalyst system is used, the FFA regression remains unchanged and the glycerolipid ester concentration is predicted from the specific band height on the right tail of the spectrogram at (1753 cm^{-1}), which present an R^2 of 0.991 for glycerolipid esters, and the FAEE is defined by difference [17,18].

The FT-IR compositional model for the FFA was contrasted with TAN titration values. It was found that at concentrations lower than 25% by mass, the error and residual values of the model reach a maximum value of 5%. As the concentration of the FFA increases, the error and residual values are reduced to approximately 2%. This verification supports the validity of the analytical method used to study FFA concentration in the HTL renewable crude from lipids. The glycerolipid ester quantification model presents a residual value at low concentrations of 7% on average and lower values at high concentrations. Besides the carbonyl stretching bonds region, there are diffused absorbance signals present in the region 915–955 cm-^{1} which may be linked the hydroxy (C-OH) asymmetric stretching and out-of-plane deformation of the acid, conjugated with acid dimer absorption band in the region 1280–1320 cm^{-1}. Deformation vibrations from the (C—C—O) bond of the acid in the region 1400–1410 cm^{-1}, and (C—O) stretching of the ester is present in the region 1100–1300 cm^{-1}. The glycerolipid shows the absorbance of the alkoxy stretching vibrations (C—O—C) of the ester in the region 1100–1175 cm^{-1}, while ethyl ester from FAEE shows the signal at approximately 1190 cm^{-1} accompanied with vibrations of the acetate in the region 1040–1060 cm^{-1}, as illustrated in Fig. 1 [17,24]. However, 500–1400 cm^{-1} is a complex IR region known as the fingerprint in which overlapping from long hydrocarbon chain stretching vibration is common. FT-IR spectrograms of the renewable crude samples are provided in Supplementary material in Fig. S.1. The single-band FT-IR quantitative model used may have limitations because of possible interference of other carbonyl bonds and heteroatoms such as amines or amides, which may come from proteins to acid interactions [1,17,18,21,24].

3.2. HTL of lipids (Blank)

Renewable crude yields obtained from the HTL of sunflower oil are comparable to experimental results reported in previous studies [6,7,13]. To achieve these values, the recovery of the product crude oil phase must be adjusted as it is an extremely sensitive process due to crude viscosity, polarity, low solubility, and tendency to stick to reactor walls [1,13]. Crude recovery in this study was initially planned to be a solvent-free process by pouring products out of the reactor. However, after running an initial set of experiments, inconsistencies were acknowledged and linked to product losses (oil phase yields as low as 72%). Therefore, product recovery had to be adjusted using ethanol to rinse the reactor and to remove crude oil stuck to the walls, as described in Section 2.3. Eventually, the major difference between the in-situ catalyst and non-catalytic HTL experiments was reduced to how much and when the ethanol was added to the system plus pH modification. HTL renewable crude solvent recovery has proven to affect crude oil yields and properties, and it is a current research topic [25–27].

Renewable crude yields and hydrolysis profile agree with values reported by *Alenezi et al. (2009)* [15]. However, the hydrolysis induction

period defined by *Alenezi et al. (2009)* was not recognised in the present results. The lowest temperature of the present study was 250 °C, in which at 30 min a hydrolysis degree of just one quarter was found, while *Alenezi et al. (2009)* reported near 70% FFA at less than 27 min. A concentration share close to three-quarters FFA was found at 350 °C and 2 min whereas *Alenezi et al. (2009)* informed around 45% at similar conditions [15,28]. Differences may be linked to heating, which as described in the method (Section 2.2), the reaction time started when the system reached 98% of the desired temperature (heating time). The heating rate has a positive effect on crude yields results and the sand fluidized bed allows an extremely quick and uniform heating rate of up to 125 °C per minute [1,7]. However, a continuous process might have a better momentum, mass, and energy diffusion than a batch system like the reactor tube used [7,29,30].

3.3. Homogeneous catalyst HTL of lipids

Co-solvents as ethanol has been tested to increase HTL oil phase yields. However, its effect on the HTL process and products has not been completely explained [31,32]. Ethanol may promote the transesterification of lipids and esterification of FFA. However, wet conditions of the HTL conversion limit the alcoholysis pathway to low pH. Alkaline conditions will promote the saponification of oils, reducing crude oil yields, which is the major reason for using acetic acid in combination with ethanol. Acid alcoholysis is less sensitive to water and FFA but requires longer residence times and higher temperatures, conditions present in the HTL of biomass [1,8,33]. To the best of our knowledge, none of the recent HTL studies using ethanol during HTL has investigated the reaction kinetics or defined the effect of ethanol in the renewable crude quality [31,32].

Renewable crude yields obtained with in-situ homogeneous catalysts (illustrated in Fig. 2) are comparable to the non-catalytic experiments (91 ± 3%). They are also in good agreement with theoretical hydrolysis and alcoholysis reaction balances and with the literature, the differences stand in crude oil functional group abundance [8–10,33]. As expected, ethanol reduces the FFA concentration while promoting the formation of FAEE from the alcoholysis of lipids and FFA. Supercritical transesterification of lipids as one of the state-of-the-art alcoholysis techniques has an optimal condition in the range 325 to 350 °C with ethanol to oil molar ratio of 33:1 to 43:1, to achieve FAEE yields of 80 to 90% [9,34]. In the present study, concentrations of up to 38% FAEE were obtained under the hydrothermal liquefaction condition with ethanol/oil molar ration of 19:1 and water/ethanol molar ratio of 7:1. Subcritical water as a major component of the reaction medium and the relatively low ethanol/water ratio affect the reaction equilibrium of hydrolysis and alcoholysis of lipids under HTL conditions [5,33,35].

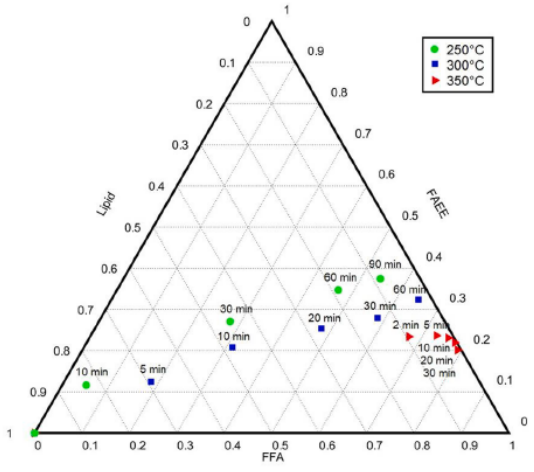

Fig. 2. Ternary compositional plot (FT-IR functional group model) for the in-situ homogeneous catalysts HTL experiments.

Temperature showed to have a substantial effect in the HTL conversion of lipids. While at 250 °C triglycerides require up to 90 min to achieve over 90% conversion, at 350 °C the reaction is as fast that after 2 min the remaining lipid concentration was lower than 10%. Furthermore, the alcoholysis reaction appeared to be indirect to temperature as at 250 °C the maximum FAEE concentration was 1.2 times the maximum achieved at 300 °C and 1.7 times the value found at 350 °C. Long residence times at 350 °C promote higher FFA concentrations, even after reaching the highest conversion of lipids, displacing the equilibrium concentration of the FAEE toward FFA. This effect, and the different degrees of equilibrium found in the crude phase, encourage to have a forward and reverse reaction paths in the kinetics model presented in Section 3.5.

3.4. Boiling point distribution and total acid number

Boiling point distribution of raw sunflower oil showed that 94% of the oil mass is above 350 °C boiling point, with a maximum mass transfer rate between 398 and 404 °C under nitrogen, according to the derivate of the mass loss (percentage) over temperature (dTG), illustrated in Supplementary material in Fig. S.2. HTL conversion reduces the percentage of over 350 °C boiling temperature crude fraction while increase 180–250 °C and 250–300 °C fractions [7,8,20]. This is achieved by the hydrolysis/fractionating of relatively high molecular weight (MW) triglycerides into three free fatty acids, which are approximately a third of the feedstock MW and have a thermal mass transfer rate peak at 275 °C under nitrogen. The measured transfer peak rate for FAEE was at 263 °C, as the difference in boiling point is minor, this technique could not differentiate FFA and FAEE in mixture. Additionally, as compositional change is negligible, there should not be major variations in HHV [8,10].

As a dynamic thermal analysis, boiling point distributions serve as an indicator of the fractionating of the glycerolipid and the quality of the renewable crude mixtures by the reduction in boiling temperature [7,21]. Despite, this is not a separation method such as GC, it does not have temperature restrictions like GC, which goes up to around 300 °C to produce volatile matter, limiting the characterisation of heavy components in the renewable crude mixture [6,36]. However, thermogravimetric analysis over 300 °C might produce low heating rate pyrolysis/cracking of the organic matter in the crude mixture samples, However, hydrocarbons and FFA in lipids are among the most thermal stable structures in biomass [8,20].

Extreme temperatures and longer residence times may affect the boiling point fractions. The most severe conditions illustrated in Fig. 3 (c) and (f), indicate that over 22% of the renewable crude is above 300 °C fractions (with approximately half of it over 350 °C). This effect may be associated with the saturation of double bonds in the FFA, the formation of other complex structures like stearolactone (*Terri, Luo, and Savage (2014)*), or the thermal stability of the mixture [6–8,20].

The enhancement of FAEE over FFA stands in crude oil acidity levels. For instance, while the glycerolipid and corresponding FAEE have a TAN number of zero, the measured TAN for oleic acid was 203.2 ± 2.9 mgKOH/g oil. As previously mentioned, TAN may work as an indicator of the concentration of FFA and as a result, it can be linked to the reaction kinetics model as a function of FFA. However, FAEE cannot be differentiated from the glycerolipids using TAN, limiting the quantification to non-catalytic experiments [15,19].

The temperature has a considerable effect on crude oil acidity. The maximum TAN value found for non-catalytic HTL at 300 and 350 °C was on average 181 mgKOH/g oil, which may indicate a hydrolysis equilibrium conversion of 89 ± 1% [15,16]. When the homogeneous catalyst system was included, the acidity values were reduced in almost all cases.

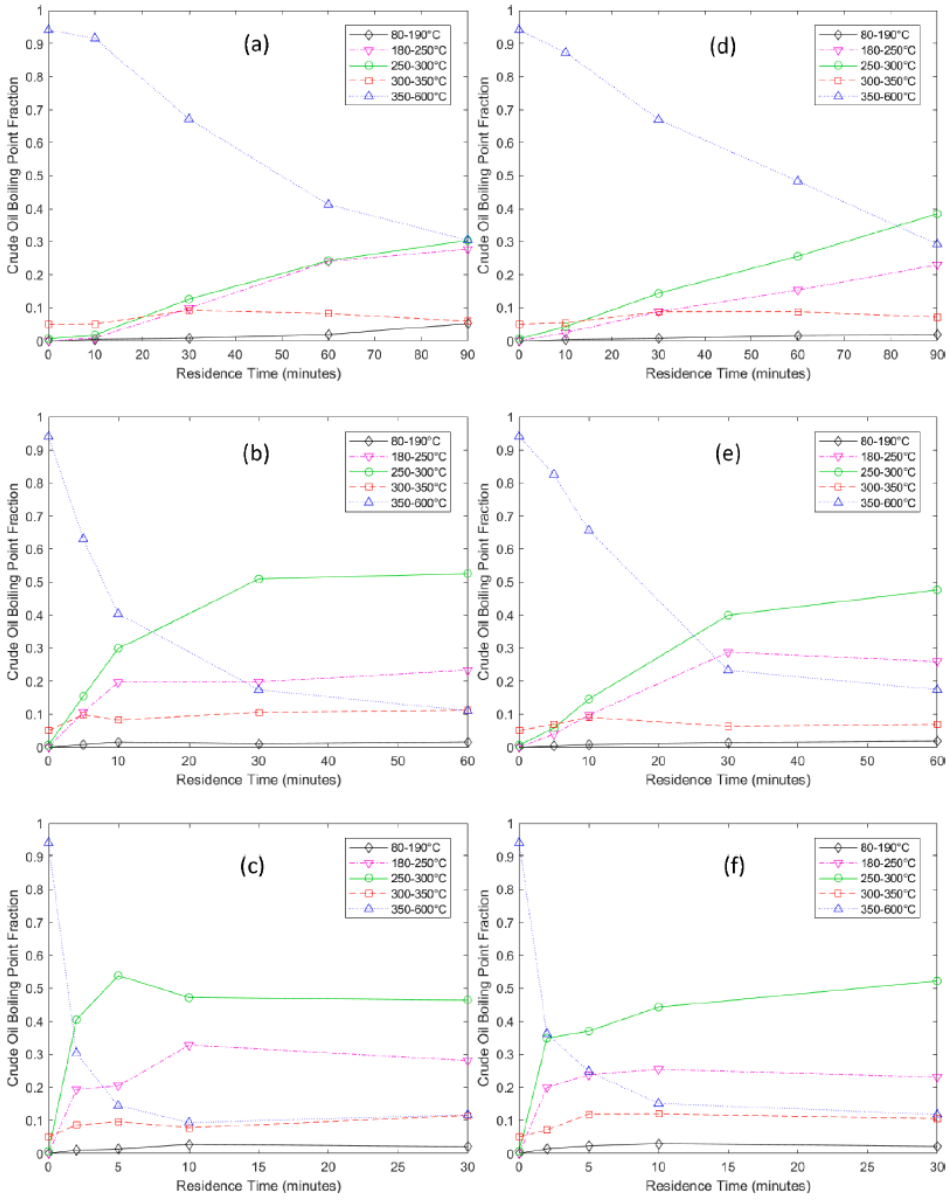

Fig. 3. Boiling point distribution of the renewable crude at (a) 250, (b) 300 and (c) 350 without catalysts, (d) 250, (e) 300 and (f) 350 with in-situ catalysts.

At 300 °C, the reduction was more significant, with the lowest difference of around 33% at 60 min and higher at lower residence times. As illustrated in Fig. 4. (a) TAN and (b) boiling point 80–300 °C results suggest that 300 °C is the ideal HTL temperature to reduce renewable crude acidity and lower boiling point fraction. However, the higher FAEE concentrations were observed at 250 °C. Boiling point distribution, TAN and functional group compositional analysis showed that the hydrolysis/fractionating reactions were not complete in any of the near-equilibrium conditions experiments.

3.5. Reaction kinetics model

The reaction pathway for the non-catalytic HTL considers the hydrolysis of the fatty acids from the triglyceride as (one-to-one) first-order reaction and the release of glycerol into the aqueous phase. Glycerol is believed to degrade into smaller alcohols, acids, and other simpler soluble compounds, from where the gaseous phase is more likely to be formed [1,7,15,27]. When ethanol and acetic acid are added to the system, hydrolysis and direct transesterification from the lipid, and the esterification of the free fatty acid released are considered as a close loop of forward and reverse reactions which reach a certain equilibrium

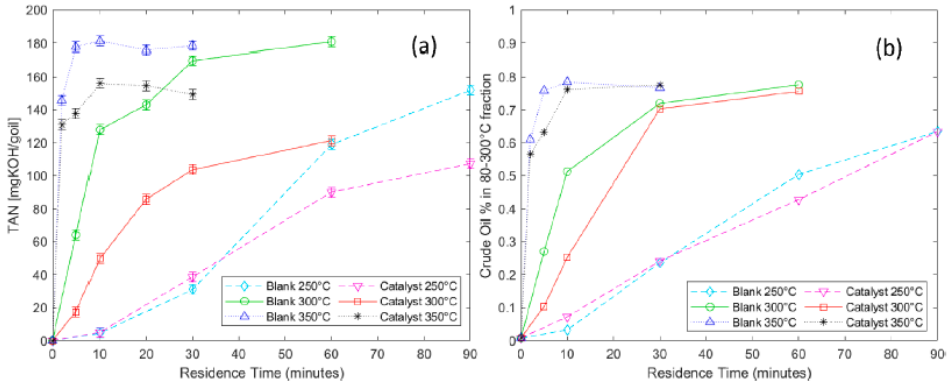

Fig. 4. TAN (a) and 80–300 °C mass fraction (b) for the HTL renewable crude with and without homogeneous catalysts.

depending on the reaction conditions, as illustrated Fig. 5 [8–10]. Consequently, the proposed kinetics model fits the average crude oil composition of the experiments closely. The squared norm of the residual function values for the non-catalytic HTL model were 3.9, 1.0, and 2.2%, while for the in-situ catalysts HTL the values were 1.3, 0.9, and 0.4% respectively for 250, 300, and 350 °C. These relatively low residual values suggest that the two models may predict phase yields and renewable oil functional composition throughout HTL with and without the homogeneous catalyst system with relatively good accuracy [18].

The differential equations for the model are (where x is mass concentration):

HTL (Non-catalytic pathway):

$$\frac{dx_a}{dt} = -k_{1F}x_a - k_2x_a + k_{1R}x_b \quad (1)$$

$$\frac{dx_b}{dt} = k_{1F}x_a - k_{1R}x_b \quad (2)$$

$$\frac{dx_c}{dt} = k_2x_a - k_3x_c \quad (3)$$

$$\frac{dx_d}{dt} = k_3x_c \quad (4)$$

With homogeneous catalyst (In-situ alcoholysis pathway):

$$\frac{dx_a}{dt} = -k_{1F}x_a + k_{1R}x_b - k_2x_a - k_{4F}x_a + k_{4R}x_e \quad (5)$$

$$\frac{dx_b}{dt} = k_{1F}x_a - k_{1R}x_b - k_{5F}x_b + k_{5R}x_e \quad (6)$$

$$\frac{dx_e}{dt} = k_{4F}x_a - k_{4R}x_e + k_{5F}x_b - k_{5R}x_e \quad (7)$$

The degree of hydrolysis at equilibrium for HTL is independent of the reaction temperature as it was defined by Lascaray (1949, 1952) and *Alenezi et al. (2009)* [12,15]. Yields at equilibrium conditions of around 80/10 for FFA/lipids were observed in the temperature range tested, as illustrated in Fig. 6(a), (b), and (c). When ethanol and acetic acid were incorporated to the system, the equilibrium concentration of the glycerolipid was displaced toward to a more complete conversion (around 3% share of the oil phase at 300 °C and higher at 350 °C). However, ethanol seems to affect the kinetics of the hydrolysis reaction as a lower conversion rate can be identified. Additionally, glycerol may generate some mono-alcohols which may react and form FAEE. But esterification is assumed to be negligible when ethanol is not used as in-situ homogeneous catalysts [8,16].

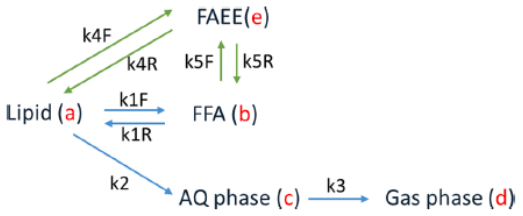

Fig. 5. Proposed reaction kinetic pathway for the HTL of lipids and in-situ transesterification.

Activation energy and the pre-exponential value obtained for the hydrolysis of sunflower oil under hydrothermal conditions are remarkably close to 98 kJ/mol and $5.2*10^6$, reported by *Alenezi et al. (2009)* as the highest values for the hydrolysis of triglycerides in the sunflower oil [15]. In the present study, the hydrolysis of lipids is modelled as one first-order reaction. The effect of diglycerides and monoglycerides is not included due to the restrictions of the functional/compositional analysis method used [18]. Furthermore, the influence of monoglycerides and diglycerides in the product profile is limited, according to the qualitative conversion plot for vegetable oils presented by *Knothe et al. (2010)* [8]. The present model also includes a reverse reaction to clarify the equilibrium degree of the system reactions [9].

The addition of ethanol increased the hydrolysis activation energy by 25% (as illustrated in Table 1). This may be because of the competing reaction with alcoholysis (direct transesterification), which accounts for almost half the value of hydrolysis [23]. Equilibrium for FAEE is indirect to reaction temperature and lower than FFA at evaluated conditions. For instance, at 250 and 300 °C, the equilibrium concentration for FAEE is reached before the FFA. The FAEE/FFA mass ratios were approximately 2/3, 1/2, and 1/3, respectively at 250, 300 and 350 °C, showing that lower temperature and longer reaction times are ideal to increase the FAEE concentration. Furthermore, at 350 °C, the FAEE/FFA ratio is reduced after reaching the maximum FAEE concentration which shows an equilibrium displacement due to the severe temperature, which is captured by the model as illustrated in Fig. 6(f).

The activation energy found for the direct alcoholysis of lipids is higher than the value reported for acid-catalysed transesterification (5% sulphuric acid) of sunflower oil (TAN of 5 to 7 mgKOH/g oil) with methanol of 50.7 kJ/mol [37]. The present alcoholysis energy value is also higher than 48.7 kJ/mol informed for the alkaline transesterification of sunflower oil with ethanol, and lower than 85.5 kJ/mol and 95 kJ/mol reported for the supercritical transesterification of sunflower oil with methanol and soybean oil with ethanol respectively [9,38,39]. Furthermore, the activation energy for the supercritical

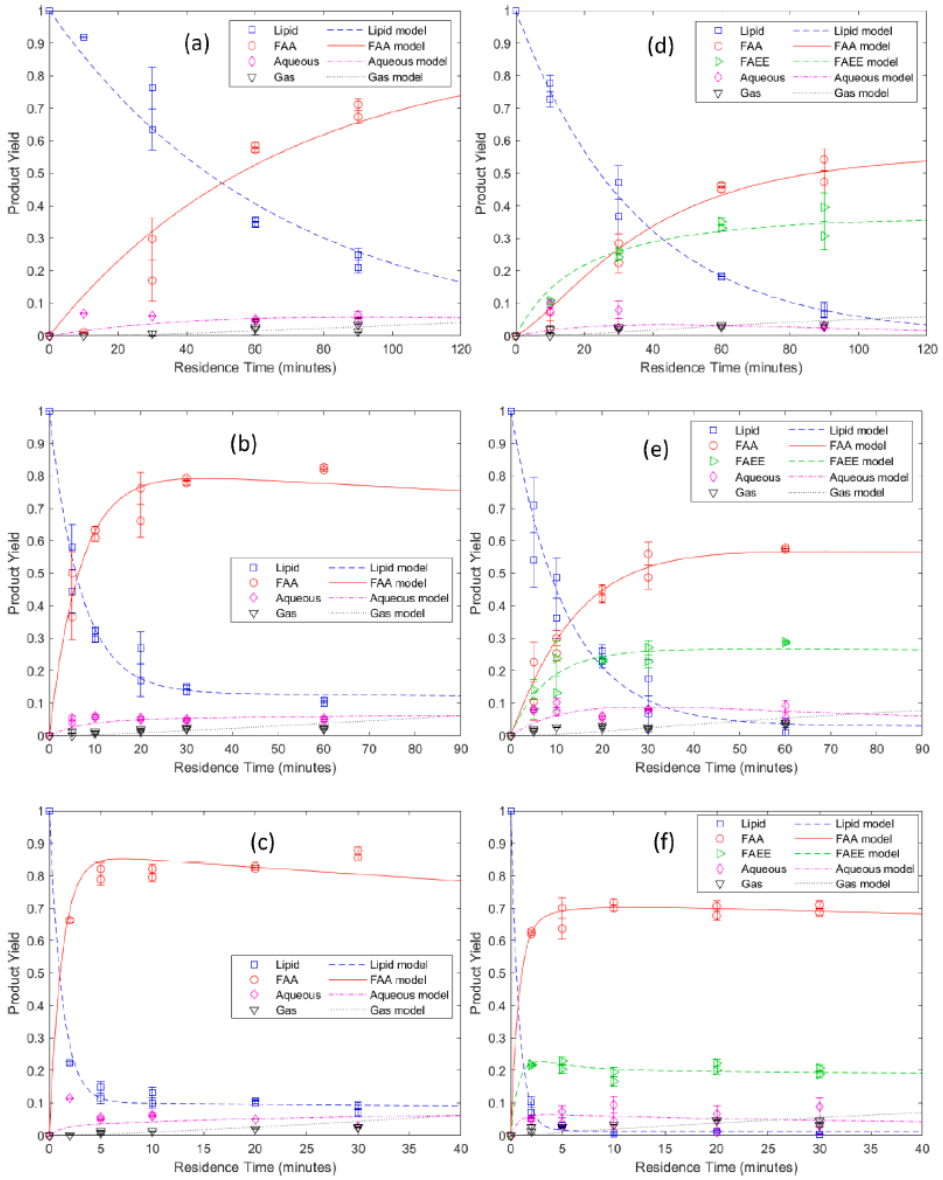

Fig. 6. Experimental and modelled yield values for the HTL of lipids. (a) 250, (b) 300 and (c) 350 °C without catalysts, (d) 250, (e) 300 and (f) 350 °C with catalysts.

esterification of oleic acid with ethanol reported by Pinnarat and Savage (2010) is 56 kJ/mol [35]. The present study involves in-situ alcoholysis, which may include transesterification of sunflower oil in a system with approximately 60% water and direct esterification of FFA released and the corresponding equilibrium. The activation energy value found for the direct alcoholysis of lipids is in good agreement with various transesterification techniques reported in the literature, despite the obvious differences in the reaction and system conditions [10].

The activation energy for the esterification of FFA is around 1/8 the value for the transesterification of lipids. This value is complex to analyse, as it heavily depends on the dynamic equilibrium of the reaction system. Although, this relatively low value may illustrate that esterification of FFA is a much quicker reaction than transesterification and the value is 1/6 of the reported activation energy for supercritical esterification of oleic acid with ethanol [35]. The equilibrium reached by the forward and reverse reactions may be included in a dynamic equilibrium constant (K_{eq}), which is equal to $k_{forward}/k_{reverse}$ and by using the Arrhenius equation with *nlparci* function, thermodynamic equilibrium energy [23,40]. The obtained values were 227.9, 612.9 and 12.9 7 kJ/mol (all negative) for hydrolysis, alcoholysis of lipids and esterification of FFA, respectively. These equilibrium energies may indicate the thermodynamic balance of the species at equilibrium conditions and it is known as an increase in internal energy from forward to reverse reactions [40].

Table 1
Kinetic parameters to fit the reaction model in Fig. 5.

Model	path	Reaction	−ln(k) [°C/sec]			lnA	Ea [kJ/mol]	R^2
			250 °C	300 °C	350 °C			
HTL (Blank)	1F	Hydrolysis Lipid to FFA	8.41	6.20	4.44	16.39 ± 1.15	107.80 ± 9.56	0.999
	1R	Hydrolysis (rev) FFA to Lipid	25.54	7.97	6.56	97.54 ± 6.11	525.64 ± 50.76	0.843
	2	Release of glycerol (AQ phase)	10.46	9.04	7.78	6.20 ± 0.77	72.49 ± 6.43	0.999
	3	Gas formation from AQ phase	8.99	8.43	7.52	0.014 ± 0.43	39.48 ± 3.57	0.964
In-situ Catalyst	1F	Hydrolysis Lipid to FFA	9.26	7.37	4.26	21.35 ± 1.46	134.20 ± 12.13	0.964
	1R	Hydrolysis (rev) FFA to Lipid	31.39	22.84	18.10	52.28 ± 3.89	362.08 ± 32.32	0.987
	2	Release of glycerol (AQ phase)	7.98	7.46	5.19	13.29 ± 1.11	103.52 ± 9.26	0.850
	3	Gas formation from AQ phase	10.39	8.72	6.54	1.46 ± 0.51	46.77 ± 4.20	0.984
	4F	Transesterification lipid to FAEE	7.31	7.10	6.97	8.75 ± 0.86	74.05 ± 7.12	0.994
	4R	Transesterification (reverse)	31.39	8.79	6.56	129.34 ± 7.93	686.92 ± 65.94	0.854
	5F	Esterification FFA to FAEE	9.22	8.52	7.48	−5.20 ± 0.10	9.12 ± 0.81	0.974
	5R	Esterification (reverse)	6.88	6.39	6.07	−1.80 ± 0.24	22.01 ± 1.96	0.996

3.6. Effect of ethanol concentration

Once the reaction kinetics are defined for both systems (blank and homogeneous catalyst), the next logical research step is to define the effect of ethanol mass loading in the system. Experiments with ethanol to sunflower oil mass ratios of 0.5:1, 1.5:1, and 2.0:1 were done at 300 °C, as the mild temperature to clarify the effect of ethanol concentration in reaction equilibrium and kinetic parameters. The obtained results suggested that higher ethanol concentrations have not substantial effect on the FAEE yield near-equilibrium of the system and the alcoholysis reaches equilibrium earlier than hydrolysis, as illustrated in the Supplementary material in Fig. S.3. This outcome may indicate a reduction in the hydrolysis reaction rate, which can be linked to the substitution of water mass by ethanol, from 70:10% to 40:40% keeping feedstock mass loading and reaction conditions constant in all cases [35,40].

The thermodynamical equilibrium of the HTL system is heavily influenced by water and the optimal cost-effective conversion is at relatively low ethanol concentration, which is beneficial for the practical use of ethanol as co-solvent during HTL. Furthermore, the renewable crude produced through HTL will require further treatment after separation to reduce the remaining acidity to levels close to 1 mgKOH/g [35].

4. Conclusion

HTL conversion of lipids as a sustainable method to produce renewable crude has been investigated, and a homogeneous catalyst system was proposed and tested to reduce renewable crude oil acidity as one of the most significant issues acknowledged to the current HTL conversion of lipids technology. Among the three temperatures tested, 300 °C appeared to produce the highest impact on reducing TAN and boiling point fractions in the renewable crude. However, lower temperatures produced higher FAEE concentrations near to equilibrium conditions. The suggested HTL and in-situ alcoholysis kinetic models could predict the yield and functional group proportion of the renewable crude oil based on the differences in the carbonyl bonds (acid and esters) present. The ethanol to oil mass ratio in the ranges tested changed the reaction rates but produced a negligible effect to control the product concentrations and degrees of equilibrium. Therefore, the information presented in this study may be useful for the HTL treatment of high lipids concentration wet biomass or in combination with other biomass types for computational fluid dynamics (CFD) design and optimization of process and equipment. Finally, the composition of renewable crude may require a better understanding as high temperatures may affect the structure of the hydrocarbons, especially the double bonds (C=C) in the FFA.

Declaration of Competing Interest

The authors declare that they have no known competing financial interests or personal relationships that could have appeared to influence the work reported in this paper.

Acknowledgments

The authors acknowledge the financial support of the Australian Research Council's Linkage Project grant (LP150101241) and our industry partner Southern Oil Refining Pty Ltd.

Appendix A. Supplementary data

Supplementary data to this article can be found online at https://doi.org/10.1016/j.cej.2021.128832.

References

[1] P. Biller, A.B. Ross, 17 - Production of biofuels via hydrothermal conversion, in Handbook of Biofuels Production (Second Edition), R. Luque, et al., Editors. 2016, Woodhead Publishing. p. 509-547.
[2] L. Xu, et al., Assessment of a dry and a wet route for the production of biofuels from microalgae: energy balance analysis, Bioresour. Technol. 102 (8) (2011) 5113–5122.
[3] P. Biller, A.B. Ross, Potential yields and properties of oil from the hydrothermal liquefaction of microalgae with different biochemical content, Bioresour. Technol. 102 (1) (2011) 215–225.
[4] A. Kruse, E. Dinjus, Hot compressed water as reaction medium and reactant, J. Supercrit. Fluids 39 (3) (2007) 362–380.
[5] A.A. Peterson, et al., Thermochemical biofuel production in hydrothermal media: a review of sub- and supercritical water technologies, Energy Environ. Sci. 1 (1) (2008).
[6] G. Teri, L. Luo, P.E. Savage, Hydrothermal treatment of protein, polysaccharide, and lipids alone and in mixtures, Energy Fuels 28 (12) (2014) 7501–7509.
[7] R. Obeid, et al., The elucidation of reaction kinetics for hydrothermal liquefaction of model macromolecules, Chem. Eng. J. 370 (2019) 637–645.
[8] 4 - Biodiesel Production, 6 - Fuel Properties, Appendix A & B, in The Biodiesel Handbook (Second Edition), G. Knothe, J. Krahl, and J. Van Gerpen, Editors. 2010, AOCS Press. p. 31-96.
[9] K.C. dos Santos, et al., Experimental and kinetic modeling of acid oil (trans) esterification in supercritical ethanol, Fuel 224 (2018) 489–498.
[10] A.W. Go, et al., Developments in in-situ (trans) esterification for biodiesel production: a critical review, Renew. Sustain. Energy Rev. 60 (2016) 284–305.
[11] Y. Chen, et al., Thermochemical conversion of low-lipid microalgae for the production of liquid fuels: challenges and opportunities, RSC Adv. 5 (24) (2015) 18673–18701.
[12] L. Lascaray, Mechanism of fat splitting, Ind. Eng. Chem. 41 (4) (1949) 786–790.
[13] P. Biller, R. Riley, A.B. Ross, Catalytic hydrothermal processing of microalgae: decomposition and upgrading of lipids, Bioresour. Technol. 102 (7) (2011) 4841–4848.
[14] S. Saka, D. Kusdiana, Biodiesel fuel from rapeseed oil as prepared in supercritical methanol, Fuel 80 (2) (2001) 225–231.
[15] R. Alenezi, et al., Hydrolysis kinetics of sunflower oil under subcritical water conditions, Chem. Eng. Res. Des. 87 (6) (2009) 867–873.
[16] R. Alenezi et al., Continuous Flow Hydrolysis of Sunflower Oil for Biodiesel. Energy Sources, Part A: Recovery, Utilization, and Environmental Effects, 2010. 32(5): p. 460-468.

[17] G. Socrates, Infrared and Raman Characteristic Group Frequencies: Tables and Charts. 2004: Wiley.
[18] D.M. Mackie et al., Simple, fast, and accurate methodology for quantitative analysis using Fourier transform infrared spectroscopy, with bio-hybrid fuel cell examples. MethodsX, 2016. 3: p. 128-38.
[19] S. Mahajan, S.K. Konar, and D.G.b. Boocock, Determining the acid number of biodiesel. Journal of the American Oil Chemists' Society, 2006. 83(6): p. 567-570.
[20] M.R. Riazi, Characterization and Properties of Petroleum Fractions. 2005: ASTM International.
[21] L. Luo, et al., Products and kinetics for isothermal hydrothermal liquefaction of soy protein concentrate, ACS Sustainable Chem. Eng. 4 (5) (2016) 2725–2733.
[22] K.J. Beers, Numerical Methods for Chemical Engineering: Applications in MATLAB. 2006: Cambridge University Press.
[23] H.S. Fogler, Elements of Chemical Reaction Engineering. 2006: Prentice Hall PTR.
[24] B.C. Smith, Infrared Spectral Interpretation: A Systematic Approach. 1998: Taylor & Francis.
[25] J. Jiang, P.E. Savage, Using Solvents To Reduce the Metal Content in Crude Bio-oil from Hydrothermal Liquefaction of Microalgae. Industrial & Engineering Chemistry Research, 2019. 58(50): p. 22488-22496.
[26] J. Lu, et al., 110th anniversary: influence of solvents on biocrude from hydrothermal liquefaction of soybean oil, soy protein, cellulose, xylose, and lignin, and their quinary mixture, Ind. Eng. Chem. Res. 58 (31) (2019) 13971–13976.
[27] A.R.K. Gollakota, N. Kishore, S. Gu, A review on hydrothermal liquefaction of biomass, Renew. Sustain. Energy Rev. 81 (2018) 1378–1392.
[28] P.H.L. Moquin, F. Temelli, Kinetic modeling of hydrolysis of canola oil in supercritical media, J. Supercrit. Fluids 45 (1) (2008) 94–101.
[29] J.D. Sheehan, P.E. Savage, Molecular and lumped products from hydrothermal liquefaction of bovine serum albumin, ACS Sustain. Chem. Eng. 5 (11) (2017) 10967–10975.
[30] J.L. Faeth, P.J. Valdez, P.E. Savage, Fast hydrothermal liquefaction of Nannochloropsis sp. to produce biocrude, Energy Fuels 27 (3) (2013) 1391–1398.
[31] S. Cheng, et al., Highly efficient liquefaction of woody biomass in hot-compressed alcohol–water co-solvents†, Energy Fuels 24 (9) (2010) 4659–4667.
[32] J. Zhang, Y. Zhang, Hydrothermal liquefaction of microalgae in an ethanol-water co-solvent to produce biocrude oil, Energy Fuels 28 (8) (2014) 5178–5183.
[33] E. Lotero et al., Synthesis of Biodiesel via Acid Catalysis. Industrial & Engineering Chemistry Research, 2005. 44(14): p. 5353-5363.
[34] K.T. Tan et al., An optimized study of methanol and ethanol in supercritical alcohol technology for biodiesel production. The Journal of Supercritical Fluids, 2010. 53 (1-3): p. 82-87.
[35] T. Pinnarat, P.E. Savage, Noncatalytic esterification of oleic acid in ethanol. The Journal of Supercritical Fluids, 2010. 53(1-3): p. 53-59.
[36] R. Obeid, et al., Reaction kinetics and characterization of species in renewable crude from hydrothermal liquefaction of mixtures of polymer compounds to represent organic fractions of biomass feedstocks, Energy Fuels 34 (1) (2020) 419–429.
[37] M. Berrios, et al., A kinetic study of the esterification of free fatty acids (FFA) in sunflower oil, Fuel 86 (15) (2007) 2383–2388.
[38] Y.T. Tsai, H.M. Lin, M.J. Lee, Biodiesel production with continuous supercritical process: non-catalytic transesterification and esterification with or without carbon dioxide, Bioresour. Technol. 145 (2013) 362–369.
[39] I. Reyero, et al., Kinetics of the NaOH-catalyzed transesterification of sunflower oil with ethanol to produce biodiesel, Fuel Process. Technol. 129 (2015) 147–155.
[40] K.G. Denbigh, K.G. Denbigh, The Principles of Chemical Equilibrium: With Applications in Chemistry and Chemical Engineering. 1981: Cambridge University Press.

The effect of ethanol as a homogeneous catalyst on the reaction kinetics of hydrothermal liquefaction of lipids

Andrés Chacón-Parra, David Lewis, Philip van Eyk

School of Chemical Engineering and Advanced Materials,

The University of Adelaide, Adelaide, SA, 5005, Australia

*Corresponding author

E-mail address: andres.chaconparra@adelaide.edu.au

Supplementary Material

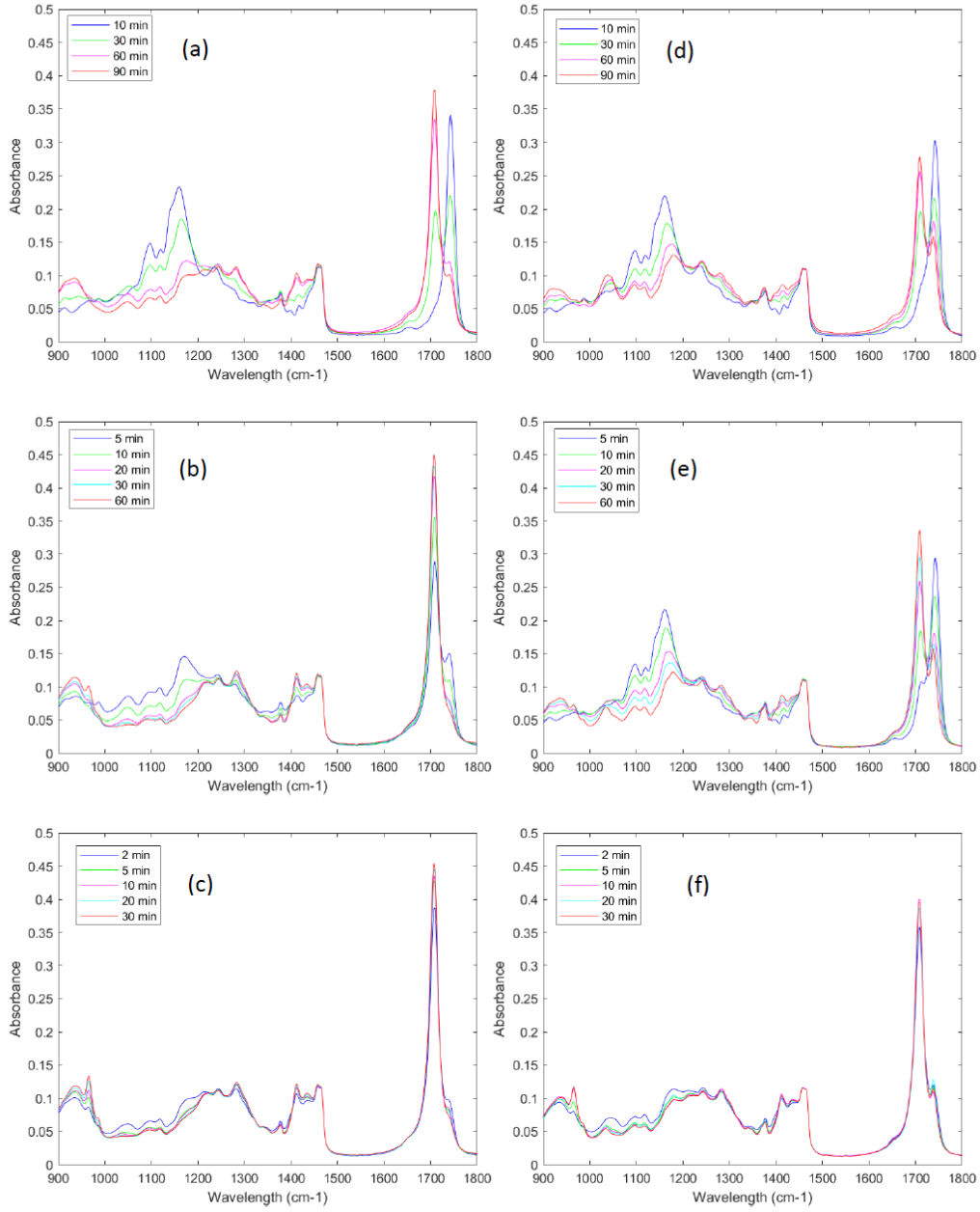

Fig S.1. FT-IR of HTL renewable crude at (a) 250, (b) 300 and (c) 350°C without catalysts, (d) 250, (e) 300 and (f) 350°C with catalysts.

2

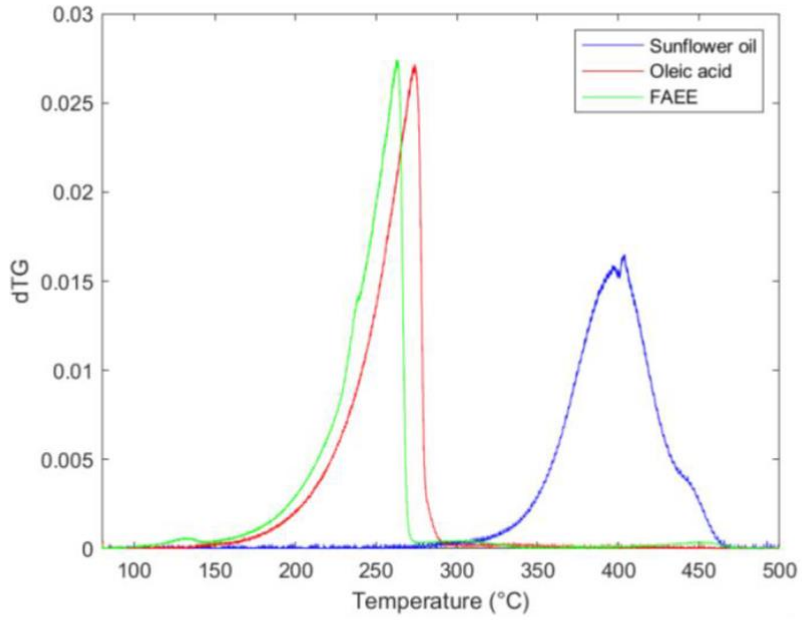

Fig S.2. dTG over temperature for sunflower oil, oleic acid and FAEE.

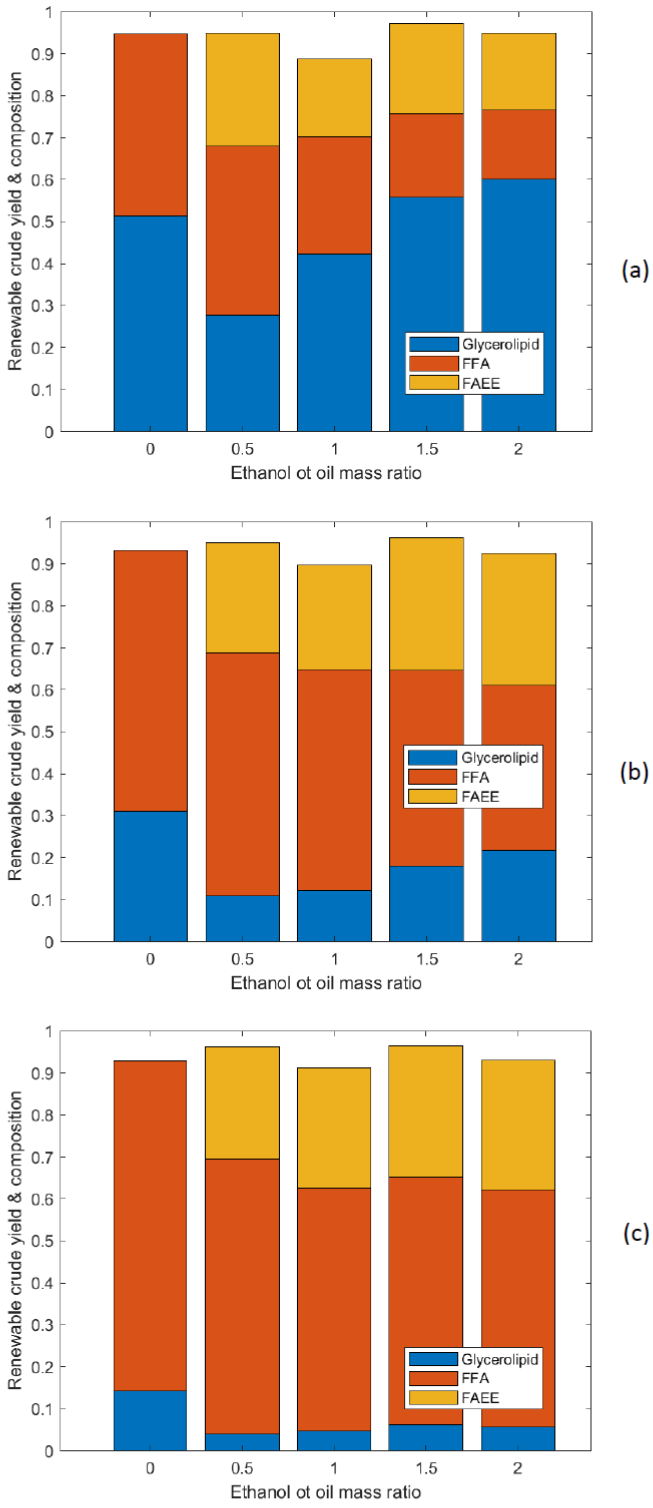

Fig S.3. Average renewable crude yield and composition over ethanol to lipid mass ratio at different residence times (a) 5 min, (b) 10 min, (c) 30 min.

4

Chapter 4

Elemental nitrogen balance, reaction kinetics and the effect of ethanol on the hydrothermal liquefaction of soy protein

Andres Chacon-Parra, David Lewis, Philip van Eyk

School of Chemical Engineering and Advanced Materials, The University of Adelaide, Adelaide, SA 5005, Australia

Chemical Engineering Journal, **425,** (2021) 130576.

Statement of Authorship

Title of Paper	Elemental nitrogen balance, reaction kinetics and the effect of ethanol on the hydrothermal liquefaction of soy protein
Publication Status	☑ Published ☐ Accepted for Publication ☐ Submitted for Publication ☐ Unpublished and Unsubmitted w ork w ritten in manuscript style
Publication Details	Chacón-Parra, A., D. Lewis, and P. van Eyk, Elemental nitrogen balance, reaction kinetics and the effect of ethanol on the hydrothermal liquefaction of soy protein. Chemical Engineering Journal, 2021. 425.

Principal Author

Name of Principal Author (Candidate)	Andres Danilo Chacon Parra
Contribution to the Paper	Design and execution of experiments and analysis. Design and optimisation of the reaction models Data interpretation Drafting of the manuscript
Overall percentage (%)	90%
Certification:	This paper reports on original research I conducted during the period of my Higher Degree by Research candidature and is not subject to any obligations or contractual agreements with a third party that would constrain its inclusion in this thesis. I am the primary author of this paper.
Signature	Date: 9/12/21

Co-Author Contributions

By signing the Statement of Authorship, each author certifies that:

i. the candidate's stated contribution to the publication is accurate (as detailed above);
ii. permission is granted for the candidate in include the publication in the thesis; and
iii. the sum of all co-author contributions is equal to 100% less the candidate's stated contribution.

Name of Co-Author	David Milton Lewis
Contribution to the Paper	Concept development Co-supervision Data interpretation
Signature	Date: 9/12/2021

Name of Co-Author	Philip Joseph van Eyk
Contribution to the Paper	Supervision Result interpretation Manuscript revision
Signature	Date: 9/12/2021

Please cut and paste additional co-auth

Chapter 4 - Elemental nitrogen balance, reaction kinetics and the effect of ethanol on the hydrothermal liquefaction of soy protein

Chemical Engineering Journal 425 (2021) 130576

Contents lists available at ScienceDirect

Chemical Engineering Journal

journal homepage: www.elsevier.com/locate/cej

Elemental nitrogen balance, reaction kinetics and the effect of ethanol on the hydrothermal liquefaction of soy protein

Andrés Chacón-Parra, David Lewis, Philip van Eyk *

School of Chemical Engineering and Advanced Materials, The University of Adelaide, Adelaide, SA 5005, Australia

ARTICLE INFO

Keywords:
Hydrothermal liquefaction
Soy protein
Reaction mechanism and kinetics
Elemental nitrogen balance
Nitrogen migration and transformation
post-HTL treatment

ABSTRACT

Hydrothermal liquefaction (HTL) is a thermochemical method to convert wet biomass and bio-waste into renewable crude and other valuable products. During HTL, water near critical point acts as a reaction medium and as a catalyst, breaking and hydrolysing bio-macromolecules into smaller compounds which interact and re-condense into different components and phases. Proteins as one of the key components in biomass plays a crucial role in the HTL process and products. Proteins are the source of nitrogen content in the HTL renewable crude, which generates environmental problems because of potential NOx emissions from combustion. Proteins also increases the pH of the aqueous phase, as over 60% of contained nitrogen is recovered in the aqueous phase as ammonia, nitrate, and soluble organic nitrogen compounds. However, the nitrogen reaction mechanism and equilibrium under HTL conditions have not been fully understood. In this study, the reaction kinetics for the product phases and nitrogen migration/transformation are elucidated by examining the yields and composition of the renewable crude and aqueous phases of HTL experiments run with a model compound soy protein, in a batch reactor at 250, 300 and 350 °C with 15% by mass feedstock. Furthermore, a co-solvent/homogeneous catalyst system has been included as a fully renewable solution to enhance the renewable crude yield, energy recovery, nitrogen content, and clarify the reaction mechanism and kinetic effects.

1. Introduction

Hydrothermal liquefaction (HTL) of biomass is a promising thermochemical method to process wet biomass and bio-waste. This versatile waste management method is of special interest because non-conventional biomass sources like sewage sludge, manure, and municipal wastes with high moisture and ash content could be treated without pre-drying [1,2]. HTL products heavily depend on feedstock type, composition, reaction temperature and residence time [1,3–5]. Proteins are an essential part of all biological organisms and represent a significant component of biomass and bio-wastes. Feedstocks rich in protein produce a renewable crude phase with high aromatic and nitrogen content, the aqueous phase with a high chemical oxygen demand (COD), ammonia (alkaline pH) and high organic nitrogen, plus malodours gaseous phase [2,6,7]. Despite some reaction pathways and kinetic models have been presented in the scientific literature, the understanding of the reaction mechanisms and equilibrium degrees of the product phases and the migration/transformation of nitrogen as a crucial element in proteins are highly fragmented and not fully elucidated [6].

Among various techniques available to analyse the renewable crude, elemental analysis (CHN/CHNS) is one of the most commonly used to determine differences in the elemental compositional of the renewable crude phase and by using Dulong formula approximation, the higher heating value (HHV), an indicator of the potential crude energy density [1,2,6,8–10]. HTL renewable crude from soy protein concentrate has shown a reduction in oxygen and nitrogen content with a slight increase in hydrogen, and HHV values close to double of the raw biomass [2,7,11]. Additionally, with reported crude oil yields of up to 30% and a substantial effect of temperature and residence time, energy recovery of up to 60% is conceivable [7,12]. Hydrogen donor solvents like ethanol have been tested to increase the crude yield. However, the effects on the heteroatom content have not been fully understood [1,13,14]. Nitrogen heteroatom in the renewable crude requires a more complete understanding as nitrogen content is considered the toughest challenge to the oil industry. HTL from rich-protein biomass may produce renewable crudes with up to 10% nitrogen content, while fuel–oil is considered between 0.1 and 1.5% [1,2,12,13].

* Corresponding author.
E-mail address: philip.vaneyk@adelaide.edu.au (P. van Eyk).

https://doi.org/10.1016/j.cej.2021.130576
Received 14 February 2021; Received in revised form 2 May 2021; Accepted 25 May 2021
Available online 30 May 2021

Chapter 4 - Elemental nitrogen balance, reaction kinetics and the effect of ethanol on the hydrothermal liquefaction of soy protein

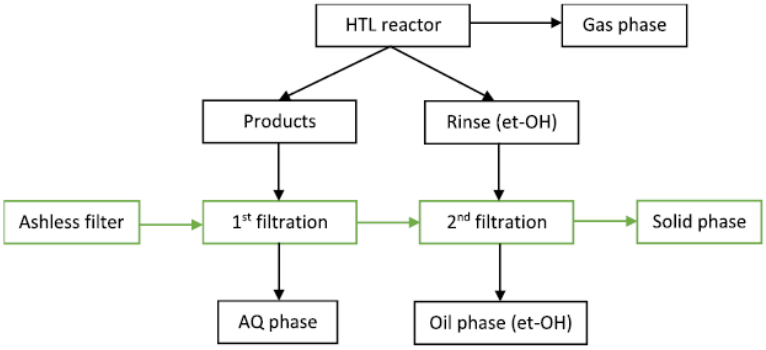

Fig. 1. Schematic separation procedure for HTL product phases.

Elucidating the nitrogen conversion in the aqueous phase (AQ) is essential to comprehend the migration and transformation reactions of nitrogen, to construct a reaction mechanism and kinetic model including the equilibrium degrees of nitrogen within the different phases of the HTL products [1,2,12]. The aqueous phase composition is also critical to define post-HTL challenges to treat and dispose the aqueous wastes. Some aqueous phase tests have been included in various studies, but the effects have not been completely explained [6,7,15]. Nitrogen in the aqueous phase could be classified as organic and inorganic nitrogen (ammonia, nitrate, and nitrite). The reactions and conversion of nitrogen under the HTL process could be integrated into an elemental nitrogen balance, counting all the HTL product phases and their equilibrium concentrations over a residence time distribution. However, the up-to-date reaction mechanism and kinetic models are oversimplified in terms of product phases without considering the fate of nitrogen (migration and transformation) and the equilibrium degrees [5,8,9,12].

In the present study, the reaction mechanism and kinetics for the hydrothermal conversion of a soy protein are investigated in a two-stage model. Initially, by fitting the experimental data to a mechanistic model defined for the phase yields and equilibrium. Follow by an elemental nitrogen balance and distribution model that clarifies the migration and transformation of nitrogen under HTL conditions. Furthermore, a renewable homogeneous catalyst and co-solvent system with ethanol and acetic acid is included to enhance crude yield and to reduce nitrogen in the renewable crude. The comparison between the non-catalytic and homogeneous catalytic experiments includes boiling point distribution, compositional differences in the crude phase, nitrogen in water tests, and energy recovery. The significance of the present study stands on the approach to understanding the elemental nitrogen migration and distribution, whilst propose a complete renewable co-solvent and homogeneous catalyst system to enhance the HTL renewable crude [5–7,12,13]. This study also addresses some of the knowledge gaps raised by L. Leng et al. (2020) [12].

2. Method

2.1. Materials and standards

A natural soy protein supplement (unflavoured) from Bulk Nutrients (Australia), composed by 89.4 +/-0.5% proteins and 13.9 +/- 0.1% Nitrogen content by mass according to the Australian National Measurement Institute analysis reports. Ethanol 100% (undenatured) and acetic acid glacial AR used a co-solvent and homogeneous catalyst, and nitrate/nitrite standards with 50, 100 and 150 mgN/L were all obtained from Chem-Supply (Australia).

2.2. Reactor and hydrothermal liquefaction experiments

A 15 ml batch reactor system (custom-built) made of Swagelok® 316 stainless steel tube, fittings and ferrules, equipped with a thermocouple and pressure transducer is fully described in a previous work, and a schematic diagram of the system is provided by *Obeid et al. (2019)* [5,16]. Soy protein powder was premixed with water to 15% (by dry mass) feedstock before adding it to the reactor tube. When ethanol (1:1 ethanol/biomass) and acetic acid were incorporated as co-solvents and homogeneous catalysts, the volumetric mass of water was reduced from 85% to 69.6% to include the two new components (15% ethanol and 0.4% acetic acid by mass). The reactor was filled to 50% of its volume capacity in all cases, purged and preloaded with nitrogen gas to a water saturation pressure under standard conditions [5,16].

Heating was accomplished with a Techne SBL-2D alumina sand fluidized bed system, equipped with a Techne TC-9D temperature and airflow controller. A heating time window to achieve 98% of the desired temperature was allowed, and the reaction was stopped in a two-step process, initially with compressed air until 100 °C and then by quenching the reactor in water. The residence time distribution is consistent with previous work with model lipids. The longest times were 90, 60 and 30 min respectively to 250 °C, 300 °C and 350 °C, and each experiment is duplicated [16].

2.3. Product recovery and separation

Gaseous phase yields were calculated by the weight difference of the nitrogen gas pre-charged, and the gases released after the reaction is completed [5,16]. Liquid and solid products were collected by pouring the reactor content into separation tubes, centrifuged at 3500 RPM for 10 min to separate solid, aqueous, and crude phases, then 100 µL of liquid phase (oil-free) samples were taken to be diluted 500 times in a 50 ml volumetric flask for aqueous tests. Additionally, 10 ml of ethanol were used to rinse the reactor and remove trapped products (oil and solids), to maximise product recovery and reduce deviations in the model as shown in Fig. 1 and described in previous work [16].

Product separation was completed in a two-step filtration process. Initially, the recovered product phase containing aqueous, solid and crude products was filtrated (first filtration) in a Buchner funnel using Whatman's Ashless Grade 42 filter papers, to recover the aqueous (oil-free) phase. Then the same filter paper (with retained crude and solids) was used to filter the reactor rinse (second filtration) as illustrated in Fig. 1. The rinse phase is composed of ethanol with crude and solids recovered from the reactor walls. It was vortexed and transferred to the product centrifuged tube and vortexed again to recover crude trapped to the tube wall by centrifugation. Then it was filtered to dissolve crude trapped in the paper and recover it all into an Erlenmeyer. The renewable crude was then dried in a sample concentrator Techne FSC400D

with a dri-block heater Techne DB200/3 set at 79 +/- 1 °C with high purity nitrogen gas flow for 8 to 12 h until constant weight to calculate crude yield. The filter paper (from the second filtration) with the solid phase was dry overnight at 105 °C to measure solid yield. The aqueous phase yield was calculated by the difference in phase yields, and the recovered aqueous sample was stored in the fridge. Despite the separation method presented differs from the scientific literature, it was aimed to maximise product recovery and separation of the different product phases with a fully water miscible and renewable solvent [5,7,12,17].

2.4. Product analysis

Elemental analysis (EA) of HTL renewable crude was carried out in a Perkin Elmer 2400 Series II CHNS/O Elemental Analyzer using CHN configuration. The analysis was conducted with approximately 4 mg of the sample (weighed to 6 d.p.) combusted at 925 °C. Results were calibrated to 4 mg of Perkin Elmer Organic Analytical Standard of Acetanilide (formula: C8H9NO) with known abundances of carbon (71.09%), hydrogen (6.71%), nitrogen (10.36%) by mass. The error range between standards was ± 0.05% for carbon, ±0.13% for hydrogen, and ± 0.12% for nitrogen; oxygen was calculated by difference, assuming sulphur is constant (0.88% from CHNS of raw soy protein) and other elements are negligible.

Boiling point distributions were measured via thermogravimetric analysis (TGA), performed in a Mettler Toledo TGA-DSC 2. The test method included an isothermal segment at 80 °C for 20 min to remove residual humidity, followed by a dynamic segment from 80 to 600 °C, with a 5 °C/min heating rate in nitrogen, then two isothermal segments at 600 °C for 20 min, one with nitrogen to remove all volatiles and finally with air to oxidize non-volatile matter. Boiling point fractions are simulated by the proportional weight loss within defined ranges of (80–180 °C), (180–250 °C), (250–300 °C), (300–350 °C), and (350–600 °C) [5,7,16,18].

The infrared (IR) spectroscopy of HTL renewable crude was conducted with a Nicolet 6700 FT-IR spectrophotometer (Thermo Fisher Scientific Inc.) Using a diamond Smart Orbit ATR (Attenuate Total Reflectance), equipped with a DTGS/KBr detector and a KBr Beamsplitter with IR source. Scanned 40 times with a resolution of 4 cm^{-1} in the range 4000–400 cm^{-1} in absorbance mode [19,20].

Total nitrogen in water via persulfate digestion was measured in a Shimadzu UV–vis 2700 using a total nitrogen HR (0 to 150 mg/L N) Hach kit (reference: Test N' Tube kit 2714100-AU) and the 10,072 TNT method for water and wastewater by Hach. Calibration was made with 4 points using Milli-Q water (blank) and the three nitrogen standards (50, 100 and 150mgN/L), digested in the dri-block heater at 105 +/- 1 °C for 30 min and measured at 430 nm (max absorbance) in PMMA micro cuvettes after acid digestion (reagent C) and cooling. Samples diluted 500 times were tested following the same procedure. Ammonia, nitrate, and nitrite were performed in a Lovibond MultiDirect photometer with Thermo fisher and Lovibond test kits. Ammonia HR (1 to 50 mg/L N) via salicylate method with Thermo ammonia HR test kit, following the Lovibond 66 test method with samples diluted 500 times. Nitrate (1 to 30 mg/L N) via chromotropic acid using vario NitraX test kit and Lovibond 265 method, and nitrite (0.01 to 0.5) via N-(1-naphthyl)-ethylenediamine with nitrite LR tablets (part 512310BT) using Lovibond 270 test method. The last two tests were done with the aqueous phase diluted 50% in water.

2.5. Kinetic modelling

Reaction kinetics were modelled with a set of first-order ordinary differential equations (ODE) system, solved in MATLAB using *ODE45* as described in previous work [16]. The reaction kinetic model has two levels, the first is to model the reaction mechanism of the product phases, which aims to predict the product yield and equilibrium degrees of protein HTL products. The second level should elucidate the elemental nitrogen distribution (migration) in the different phases and the nitrogenous transformations within the aqueous phase with a defined reaction mechanism.

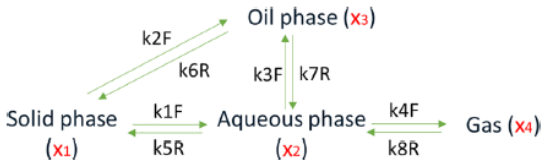

Fig. 2. Proposed reaction mechanism for the product phases of protein HTL.

The reaction constants (k) were obtained via multivariable optimisation using *lsqcurvefit* function by fitting the experimental concentration values (average) to the set of reaction constants at each temperature over the residence time frame by minimizing the squared norm of the residual function in a *k* range from 0 to 1 as described in previous work (the higher limit was increased to 10 when optimisation values were close to 1) [16]. The error bars of the experimental product yields plotted correspond to the standard deviation of the data at each point [21]. The activation energies and pre-exponential factors were calculated with the Arrhenius equation using *nlparci* function to compute the regression within 95% confidence intervals [5,16,21–23].

3. Results and discussion

3.1. Product phase reaction kinetics model

Soy protein is a fine powder, which in contact with water creates a highly viscous suspension difficult to integrate. Initial experiments with 20% by mass produced some low-density coke almost impossible to recover and separate. For this reason, the feedstock slurry had to be reduced to 15% by mass to obtain a homogeneous paste. Homogeneity of the biomass seems to be a critical condition to produce reproducible phase results [1,2]. Proteins are highly reactive under hydrothermal conditions and their decomposition forms large quantity of water-soluble compounds, and a renewable crude oil (thick and dark) [10]. After quick heating to 250 °C, water hydrolyses 60% of the protein and generates approximately 10% of ethanol-soluble renewable crude, which after drying appears to be a complete solid (tar) product. This zero-time point is of crucial importance for an ideally isothermal Arrhenius reaction kinetic model, even with a high heating rate of up to 125 °C/min, as hydrolysis appears to be instantaneous and takes place during heating [1,5,16].

The first-stage (product phase) reaction mechanism and kinetic model proposed in this study are not much different from previously reported models [5,7,8,17]. The initial feedstock is modelled as solid, which hydrolyse into aqueous and oily phases (partial breaking), as shown in Fig. 2. The reaction network aimed to synthesise the different phases of the hydrolysis and recondensation reactions of polypeptides, peptides, amino acids, and other intermediates. The difference of the present product phase model stands in the reaction loop with forward and reverse reactions which aimed to characterise the degrees of equilibrium in all phases at tested conditions [1,6,12,15]. Additionally, as zero residence time produced a low gas yields, the gaseous products are expected to be produced only from the aqueous phase where gas formation reactions are more probable [16,24].

The differential equations for the kinetics model from the reaction mechanism shown in Fig. 2 are:

$$\frac{dx_1}{dt} = -(k_{1F} + k_{2F})x_1 + k_{5R}x_2 + k_{6R}x_3 \quad (1)$$

$$\frac{dx_2}{dt} = k_{1F}x_1 + k_{7R}x_3 + k_{8R}x_4 - (k_{3F} + k_{4F} + k_{5R})x_2 \quad (2)$$

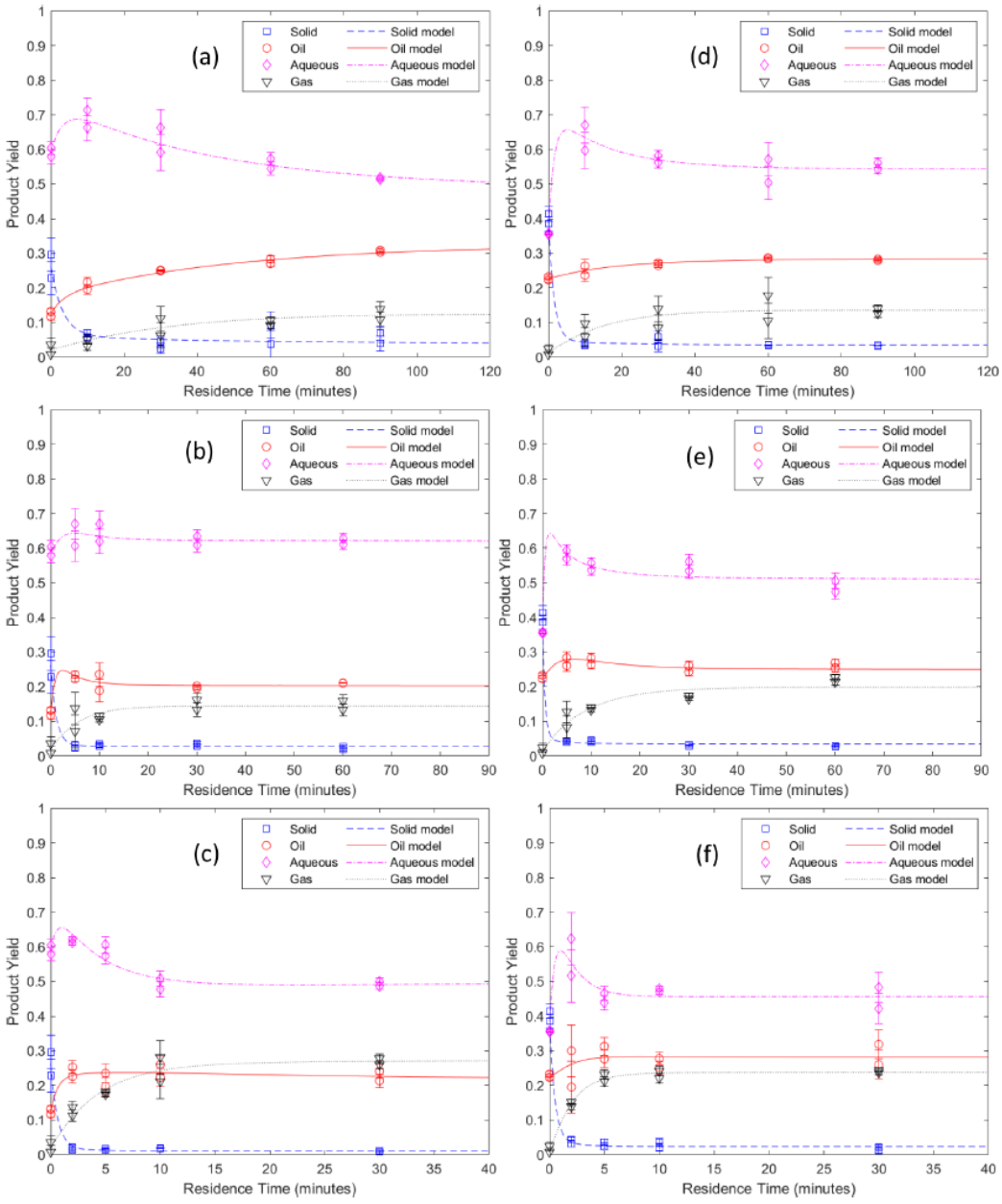

Fig. 3. Experimental and modelled phase (mass) yield values for the HTL of soy protein at (a) 250 °C, (b) 300 °C and (c) 350 °C without catalysts, (d) 250 °C, (e) 300 °C and (f) 350 °C with in-situ homogeneous catalysts.

$$\frac{dx_3}{dt} = k_{2F}x_1 + k_{3F}x_2 - (k_{6R} + k_{7R})x_3 \quad (3)$$

$$\frac{dx_4}{dt} = k_{4F}x_2 - k_{8R}x_4 \quad (4)$$

The present mechanistic and kinetic model predicts the experimental phase distribution with a relatively higher accuracy than previous studies, as shown in Fig. 3. The squared norm of the residual function value was on average 0.16% with a maximum value of 0.28% [21]. In all cases the aqueous phase showed to be an intermediate reagent, growing until complete hydrolysis of the solids, and decreasing to rise the crude and gas yields [1,12]. The solid phase helped to comprehend hydrolysis, while the balance between the renewable crude oil and aqueous phases, and further gaseous phase illustrate the effect of temperature and residence time and concentrations near equilibrium conditions [7].

Table 1
Kinetic parameters to fit the phase reaction model in Fig. 2.

Model	Reaction path	k	-ln(k) [min^{-1}]			lnA	EA [kJ/mol]	R^2
			250 °C	300 °C	350 °C			
Blank HTL	Solid to AQ	1F	2.58	0.55	0.43	11.4 ± 1.11	59.63 ± 5.8	0.831
	Solid to Crude oil	2F	1.53	1.26	0.10	7.07 ± 0.68	38.1 ± 3.66	0.851
	AQ to Crude oil	3F	18.31	2.25	30.86	−81.26 ± 18.4	−303.92 ± 68.8	0.153
	AQ to Gas	4F	5.29	3.26	2.48	12.58 ± 1.14	77.08 ± 6.98	0.959
	AQ to Solid	5R	8.23	9.13	9.24	−14.76 ± 1.4	−27.94 ± 2.66	0.868
	Crude oil to Solid	6R	3.73	3.25	3.35	−1.15 ± 0.13	10.85 ± 1.22	0.626
	Crude oil to AQ	7R	4.72	0.91	3.39	5.60 ± 1.28	40.81 ± 9.29	0.152
	Gas to AQ	8R	3.90	1.79	1.88	9.33 ± 0.95	56.19 ± 5.72	0.760
In-situ Catalysts	Solid to AQ	1F	4.92	3.19	2.88	8.16 ± 0.63	56.08 ± 5.26	0.894
	Solid to Crude oil	2F	0.49	−0.59	−0.83	7.95 ± 0.7	36.26 ± 3.18	0.913
	AQ to Crude oil	3F	4.51	2.18	2.51	8.78 ± 1.05	59.19 ± 6.38	0.677
	AQ to Gas	4F	4.36	3.37	1.76	11.54 ± 0.76	69.74 ± 6.31	0.966
	AQ to Solid	5R	31.34	9.00	28.50	0.15 ± 7.02	109.5 ± 58.4	0.003
	Crude oil to Solid	6R	3.19	2.09	2.05	4.23 ± 0.37	31.67 ± 3.1	0.818
	Crude oil to AQ	7R	3.82	1.44	1.99	8.50 ± 0.72	51.78 ± 5.98	0.589
	Gas to AQ	8R	2.98	2.42	1.11	8.32 ± 0.96	49.78 ± 4.59	0.925

Co-solvent and homogeneous catalyst system seem to promote the partial breaking of the protein, generating higher and more stable crude yields from zero-residence time. The ethanol under the hydrothermal reaction conditions might prevent the H_3O^+ hydrolysis of nitrogen heteroatom from subcritical water ions into the aqueous phase [1,4]. The effect of ethanol as a co-solvent, hydrogen donor and homogeneous catalysts has been limited to the increase in the renewable crude yield while reduce the solid yield. However, the reaction mechanism, kinetics and equilibrium are fragmented and limited to solvent extraction prior GC–MS characterisation [12–14].

The renewable crude yield had an average of 25.2% with a range between 18.8 and 31.9%, without counting zero residence time. Renewable crude yields obtained are in good agreement with *Luo et al. (2016)* despite the differences in method [7]. However, the reaction kinetics seems to be much faster in the present study, as the product phase yield values near-equilibrium were reached much faster even at 250 °C (the lowest temperature). Additionally, gaseous yields were higher with an average of 15% and a range between 3.2 and 28.1%, compared to a maximum of approximately 20% reached at 350 °C for 60 min by *Luo et al. (2016)* [7].

When the co-solvent and homogeneous catalysts were incorporated, the zero-time crude yield increased from 12 to 22% on average. This may suggest that ethanol promotes the partial fractionating of polypeptides into mid-molecular weight oily compounds rather than directly into water soluble mixtures [6,7]. Sub and supercritical ethanol alcoholysis with ethanol produce secondary and ternary amines, and amides because of alcohols alkylation and etherification ability [13,14]. Additionally, the renewable crude yields near-equilibrium were higher than their respective blank HTL at 300 and 350 °C. For the case of non-catalytic HTL, A reaction temperature of 250 °C produced the highest crude yield. However, the transformations (quality and composition) of these low temperature experiments were small in terms of low volatile fractions, elemental composition and energy density as discussed in section 3.2.

The kinetic parameters presented in Table.1 are difficult to contrast and compare with previously reported studies as the values heavily depend on the kinetic approach defined in Fig. 2. The optimisation at each temperature was completely autonomous (Matlab *lsqcurvefit* function), and the coefficient of determination (R^2) despite being calculated using *nlparci* function, were independent of the kinetic constants *k* optimisation [21–23]. For the non-catalytic HTL the activation energies for the hydrolysis into aqueous (1F), crude phase (2F) and the gaseous phase formation (4F) were 59.6 ± 5.8, 38.1 ± 3.7 and 77.1 ± 7.0 kJ/mol, with relatively high R^2 values. These activation energies were reduced between 5 and 10% when ethanol and acetic acid were integrated as co-solvent and homogeneous catalysts, which may be an indicator of the positive effect of the in-situ catalysts in the system, plus slightly higher R^2 values [22].

The activation energy and pre-exponential values of 58.6 kJ/mol and 10.37, reported by *Luo et al. (2016)* for the renewable crude formation from the aqueous phase are in relative agreement with the kinetic values reported for the hydrolysis into the aqueous and oily phases, despite the differences in the reaction mechanism [7]. The reactions which showed R^2 values lower than 0.6, presented reaction constants *k* at 300 °C relatively out of trend, possibly because the multivariable optimisation is a purely mathematical solution by minimising the square norm of the residual function with a relatively wide range for *k* (0 to 1) [21,23]. The addition of more intermediate temperature values could produce more reliable Arrhenius parameters.

3.2. Boiling point distribution, elemental composition, and FT-IR.

Boiling point fractions compute the potential boiling point distribution and may be condensed in three key ranges, low boiling point fraction (80 to 300 °C), high boiling point (300 to 600 °C), and the non-volatile fraction (oxidation/combustion) at 600 °C, of the renewable crude [18]. These three segments serve as an indicator of the breaking/fractionation by the reduction in boiling point, and the effect of temperature and residence time. Additionally, the low temperature fraction may include the potential volatile fractions in the fuel–oil range, as illustrated in Fig. 4 (a). Most of the changes in the volatile matter fractions happened in the initial 5 to 10 min [5,7,16]. Additionally, in the high boiling fraction, temperature (above 300 °C) may produce pyrolysis and decomposition rather than merely volatilisation [18]. The complete boiling point distributions of all renewable crude experiments are provided in Supplementary Material Fig. S1.

The 180–250 °C fraction is increased with temperature, while the 300–350 °C fraction is reduced for the non-catalytic HTL. When the homogeneous catalysts were included, the 80–180 °C fraction increased by dropping the 350–600 °C fraction, until reaching values close to the 180–250 °C fraction. These results may suggest a more complete fractionation increasing the portion of 180–250 °C fraction with temperature, and 80–180 °C fraction with the homogeneous catalysts and temperature. This was an expected and desired effect for the HTL conversion, despite the controversy of TGA as an analytical method to measure the conversion of HTL products, without a characterisation [7,16,18].

Correspondingly, elemental analysis (CHN) of the renewable crude showed an increase in carbon and hydrogen content, while nitrogen and oxygen decreased over residence times as illustrated in Fig. 5. The temperature also showed to have a significant effect in the elemental composition of the renewable crude produced [6–8,12]. However, the

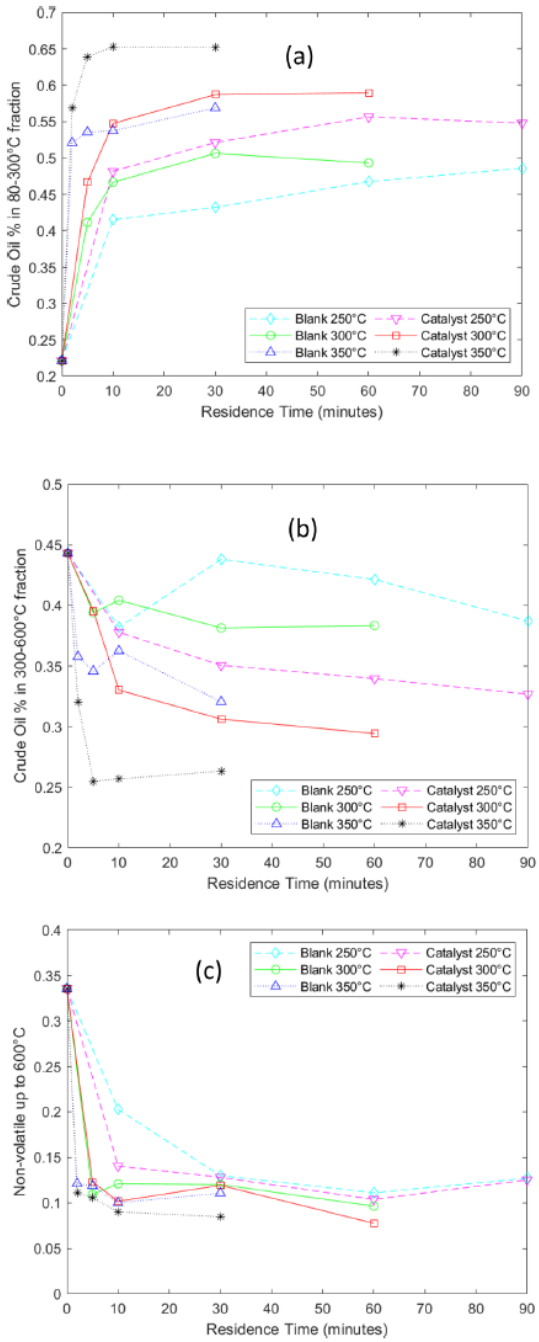

Fig. 4. Renewable crude mass fractions in the boiling point ranges of 80–300 °C (a), 300–600 °C (b) and the non-volatiles at 600 °C (c).

oxygen content with the co-solvent and homogeneous catalyst system showed to be relatively higher than the non-catalytic counter-part, reducing the carbon content, another observation which supports the alkylation/etherification effect of ethanol during the HTL of proteins. Hydrogen and nitrogen content seem not to be significantly affected by the co-solvent/catalyst system [13].

Non-catalytic HTL generates renewable crude with higher carbon and relatively lower oxygen, which generated a higher HHV (Dulong formula), as illustrated in Fig. 6 (a). When the homogeneous catalysts were used, the ethanol produced higher oxygen content in the renewable crude, reducing the relative carbon content and lowering HHV by the way, which may be linked to the formation of amides. However, as the renewable crude yields are relatively higher, the energy recovery values (Theoretical HHV times the average crude yield) were higher with the in-situ catalyst. Therefore, a higher proportion of low boiling point factions (80–180 °C), coupled with higher energy recovery, could be in fact more important than just HHV.

Elemental composition and HHV values obtained were in good agreement with *Luo et al. (2016)* [7]. For instance, The CHN composition obtained for plain HTL at 350 °C and 30 min values were 73.7, 9.9 and 9.4 respectively, compared to 73.7, 9.67 and 6.35 obtained at 350 °C for 90 min by *Luo et al. (2016)*, despite the differences in raw materials, system, and method. Additionally, as the sulphur content has been reported relatively low and unchanged during the HTL in the scientific literature [7,8,12,25]. A sulphur content of 0.88% was measured from the raw soy protein (CHNS) and defined as constant in the present study. The highest HHV value obtained was almost 38 MJ/kg compared to 37 MJ/kg obtained by *Luo et al. (2016)*. However, the energy recovery values are not equivalent because in this study the maximum renewable crude yield was not obtained at the maximum HHV, as illustrated in Fig. 3. The temperature had a negative effect in near equilibrium crude yields, leaving the maximum energy recovery of non-catalytic experiments to 40% [7,12]. Van Krevelen diagrams with H/C and O/C ratios are available in the Supplementary Material Fig. S2.

FT-IR provide a general overview of the functional groups present in the renewable crude. The groups present in all samples include amides (I and II), amines and imides, which are in the range 1550 to 1700 cm^{-1} are presented in Supplementary Material Fig. S3 [19]. The peak in the region 1630 to 1680 cm^{-1} is common to the stretching of the carbonyl bond (C = O) present in the amide (I), which is particularly higher in in-situ catalyst (co-solvent) product oils. However, severe conditions might convert them into heterocyclic compound such as pyridines, which also have C = O stretching in the region 1630 to 1690 cm^{-1}, making it extremely difficult and subjective to characterise in a mixture without prior separation [19].

3.3. Aqueous phase tests and transformations of nitrogen.

The characterisation and quantification of nitrogen species in water has been used for decades in the treatment of wastewater. Nitrogen is an environmental pollutant which can harm aquatic ecosystems (plants and animal life). For this reason, nitrogen composition in the aqueous phase is an important parameter to control, and the post-HTL water needs to be integrated with wastewater effluents for biological nutrient removal (BNR) prior to discharge into bodies of water. However, the concentration of various nitrogen species might have a negative impact on the kinetic growth of the bacteria which undertake the biological treatment. For instance, if ammonia concentration overweights the total organic carbon (TOC), the wastewater would be difficult to treat biologically. Therefore, understanding the nitrogen balance of the aqueous waste is crucial for aqueous waste treatment [1,26–28]. The organic nitrogen is quite complex as it includes all sources of water-soluble nitrogen linked to carbon atoms like amino acid, amides, amides, imides and more, which are difficult to separate and even more to analyse in mixtures [6,15]. Inorganic nitrogen is readily analysed with colorimetric test kits and it comprises mostly ammonia (NH_3/NH_4^+) and nitrogen oxide ions (NO_x^-), mainly nitrate (NO_3^-) and nitrite (NO_2^-), commercially available [26].

Accounting for the aqueous phase in hydrothermal processing is quite complex as water is a reagent and sub-product of the hydrolysis

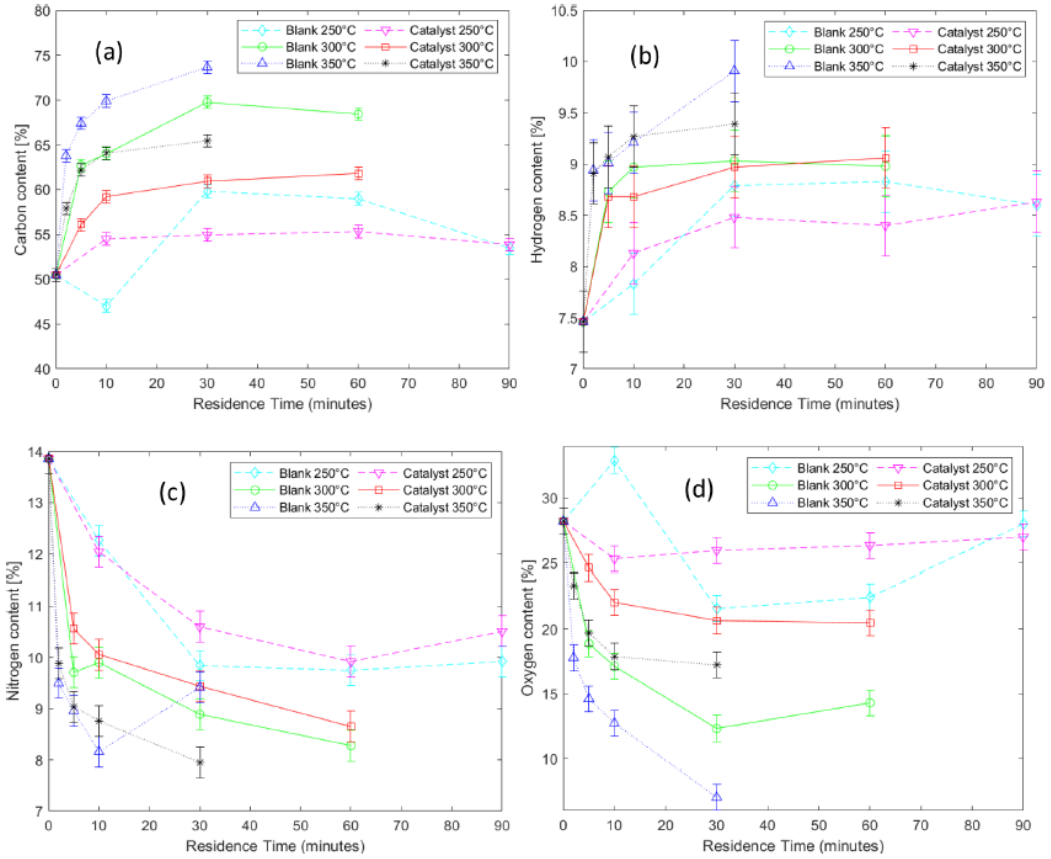

Fig. 5. Elemental composition (CHN) of the HTL renewable crude, (a) carbon, (b) hydrogen, (c) nitrogen (d) oxygen.

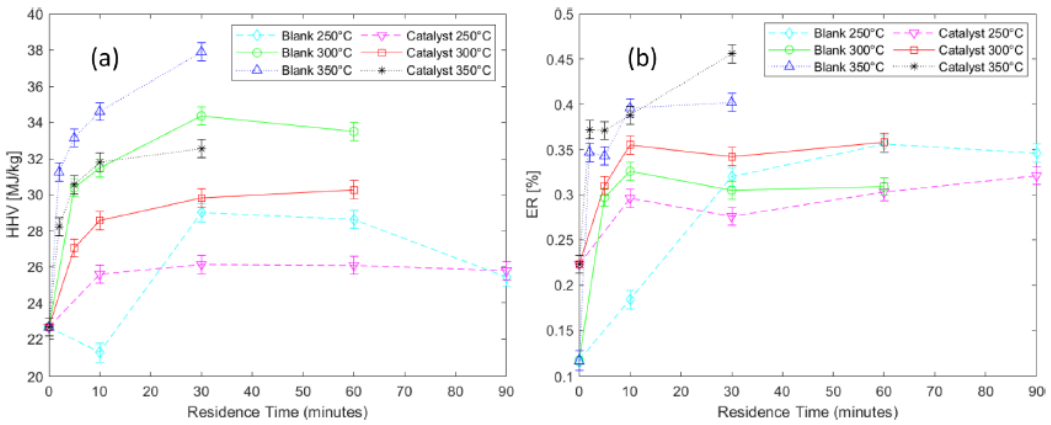

Fig. 6. Renewable crude oil HHV-Dulong (a) and energy recovery (b).

and decomposition of biomass [1,4]. Additionally, water might easily evaporate or stay as residual humidity during separation steps (extraction and filtration) and drying. For these reasons, the aqueous phase yields must be measured by difference. However,100 µL aqueous samples were taken and diluted 500 times, immediately after product collection and centrifugation to reduce possible interference from changes in the aqueous phase. Nitrate and nitrite tests were measured with the recovered aqueous phase after separation, diluted 50% in water to produce a reading value in test ranges. The concentration values of these two nitrogen oxide ions were extremely low in contrast to total

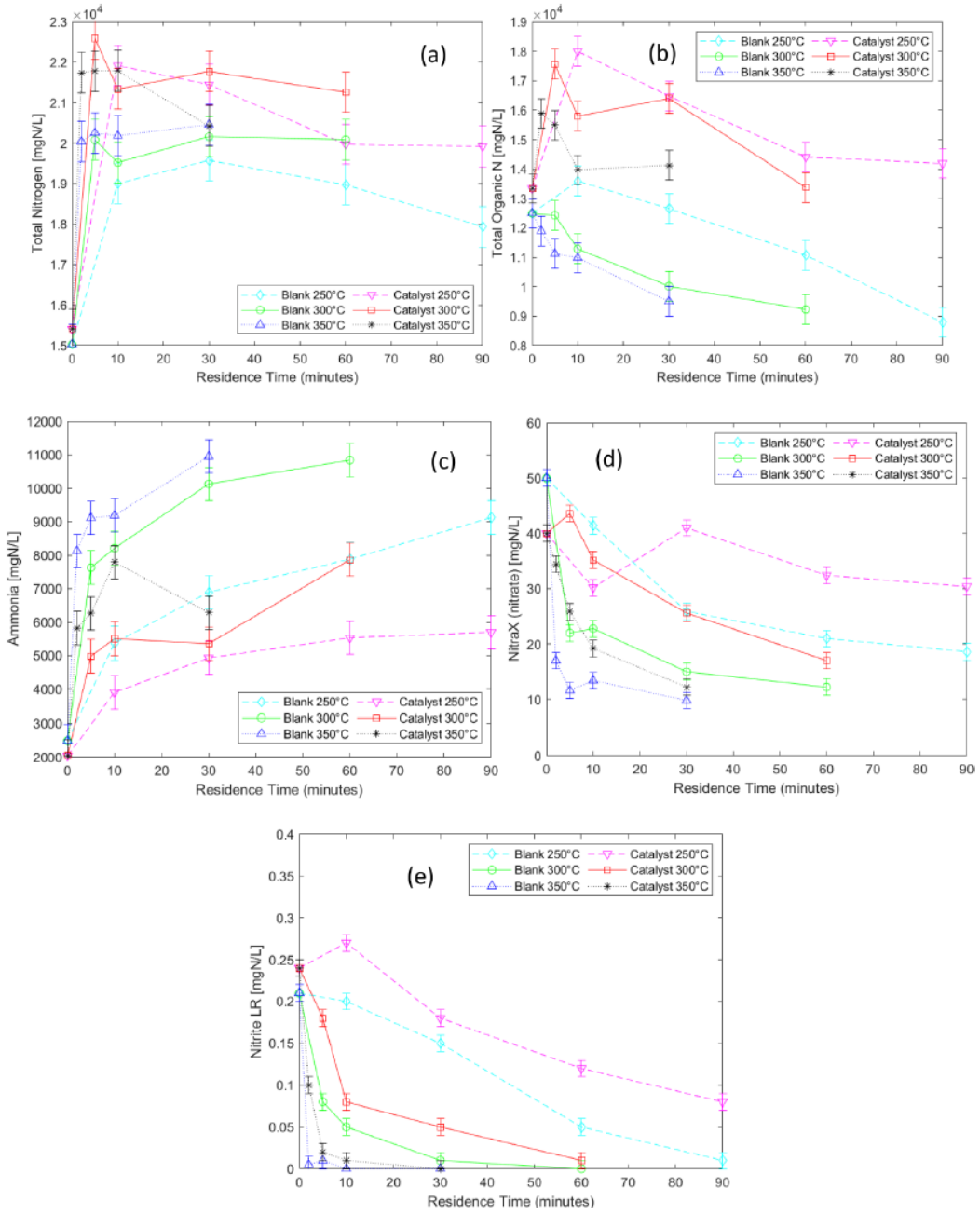

Fig. 7. Nitrogen in water tests (a) Total Nitrogen, (b) Organic Nitrogen by difference, (c) Ammonia, (d) Nitrate, and (e) Nitrite.

nitrogen and ammonia.

Results of the nitrogen concentration in water (shown in Fig. 7) are in agreement with the results presented by *Jena et al. (2011)* in which the total nitrogen and ammonia reported values were 16,200 and 12,700 mgN/L, despite the differences in feedstock and procedure [15,29]. The total nitrogen reached the highest value in the initial 5 to 10 min, in agreement with hydrolysis. Then the organic nitrogen balances with ammonia (ammonification) to the near-equilibrium concentration, with a significant effect of the temperature. Ammonia became the highest proportion of nitrogen in the aqueous phase of non-catalytic experiments at 300 °C and 350 °C. The in-situ co-solvent and homogeneous catalyst system showed a slightly higher total nitrogen despite the lower hydrolysis rate and higher crude yields, while ammonia showed to be lower in all cases compared to the corresponding plane HTL results

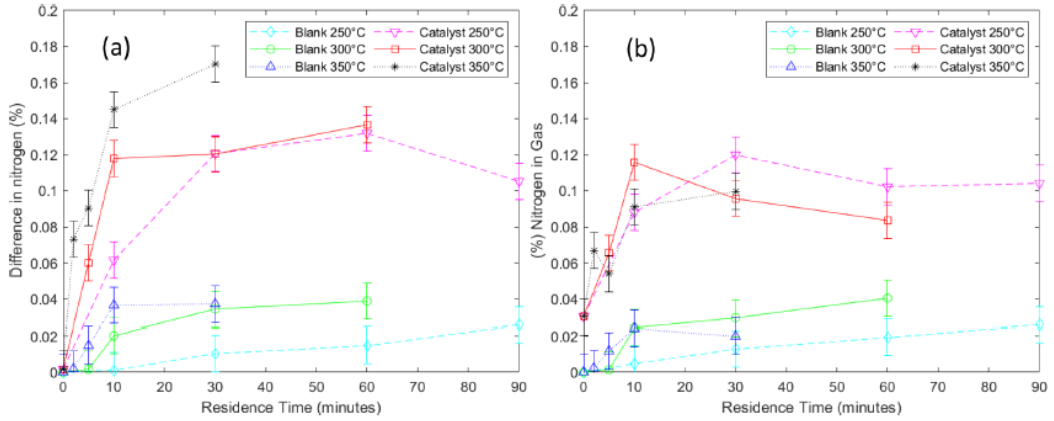

Fig. 8. Nitrogen difference/balance (a) and mass fraction of N in the gas phase.

[15,26,28–30]. The nitrate and nitrite concentrations presented a negligible fraction in the aqueous phase and showed a decreasing pattern, possibly because of the severity of the conditions and a lack of free oxygen for nitrification [28].

The homogeneous catalyst and co-solvent system produced a relatively higher total nitrogen and lower ammonia concentrations, this may be associated with lower hydrogen donor effect of subcritical water in conjunction with the synergetic effect of ethanol as an alkylation and etherification reagent [13,31]. The effect of a hydrogen donator and acceptor ought to remove heteroatoms by hydrogen donation/substitution. However, ethanol to biomass ratio of 1:1 by mass formed amides and amines producing higher renewable crude yields, which with similar nitrogen content produced higher nitrogen retention in the renewable crude phase (lower nitrogen removal). Likewise, this effect could indicate that the alkylation effect of alcohols might generate a unique structure (not characterised) which may be counted in the total nitrogen test [30].

The nitrite test works as a qualitative indicator. The colorimetric test method used due to the extremely low concentrations is not especially appropriate (it goes from light yellow to pale purple). The aqueous phase presented a light yellow colour which, after being subtracted as zero reading, presented a minor change in colour with the nitrile reagent, affecting the reliability of the test. Additionally, some nitrite tests presented readings under-range. Furthermore, the solid phase yields at equilibrium conditions were in the range 3 to 4% (Fig. 3), with approximately 8% nitrogen content according to a total nitrogen persulfate digestion undertaken with a mix of the solid sample recovered. This value is defined as the tentative nitrogen content for the solid phase which is of crucial importance to complete the nitrogen balance in section 3.4.

3.4. Nitrogen balance, migration and transformation of N.

Before defining the nitrogen distribution model, the elemental nitrogen balances suggested that there was a missing portion of nitrogen, which by difference should be considered and modelled in the gas phase, as illustrated in Fig. 8. The nitrogen in the gas phase is extremely difficult to analyse and characterise as the system is pre-charged with nitrogen gas (N_2) as an inert pre-pressure gas to keep the pressure over water saturation pressure [1,3,4]. The nitrogen gas concentrations for the non-catalytic experiments were between 0 and 4% and increased with the homogeneous catalyst/co-solvent system, starting from 3% at zero-time to a maximum value of approximately 12% by mass. Despite these values being calculated by difference (balances) and may summarise the error of the product phase recovered, and nitrogen analysis done, the trends and changes are clear. The homogeneous catalyst system seems to promote the migration/transformation of nitrogen into a gaseous form [30].

From observations made in this investigation with the elemental nitrogen balance, the organic and inorganic nitrogen in the aqueous phase, elemental nitrogen in the crude phase and the potential nitrogen in the solid, A reaction mechanism for the migration and transformation of nitrogen under HTL is proposed as follows in Fig. 9.

The differential equations for the nitrogen balance mechanism model

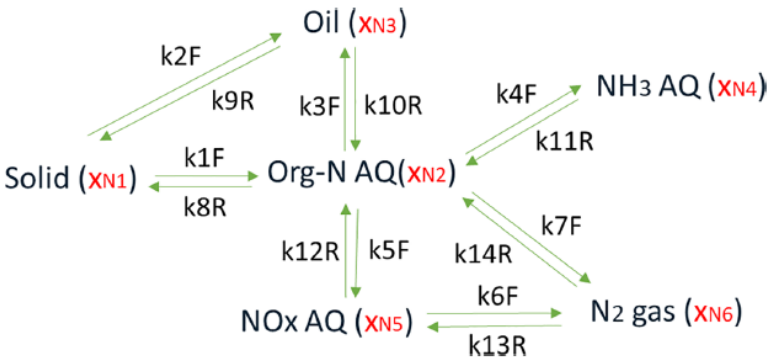

Fig. 9. Nitrogen migration and transformation reaction mechanism for protein HTL.

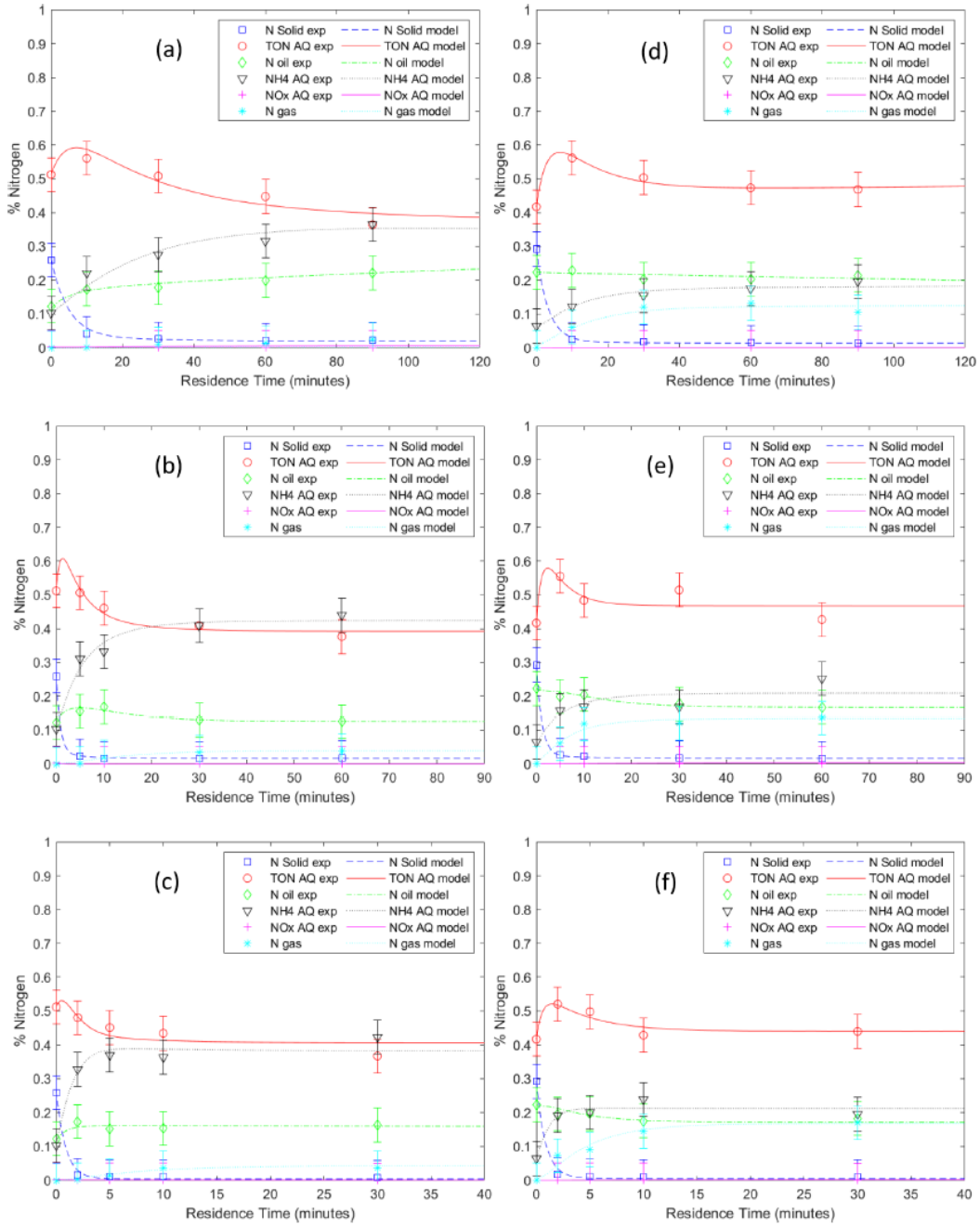

Fig. 10. Experimental and modelled nitrogen balance and distribution in different phases and forms. (a) 250, (b) 300 and (c) 350 without catalysts, (d) 250, (e) 300 and (f) 350 with catalysts.

Table 2
Kinetic parameters to fit the Nitrogen distribution reaction model in Fig. 9.

path	Elemental NdistributionReaction	Non-catalytic HTL -ln(k) [min^{-1}]			In-situ homogeneous catalyst -ln(k) [min^{-1}]		
		250 °C	300 °C	350 °C	250 °C	300 °C	350 °C
1	Solid-N to AQ-N	1.77	0.55	0.19	1.17	1.18	−0.46
2	Solid-N to Crude oil-N	3.19	2.25	1.73	13.40	2.96	17.94
3	AQ-N to Crude oil-N	10.08	3.29	5.55	5.02	2.96	1.04
4	Org-N AQ to NH3	3.94	2.34	1.00	4.32	3.14	1.36
5	Org-N AQ to NOx	3.55	22.70	8.84	5.21	9.74	27.18
6	NOx to N2 gas	2.98	2.54	2.75	0.01	3.69	−1.63
7	Org-N AQ to N2 gas	5.41	5.66	4.84	4.23	3.42	2.86
8	AQ-N to Solid-N	4.66	8.71	8.98	4.77	7.30	3.40
9	crude oil-N to Solid-N	6.44	2.53	4.32	6.02	4.20	13.54
10	Crude oil-N to AQ-N	11.52	3.00	9.21	4.27	2.01	0.10
11	NH3 to Org-N AQ	3.83	2.41	0.95	3.43	2.38	0.60
12	NOx to Org-N AQ	−1.14	3.09	7.78	0.01	8.91	18.50
13	N2 gas to NOx	0.82	6.42	7.98	10.42	6.37	3.12
14	N2 gas to Org-N AQ	9.17	3.58	2.73	2.68	2.18	1.93
	Optimisation Res-norm	0.55%	0.35%	0.70%	0.15%	1.12%	0.32%

are (where xN is N fraction):

$$\frac{dx_{N1}}{dt} = -(k_{1F}+k_{2F})x_{N1} + k_{8R}x_{N2} + k_{9R}x_{N3} \quad (5)$$

$$\frac{dx_{N2}}{dt} = k_{1F}x_{N1} + k_{10R}x_{N3} + k_{11R}x_{N4} + k_{12R}x_{N5} + k_{14R}x_{N6} - (k_{3F}+k_{4F}+k_{5F}+k_{7F}+k_{8R})x_{N2} \quad (6)$$

$$\frac{dx_{N3}}{dt} = k_{2F}x_{N1} + k_{3F}x_{N2} - (k_{9R}+k_{10R})x_{N3} \quad (7)$$

$$\frac{dx_{N4}}{dt} = k_{4F}x_{N2} - k_{11R}x_{N4} \quad (8)$$

$$\frac{dx_{N5}}{dt} = k_{5F}x_{N2} + k_{13R}x_{N6} - (k_{12R}+k_{6F})x_{N5} \quad (9)$$

$$\frac{dx_{N6}}{dt} = k_{7F}x_{N2} + k_{6F}x_{N5} - (k_{13R}+k_{14R})x_{N6} \quad (10)$$

The presented model aimed to incorporate the distribution, transformation, and equilibrium of various nitrogen phases and species in an HTL system. Most of the nitrogen transformation happened within the aqueous phase, as in this phase the nitrogen is mostly recovered [1]. However, the functional structure of the nitrogen bonds changed because of the severity of the conditions [6,7]. The reaction happening in the aqueous phase includes ammonification (the hydrolysis of nitrogen from organic nitrogen to ammonia) and denitrification (from nitrogen oxide ions to nitrogen gas). Additionally, there seems to be a direct transformation of ammonia to nitrogen gas, which is known as anammox (anaerobic ammonium oxidation), this usually happens in a low to non-oxygen environment and produces nitrogen gas (N_2O and N_2) from the bacterial oxidation of ammonia [26,28]. However, this reaction may be limited to the ammonia produced in the plane HTL experiments, not the in-situ co-solvent and homogeneous catalyst as the ammonia concentration is lower coupled with higher nitrogen gas formation.

Including ethanol and acetic acid limit the ammonia conversion from the organic nitrogen, whilst increasing the total nitrogen in water and promoting nitrogen content in the gas phase (as illustrated in Fig. 10). This observation suggested that instead of promoting the ammonification and probably ammonia oxidation reaction, the co-solvent and homogeneous catalysts system produced an intermediate which later reacts to produce nitrogen in gas form. This hypothesis could be supported by the synthesis made by *Soler-Jofra et al. (2020)* for hydroxylamine as an intermediate of the bacterial anaerobic ammonia oxidation (Anammox) [30]. However, in this case, temperature and homogeneous co-solvents produced the substitution and oxidation reactions (from the alkylation ability of ethanol). The lack of free oxygen creates completely unique conditions in the reaction network of nitrogen under HTL conditions with sub and supercritical ethanol as co-solvent and catalyst [7,26,30].

Derivatives of hydroxylamine as an intermediate could be formed from breaking and substitution reactions of organic nitrogen with ethanol, limiting the release of ammonia [30]. The hydroxylamine should be included in the total nitrogen (TN) measurement and counted as organic nitrogen despite it is not (It does not contain carbon atoms), depending on the hydroxyl hydrogen substitutes. Furthermore, hydroxylamine generates NO_2 and NO_3 ions, which then produce N_2O and N_2 via the denitrification reaction. However, these ideas could not be verified. Nitrate and nitrite shown a clear decreasing profile, which may indicate these may not be the only intermediates for nitrogen gas formation during HTL, whilst nitrite concentration was as low that it was not included in the model. Likewise, the detection and quantification of hydroxylamine is currently considered an analytical bottleneck [12,30].

The reaction kinetics parameters to fit the elemental nitrogen balance model in Fig. 9 are presented in Table 2. These values follow similar patterns to the product phase mechanism model and integrate some of the nitrogen transformations happening in the aqueous phase. But in this case the optimisation is a bit more complex because of an increase in the number of equation and variables, coupled with the subjectivity and limitations of the suggested model. However, the squared norm of the residual function values were still relatively low [21,23]. The activation energy for the hydrolysis of nitrogen from the solid to the aqueous and crude phases were 46.2 ± 3.9 and 38.8 ± 3.6 kJ/mol respectively, while the ammonification reaction (plane HTL) had an activation energy of 79.5 ± 7.1 kJ/mol. The homogeneous catalyst and co-solvent system produced an activation energy of 37.2 ± 3.3 kJ/mol for the transformation of nitrogen from the organic nitrogen in the aqueous phase to the gas phase and 107.7 ± 9.6 kJ/mol for the migration of nitrogen from the aqueous phase to the crude phase.

The reaction constants k of the N fate model are difficult to contrast and discuss because of the lack of specific scientific literature, and because they heavily depend on the loop reaction mechanism defined in Fig. 9 [22]. The reverse reaction pathways of the proposed mechanism define the degrees of equilibrium and help to fit the data from reaction experiments into the Arrhenius model. These reverse reaction k values may not have individual significance, apart from limiting and fitting the model. However, the dynamic equilibrium constant (K_{eq}), which may be calculated by the ratio $k_{forward}/k_{reverse}$ may indicate the thermodynamic equilibrium of the species near equilibrium concentration [32]. The N fate model integrates the product phase and elemental nitrogen composition with the reactions happening in the aqueous phase and

equilibrium degrees, as a last and summary step of the nitrogenous transformations of proteins under HTL.

4. Conclusion

The HTL conversion of a model compound protein has been investigated to propose a more complete reaction mechanism and kinetic model for the product phases, then product yield phases were coupled with an elemental nitrogen balance to produce a fate of nitrogen (migration and transformation) reaction mechanism and kinetic models. The information presented in this study could be useful to understand the conversion of nitrogen as a key element in protein biomass, nitrogen content in the renewable crude is an environmental threat for refining and combustion, while clarifying the transformation of nitrogen in the aqueous phase not only helped to comprehend the nitrogenous transformations. They also help to identify the post-HTL treatment required for the aqueous waste before being integrated with wastewater effluents. Additionally, a co-solvent and homogeneous catalyst system has been incorporated and tested to increase renewable crude yield and quality. The comparison includes boiling point distribution, elemental analysis, and energy recovery. However, the specific composition and functionalities of the nitrogen species in the renewable crude and the organic nitrogen in the aqueous remain relatively unknown and should be further investigated, despite the difficulties that organic-nitrogen heteroatoms generate to most analytical techniques available.

Declaration of Competing Interest

The authors declare that they have no known competing financial interests or personal relationships that could have appeared to influence the work reported in this paper.

Acknowledgments

The authors acknowledge the financial support of the Australian Research Council's Linkage Project grant (LP150101241).

Appendix A. Supplementary data

Supplementary data to this article can be found online at https://doi.org/10.1016/j.cej.2021.130576.

References

[1] P. Biller, A.B. Ross, et al., in: *17 - Production of biofuels via hydrothermal conversion*, in *Handbook of Biofuels Production (Second Edition)*, Woodhead Publishing, 2016, pp. 509–547.
[2] Y. Zhang, W.T. Chen, in: *5 - Hydrothermal liquefaction of protein-containing feedstocks*, in *Direct Thermochemical Liquefaction for Energy Applications*, Woodhead Publishing, 2018, pp. 127–168.
[3] A. Kruse, E. Dinjus, Hot compressed water as reaction medium and reactant, The Journal of Supercritical Fluids 39 (3) (2007) 362–380.
[4] A.A. Peterson, F. Vogel, R.P. Lachance, M. Fröling, M.J. Antal, Jr., J.W. Tester, Thermochemical biofuel production in hydrothermal media: A review of sub- and supercritical water technologies, Energy Environ. Sci. 1 (1) (2008) 32.
[5] R. Obeid, D. Lewis, N. Smith, P. van Eyk, The elucidation of reaction kinetics for hydrothermal liquefaction of model macromolecules, Chem. Eng. J. 370 (2019) 637–645.
[6] J. Lu, H. Li, Y. Zhang, Z. Liu, Nitrogen Migration and Transformation during Hydrothermal Liquefaction of Livestock Manures, ACS Sustainable Chem. Eng. 6 (10) (2018) 13570–13578.
[7] L. Luo, J.D. Sheehan, L. Dai, P.E. Savage, Products and Kinetics for Isothermal Hydrothermal Liquefaction of Soy Protein Concentrate, ACS Sustainable Chem. Eng. 4 (5) (2016) 2725–2733.
[8] J.D. Sheehan, P.E. Savage, Products, Pathways, and Kinetics for the Fast Hydrothermal Liquefaction of Soy Protein Isolate, ACS Sustainable Chem. Eng. 4 (12) (2016) 6931–6939.
[9] C. Jazrawi, P. Biller, Y. He, A. Montoya, A.B. Ross, T. Maschmeyer, B.S. Haynes, Two-stage hydrothermal liquefaction of a high-protein microalga, Algal Research 8 (2015) 15–22.
[10] Chen, W.-T., Hydrothermal liquefaction of protein-containing feedstocks. 2017.
[11] Zhang, Y., et al., Mild Hydrothermal Liquefaction of High Water Content Agricultural Residue for Bio-Crude Oil Production: A Parametric Study. Energies, 2018. 11(11).
[12] L. Leng, W. Zhang, H. Peng, H. Li, S. Jiang, H. Huang, Nitrogen in bio-oil produced from hydrothermal liquefaction of biomass: A review, Chem. Eng. J. 401 (2020) 126030.
[13] K.M. Isa, T.A.T. Abdullah, U.F.M. Ali, Hydrogen donor solvents in liquefaction of biomass: A review, Renew. Sustain. Energy Rev. 81 (2018) 1259–1268.
[14] J. Zhang, Y. Zhang, Hydrothermal Liquefaction of Microalgae in an Ethanol–Water Co-Solvent To Produce Biocrude Oil, Energy Fuels 28 (8) (2014) 5178–5183.
[15] J.S. Martinez-Fernandez, S. Chen, Sequential Hydrothermal Liquefaction characterization and nutrient recovery assessment, Algal Research 25 (2017) 274–284.
[16] A. Chacón-Parra, D. Lewis, P. van Eyk, The effect of ethanol as a homogeneous catalyst on the reaction kinetics of hydrothermal liquefaction of lipids, Chem. Eng. J. 414 (2021) 128832.
[17] G. Teri, L. Luo, P.E. Savage, Hydrothermal Treatment of Protein, Polysaccharide, and Lipids Alone and in Mixtures, Energy Fuels 28 (12) (2014) 7501–7509.
[18] Riazi, M.R., Characterization and Properties of Petroleum Fractions. 2005: ASTM International.
[19] Socrates, G., Infrared and Raman Characteristic Group Frequencies: Tables and Charts. 2004: Wiley.
[20] D.M. Mackie, J.P. Jahnke, M.S. Benyamin, J.J. Sumner, Simple, fast, and accurate methodology for quantitative analysis using Fourier transform infrared spectroscopy, with bio-hybrid fuel cell examples, MethodsX 3 (2016) 128–138.
[21] Law, V.J., Numerical Methods for Chemical Engineers Using Excel, VBA, and MATLAB. 2013: CRC Press, Taylor & Francis Group.
[22] Fogler, H.S., Elements of Chemical Reaction Engineering. 2006: Prentice Hall PTR.
[23] Beers, K.J., Numerical Methods for Chemical Engineering: Applications in MATLAB. 2006: Cambridge University Press.
[24] P.J. Valdez, V.J. Tocco, P.E. Savage, A general kinetic model for the hydrothermal liquefaction of microalgae, Bioresour. Technol. 163 (2014) 123–127.
[25] J. Lu, Z. Liu, Y. Zhang, P.E. Savage, 110th Anniversary: Influence of Solvents on Biocrude from Hydrothermal Liquefaction of Soybean Oil, Soy Protein, Cellulose, Xylose, and Lignin, and Their Quinary Mixture, Ind. Eng. Chem. Res. 58 (31) (2019) 13971–13976.
[26] Burton, F.L., et al., Wastewater Engineering: Treatment and Resource Recovery. 2013: McGraw-Hill Education.
[27] L. Xu, D.W.F. (Wim) Brilman, J.A.M. Withag, G. Brem, S. Kersten, Assessment of a dry and a wet route for the production of biofuels from microalgae: Energy balance analysis, Bioresour. Technol. 102 (8) (2011) 5113–5122.
[28] Snoeyink, V.L. and D. Jenkins, Water chemistry. 1980: Wiley.
[29] U. Jena, N. Vaidyanathan, S. Chinnasamy, K.C. Das, Evaluation of microalgae cultivation using recovered aqueous co-product from thermochemical liquefaction of algal biomass, Bioresour. Technol. 102 (3) (2011) 3380–3387.
[30] A. Soler-Jofra, J. Perez, M.C.M. van Loosdrecht, Hydroxylamine and the nitrogen cycle: A review, Water Res. 190 (2020), 116723.
[31] A. Duereh, R.L. Smith Jr., Strategies for using hydrogen-bond donor/acceptor solvent pairs in developing green chemical processes with supercritical fluids, The Journal of Supercritical Fluids 141 (2018) 182–197.
[32] Denbigh, K.G. and K.G. Denbigh, The Principles of Chemical Equilibrium: With Applications in Chemistry and Chemical Engineering. 1981: Cambridge University Press.

Elemental nitrogen balance, reaction kinetics and the effect of ethanol on the hydrothermal liquefaction of soy protein

Andrés Chacón-Parra, David Lewis, Philip van Eyk

School of Chemical Engineering and Advanced Materials,

The University of Adelaide, Adelaide, SA, 5005, Australia

*Corresponding author

E-mail address: philip.vaneyk@adelaide.edu.au

Supplementary Material

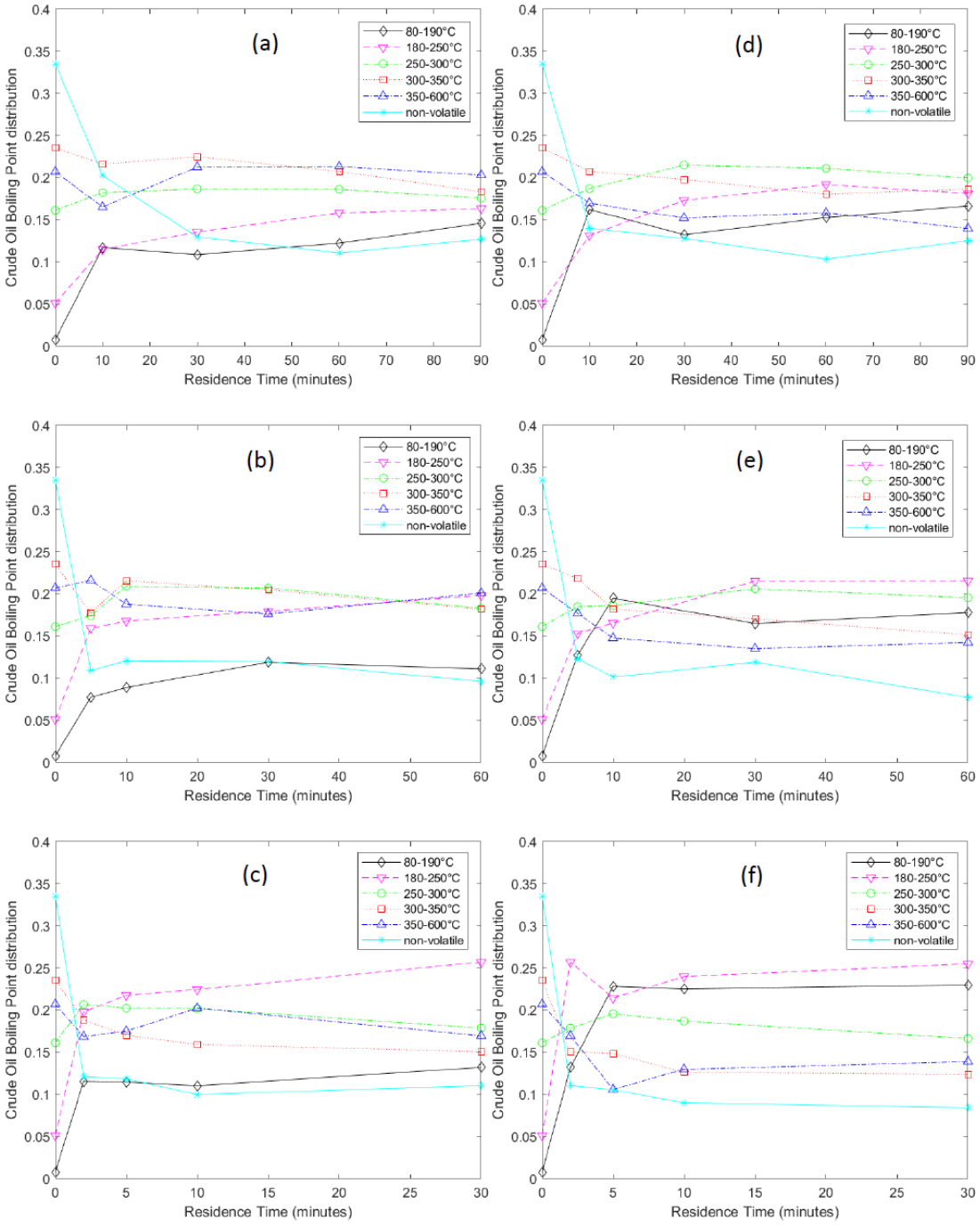

Figure S.1. HTL renewable crude boiling point distribution at (a) 250°C, (b) 300°C and (c) 350°C without catalysts, (d) 250°C, (e) 300°C and (f) 350°C with in-situ catalysts.

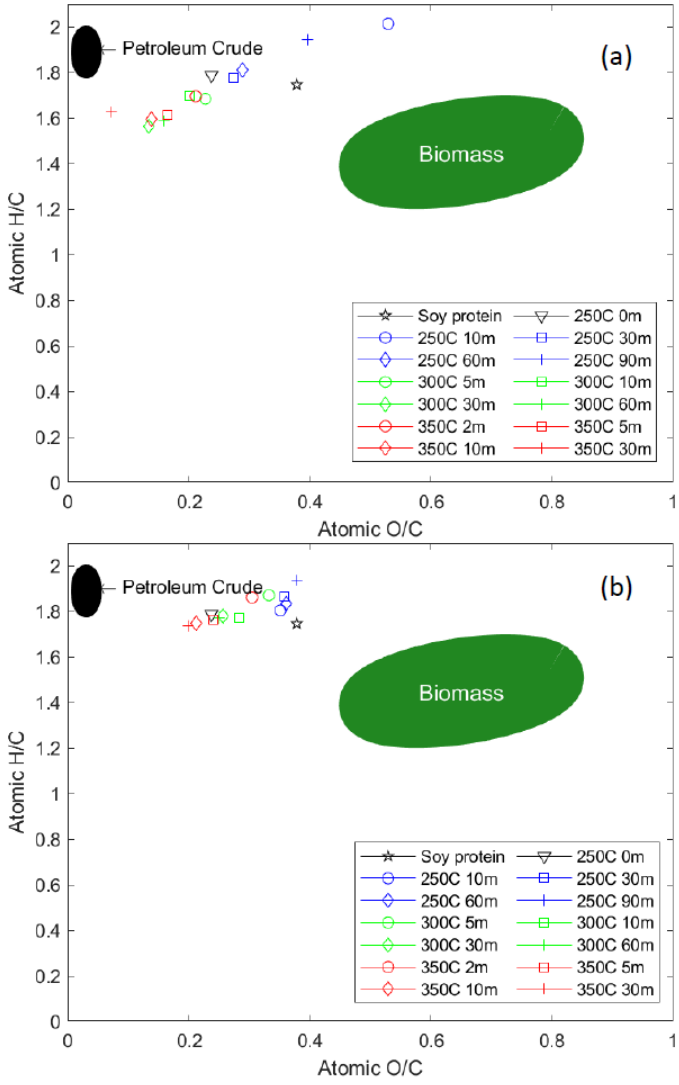

Figure S.2. Van Krevelen diagram of (a) plane HTL and (b) in-situ catalysts HTL.

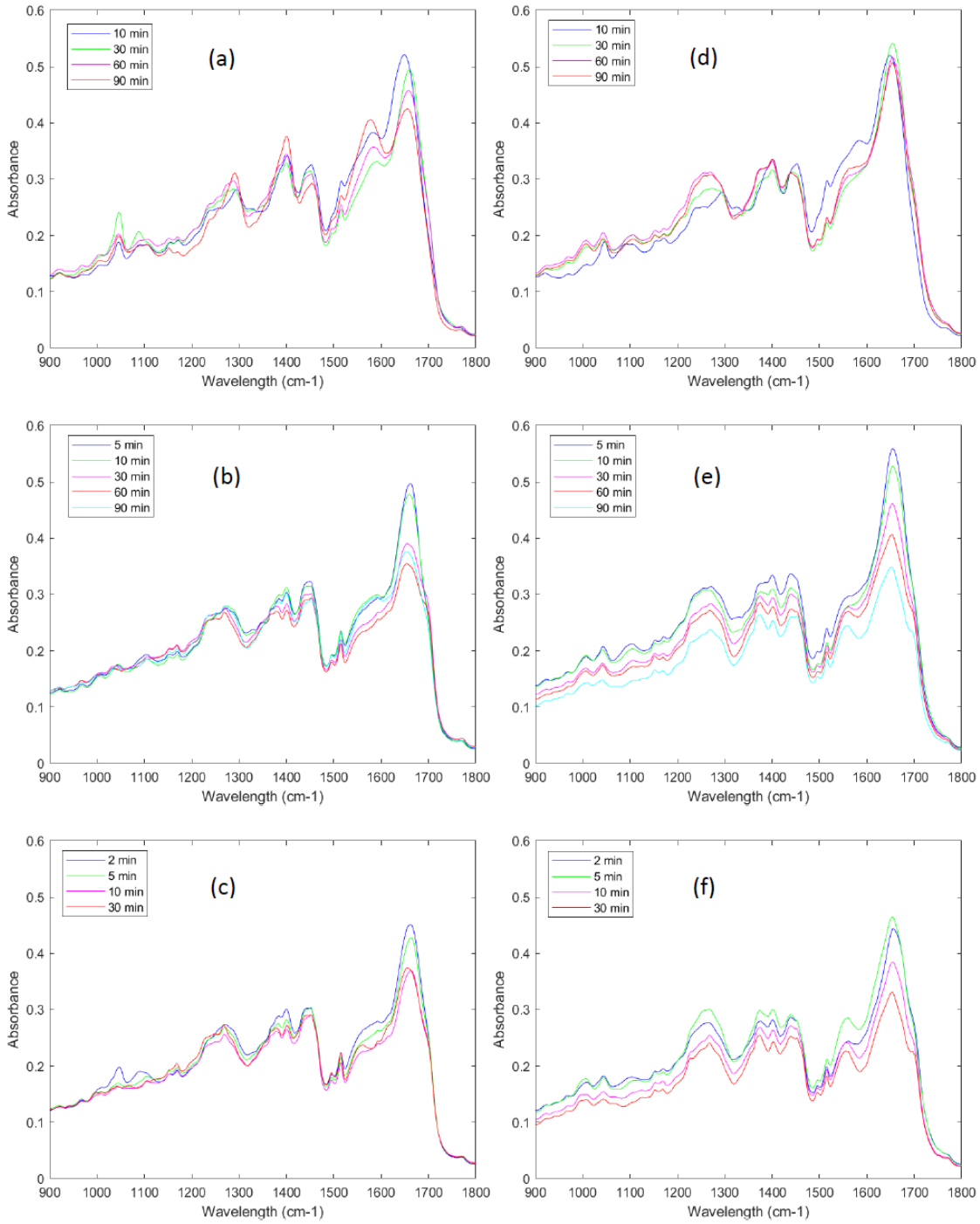

Figure S.3. FT-IR of HTL renewable crude at a) 250, b) 300 and c) 350°C without catalysts, d) 250, e) 300 and f) 350°C with catalysts.

Chapter 5

A multi-component reaction kinetics model for the hydrothermal liquefaction of carbohydrates and co-liquefaction to produce 5-ethoxymethyl furfural

Andres Chacon-Parra[a], David Lewis[a], Marianne Glasius[b], Philip van Eyk[a]

[a]School of Chemical Engineering and Advanced Materials, The University of Adelaide, Adelaide, SA 5005, Australia

[b]Department of Chemistry, Aarhus University, 8000 Aarhus C, Denmark

Fuel, **311**, (2022) 122499.

Chapter 5 - A multi-component reaction kinetics model for the hydrothermal liquefaction of carbohydrates and co-liquefaction to produce 5-ethoxymethyl furfural

Statement of Authorship

Title of Paper	A multi-component reaction kinetics model for the hydrothermal liquefaction of carbohydrates and co-liquefaction to produce 5-ethoxymethyl furfural
Publication Status	☑ Published ☐ Accepted for Publication ☐ Submitted for Publication ☐ Unpublished and Unsubmitted work written in manuscript style
Publication Details	Chacón-Parra, A., D. Lewis, M. Glasius, and P. van Eyk, A multi-component reaction kinetics model for the hydrothermal liquefaction of carbohydrates and co-liquefaction to produce 5-ethoxymethyl furfural. Fuel, 2022. 311: p. 122499.

Principal Author

Name of Principal Author (Candidate)	Andres Danilo Chacon Parra
Contribution to the Paper	Conceptualisation, Investigation, Methodology, Formal analysis, Data curation, Writing - original draft
Overall percentage (%)	85%
Certification:	This paper reports on original research I conducted during the period of my Higher Degree by Research candidature and is not subject to any obligations or contractual agreements with a third party that would constrain its inclusion in this thesis. I am the primary author of this paper.
Signature	Date: 9/12/21

Co-Author Contributions

By signing the Statement of Authorship, each author certifies that:

i. the candidate's stated contribution to the publication is accurate (as detailed above);
ii. permission is granted for the candidate in include the publication in the thesis; and
iii. the sum of all co-author contributions is equal to 100% less the candidate's stated contribution.

Name of Co-Author	David Milton Lewis
Contribution to the Paper	Supervision, Funding acquisition, Writing - review & editing
Signature	Date: 9/12/2021

Name of Co-Author	Marianne Glasius
Contribution to the Paper	Data curation, Validation, Writing - review & editing
Signature	Date: 17 December 2021

Chapter 5 - A multi-component reaction kinetics model for the hydrothermal liquefaction of carbohydrates and co-liquefaction to produce 5-ethoxymethyl furfural

Name of Co-Author	Philip Joseph van Eyk
Contribution to the Paper	Supervision, Conceptualisation, Resources, Writing - review & editing
Signature	Date 9/12/2021

Please cut and paste additional co-author panels here as required.

Chapter 5 - A multi-component reaction kinetics model for the hydrothermal liquefaction of carbohydrates and co-liquefaction to produce 5-ethoxymethyl furfural

Fuel 311 (2022) 122499

Contents lists available at ScienceDirect

Fuel

journal homepage: www.elsevier.com/locate/fuel

Full Length Article

A multi-component reaction kinetics model for the hydrothermal liquefaction of carbohydrates and co-liquefaction to produce 5-ethoxymethyl furfural

Andrés Chacón-Parra [a,1], David Lewis [a,2], Marianne Glasius [b,3], Philip van Eyk [a,4,*]

[a] School of Chemical Engineering and Advanced Materials, The University of Adelaide, Adelaide, SA 5005, Australia
[b] Department of Chemistry, Aarhus University, Langelandsgade 140, 8000 Aarhus C, Denmark

ARTICLE INFO

Keywords:
Hydrothermal liquefaction
Carbohydrates
Multi-component reaction kinetics
Shrinking core model
Co-liquefaction
5-Ethoxymethyl furfural

ABSTRACT

Hydrothermal liquefaction (HTL) as a waste management technology has been investigated to produce renewable bio-crude and other valuable products from wet biomass and bio-waste. However, carbohydrates as a vital component in biomass have shown to increase the complexity of the process. Undesirable solid yields produced by the carbonisation/re-condensation of reactive carbohydrate intermediates could limit the renewable crude yield and recovery. In the present study, the reaction mechanism and kinetic models for the HTL of monosaccharides and polysaccharides are investigated using gas chromatography–mass spectrometry (GC–MS) and high-performance liquid chromatography (HPLC) to characterise, validate and quantify the most abundant organic species in the aqueous phase. The experimental data and models presented provide an unbiased understanding of the carbohydrate decomposition during HTL conversion, while the analysis of solid products clarifies solid transformations and integrates both phases into a more comprehensive reaction mechanism approach, including a shrinking core model for cellulose. Finally, ethanol and acetic acid were added as co-solvents to elucidate the effects of a fully renewable hydrogen donor solvent system to generate 5-ethoxymethyl furfural and ethyl levulinate (validated with GC–MS), two renewable fuel additives and promising tunable monomers candidates. Experiments were conducted with glucose, fructose, and cellulose in a batch reactor with 20% by mass premixed feedstock at 250 °C and 300 °C.

1. Introduction

Hydrothermal liquefaction (HTL) of wet biomass and bio-waste is a promising solution for waste management and renewable energy production, which brings attention to non-conventional wet biomass sources such as municipal sewage sludge, municipal wastes, and algae [1–3]. HTL takes advantage of the extraordinary properties of sub-critical water (250 °C to 375 °C, over saturation pressure) to break and hydrolyse major biomass linkages, and as a reaction medium, water allows intermediates to react and re-condense into different compounds and phases [1,2,4–6]. The products of HTL heavily depend on process conditions, feedstock type, and composition. Carbohydrates, as a key biomass component, produce considerable fractions of undesirable hydrochar (solid char), while reducing the renewable crude yields and increase the complexity of the process and separation afterwards [1–5].

Reported renewable crude yields of less than 6% (with dichloromethane extraction) and the negligible effect of temperature and residence time have been reported from the HTL of glucose [7–9]. 5-Hydroxymethyl furfural (5-HMF) and levulinic acid are recognised as the most prominent and valuable products from six-carbon monosaccharides degradation under subcritical water [7,10–16]. The characterisation of aqueous phases via gas chromatography-mass spectrometry (GC–MS) with direct injection or solvent extraction (and derivatization) have suggested various components and compositions

* Corresponding author.
E-mail address: philip.vaneyk@adelaide.edu.au (P. van Eyk).
[1] 0000-0002-7615-0238
[2] 0000-0002-5322-1873
[3] 0000-0002-4404-6989
[4] 0000-0003-3768-2044

https://doi.org/10.1016/j.fuel.2021.122499
Received 19 August 2021; Received in revised form 14 October 2021; Accepted 31 October 2021
Available online 11 November 2021

Chapter 5 - A multi-component reaction kinetics model for the hydrothermal liquefaction of carbohydrates and co-liquefaction to produce 5-ethoxymethyl furfural

highly influenced by the specific conditions of the analytical method used [7,8,13,17–20]. A highly hydrophobic solid (hydrochar) product phase might have some potential uses as functionalised material for absorbents, support for catalysts and soil recovery. However, hydrochar besides energy storage purposes is not attractive from an energy perspective [1,4,13,21–23]. Hydrochar is formed by humins, a heterogeneous carbonaceous structure produced by the nucleation reaction of furan ring radicals, mostly 5-HMF and ring-opening, typically levulinic acid [13,14,24–30]. The morphological and structural differences of hydrochar from monosaccharides and polysaccharides have been studied, and some reaction pathways have been established [2,16,22,31–36]. However, the kinetics and reaction mechanism of monosaccharides and the direct solid transformation of cellulose (polysaccharides) are barely studied [14,15,37–39].

The hydrothermal conversion of cellulose as one of the most abundant natural polymers on earth has been investigated for more than a century [4,21,36,40]. However, most of the reported scientific literature is focused on understanding the cellulose degradation mechanisms (hydrolysis), defining the product yields, and proposing bulk mechanism and basic reaction kinetic models, including some shrinking core models [14,35,38,41–46]. Chuntanapum and Matsumura (2010) presented a reaction mechanism considering 5-HMF and furfural as intermediates for hydrochar formation, with many unknown organic compounds [47–50]. Yin and Tan (2012) presented a reaction pathway as a function of reaction medium pH with apparent differences in reaction mechanism pathways [50,51]. To the best of our knowledge, studies presenting a reaction kinetic model which integrates the liquid and solid phases, also valuable for process modelling and optimisation, are limited [46,52–54]. Additionally, there may be some valuable products in the aqueous phase which might be the foundation of new sustainable fuel additive and polymers based in 5-HMF and levulinic acid [15,26,35,54–56]. However, these promising organic species have been only produced via solid acid catalysts [55,57–60]. Ethanol as a hydrogen donor solvent over subcritical water conditions (co-liquefaction) may promote the alkylation/etherification of 5-HMF and levulinic acid under autogenous conditions, while improving the renewable bio-crude yield and properties from other biomass key components [57,61–64].

In this study. GC–MS and HPLC were used to identify and quantify the most abundant species in the aqueous phase from HTL of glucose and fructose. The yields of all detected species are included in a multi-component reaction mechanism and kinetic model, balanced with the unknown as total organic carbon (TOC) and water released (dehydration). The solid product phases were analysed using thermogravimetric analysis-mass spectrometry (TG-MS), particle size distribution and scanning electron microscope coupled with energy dispersive X-ray spectroscopy (SEM/EDS) to determine the volatilisation profile, liquid dispersion particle size distribution, morphology and relative (O/C) composition of the solid particles (hydrochar) from HTL [31,32]. The derivate thermogravimetric analysis (dTG) of HTL solid products from cellulose was used to estimate the unreacted feedstock in the solid phase, based on the characteristic decomposition of cellulose and hydrochar [65]. The estimation of cellulose in hydrochar is then integrated to produce a multi-component and shrinking core reaction kinetic models for the HTL of cellulose. Finally, ethanol and acetic acid were included in a co-liquefaction conversion to clarify the effects of this commonly used hydrogen donor solvent system over the HTL conversion of carbohydrates, and to generate some valuable water-soluble organics which may revolutionise synthetic bio-fuels and green polymer industries [55,57,58]. The significance of the present study stands on integrating liquid and solid phase analysis to provide a more complete understanding of the HTL reaction mechanism of carbohydrates, and the co-liquefaction to produce functional ester and ether with potential value as fuel additives and tunable monomers, and a remarkable green chemistry alternative from carbohydrates [55,58].

2. Materials and method

2.1. Materials and standards

D-fructose analytical reagent (AR), D-glucose anhydrous laboratory reagent (LR) and Cellulose Microcrystalline extra pure (with an average particle size of 90 μm, Acros Organics) from Chem-supply were selected as mono and polysaccharides. Ethanol 100% (undenatured) used as a solvent and homogeneous catalyst and acetic acid glacial AR were also provided from Chem-Supply. 5-Hydroxymethyl furfural (>99% purity), 5-Methyl furfural (>99%), Furfural (>99%), 3-Methyl-1,2-cyclopentanedione (>99%), 2-Butanone (>99.7%), Levulinic acid (>98%), formic acid (>95%), 2,5-Hexanedione (>98%) and trans 2-Pentenoic acid (>98%) were provided by Sigma Aldrich and used as standards for HPLC characterisation and quantification.

2.2. Batch reactor and heating system

A customised reactor system (15 ml nominal volume) made with 20 cm of a ½ inch 316 stainless steel tube, fitting, and ferrules (Swagelok®), extended and equipped with a type K thermocouple, pressure transducer and ball valve, a diagram of the batch reactor system is provided in previous works [43,63]. Carbohydrate feedstocks were premixed in water to 20% by mass. When ethanol and acetic acid were added as co-solvent and homogeneous catalyst system, the water mas load was reduced from 80% to 59.6% to include the two new co-solvents (20% ethanol and 0.4% acetic acid by mass) in the system. The reactor was filled to 50% of its nominal volume capacity in all cases, purged, and pre-pressurised with nitrogen gas (to keep water under subcritical conditions) [63].

Heating was accomplished with an alumina sand fluidised bed system (Techne SBL-2D), set with a temperature controller (Techne TC-9D). The system can reach a heating ramp of up to 125 °C/min, which is ideal for reaction kinetic. The reaction was counted as started when the system reached 98% of the desired temperature and stopped in a two-step cooling process, by blowing compressed air until 100 °C followed by a water quench bath [63,64]. The residence time distribution was in relative agreement with previous work on the HTL of lipids and proteins (with a pre-defined time step "η" of 5 min, in agreement with reaction conditioning time). The longest time was 30 min for 250 °C and 300 °C. Finally, 350 °C was considered an extreme temperature for carbohydrates based on the scientific literature [9,12,63,66].

2.3. Hydrothermal liquefaction experiments and product separation

Each experiment was performed twice. However, every run served only one of two specific purposes. The first was to produce and collect an unaffected and representative aqueous phase sample for HPLC, and solid phase for thermogravimetric, SEM and particle size analysis (once dry by forced convection, the solids may lose specific properties) [67]. The second run was undertaken to quantify all bulk product phase yields, rinsing the reactor system to minimise mass losses and drying the solids [63]. This method reduced possible deviation from human errors and external factors.

In both cases, the gaseous phase yield was measured by weight difference, accounting for the pre-charged nitrogen gas and the amount total of gas vented after the reaction was completed [43,63]. Solid and liquid products were collected by pouring the reactor content into centrifuge tubes and pushing solids out of the reactor with a stainless-steel bar to maximise product recovery. Then the sample was centrifuged for 10 min at 3500 RPM to separate the solid and aqueous products. A 2 ml liquid sample was taken and filtered with a 0.22 μm cellulose acetate KX Syringe filter into a chromatography vial and refrigerated for analysis. The solids were poured directly into a Buchner separation funnel (with Whatman's Ashless Grade 42 filter papers) in the second run. Then the reactor was rinsed with deionised water to

Chapter 5 - A multi-component reaction kinetics model for the hydrothermal liquefaction of carbohydrates and co-liquefaction to produce 5-ethoxymethyl furfural

maximise solid recovery. The filter papers were then dried at 105 °C overnight to quantify solid yields [63,64].

2.4. Product analysis

An initial characterisation of the organic species in the aqueous phase was undertaken on an Agilent 7977B/7890B Gas Chromatography GC–MS. Separation was accomplished using a Perkin Elmer Elite-FFAP capillary column (30 m × 0.32 mm × 0.25um) with a 2 ml/min flow of helium carrier gas. A 1 ± 0.1 µL aqueous sample was manually injected into the GC system in split mode (20:1). The oven temperature was programmed to start at 50 °C, held for one minute, followed by a 10 °C/minute ramp to 150 °C, then a ramp of 25 °C/minute to 250 °C with a final hold of 25 min. The mass spectrometer (5977B MSD) scanned from *m/z* 40–500. The compounds were tentatively identified with the NIST14 Spectral Library data base using ChemStation MS data analysis module (Agilent software) [7].

Quantification was accomplished via HPLC. The analysis was conducted using a Shimadzu LC-20AD (XR) HPLC system, equipped with a SIL-20A auto-sampler, a CTO-20A column oven, and an Optilab T-Rex Wyatt refractive index detector in deferential RI mode (dRI). The separation was accomplished with an ion-exclusion column system, Phenomenex Rezex ROA-organic acid H+, 300x7.80 mm (00H0138K0), with the corresponding guard column (03B-0138-K0) and 0.5 ml/min flow rate of 0.005 N sulfuric acid (isocratic) with sample injection volume of 0.5 µL. The temperatures of the column and detector were 60 °C and 40 °C respectively, with a maximum retention time of 90 min. The dRI data was auto background line subtracted using Astra software (Wyatt) and exported to raw data then plotted in Matlab and integrated using *trapz* function, which computes an approximation of the integral area via trapezoidal method (Riemann sum) [68]. Quantification was accomplished using peak area with at least six different volume injections (0.2 to 2 µL) of each standard to reduce the human error [69].

Thermogravimetric analysis with mass-spectrometry (TG-MS) of solid products was performed in a NETZSCH simultaneous thermal analyser (STA) 449 F5 Jupiter, equipped with a (quadrupole mass spectrometer) QMS 403 D Aëolos in MID (Multiple Ion Detection measurements) mode, with SEM (Channeltron) detector configured at 70 eV, and temperatures of 280 °C and 300 °C for the transfer line and QMS, respectively. The method run started with an isothermal segment for 20 min at 80 °C to remove any residual humidity, followed by a ramp at a 5 °C/min from 80 to 600 °C, with 50 ml/min nitrogen gas flow rate, finally an isothermal segment at 600 °C with air to determine combustible matter. The first derivative of the mass loss (percentage) over temperature (dTG) is plotted with the *m/z* signals from ion fragments detected in volatiles [43,67,70].

Scanning electron microscope (SEM) images were taken in a FEI Quanta 450 High Resolution Field Emission Scanning Electron Microscope equipped with an Everhart-Thornley detector (ETD) using high vacuum mode with samples coated in platinum (10 nm). Additionally, energy dispersive spectroscopy (EDS) as a surface assessment for O/C compositional ratio was accomplished with an Oxford Ultim Max EDS detector using Oxford AZtec processing software for live mapping and data processing. Finally, the particle size distribution analysis of the solids was conducted in a Malvern Mastersizer APA2000 (laser diffraction) particle size analyser equipped with a Hydro 200MU liquid dispersion unit. Run with water (dispersant) at 900 RPM pump speed and 10 as ultrasonic level displacement. Set for carbon particles in the range (0.02 to 2000 µm) with an obscuration level from 5 to 10%.

2.5. Kinetic modelling

Reaction kinetics were modelled using a set of first-order ordinary differential equations (ODE) based on defined reaction mechanisms, solved using *ODE45* in MATLAB [43,63]. The reaction constants (k) for each set of conditions were obtained using *lsqcurvefit* function via multivariable optimisation by fitting the experimental yield values to the set of reaction constants over the defined residence time range by minimising the squared norm of the residual function. As only two temperature points were obtained (knowing that 350 °C is too extreme for carbohydrate conversion), the activation energies and pre-exponential factors were not calculated. Although, the *k* values are provided for further calculations [43,63,68,71].

3. Results and discussion

3.1. Aqueous phase characterisation and quantification

Carbohydrates and conjugates are commonly separated, characterised and quantified with HPLC using Refractive Index (RI) detectors. Among the different stationary phases available, ion-exchange combined with size-exclusion could be considered the most appropriate to separate complex mixtures of saccharides and products of its degradation [9,47,48]. The decomposition of sugars during HTL produces organic acids, ketones, alcohols and some heterocyclic compounds [66,69]. Additionally, as functional groups in carbohydrates are virtually undetectable by UV detectors, differential RI detectors elude the refractive index difference between the mobile phase and the sample (under isocratic conditions) [9]. Taking these factors into consideration, a Phenomenex Rezex Organic Acids (ROA) column was chosen as a stationary phase, as this is ideal for organic acids in combination with carbohydrates, alcohols, fatty acids, or neutral compounds. Chromatograms of the HTL products of glucose, fructose and cellulose are presented in Supplementary Material Fig S.3. However, identification of the peaks was challenging as the relevant scientific literature is fragmented, suggesting dissimilar intermediates [4,7–9,11–13,18,48,52]. Therefore, GC–MS analysis was performed to tentatively identify products before standards acquisition for LC validation and quantification. The GC–MS chromatograms and identification are available in the Supplementary Material Fig S.1 and Table S.2.

The major peaks detected are identified in Table. 1. There were three unknown peaks (A1, A2 and A3), which according to the scientific literature might be erythrose, pyruvaldehyde and 1,6-anhydroglucose respectively [9]. Sasaki et al. (2000) used a sugar KS-801 ligand exchange and size exclusion column with a refractive index detector. Despite the difference in ligand ion used, the distribution of glucose, fructose, 5-HMF and furfural peaks is analogous, with a factor of approximately 1.6 for the ROA H^+ [9]. Additionally, the A3 unknown peak was observed at relatively high concentration with glucose, which may be linked to a specific degradation product [9,11,26,46,48]. The unknowns were semi-quantified with similar refractive index and length

Table 1
Liquid chromatography peak identification.

Reagent	Retention time peak (min)	Formula	Abbreviation
Glucose	12.8	$C_6H_{12}O_6$	Glu
Fructose	13.9	$C_6H_{12}O_6$	Fru
A1* (Erythrose)	14.4	$C_4H_8O_4$	–
A2* (Pyruvaldehyde)	15.5	$C_3H_4O_2$	–
A3* (1,6-Anhydroglucose)	16.7	$C_6H_{10}O_5$	–
Formic A	18.3	CHOOH	FA
Acetic A	19.6	CH_3COOH	AA
Levulinic acid	20.6	$C_5H_8O_3$	LA
trans-2-Pentenoic acid	25.3	$C_5H_8O_2$	t-PA
Ethanol	27.2	C_2H_5OH	E-OH
2,5-Hexanedione	28.7	$C_6H_{10}O_2$	HEX
2-butanone	32.6	C_4H_8O	BUT
5-hydroxymethyl furfural	35.8	$C_6H_6O_3$	HMF
3-Methyl-1,2-cyclopentanedione	37.7	$C_6H_8O_2$	MCP
Furfural	51.2	$C_5H_5O_2$	FUR
5-Methyl furfural	73.3	$C_6H_6O_2$	MFU

*No characterised peak, semi quantified and named based on the literature [9].

standard compounds, then included in the TOC and water to complete the mass balance for the reaction kinetic models presented in Sections 3.2, 3.4 and 3.5.

For each of the three carbohydrates tested (glucose, fructose, and cellulose) a zero (0) residence time test was run. This zero-time is of crucial importance to model isothermal reaction kinetics (Arrhenius). For glucose and cellulose, the zero-residence time experiments showed peaks in the chromatograms before glucose. To the best of our knowledge, these peaks might correspond to some oligomers, which do not interact with the ion-exclusion system and elude early [9,47,48]. However, these were not counted in the quantification model. They were included in TOC and water, which contain all the unknowns, RI non-detected species and water released [46].

Glucose and fructose have an O/C ratio of 1.33, while cellulose has an approximate O/C ratio of 1.11 (based on the monomeric structure formula). HTL reduces this relatively high oxygen content via dehydration (H_2O) and decarboxylation (CO_2) reactions [13,14,47]. However, the amount of water released into the aqueous phase cannot be easily determined, as water is a reaction medium, solvent, and catalyst under HTL conditions. Water is consumed and produced from hydrolysis, ring opening and carboxylic acid nucleophilic substitution reactions, affecting the concentration of all organic species [1,4,14,46,51]. For this reason, water released from the dehydration cannot be separated from the TOC, which was calculated by difference (leftover) from the initial mass and the sum of all quantified organic compounds.

3.2. Reaction mechanism and kinetics for the HTL of monosaccharides

Concentrations of all compounds identified and quantified with GC–MS and HPLC of the aqueous phase from HTL of glucose are shown in the Supplementary Material Table S.4. As the data revealed, the concentration of glucose is reduced from 200 to 125.8 mg/ml during heating-up to 250 °C (zero time), and fructose showed even more severe reduction with a concentration of 9.8 mg/ml just after heating as illustrated in the Supplementary Material Table S.5. These observations indicate the high reactivity of monosaccharides in subcritical water [9,14,16]. The next reasonable observation is the isomerisation of both monosaccharides, which is widely acknowledged and discussed in the scientific literature [4,9,11–13].

Glucose decomposition during HTL seems to be slower than fructose, and fructose appears to be a substantial intermediate of glucose despite the low concentration (as it is highly reactive) over the residence time distribution [4,39]. Likewise, fructose seems to be extremely fugacious and the concentrations of 5-HMF, methyl cyclopentadiene and levulinic acid were substantial as intermediates of hydrochar formation [3,4,14–16,48]. For example, maximum values of 51 and 12 mg/ml for 5-HMF and methyl cyclopentadiene, respectively, were found at zero-time in the HTL decomposition of fructose. Similarly, unknowns A3

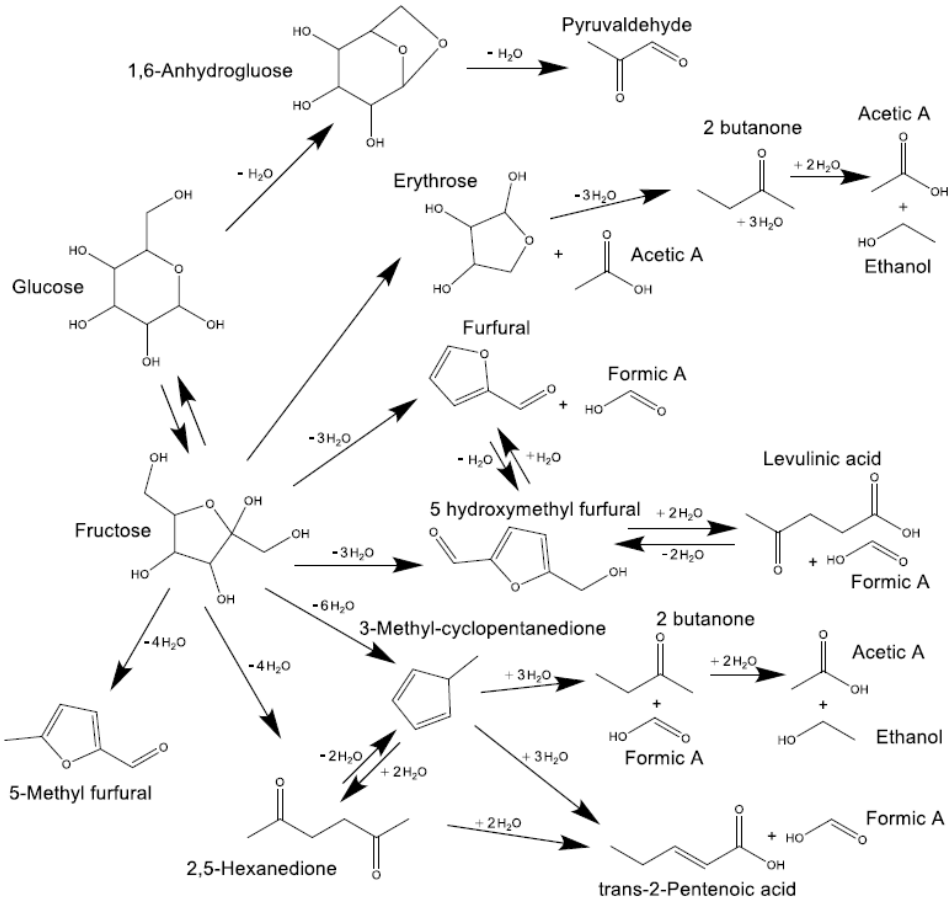

Fig. 1. Proposed decomposition mechanism for glucose and fructose during HTL.

and A2 showed relatively high levels of direct glucose decomposition, while A1 was particularly higher from fructose decomposition [4,9,13,26,72].

Based on the identified species, the number of carbons, the functionalities of the structures, and the concentration profiles provided in the Supplementary Material Tables S.4 and S.5. A reaction mechanism is proposed and illustrated in Fig. 1. Isomerisation of glucose and fructose clearly goes in two directions, as illustrated in the glucose and fructose experiments [4,13,39]. Because of the furanose structure of fructose, it seems to be a transitional compound of most detected organic products, including 5-HMF and 5-methyl furfural from fructose dehydration, 3-methyl cyclopentanedione from dehydration and ring closure (rearrangement), and hexanedione (ring opening) [3,9,48]. There also seems to be a partial degradation of structures like erythrose, with is modelled to produce acetic acid as a by-product. Furfural is modelled to form from the dehydration and breaking of fructose producing formic acid and in equilibrium with 5-HMF (HMF and furfural follows relatively similar patterns). Levulinic acid is well known to be a product of C-O cleavage (ring opening) and C–C cleavage (breaking) from 5-HMF [4,13,26,49,73]. Butanone and *trans*-pentenoic acid are expected products from the breaking of 3-methyl cyclopentadiene, hexanedione and erythrose. However, 3-methyl cyclopentadiene appears to be more likely to form butanone following the dehydration path and *trans*-pentenoic acid from the degradation of hexanedione [2,4,15,39,74]. The only apparent direct intermediate of glucose appears to be 1,6-anhydroglucose, which then degrades into pyruvaldehyde before forming humins structure and the solid particles (hydrochar) [3,4,9,37]. The solid phases are discussed in Section 3.3. This specific reaction mechanism pathway (illustrated in Fig. 1) is produced based on observations, the scientific literature and the causal relation of the concentration profiles. The actual HTL conversion may differ from what is presented (measured concentrations are provided in Supplementary Material).

The experimental and modelled yields of products from HTL of glucose with sixteen species defined are illustrated in Fig. 2. Solid char is the most prominent product which accounts for approximately 50% of the mass yield, followed by TOC and water released into the aqueous phase and gaseous phase (CO_2) from the dehydrogenation of formic acid as the shortest and simplest organic structure formed from the degradation of carbohydrates, also referred as decarboxylation [4,12,26]. However, because of the subcritical water conditions of HTL, CO_2 is modelled to form from formic acid. The temperature 300 °C seems to be a severe for the conversion of monosaccharides, as the concentration of all intermediates is much lower compared to 250 °C and remained relatively unchanged after 5 min residence time [7,11,12]. The complete reaction model and equation system used to complete Fig. 2. is presented in Section 3.4. Despite the model contain 16 variables to fit and optimise simultaneously, the predicted profiles presented a good agreement with the experimental data.

The renewable bio-crude fraction presented in the scientific literature typically corresponds to organic species which were extracted using organic solvent and derivation reagents in most cases [7,8,13,18–20,22]. However, in the present study, all organic compounds are accounted within the aqueous phase after centrifugation and filtration, as all species are soluble in water [9,48]. There could be some solubilisation of hydrophobic species (mostly phenolic) adsorbed to the solid particles during the solvent extraction as more complex structures have been detected with GC–MS when the extraction is done to the solid and liquid phases together [7,8,18]. In the GC–MS initial characterisation undertaken in the present study, the sample was directly injected with no solvent extraction (the same samples used for HPLC) as described in Section 2.4.

Fructose experimental and modelled concentrations are illustrated in Fig. 3. The results suggest that fructose is more reactive than glucose, and hydrochar yields produced are higher than from glucose [16]. The model cannot recognise substantial differences between the two reaction temperatures tested (250 °C and 300 °C), despite that the model

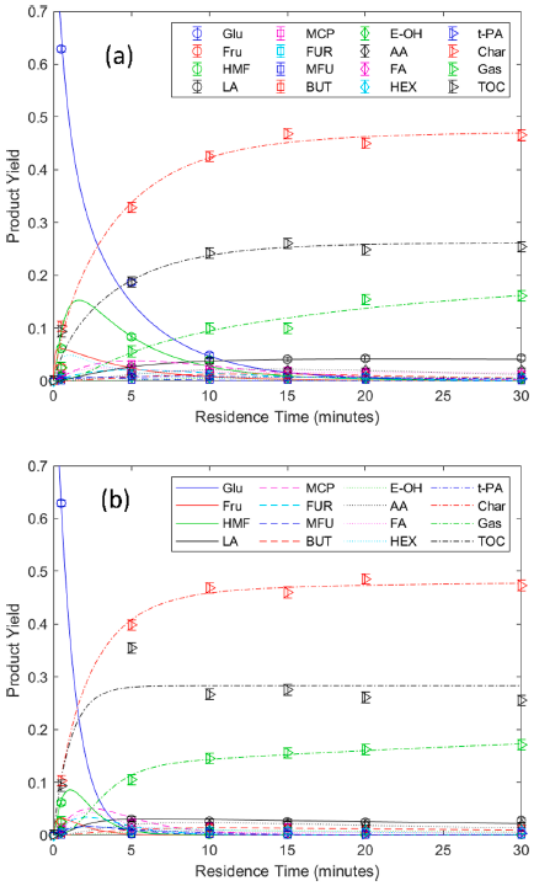

Fig. 2. Experimental points and modelled concentration profiles for the HTL of glucose at 250 °C (a) and at 300 °C (b). Abbreviations listed in Table. 1.

used is the same [13,14,25,26,75]. The concentration of valuable intermediates is lower than from glucose, and zero residence time seems to be the only point which presented high organic concentration in the aqueous species (also shown in experimental data provided in the Supplementary Material Tables S.4 and S.5).

The solid hydrochar product is formed by humins, a heterogeneous carbonaceous material produced by the nucleation of furan ring radicals, 5-HMF and ring opening typically levulinic acid, followed by the coalescence and crosslinking of particles to grow their size [13,14,24,25,28,48,66]. Hydrochar and humins have received little attention, as these are not as valuable as other product phases [1,26]. However, as solids are the most significant product portion of HTL of carbohydrates, and to provide a better understanding of the reaction kinetics and impact of the conditions, it is necessary to analyse the aqueous phase in conjunction to the other product phases [13,14,26,74].

3.3. Hydrochar characterisation and cellulose estimation

Oil fractions trapped in the solids which have been measured via thermal volatilisation by Source Rock Analysis (SRA) and thermogravimetric analysis might be debatable because of the thermal decomposition of cross-linked hydrocarbon in the solid products [7,8,70]. Hydrochar is a relatively low-porosity structure formed by clusters of

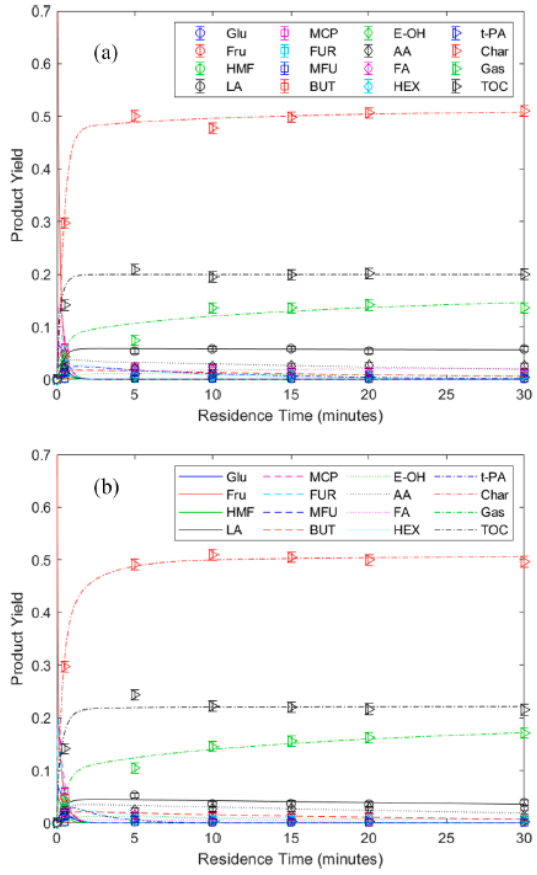

Fig. 3. Experimental points and modelled concentration profiles for the HTL of fructose at 250 °C (a) and at 300 °C (b).

highly hydrophobic spheres [25,26,32,33]. However, these spheric particles may contain relatively weak chemical bonds (chemisorption), on the edges of the aromatic structures, which could degrade and cleave/volatilise at medium temperatures and can be extracted with low-polarity solvents prior to GC–MS characterisation [7,8,18,34,48,67,74].

The TG-MS of raw glucose, fructose and cellulose are presented in the Supplementary Material Fig S.6. The dehydration before the thermal decomposition for glucose and fructose, produce up to 15 and 10% mass of water at temperatures of 250 °C and 200 °C, respectively. Followed by the decomposition and volatilisation of some low mass-to-charge ratio (m/z). Glucose is particularly more resistant than fructose to thermal degradation, which may be linked to the relative reactivity of both under HTL conditions, despite the differences of HTL and the slow heating rate pyrolysis of TGA [13,14]. The m/z ratios of the volatilised matter are 41, 43 and 55 m/z, which apart from being general ionisation fragment ions, might be associated to C_3H_5, C_3H_7, CH_3CO and C_4H_7 from the partial breaking of the pyran and furanose ring structures of the monosaccharides after dehydration [4,14,67,74].

The TG mass loss profiles and mass spectra of the hydrochar from glucose and fructose HTL hydrochar remained relatively unchanged over the residence time distribution, with an average of 44.9 and 44.8% +/- 1% mass in the range 110 °C to 600 °C (or volatile fraction) for glucose and fructose, respectively; and 51.4 and 53.6% +/- 1% in the combustible range at 600 °C. Fructose HTL hydrochar showed more similar thermogravimetric profiles than glucose at varying residence times. Additionally, the m/z of the decomposition products (for the volatile fraction) show signals of 41, 43 and 55 m/z, as illustrated in Supplementary Material Fig S.7. However, 43 m/z may be associated with decarboxylation (CO_2 – 44 m/z) from the thermal decomposition of carbon particles, which cannot be separated due to the QMS resolution (0.5 u to 1.5 u) [67].

SEM images of some monosaccharide hydrochars are provided in the Supplementary Material Fig S.8. The pictures illustrate the clusters formed by relatively spherical microparticles which, once dry, seem to overlap on the edge boundaries with the neighbouring particles from a solid perspective [14,22,25,33]. SEM images and EDS relative compositional data from glucose and fructose HTL hydrochars, provide a better understanding of the nucleation and coalescence reactions involved in the formation of the solid particles and the relatively lower O/C ratio of 0.43 (from EDS), which is 1/3 of the original O/C ratio. Additionally, humins seem to start at 0.1 µm equivalent diameter at 5 min residence time for glucose experiments and coalesce (cross-link) to a nominal diameter of 3 µm [14,25,26]. The microscopy image of this experiment showed a relatively continuous surface on SEM images (not included due to lack of contrast to focus on the microscopy).

SEM data is supported by the particle size distributions measured in liquid dispersion with a laser diffraction particle size analyser presented in Fig. 4. These provide a more realistic perspective of the particle size distribution of the carbon particles (hydrochar) in water over the residence time distribution [14]. The particle size distributions illustrate the polymodal distribution and the relative growth in size over the residence time distribution. Fructose hydrochar showed a less disperse distribution with relatively larger particles than glucose hydrochar [14,32,33]. The relatively higher dispersity of glucose hydrochar (with a fraction entering the nanoparticles range) could be the reason for a continuous surface observed on the SEM at 5 min and the relatively amorphous surface of the microparticles cluster [76].

For the case of cellulose, the crystalline structure of the polysaccharide provides higher resistance to thermal degradation, which is confirmed by the thermogravimetric analysis having only one mass loss peak at 300 °C and stronger signals of ions with higher mass-to-charge ratios (m/z) [65,73]. This relatively strong and clear decomposition peak is valuable as it represents the high resistance of the microcrystalline structure of polysaccharides as cellulose [31,37,43–45,65,73]. Thermogravimetric diagrams of cellulose HTL hydrochar over residence time showed a flattened behaviour as illustrated in Fig. 5 (a). This change could be useful to estimate the non-reacted cellulose, as it has a strong and clear transformation from 280 °C to 350 °C. Indeed, Carrier et al. (2011) have used the TGA profile to determine the composition of α-cellulose in lignocellulosic biomass based on chemical structure differences [65]. In the present study, cellulose is the only component different from the hydrochar that should be present in the solid particles, making the quantification even clearer. Area integration of derivative TG (dTG) over temperatures using *trapz* function in Matlab transformation between 280 °C and 350 °C provide and approximation of unreacted cellulose remaining in the solid phase (shown in Fig. 5 (b and c). [65].

The effect of the HTL conversion on the relatively resistant crystalline structure of cellulose is also different to the monosaccharides [73]. Hydrolysis is a controlling reaction limiting the formation of intermediates. There also seems to be a reduction over the first 10 min from 100 to 10 µm (50% percentile of the distribution), follow by an increase in diameter to approximately 56 µm shown in Fig. 4 (C). However, as SEM images provided in the Supplementary Material Fig S.9 illustrates that cellulose hydrochar particles are more amorphous than the monosaccharide hydrochars and presented a relatively wider peak on the size distribution graph. Additionally, there were spheric particles attached to amorphous bigger particles in hydrochar with apparent differences in the O/C composition (EDS) from raw cellulose.

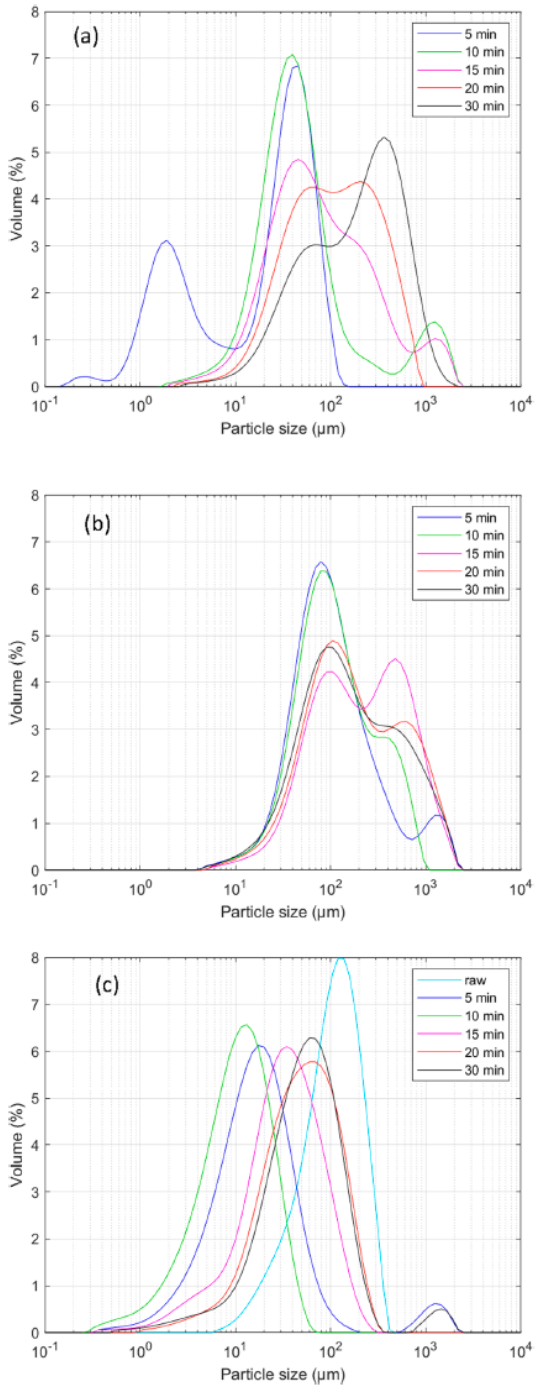

Fig. 4. Particle size distribution of the hydrochar from (a) glucose, (b) fructose and (c) cellulose HTL at 250 °C, over the residence time distribution.

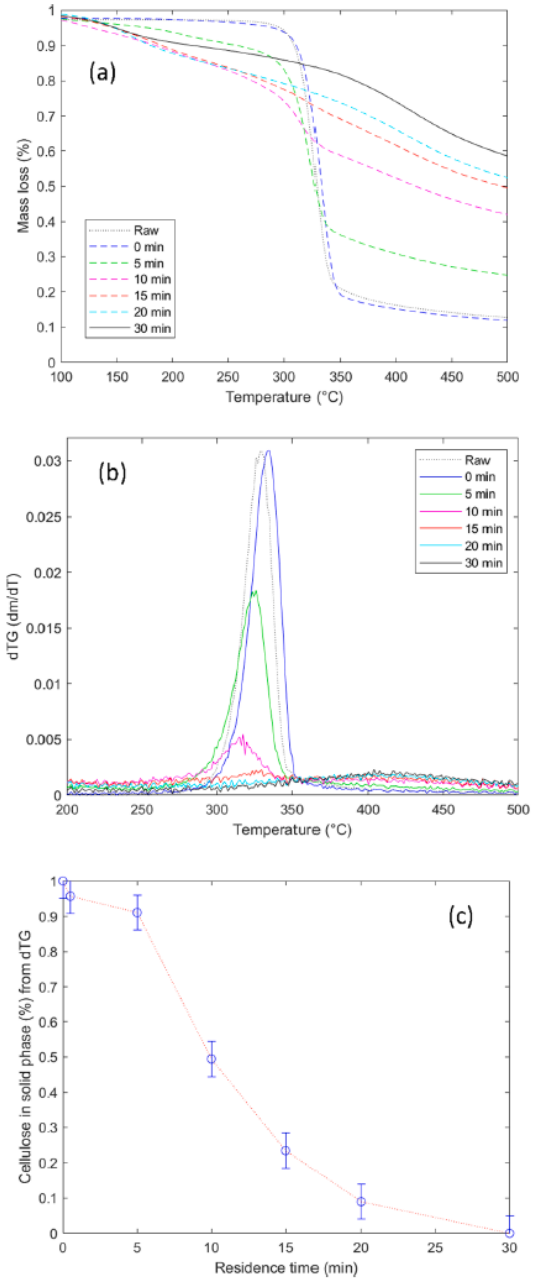

Fig. 5. Cellulose thermogravimetric mass loss for the HTL of cellulose at 250 °C (a), first derivate of TG (dTG) (b), and concentration estimation based on dTG (c).

This difference might support the two different reaction mechanism pathways of the polysaccharide, the secondary char or wet pathway (hydrolysis) and the solid-state transformation of primary char (carbonisation) from cellulose [15,31,32,73].

3.4. Multi-component and shrinking core reaction models for the HTL of cellulose

By including the residual cellulose in hydrochar product estimation, the reaction kinetic model is now complete. All organic species in the aqueous phase and the product phases could be modelled with the proposed mechanism illustrated in Fig. 6.

The differential equation system of the model is (where × is mass yield):

$$\frac{dx_1}{dt} = -(k_1+k_{22})x_1 + k_2x_2 + k_{23}x_{16} + k_{33}x_{17} \quad (1)$$

$$\frac{dx_2}{dt} = k_1x_1 - (k_2+k_3+k_5+k_7+k_8+k_9+k_{20})x_2 + k_4x_3 + k_6x_5 + k_{21}x_{16} \quad (2)$$

$$\frac{dx_3}{dt} = k_3x_2 + k_{11}x_6 + k_{13}x_4 - (k_4+k_{10}+k_{12}+k_{26})x_3 \quad (3)$$

$$\frac{dx_4}{dt} = k_{12}x_3 - k_{13}x_4 - k_{27}x_4 \quad (4)$$

$$\frac{dx_5}{dt} = k_5x_2 + k_{16}x_{12} - (k_6+k_{14}+k_{15}+k_{17})x_5 \quad (5)$$

$$\frac{dx_6}{dt} = k_7x_2 + k_{10}x_3 - (k_{11}+k_{26})x_6 \quad (6)$$

$$\frac{dx_7}{dt} = k_9x_2 - k_{32}x_7 \quad (7)$$

$$\frac{dx_8}{dt} = k_{14}x_5 - k_{19}x_8 \quad (8)$$

$$\frac{dx_9}{dt} = k_{19}x_8 \quad (9)$$

$$\frac{dx_{10}}{dt} = k_{19}x_8 \quad (10)$$

$$\frac{dx_{11}}{dt} = k_7x_2 + k_{12}x_3 + (k_{14}+k_{17})x_5 + k_{18}x_{12} - k_{29}x_{11} + k_{30}x_{15} \quad (11)$$

$$\frac{dx_{12}}{dt} = k_8x_2 + k_{15}x_5 - (k_{16}+k_{18}+k_{31})x_{12} \quad (12)$$

$$\frac{dx_{13}}{dt} = k_{17}x_5 + k_{18}x_{12} - k_{28}x_{13} \quad (13)$$

$$\frac{dx_{14}}{dt} = k_{26}x_3 + k_{27}x_4 + k_{25}x_6 + k_{32}x_7 + k_{31}x_{12} + k_{28}x_{13} + k_{24}x_{16} + k_{34}x_{17} - k_{35}x_{14} \quad (14)$$

$$\frac{dx_{15}}{dt} = k_{29}x_{11} - k_{30}x_{15} \quad (15)$$

$$\frac{dx_{16}}{dt} = k_{22}x_1 + k_{20}x_2 - (k_{21}+k_{23}+k_{24})x_{16} \quad (16)$$

$$\frac{dx_{17}}{dt} = -(k_{33}+k_{34})x_{17} + k_{35}x_{14} \quad (17)$$

x_1 to x_{17} correspond to mass yields of identified components in Fig. 6,

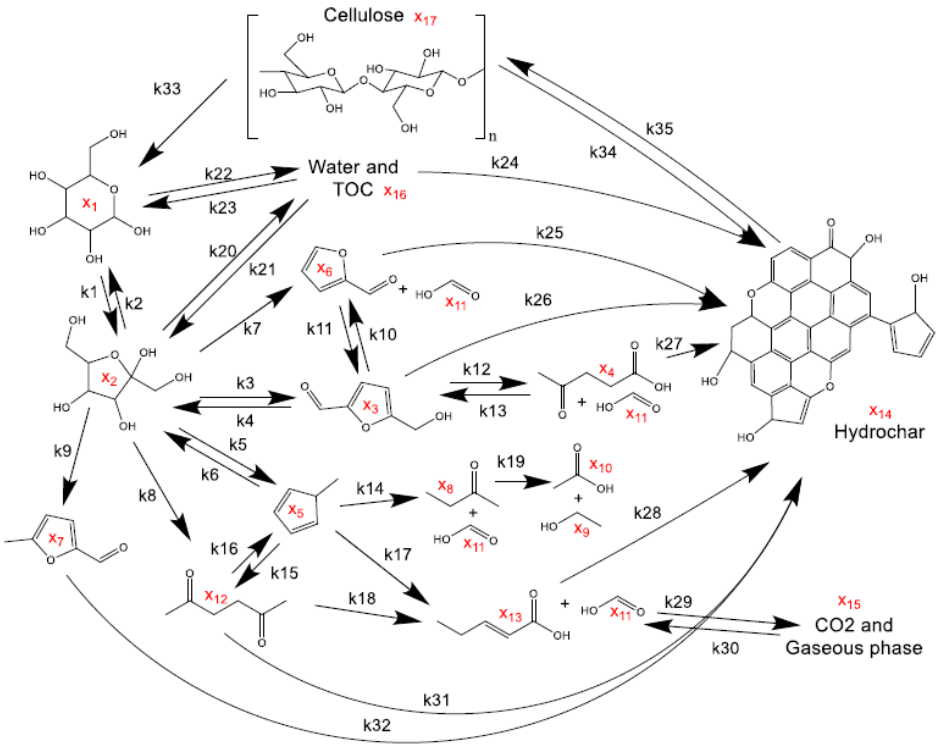

Fig. 6. Complete proposed reaction pathway model for the HTL of carbohydrates. *Note:* Hydrochar structure has been . adapted from [22,34]

named in Table. 1. For glucose and fructose experiments, x_{17} is not included, which also removes k_{33} to k_{35} out of the ODE system. As illustrated in Fig. 6, cellulose is supposed to produce only glucose as a product of hydrolysis, oligomers and other intermediate products are included in the TOC. However, cellulose also presented a direct solid reaction transformation, which is being investigated and discussed in the scientific literature [22,32,37,77]. It is also important to acknowledge the limitation of the *lsqcurvefit* function, which allows up to 37 unknown variables to fit per optimisation [78].

As shown in Fig. 7, the hydrolysis of cellulose is controlling the reaction and, in contrast to reaction kinetics of monosaccharides, the effect of temperature is not as severe. However, at 300 °C, the abundance of intermediates in the aqueous phase is limited because of the high reactivity of monosaccharides and intermediates [44,52,73,74,79,80]. From the two temperatures tested, the difference in glucose as the main intermediate of cellulose hydrolysis is reduced from 65.4 to 0.36 mg/ml as the highest glucose concentrations reported at 250 and 300 °C respectively, these results may suggest that temperature closer and over 300 °C is not ideal for the conversion of polysaccharides, as the concentration of intermediates in the aqueous phase would be negligible [9,51,81]. High temperature conversion may promote the direct solid transformation (carbonisation) of polysaccharides, preventing monosaccharides and intermediates to interact with other biomass structures

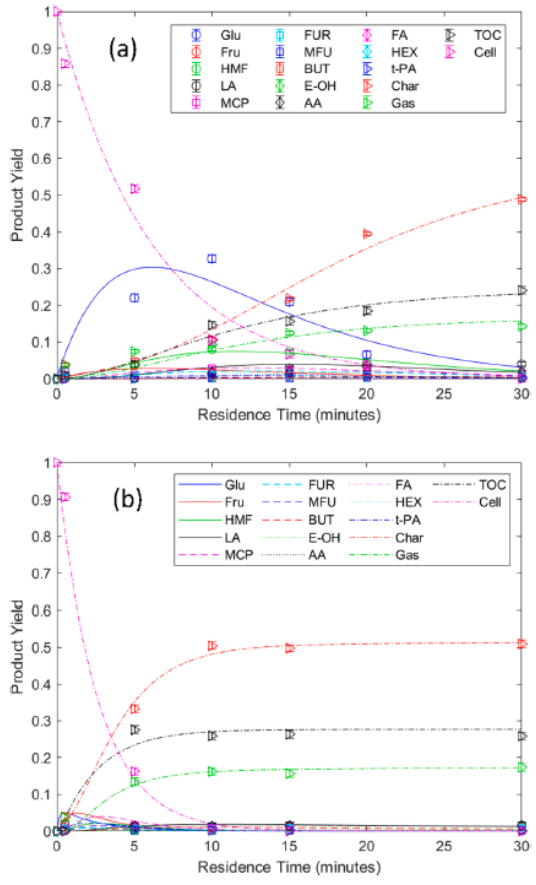

Fig. 7. Experimental points and modelled concentration profiles for the HTL of cellulose at 250 °C (a) and at 300 °C (b).

to form structures that may enrich the renewable crude yields (Maillard reaction) while increasing the complexity of the separation [8,82,83]. This might be the reason for a two-step HTL process with low initial temperature to break and hydrolyse the bio-macromolecules in the first stage, and higher temperature at a second stage, to promote the interaction and re-condensation of valuable product phases [1,84].

Some studies have modelled the hydrothermal conversion of cellulose as a shrinking core reaction based on the characteristic decomposition of the natural polymer. However, as the crystalline cellulose has no porosity, the diffusion of water is limited to the surface of the modelled particle [17,44–46,52]. To the best of our knowledge, none of the shrinking core approximations up-to-date have presented experimental data of the particle size distribution. Additionally, suggested models only incorporate the hydrolysis of cellulose and the mass transfer (diffusion) coefficient. The effect of hydrochar formation is not captured in the models [44,46]. If the 50% percentile of the particle size distributions from the HTL of cellulose at 250 °C (Fig. 4(c)) are analysed with the concentrations of cellulose, glucose and hydrochar (Fig. 7(a)). A functional shrinking core model based on product yield concentrations can be produced as illustrated in Fig. 8.

The suggested model is a combination of hydrolysis, glucose diffusion at the surface and hydrochar formation, as one first order reaction based on the product yield profiles for the three components as shown in Eq. (18) to (20) [71]. With the correspondent optimised constraints, illustrated in Fig. 8 (c). The model is then simplified to Eq. (21). To integrate the initial particle size R_0, final particle size R, and the maximum diffusion rate of glucose at the surface Δr, as a function of the normalised yield of each of the three components [44,46,71]. The model is a simplified representation of the 50% percentile particle size of the solid products from the HTL of cellulose. It is possible because of the mono-modal distribution and relatively similar full width at half maximum (FWHM), shown in Fig. 4(c).

$$Particlesize = Cellulose_{hydrolysis} - Glucose_{difussionatsurface} + Char_{formation}$$

$$\rho\frac{d}{dt}\left(\frac{4}{3}\pi r^3\right) = b_1{*}\frac{dx_{17}}{dt} - b_2{*}\frac{dx_1}{dt} + b_3{*}\frac{dx_{14}}{dx} = \rho\frac{d\varphi}{dt} \tag{19}$$

The optimisation of the equation model using *lsqcurvefit* to fit the constants b with the 50% percentile particle size and concentrations profile produce the next results.

$$\rho\frac{d\varphi}{dt} = 102.7{*}\frac{dx_{17}}{dt} - 40.47{*}\frac{dx_1}{dt} + 114.69{*}\frac{dx_{14}}{dx} \tag{20}$$

$$\rho\frac{d\varphi}{dr} = R_0{*}\frac{dx_{17}}{dt} - \left(\frac{\Delta r}{x_1^{max}}\right){*}\frac{dx_1}{dt} + \left(\frac{R}{x_{14}^{\infty}}\right){*}\frac{dx_{14}}{dx} \tag{21}$$

$$\rho\int_{R_0}^{r}\frac{d\varphi}{dr} = \rho\int_0^t\frac{d\varphi}{dt} = 102.7{*}\int_0^t\frac{dx_{cell}}{dt} - \left(\frac{13.27}{x_{glu}^{max}}\right){*}\int_0^t\frac{dx_{glu}}{dt} + \left(\frac{56.04}{x_{char}^{\infty}}\right){*}\int_0^t\frac{dx_{char}}{dt} \tag{22}$$

3.5. Co-liquefaction with ethanol to produce high-value organics

Ethanol has been assessed to increase the renewable crude yield during HTL. However, the reaction mechanisms involved are not completely clear [61]. Ethanol may produce transesterification of triglycerides from lipids (under acidic conditions) and promote the formation of amides and amines, increasing the renewable crude yield from protein by the alkylation/etherification ability of alcohols [61–64,74]. The addition of ethanol as a co-solvent and homogeneous catalyst in the HTL co-conversion of carbohydrates has not been considered before to produce valuable aqueous soluble organics [61,85]. HPLC chromatograms of aqueous phase from the HTL of glucose, fructose, and cellulose at 250 °C from the co-liquefaction with ethanol are shown in

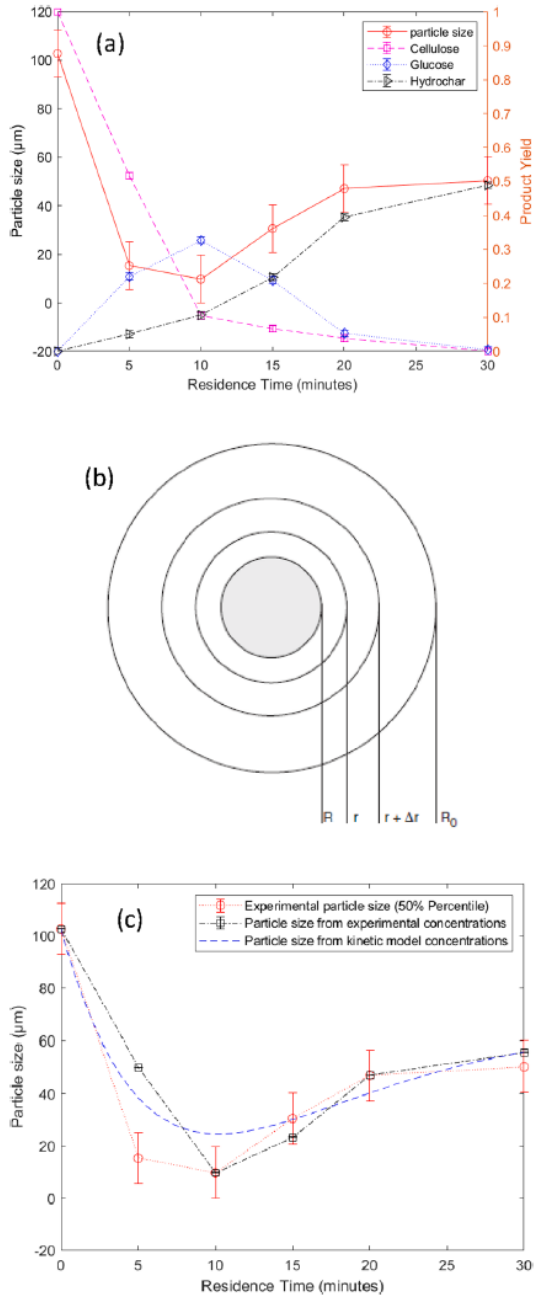

Fig. 8. Experimental particle size and concentration profiles for the HTL of cellulose at 250 °C (a), a shrinking core schematic diagram for spheres [71] (b), the shrinking core modelled results from data and kinetic model (c).

Supplementary Material Fig S.10. These chromatograms present larger and sharper peaks (with larger peak area) than the corresponding plain HTL in Supplementary Material Fig S.3, which might serve as an indication of the synergetic effect of ethanol near the critical point and the reduction in hydrochar due to the alkylation effect [59,61,74,85–87].

The concentration of glucose from the HTL of glucose experiment presented a reduction from 125.8 to 70.9 mg/ml at zero residence time by including the co-solvent and homogeneous catalyst system [13,26]. The concentration of fructose was increased from 5.1 to 12.5 mg/ml. Additionally, concentrations of 59.8, 93.6, 31.3 and 11.9 mg/ml for fructose, 5-HMF, methyl cyclopentadiene and furfural respectively, at zero residence time for the HTL of fructose. These values may confirm the positive effect of ethanol to reduce the decomposition of fructose as a highly reactive monosaccharide and intermediate with nearly half of the initial feedstock mass concentration converted into 5-HMF, which is the source of a promising synthetic biofuels [14,15,55,58,86].

Ethanol seems to promote isomerisation into fructose, which reduces the cleavage of this highly reactive intermediate [13,14,61]. Furthermore, there was a new peak at 63.5 min, which follows a similar pattern to the 5-HMF concentration and may correspond to etherification of 5-HMF because of the alkylation/etherification ability of ethanol. If this new peak is semi-quantified (with the 5-HMF standard calibration) concentrations of 9 mg/ml for glucose HTL at zero residence time and 14.5 mg/ml for fructose HTL at 5 min could be good estimations. 5-ethoxymethyl furfural (5-EMF) has been investigated in the literature as a potential fuel additive and component for biodiesel production [55,57–59]. However, heterogeneous solid acid catalysis such as Amberlyst-131 and MCM-41 among others have been integrated in the reaction formation from 5-HMF with ethanol [57,58,86,88,89]. The actual in-situ co-liquefaction only involves near critical point ethanol and subcritical water (with relatively high acidity due to the cleavage of saccharides). The presence of 5-ethoxymethyl furfural and ethyl levulinate (EL) was established (tentative identification) with the GC–MS analysis to one product sample from the HTL co-conversions of glucose with ethanol. Ethyl levulinate was contrasted with the NIST14 library, but the mass spectrum of 5-EMF was not found in the literature. The identification is based on a mass-to-charge ratio of 154.1 with many similarities to the 5-HMF fragmentation spectrum, as illustrated in the Supplementary Material Fig S.12.

The experimental and modelled concentrations are presented in Fig. 9. The initial concentrations of ethanol and acetic acid added to the reaction were subtracted from the model to centre the product yields on the feedstock conversion. Cellulose showed a distinct pattern over the co-liquefaction as the hydrolysis of the glycosidic bond of cellulose rules the reaction. The decomposition of cellulose was reduced. However, at 10 min residence time, the concentration of glucose was increased from 65.4 to 104.3 mg/ml with the co-solvent. Similarly, the concentrations of intermediates were relatively higher with ethanol. The effect of ethanol with carbohydrates seems to be mostly catalytic, as the changes in ethanol concentration were negligible (based on the initial concentration of ethanol as feedstock), reducing the high reactivity of the furanic structures. However, a delay of 1.37 min on the MS detector to prevent signal saturation due to the high concentration of water and ethanol might have probably missed smaller compounds like diethyl ether which are known to be formed from ethanol dehydration in acid hydrothermal conditions [87].

Undeniably the concentrations of valuable intermediates were higher by including ethanol and acetic acid in a co-liquefaction of carbohydrates, and more intermediates in the aqueous phase could probably result in more interactions with proteins and lipids to increase the renewable crude yield as the desirable product of HTL rather than undesirable solid products. Future work should consider the continuous hydrothermal conversion of saccharides and co-liquefaction of rich-carbohydrates biomass sources to produce valuable soluble organics, and the recovery of 5-EMF, EL and ethanol from the aqueous phase. Interactions like Maillard reaction should also be considered and they play a crucial role limiting the formation of 5-EMF and EL [52,84,90–93].

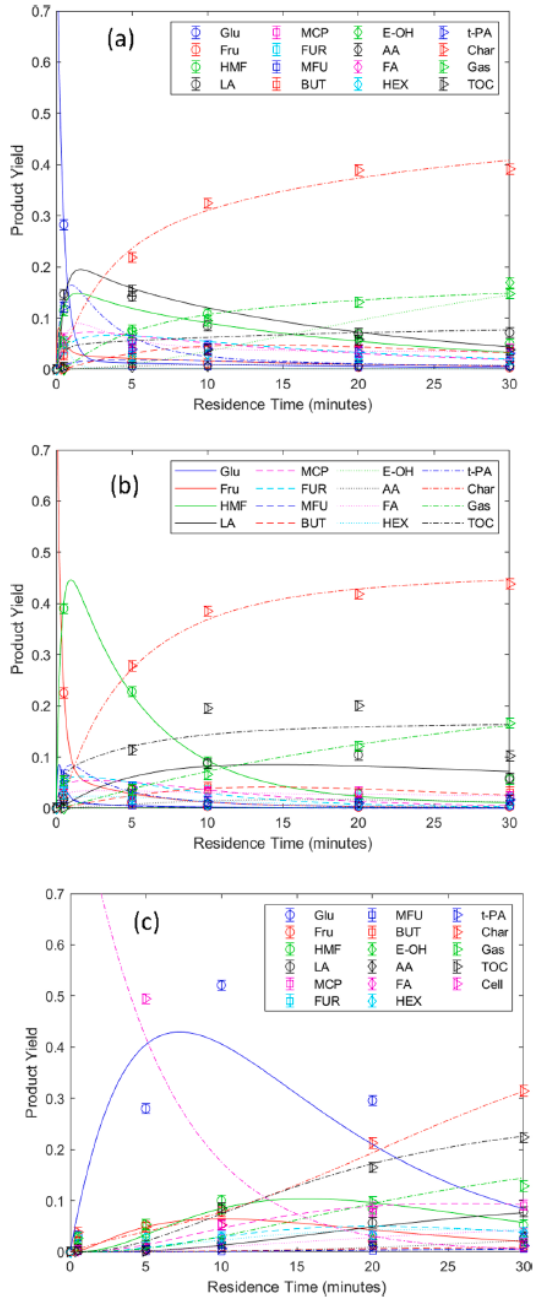

Fig. 9. Experimental points and modelled concentration profiles for the co-liquefaction of glucose (a), fructose (b) and cellulose (c) with ethanol at 250 °C.

4. Conclusion

The composition of the most abundant organic species in the aqueous phase from the HTL of carbohydrates over a residence time distribution was analysed using GC–MS and HPLC. The product profiles were included in a multi-component reaction mechanism and kinetics model, including all the product phases of the HTL conversion. Furthermore, the solid products have been characterised using TG-MS, particle size distribution and SEM/EDS to integrate the effect of subcritical water in hydrochar formation with the aqueous product interactions. Then the composition of cellulose hydrochar was estimated based on the thermal degradation of cellulose and glucose hydrochar. The estimation was integrated into the reaction kinetics model of the polysaccharide to complete the reaction mechanism by differentiating unreacted cellulose from hydrochar in the solid products, and to suggest a shrinking core model based on hydrolysis of cellulose, diffusion of glucose, and hydrochar formation to predict the 50% percentile particle size. Finally, the co-liquefaction of carbohydrates with ethanol lightens the production of 5-ehtoxymethyl furfural and ethyl levulinate, two promising renewable organics with potential applications as fuel additives and monomer for a new generation of sustainable products from carbohydrates.

CRediT authorship contribution statement

Andrés Chacón-Parra: Conceptualization, Investigation, Methodology, Formal analysis, Data curation, Writing – original draft. **David Lewis:** Supervision, Funding acquisition, Writing – review & editing. **Marianne Glasius:** Data curation, Validation, Writing – review & editing. **Philip van Eyk:** Supervision, Conceptualization, Resources, Writing – review & editing.

Declaration of Competing Interest

The authors declare that they have no known competing financial interests or personal relationships that could have appeared to influence the work reported in this paper.

Acknowledgments

The authors acknowledge the financial support of the Australian Research Council's Linkage Project grant (LP150101241) with industry partner Southern Oil Refining, and the contribution of Tony Hall (from the Faculty of Sciences of The University of Adelaide) with unbiased GC-MS analysis and tentative identification of organic compounds.

Appendix A. Supplementary data

Supplementary data to this article can be found online at https://doi.org/10.1016/j.fuel.2021.122499.

References

[1] Biller P, Ross AB, et al. In: *17 - Production of biofuels via hydrothermal conversion*, in *Handbook of Biofuels Production (Second Edition)*. Woodhead Publishing; 2016. p. 509–47.
[2] Kruse A, Funke A, Titirici M-M. Hydrothermal conversion of biomass to fuels and energetic materials. Curr Opin Chem Biol 2013;17(3):515–21.
[3] Titirici M-M, Funke A, Kruse A. *Hydrothermal Carbonisation of Biomass*, in *Recent Advances in Thermo-Chemical Conversion of*. Biomass. 2015:325–52.
[4] Peterson AA, Vogel F, Lachance RP, Fröling M, Antal, Jr. MJ, Tester JW. Thermochemical biofuel production in hydrothermal media: A review of sub- and supercritical water technologies. Energy Environ. Sci. 2008;1(1):32. https://doi.org/10.1039/b810100k.
[5] Gollakota ARK, Kishore N, Gu S. A review on hydrothermal liquefaction of biomass. Renew. Sustain. Energy Rev. 2018;81:1378–92.
[6] Xu L, (Wim) Brilman DWF, Withag JAM, Brem G, Kersten S. Assessment of a dry and a wet route for the production of biofuels from microalgae: Energy balance analysis. Bioresour. Technol. 2011;102(8):5113–22.
[7] Obeid R, Lewis DM, Smith N, Hall T, van Eyk P. Reaction kinetics and characterisation of species in renewable crude from hydrothermal liquefaction of monomers to represent organic fractions of biomass feedstocks. Chem. Eng. J. 2020;389:124397. https://doi.org/10.1016/j.cej.2020.124397.
[8] Teri G, Luo L, Savage PE. Hydrothermal Treatment of Protein, Polysaccharide, and Lipids Alone and in Mixtures. Energy Fuels 2014;28(12):7501–9.
[9] Sasaki M, Fang Z, Fukushima Y, Adschiri T, Arai K. Dissolution and Hydrolysis of Cellulose in Subcritical and Supercritical Water. Ind. Eng. Chem. Res. 2000;39(8):2883–90.

Chapter 5 - A multi-component reaction kinetics model for the hydrothermal liquefaction of carbohydrates and co-liquefaction to produce 5-ethoxymethyl furfural

[10] Srokol Z, Bouche A-G, van Estrik A, Strik RCJ, Maschmeyer T, Peters JA. Hydrothermal upgrading of biomass to biofuel; studies on some monosaccharide model compounds. Carbohydr Res 2004;339(10):1717–26.
[11] Matsumura Y, Yanachi S, Yoshida T. Glucose Decomposition Kinetics in Water at 25 MPa in the Temperature Range of 448–673 K. Ind. Eng. Chem. Res. 2006;45(6): 1875–9.
[12] Knežević D, van Swaaij WPM, Kersten SRA. Hydrothermal Conversion of Biomass: I, Glucose Conversion in Hot Compressed Water. Ind. Eng. Chem. Res. 2009;48 (10):4731–43.
[13] Poerschmann J, Weiner B, Koehler R, Kopinke F-D. Hydrothermal Carbonization of Glucose, Fructose, and Xylose—Identification of Organic Products with Medium Molecular Masses. ACS Sustainable Chem. Eng. 2017;5(8):6420–8.
[14] Jung D, Zimmermann M, Kruse A. Hydrothermal Carbonization of Fructose: Growth Mechanism and Kinetic Model. ACS Sustainable Chem. Eng. 2018;6(11): 13877–87.
[15] Girisuta B, Janssen LPBM, Heeres HJ. Kinetic Study on the Acid-Catalyzed Hydrolysis of Cellulose to Levulinic Acid. Ind. Eng. Chem. Res. 2007;46(6): 1696–708.
[16] Patil SKR, Heltzel J, Lund CRF. Comparison of Structural Features of Humins Formed Catalytically from Glucose, Fructose, and 5-Hydroxymethylfurfuraldehyde. Energy Fuels 2012;26(8):5281–93.
[17] Burnham AK, Zhou X, Broadbelt LJ. Critical Review of the Global Chemical Kinetics of Cellulose Thermal Decomposition. Energy Fuels 2015;29(5):2906–18.
[18] Madsen RB, Biller P, Jensen MM, Becker J, Iversen BB, Glasius M. Predicting the Chemical Composition of Aqueous Phase from Hydrothermal Liquefaction of Model Compounds and Biomasses. Energy Fuels 2016;30(12):10470–83.
[19] Madsen RB, Jensen MM, Mørup AJ, Houlberg K, Christensen PS, Klemmer M, et al. Using design of experiments to optimize derivatization with methyl chloroformate for quantitative analysis of the aqueous phase from hydrothermal liquefaction of biomass. Anal Bioanal Chem 2016;408(8):2171–83.
[20] Madsen RB, Glasius M. How Do Hydrothermal Liquefaction Conditions and Feedstock Type Influence Product Distribution and Elemental Composition? Ind. Eng. Chem. Res. 2019;58(37):17583–600.
[21] Kambo HS, Dutta A. A comparative review of biochar and hydrochar in terms of production, physico-chemical properties and applications. Renew. Sustain. Energy Rev. 2015;45:359–78.
[22] Baccile, N., et al., *Characterisation of Hydrothermal Carbonisation Materials*, in *Sustainable Carbon Materials from Hydrothermal Processes*. 2013. p. 151-211.
[23] Titirici M-M, White RJ, Falco C, Sevilla M. Black perspectives for a green future: hydrothermal carbons for environment protection and energy storage. Energy Environ. Sci. 2012;5(5):6796. https://doi.org/10.1039/c2ee21166a.
[24] Girisuta B, Janssen LPBM, Heeres HJ. A kinetic study on the decomposition of 5-hydroxymethylfurfural into levulinic acid. Green Chem. 2006;8(8):701–9.
[25] vanZandvoort I, Wang Y, Rasrendra CB, vanEck ERH, Bruijnincx PCA, Heeres HJ, et al. Formation, molecular structure, and morphology of humins in biomass conversion: influence of feedstock and processing conditions. ChemSusChem 2013; 6(9):1745–58.
[26] Rasmussen H, Sørensen HR, Meyer AS. Formation of degradation compounds from lignocellulosic biomass in the biorefinery: sugar reaction mechanisms. Carbohydr Res 2014;385:45–57.
[27] Zhang Mu, Yang H, Liu Y, Sun X, Zhang D, Xue D. First identification of primary nanoparticles in the aggregation of HMF. Nanoscale Res. Lett. 2012;7(1). https://doi.org/10.1186/1556-276X-7-38.
[28] Tsilomelekis G, Orella MJ, Lin Z, Cheng Z, Zheng W, Nikolakis V, et al. Molecular structure, morphology and growth mechanisms and rates of 5-hydroxymethyl furfural (HMF) derived humins. Green Chem. 2016;18(7):1983–93.
[29] Patil SKR, Lund CRF. Formation and Growth of Humins via Aldol Addition and Condensation during Acid-Catalyzed Conversion of 5-Hydroxymethylfurfural. Energy Fuels 2011;25(10):4745–55.
[30] He Q, Yu Y, Wang J, Suo X, Liu Y. Kinetic Study of the Hydrothermal Carbonization Reaction of Glucose and Its Product Structures. Ind. Eng. Chem. Res. 2021;60(12): 4552–61.
[31] Sevilla M, Fuertes AB. The production of carbon materials by hydrothermal carbonization of cellulose. Carbon 2009;47(9):2281–9.
[32] Falco C, Baccile N, Titirici MM. Morphological and structural differences between glucose, cellulose and lignocellulosic biomass derived hydrothermal carbons. Green Chem. 2011;13(11):3273–81.
[33] Sevilla M, Fuertes A. Chemical and structural properties of carbonaceous products obtained by hydrothermal carbonization of saccharides. Chemistry 2009;15(16): 4195–203.
[34] Baccile N, Laurent G, Babonneau F, Fayon F, Titirici M-M, Antonietti M. Structural Characterization of Hydrothermal Carbon Spheres by Advanced Solid-State MAS 13C NMR Investigations. The Journal of Physical Chemistry C 2009;113(22): 9644–54.
[35] Dussan K, Girisuta B, Haverty D, Leahy JJ, Hayes MHB. Kinetics of levulinic acid and furfural production from Miscanthus×giganteus. Bioresour. Technol. 2013; 149:216–24.
[36] Yang W, Shimanouchi T, Wu S, Kimura Y. Investigation of the Degradation Kinetic Parameters and Structure Changes of Microcrystalline Cellulose in Subcritical Water. Energy Fuels 2014;28(11):6974–80.
[37] Dinjus E, Kruse A, Tröger N. Hydrothermal Carbonization - 1. Influence of Lignin in Lignocelluloses. Chem. Eng. Technol. 2011;34(12):2037–43.
[38] Jatzwauck M, Schumpe A. Kinetics of hydrothermal carbonization (HTC) of soft rush. Biomass Bioenergy 2015;75:94–100.
[39] Funke A, Ziegler F. Hydrothermal carbonization of biomass: A summary and discussion of chemical mechanisms for process engineering. Biofuels, Bioprod. Biorefin. 2010;4(2):160–77.
[40] Bobleter O. Hydrothermal degradation of polymers derived from plants. Prog. Polym. Sci. 1994;19(5):797–841.
[41] Reza MT, Yan W, Uddin MH, Lynam JG, Hoekman SK, Coronella CJ, et al. Reaction kinetics of hydrothermal carbonization of loblolly pine. Bioresour Technol 2013; 139:161–9.
[42] Martinez-Fernandez JS, Chen S. Sequential Hydrothermal Liquefaction characterization and nutrient recovery assessment. Algal Research 2017;25: 274–84.
[43] Obeid R, Lewis D, Smith N, van Eyk P. The elucidation of reaction kinetics for hydrothermal liquefaction of model macromolecules. Chem. Eng. J. 2019;370: 637–45.
[44] Kamio E, Sato H, Takahashi S, Noda H, Fukuhara C, Okamura T. Liquefaction kinetics of cellulose treated by hot compressed water under variable temperature conditions. J. Mater. Sci. 2008;43(7):2179–88.
[45] Galgano A, Blasi CD. Modeling Wood Degradation by the Unreacted-Core-Shrinking Approximation. Ind. Eng. Chem. Res. 2003;42(10):2101–11.
[46] Jayathilake M, Rudra S, Rosendahl LA. Hydrothermal liquefaction of wood using a modified multistage shrinking-core model. Fuel 2020;280:118616.
[47] Chuntanapum A, Matsumura Y. Char Formation Mechanism in Supercritical Water Gasification Process: A Study of Model Compounds. Ind. Eng. Chem. Res. 2010;49 (9):4055–62.
[48] Chuntanapum A, Matsumura Y. Formation of Tarry Material from 5-HMF in Subcritical and Supercritical Water. Ind. Eng. Chem. Res. 2009;48(22):9837–46.
[49] Antal MJ, Mok WSL, Richards GN. Mechanism of formation of 5-(hydroxymethyl)-2-furaldehyde from d-fructose and sucrose. Carbohydr. Res. 1990;199(1):91–109.
[50] García-Bordejé E, Pires E, Fraile JM. Parametric study of the hydrothermal carbonization of cellulose and effect of acidic conditions. Carbon 2017;123: 421–32.
[51] Yin S, Tan Z. Hydrothermal liquefaction of cellulose to bio-oil under acidic, neutral and alkaline conditions. Appl. Energy 2012;92:234–9.
[52] Paksung N, Pfersich J, Arauzo PJ, Jung D, Kruse A. Structural Effects of Cellulose on Hydrolysis and Carbonization Behavior during Hydrothermal Treatment. ACS Omega 2020;5(21):12210–23.
[53] Knežević D, et al. High-Throughput Screening Technique for Conversion in Hot Compressed Water: Quantification and Characterization of Liquid and Solid Products. Ind. Eng. Chem. Res. 2007;46(6):1810–7.
[54] Gollakota A, Savage PE. Fast and Isothermal Hydrothermal Liquefaction of Polysaccharide Feedstocks. ACS Sustainable Chem. Eng. 2020;8(9):3762–72.
[55] Liu X, Wang R. In: Biomass, Biofuels, Biochemicals. Elsevier; 2020. p. 355–75. https://doi.org/10.1016/B978-0-444-64307-0.00013-5.
[56] Qi L, Mui YF, Lo SW, Lui MY, Akien GR, Horváth IT. Catalytic Conversion of Fructose, Glucose, and Sucrose to 5-(Hydroxymethyl)furfural and Levulinic and Formic Acids in γ-Valerolactone As a Green Solvent. ACS Catal. 2014;4(5):1470–7.
[57] Allen, M.C., *Creating Renewable Tunable Polymers from Hydroxymethylfurfural*, in *Chemical Engineering*. 2017, University of Maine: Electronic Theses and Dissertations.
[58] Zhu C, Wang H, Liu Q, Wang C, Xu Y, Zhang Qi, et al. In: Biomass, Biofuels, Biochemicals. Elsevier; 2020. p. 61–94. https://doi.org/10.1016/B978-0-444-64307-0.00003-2.
[59] Xiang Y, Wen S, Tian Yi, Zhao K, Guo D, Cheng F, et al. Efficient synthesis of 5-ethoxymethylfurfural from biomass-derived 5-hydroxymethylfurfural over sulfonated organic polymer catalyst. RSC Adv. 2021;11(6):3585–95.
[60] Unlu D, Durmaz Hilmioglu N. Synthesis of Ethyl Levulinate as a Fuel Bioadditive by a Novel Catalytically Active Pervaporation Membrane. Energy Fuels 2016;30(4): 2997–3003.
[61] Cheng S, D'cruz I, Wang M, Leitch M, Xu C(. Highly Efficient Liquefaction of Woody Biomass in Hot-Compressed Alcohol−Water Co-solvents†. Energy Fuels 2010;24(9):4659–67.
[62] Tan KT, Gui MM, Lee KT, Mohamed AR. An optimized study of methanol and ethanol in supercritical alcohol technology for biodiesel production. The Journal of Supercritical Fluids 2010;53(1-3):82–7.
[63] Chacón-Parra A, Lewis D, van Eyk P. The effect of ethanol as a homogeneous catalyst on the reaction kinetics of hydrothermal liquefaction of lipids. Chem. Eng. J. 2021;414:128832.
[64] Chacón-Parra A, Lewis D, van Eyk P. Elemental nitrogen balance, reaction kinetics and the effect of ethanol on the hydrothermal liquefaction of soy protein. Chem. Eng. J. 2021;425:130576. https://doi.org/10.1016/j.cej.2021.130576.
[65] Carrier M, Loppinet-Serani A, Denux D, Lasnier J-M, Ham-Pichavant F, Cansell F, et al. Thermogravimetric analysis as a new method to determine the lignocellulosic composition of biomass. Biomass Bioenergy 2011;35(1):298–307.
[66] Sasaki M, Adschiri T, Arai K. Kinetics of cellulose conversion at 25 MPa in sub- and supercritical water. AIChE J. 2004;50(1):192–202.
[67] Jayaraman K, Kok MV, Gokalp I. Thermogravimetric and mass spectrometric (TG-MS) analysis and kinetics of coal-biomass blends. Renewable Energy 2017;101: 293–300.
[68] Beers, K.J., *Numerical Methods for Chemical Engineering: Applications in MATLAB*. 2006: Cambridge University Press.
[69] Llano T, Quijorna N, Andrés A, Coz A. Sugar, acid and furfural quantification in a sulphite pulp mill: Feedstock, product and hydrolysate analysis by HPLC/RID. Biotechnol Rep (Amst) 2017;15:75–83.
[70] Riazi, M.R., *Characterisation and Properties of Petroleum Fractions*. 2005: ASTM International.
[71] Fogler, H.S., *Elements of Chemical Reaction Engineering*. 2006: Prentice Hall PTR.

Chapter 5 - A multi-component reaction kinetics model for the hydrothermal liquefaction of carbohydrates and co-liquefaction to produce 5-ethoxymethyl furfural

[72] Titirici M-M, Antonietti M, Baccile N. Hydrothermal carbon from biomass: a comparison of the local structure from poly- to monosaccharides and pentoses/hexoses. Green Chem. 2008;10(11):1204–12.
[73] Möller M, Harnisch F, Schröder U. Hydrothermal liquefaction of cellulose in subcritical water—the role of crystallinity on the cellulose reactivity. RSC Adv. 2013;3(27):11035–44.
[74] Ruppert AM, Weinberg K, Palkovits R. Hydrogenolysis goes bio: from carbohydrates and sugar alcohols to platform chemicals. Angew Chem Int Ed Engl 2012;51(11):2564–601.
[75] Luijkx GCA, van Rantwijk F, van Bekkum H. Hydrothermal formation of 1,2,4-benzenetriol from 5-hydroxymethyl-2-furaldehyde and d-fructose. Carbohydr. Res. 1993;242:131–9.
[76] Polte J. Fundamental growth principles of colloidal metal nanoparticles – a new perspective. CrystEngComm 2015;17(36):6809–30.
[77] Jatzwauck, M.S., *Kinetik der Hydrothermalen Karbonisierung von Modellsubstanzen und Biomassen*. 2015.
[78] Law, V.J., *Numerical Methods for Chemical Engineers Using Excel, VBA, and MATLAB*. 2013: CRC Press, Taylor & Francis Group.
[79] Karayıldırım T, Sınağ A, Kruse A. Char and Coke Formation as Unwanted Side Reaction of the Hydrothermal Biomass Gasification. Chem. Eng. Technol. 2008;31(11):1561–8.
[80] Álvarez-Murillo A, Sabio E, Ledesma B, Román S, González-García CM. Generation of biofuel from hydrothermal carbonization of cellulose. *Kinetics modelling*. Energy 2016;94:600–8.
[81] Lu X, Pellechia PJ, Flora JRV, Berge ND. Influence of reaction time and temperature on product formation and characteristics associated with the hydrothermal carbonization of cellulose. Bioresour. Technol. 2013;138:180–90.
[82] Obeid R, Lewis DM, Smith N, Hall T, van Eyk P. Reaction Kinetics and Characterization of Species in Renewable Crude from Hydrothermal Liquefaction of Mixtures of Polymer Compounds To Represent Organic Fractions of Biomass Feedstocks. Energy Fuels 2020;34(1):419–29.
[83] Lu J, Liu Z, Zhang Y, Savage PE. 110th Anniversary: Influence of Solvents on Biocrude from Hydrothermal Liquefaction of Soybean Oil, Soy Protein, Cellulose, Xylose, and Lignin, and Their Quinary Mixture. Ind. Eng. Chem. Res. 2019;58(31):13971–6.
[84] Jazrawi C, Biller P, He Y, Montoya A, Ross AB, Maschmeyer T, et al. Two-stage hydrothermal liquefaction of a high-protein microalga. Algal Research 2015;8:15–22.
[85] Isa KM, Abdullah TAT, Ali UFM. Hydrogen donor solvents in liquefaction of biomass: A review. Renew. Sustain. Energy Rev. 2018;81:1259–68.
[86] Flannelly T, Dooley S, Leahy JJ. Reaction Pathway Analysis of Ethyl Levulinate and 5-Ethoxymethylfurfural fromd-Fructose Acid Hydrolysis in Ethanol. Energy Fuels 2015;29(11):7554–65.
[87] Aghbashlo M, et al. Exergy, economic, and environmental assessment of ethanol dehydration to diesel fuel additive diethyl ether. Fuel 2022;308:121918.
[88] Morales G, Melero JA, Paniagua M, Iglesias J, Hernández B, Sanz M. Sulfonic acid heterogeneous catalysts for dehydration of C6-monosaccharides to 5-hydroxymethylfurfural in dimethyl sulfoxide. Chin. J. Catal. 2014;35(5):644–55.
[89] Morales G, Paniagua M, Melero JA, Iglesias J. Efficient production of 5-ethoxymethylfurfural from fructose by sulfonic mesostructured silica using DMSO as co-solvent. Catal. Today 2017;279:305–16.
[90] Fan Y, Hornung U, Dahmen N, Kruse A. Hydrothermal liquefaction of protein-containing biomass: study of model compounds for Maillard reactions. Biomass Convers. Biorefin. 2018;8(4):909–23.
[91] Qiu Yi, Aierzhati A, Cheng J, Guo H, Yang W, Zhang Y. Biocrude Oil Production through the Maillard Reaction between Leucine and Glucose during Hydrothermal Liquefaction. Energy Fuels 2019;33(9):8758–65.
[92] Zhang C, Tang X, Sheng L, Yang X. Enhancing the performance of Co-hydrothermal liquefaction for mixed algae strains by the Maillard reaction. Green Chem. 2016;18(8):2542–53.
[93] Hietala DC, Savage PE. A molecular, elemental, and multiphase kinetic model for the hydrothermal liquefaction of microalgae. Chem. Eng. J. 2021;407:127007. https://doi.org/10.1016/j.cej.2020.127007.

A multi-component reaction kinetics model for the hydrothermal liquefaction of carbohydrates and co-liquefaction to produce 5-ethoxymethyl furfural

Andrés Chacón-Parra, † David Lewis, † Marianne Glasius, ‡ Philip van Eyk†

† School of Chemical Engineering and Advanced Materials,

The University of Adelaide, Adelaide, SA, 5005, Australia

‡ Department of Chemistry, Aarhus University,

Langelandsgade 140, 8000 Aarhus C, Denmark

*Corresponding author

E-mail address: philip.vaneyk@adelaide.edu.au

Supplementary material

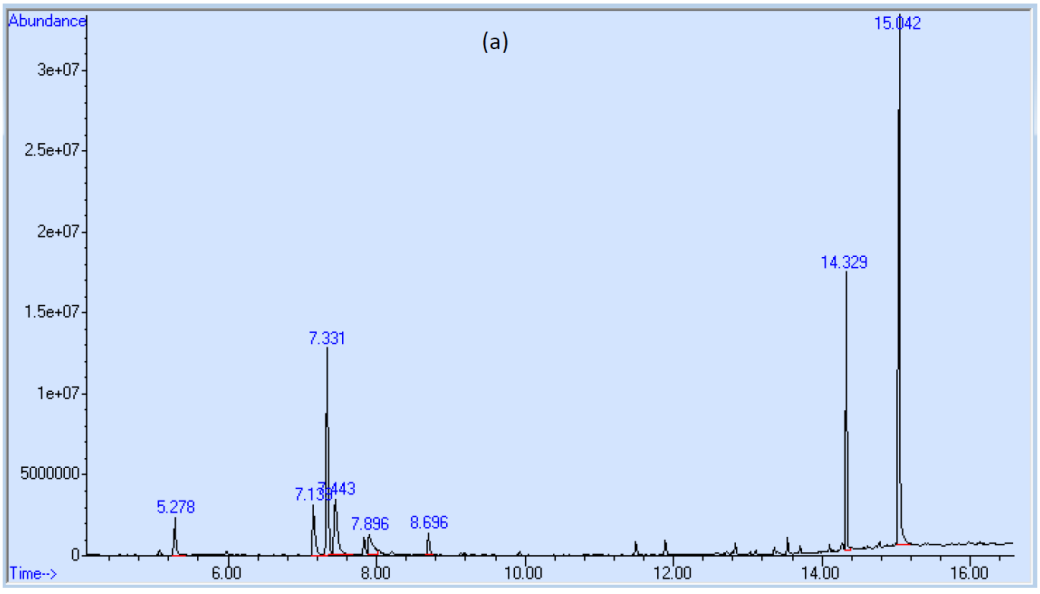

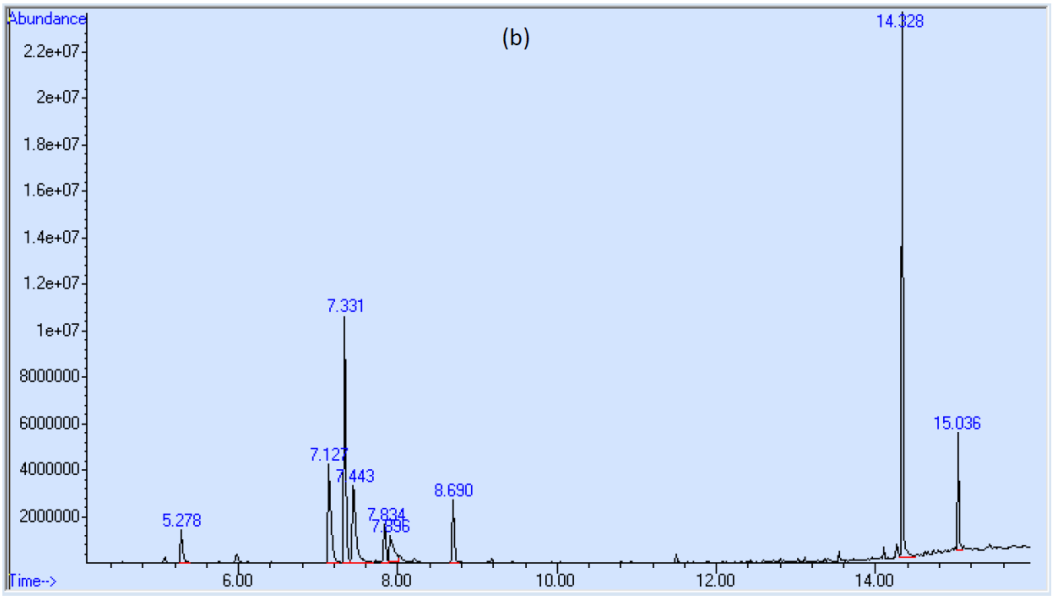

Figure S.1. Total Ion Chromatogram (TIC) from GC-MS of the HTL of glucose (a) and fructose (b) at 250°C for 5 min.

Table S.2. Identification of the ten largest TIC peaks from the GC-MS of the HTL of glucose and fructose at 250°C for 5 min.

Name	Retention time [min]	Match factor	R-match factor	Probability [%]
Acetic acid	7.13	969	969	85.2
Furfural	7.33	949	953	60.4
2-Butanone	7.44	871	903	40.1
2,5-Hexanedione	7.83	785	928	78.4
Formic acid	7.90	954	965	81.0
5-Methyl furfural	8.69	881	944	94.0
3-Methyl-cyclopentanedione	11.49	921	932	40.4
trans-2-Pentenoic acid	11.89	879	926	54.9
Levulinic acid	14.33	839	883	88.0
5 hydroxymethyl furfural	15.04	920	927	95.9

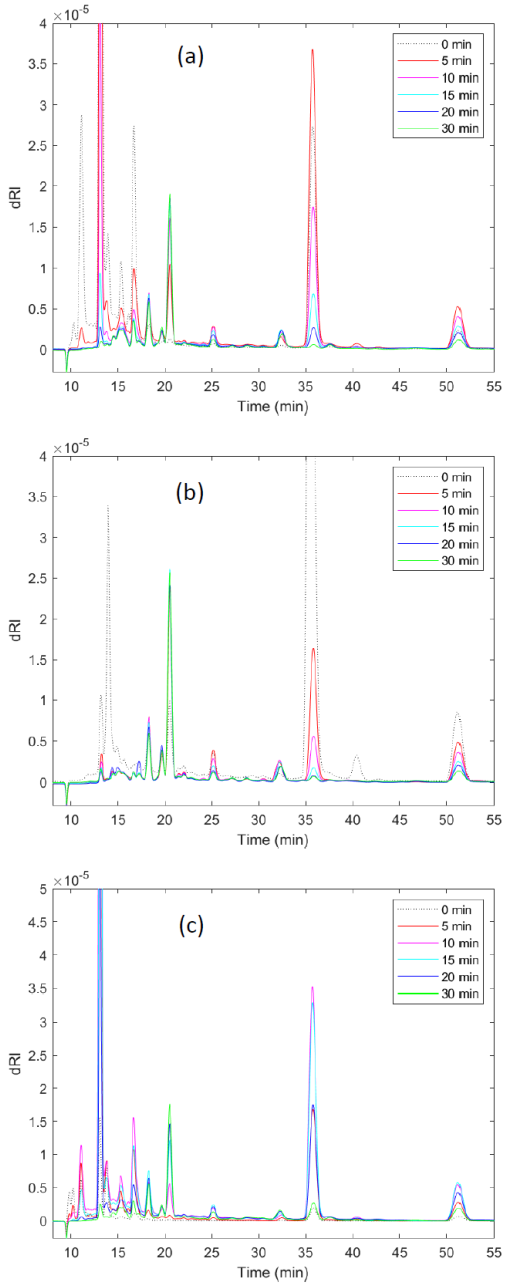

Figure S.3. HPLC/RID chromatograms of the HTL products of glucose (a), fructose (b), and cellulose (c) at 250°C, over a residence distribution time of (0 to 30 min).

Note: *Methyl furfural presented a relatively weak peak which reduced the visibility of the chromatograms, so the plotting time was cut to 55 minutes.*

Table S.4. Concentration of detected species in AQ phase from the HTL of glucose at 250°C.

[mg/ml]	0 min	5 min	10 min	15 min	20 min	30 min	Tolerance
Glucose	125.8	37.3	9.7	2.5	1.0	0.5	± 0.2
Fructose	5.1	2.2	1.0	0.7	0.7	0.6	± 0.2
A1* (Erythrose)	2.8	1.6	1.1	1.0	0.9	0.9	± 0.2
A2* (Pyruvaldehyde)	5.8	3.7	2.7	2.4	2.2	2.1	± 0.2
A3* (1,6-Anhydrogluose)	8.8	3.9	2.0	1.5	1.4	1.3	± 0.2
Formic acid	2.6	4.1	3.6	3.4	3.1	2.9	± 0.1
Acetic acid	1.7	3.4	3.4	3.7	3.8	3.8	± 0.1
Levulinic acid	1.0	5.2	7.5	8.1	8.4	8.6	± 0.2
trans-2-Pentenoic acid	0.5	1.7	1.6	1.4	1.1	0.7	± 0.1
Ethanol	0.8	1.5	1.3	1.3	1.3	1.0	± 0.1
2,5-Hexanedione	1.3	1.7	1.6	1.5	1.5	1.4	± 0.1
2 butanone	0.6	1.6	1.9	2.2	2.2	1.9	± 0.1
5 hydroxymethyl furfural	12.3	16.7	7.9	3.2	1.3	0.4	± 0.2
3-Methyl-cyclopentanedione	2.2	6.4	4.3	3.9	3.3	1.0	± 0.1
Furfural	1.7	3.7	2.8	2.1	1.5	0.8	± 0.1
5-Methyl furfural	0.1	0.3	0.3	0.3	0.3	0.1	± 0.1

Table S.5. Concentration of detected species in AQ phase from the HTL of fructose at 250°C.

[mg/ml]	0 min	5 min	10 min	15 min	20 min	30 min	Tolerance
Glucose	3.4	1.0	0.8	0.6	0.5	0.6	± 0.2
Fructose	9.8	0.7	0.6	0.6	0.7	0.6	± 0.2
A1* (Erythrose)	3.5	0.9	0.8	0.8	1.1	0.8	± 0.2
A2* (Pyruvaldehyde)	3.0	1.4	1.4	1.4	1.5	1.4	± 0.2
A3* (1,6-Anhydrogluose)	1.4	0.7	0.7	0.6	0.7	0.7	± 0.2
Formic acid	3.7	3.7	3.7	3.4	3.1	2.9	± 0.1
Acetic acid	4.4	4.4	4.9	5.1	5.4	5.1	± 0.1
Levulinic acid	5.1	10.8	11.6	11.7	10.8	11.6	± 0.2
trans-2-Pentenoic acid	2.2	2.2	1.7	1.2	0.9	0.8	± 0.1
Ethanol	2.1	1.2	1.3	1.2	1.2	1.3	± 0.1
2,5-Hexanedione	2.0	1.4	1.5	1.4	1.4	1.5	± 0.1
2 butanone	1.5	1.6	1.9	1.8	1.5	1.8	± 0.1
5 hydroxymethyl furfural	51.0	7.4	2.6	0.9	0.5	0.5	± 0.2
3-Methyl-cyclopentanedione	12.1	5.0	4.5	3.0	2.0	2.7	± 0.1
Furfural	5.9	3.3	2.6	1.9	1.5	1.1	± 0.1
5-Methyl furfural	0.4	0.5	0.5	0.4	0.3	0.3	± 0.1

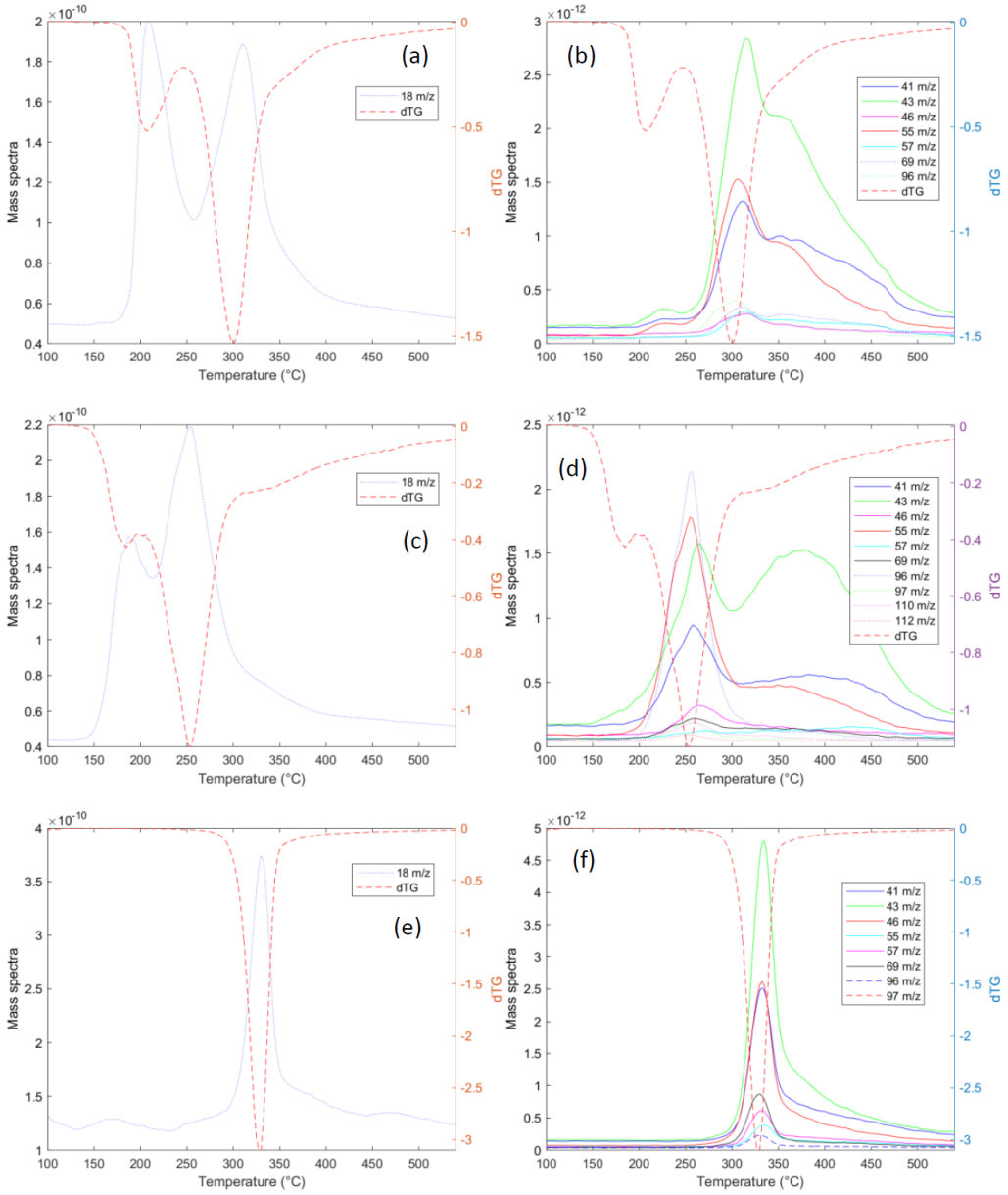

Figure S.6. dTG-MS of glucose (a-b), fructose (c-d) and cellulose (e-f) with MS signals of water (left) and organics (right).

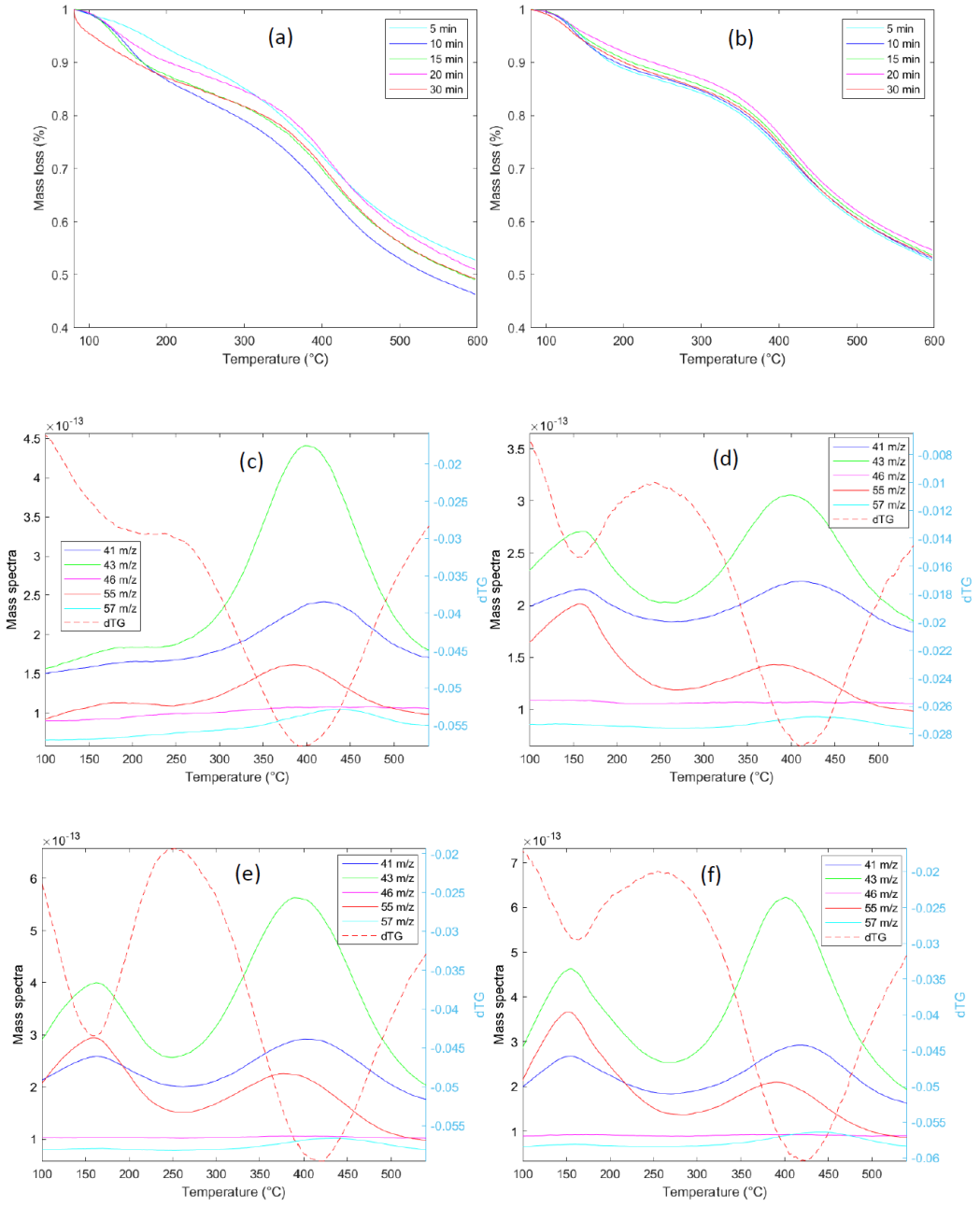

Figure S.7. Thermogravimetric mass loss of (a) glucose HTL and (b) fructose HTL at 250°C, over the residence time distribution and dTG-MS of glucose (c-d) and fructose (e-f) at 5 and 20 minutes residence time respectively.

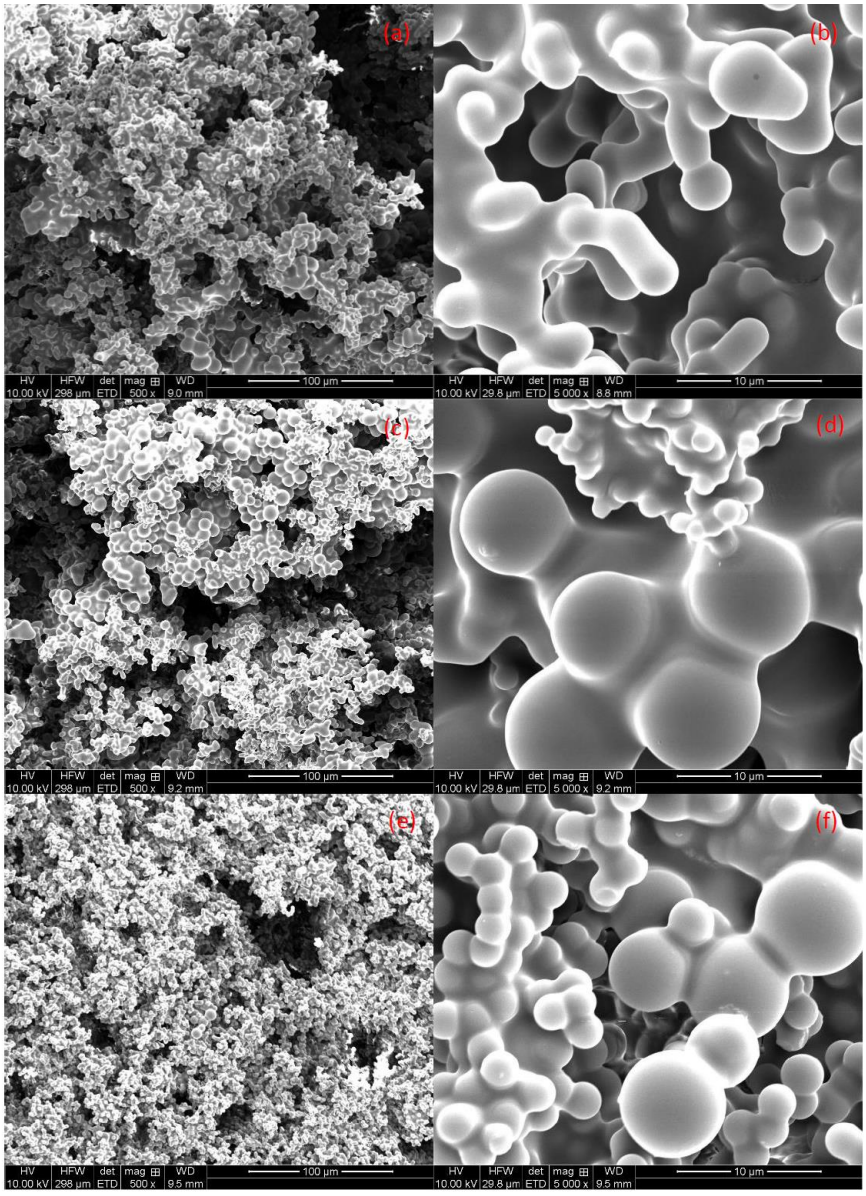

Figure S.8. SEM images of fructose HTL at 250°C for 5 min (a, b), 30 min (c, d) and glucose HTL at 30min (e, f)

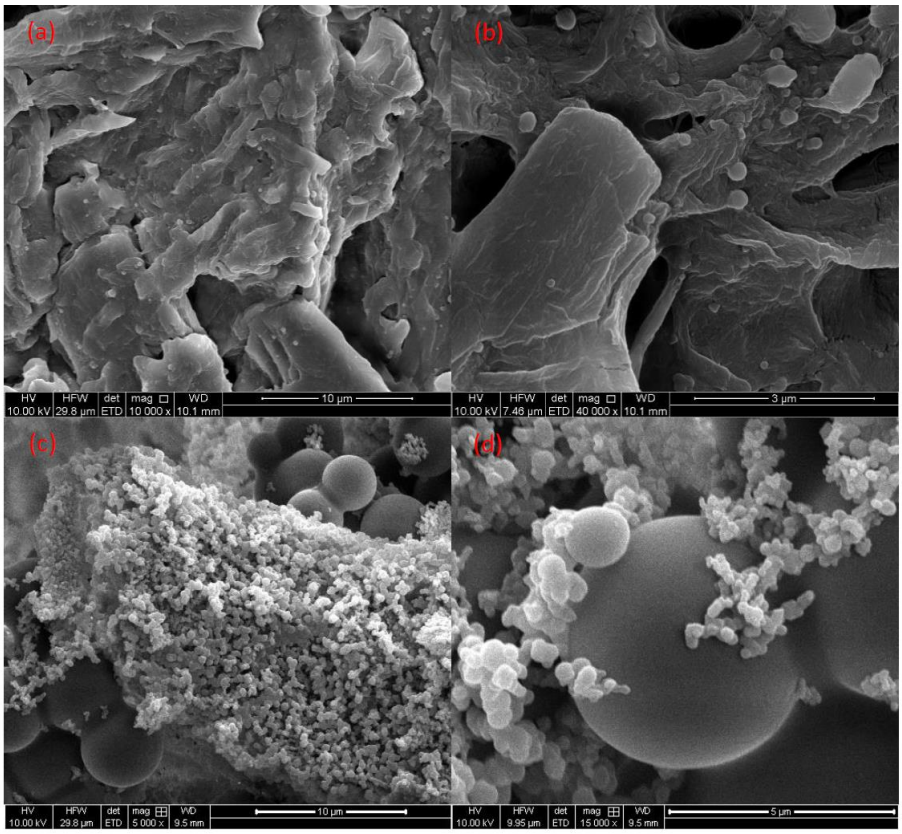

Figure S.9. SEM images of cellulose HTL at 250°C for 5 min (a, b) and 30 min (c, d)

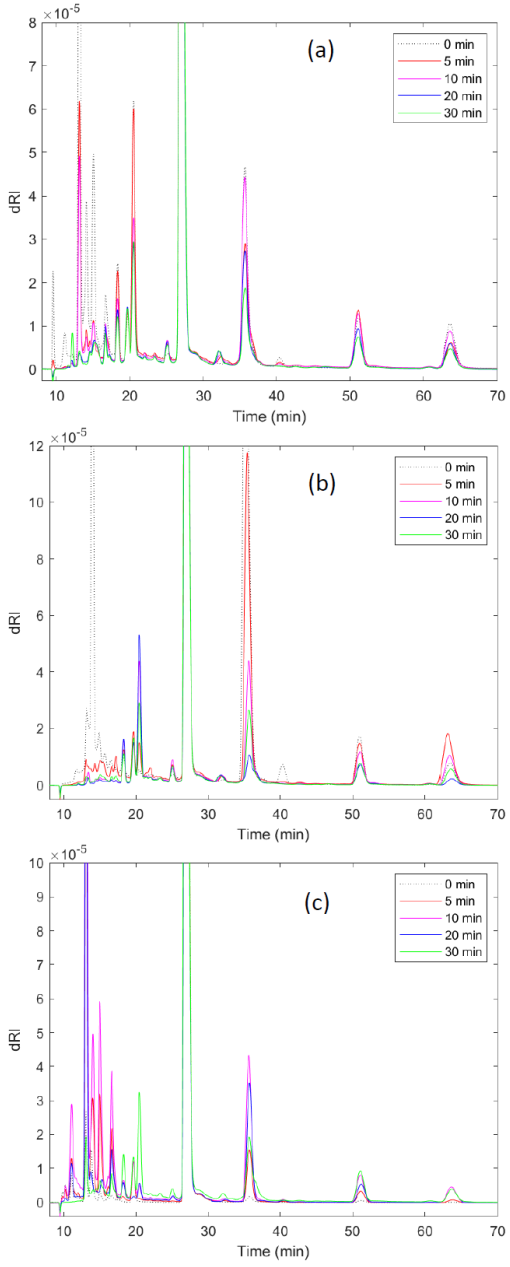

Figure S.10. LC/RID chromatograms for the co-liquefaction of glucose (a) fructose (b) and cellulose with ethanol and acetic acid at 250°C.

Table S.11. Constant values k for the optimizations of glucose, fructose and cellulose, and the in-situ co-solvents and homogeneous catalysts.

-ln(*k*)	Glucose		Fructose		Cellulose		Co-liquefaction/co-solvents		
	250°C	300°C	250°C	300°C	250°C	300°C	Glucose	Fructose	Cellulose
k1	-0.65	-0.83	15.21	10.96	0.03	-0.81	-0.86	-1.64	2.24
k2	-2.30	1.07	0.72	-0.90	-1.86	0.19	-0.32	-0.28	7.42
k3	3.92	1.60	2.38	2.30	3.55	2.24	1.33	0.76	0.97
k4	2.85	2.94	2.65	2.72	1.59	2.96	2.17	1.86	2.32
k5	3.26	1.25	2.04	0.59	3.27	3.26	0.86	-0.61	2.07
k6	27.25	5.78	4.45	8.85	3.07	18.28	2.37	1.75	8.57
k7	2.72	0.15	10.19	3.97	1.97	1.53	0.48	1.53	2.86
k8	-0.21	-1.66	-1.26	-2.45	0.81	0.82	-0.83	2.34	2.73
k9	12.31	5.42	2.16	0.79	17.49	30.82	30.23	3.25	5.52
k10	5.21	2.23	6.30	5.57	29.36	31.41	6.49	2.17	2.72
k11	2.61	2.38	1.24	0.01	3.31	1.59	3.28	2.69	7.98
k12	31.32	11.77	18.78	8.12	31.32	22.82	5.55	3.49	3.32
k13	1.54	0.05	0.78	-0.71	1.77	1.44	-0.92	-0.85	15.04
k14	3.35	-1.29	2.15	-1.78	24.04	30.84	-0.08	15.86	4.08
k15	2.17	9.58	2.56	13.01	2.22	1.77	2.71	14.39	3.96
k16	1.77	3.74	2.16	0.42	3.43	3.89	2.13	2.21	10.97
k17	3.01	2.84	3.37	2.73	4.42	1.84	4.51	-0.86	6.03
k18	3.53	8.28	3.74	4.41	3.81	2.35	5.53	2.13	6.07
k19	30.64	3.03	7.81	-1.18	30.70	30.98	30.86	3.45	1.69
k20	3.21	1.07	2.17	0.58	3.72	2.90	-0.84	13.33	1.77
k21	3.50	3.52	3.44	3.47	3.68	3.76	2.15	19.43	8.89
k22	5.82	4.14	8.38	16.45	1.63	30.85	2.97	5.56	6.88
k23	13.54	6.69	10.86	13.46	2.21	1.31	30.78	0.08	11.58
k24	0.49	0.49	-0.77	-1.65	1.99	0.27	3.88	11.30	10.16
k25	15.09	8.77	14.88	12.02	31.16	30.67	30.99	0.55	1.74
k26	16.42	9.29	7.32	22.54	30.90	24.13	30.88	1.04	6.70
k27	0.79	0.41	1.02	0.63	-1.48	-2.01	1.69	3.83	8.09
k28	31.00	0.94	12.16	-3.84	2.18	30.84	2.98	15.39	17.93
k29	8.08	6.46	6.56	9.22	25.33	30.87	-1.06	2.31	-1.93
k30	2.41	-0.09	1.00	0.23	13.52	30.84	3.56	10.08	-0.70
k31	13.21	4.37	3.82	3.22	14.86	19.47	31.09	3.21	2.46
k32	22.79	2.35	0.14	-1.55	1.18	0.43	-0.01	6.19	17.23
k33	--	--	--	--	17.76	19.73	--	--	1.82
k34	--	--	--	--	1.91	1.46	--	--	4.52
k35	--	--	--	--	4.59	2.22	--	--	8.91

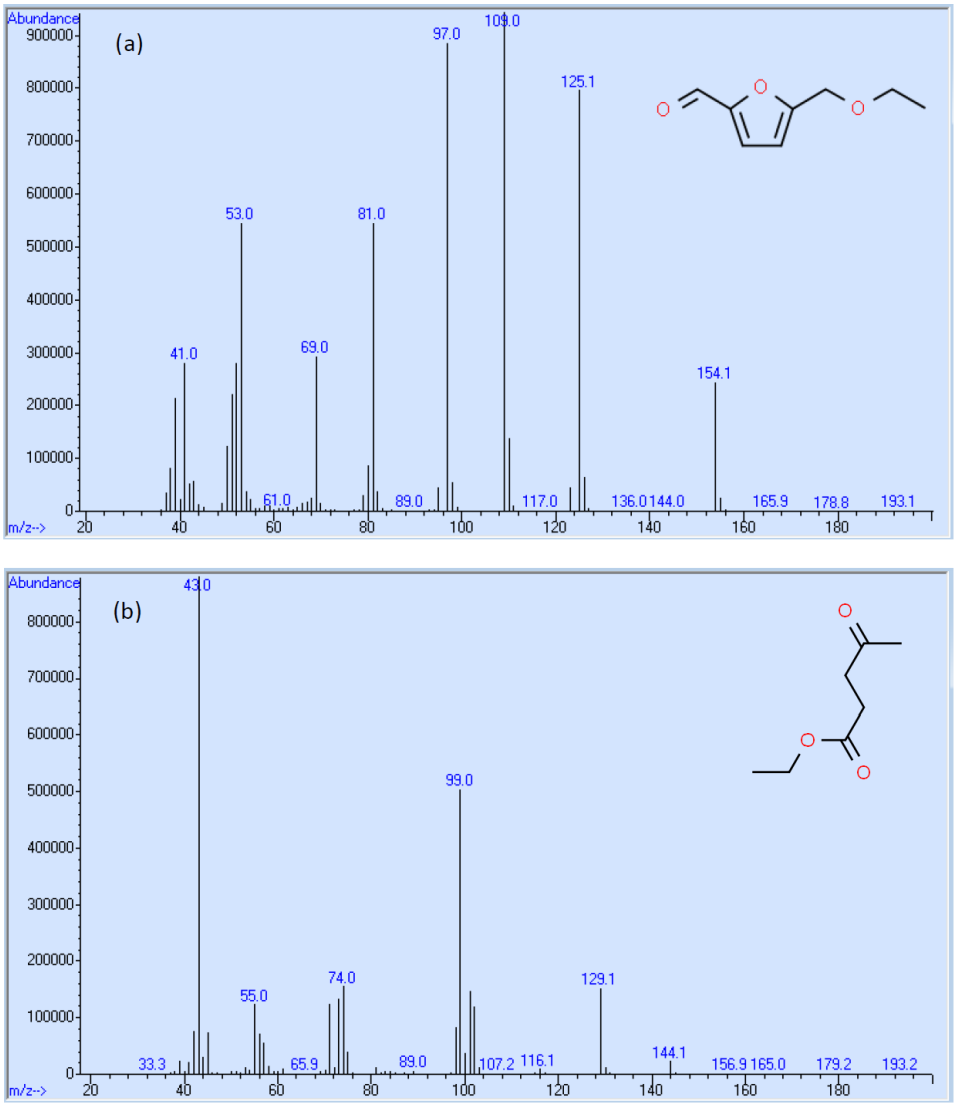

Figure S.12. Tentative spectrum of 5-Ethoxy methyl furfural (5-EMF) (a) and Ethyl levulinate (b) found in the GC-MS of the HTL of glucose with co-solvents and homogeneous catalysts.

Chapter 6

Elucidating the Maillard reaction mechanism in the hydrothermal liquefaction of binary model compound mixtures and spirulina

Andres Chacon-Parra[a], Tony Hall[b], David Lewis[a], Marianne Glasius[c], Philip van Eyk[a]

[a]School of Chemical Engineering and Advanced Materials, The University of Adelaide, Adelaide, SA 5005, Australia

[b]Faculty of Sciences, The University of Adelaide, Adelaide, South Australia 5005, Australia

[c]Department of Chemistry, Aarhus University, 8000 Aarhus C, Denmark

Submitted to ACS Sustainable Chemistry & Engineering, in ACS manuscript style.

Statement of Authorship

Title of Paper	Elucidating the Maillard reaction mechanism in the hydrothermal liquefaction of binary model compound mixtures and spirulina
Publication Status	☐ Published ☐ Accepted for Publication ☑ Submitted for Publication ☐ Unpublished and Unsubmitted w ork w ritten in manuscript style
Publication Details	Chacón-Parra, A., T. Hall, D. Lewis, M. Glasius, and P. van Eyk, Elucidating the Maillard reaction mechanism in the hydrothermal liquefaction of binary model compound mixtures and spirulina. Submitted to ACS Sustainable Chemistry & Engineering (id: sc-2022-00688d)

Principal Author

Name of Principal Author (Candidate)	Andres Danilo Chacon Parra
Contribution to the Paper	Conceptualisation, Investigation, Methodology, Formal analysis, Data curation, Writing - original draft
Overall percentage (%)	80%
Certification:	This paper reports on original research I conducted during the period of my Higher Degree by Research candidature and is not subject to any obligations or contractual agreements with a third party that would constrain its inclusion in this thesis. I am the primary author of this paper.
Signature	Date 11/02/2022

Co-Author Contributions

By signing the Statement of Authorship, each author certifies that:

i. the candidate's stated contribution to the publication is accurate (as detailed above);
ii. permission is granted for the candidate in include the publication in the thesis; and
iii. the sum of all co-author contributions is equal to 100% less the candidate's stated contribution.

Name of Co-Author	Tony Hall
Contribution to the Paper	Methodology, Data curation, Writing - review & editing
Signature	Date 16/02/2022

Name of Co-Author	David Milton Lewis
Contribution to the Paper	Supervision, Funding acquisition, Writing - review & editing
Signature	Date 11/02/2022

Name of Co-Author	Marianne Glasius		
Contribution to the Paper	Validation, Writing - review & editing		
Signature		Date	17 December 2021

Name of Co-Author	Philip Joseph van Eyk		
Contribution to the Paper	Supervision, Conceptualisation, Resources, Writing - review & editing		
Signature		Date	21-Feb-2022

Please cut and paste additional co-author panels here as required.

Elucidating the Maillard reaction mechanism in the hydrothermal liquefaction of binary model compound mixtures and spirulina

Andrés Chacón-Parra, † Tony Hall, ♯ David Lewis, † Marianne Glasius, □ Philip van Eyk†

† School of Chemical Engineering and Advanced Materials,

The University of Adelaide, Adelaide, SA, 5005, Australia

♯ Faculty of Sciences, The University of Adelaide,

Adelaide, South Australia 5005, Australia

□ Department of Chemistry, Aarhus University,

8000 Aarhus C, Denmark

*Corresponding author

E-mail address: philip.vaneyk@adelaide.edu.au

Abstract

Hydrothermal liquefaction (HTL) transforms wet biomass and bio-waste feedstocks into water-insoluble bio-crude and valuable water-soluble organic products. HTL takes advantage of the exceptional properties of water near the critical point to break bio-macromolecule linkages and, as a reaction medium, sub-critical water ions allow the reaction and re-condensation of intermediates into various structures and product phases. Among the different reaction mechanisms involved in the hydrothermal conversion, the synergetic interaction between protein and carbohydrate intermediates, known as the Maillard reactions, can boost the renewable bio-crude yield up to 25% higher than solely free fatty acid hydrolysis from lipids. However, the actual reaction mechanisms are not fully understood. In this study, the Maillard reactions have been investigated with a Central Composite Design (CCD) to validate the impact of mass ratio (carbohydrate/protein) over temperature and residence time, via product response analysis, including product yields, boiling point distribution, aqueous tests, elemental, and chemical compositions. Then, the GC-MS data is used to propose a potential pathway followed by levulinic acid from carbohydrates as a candidate to produce proline via Maillard interactions before amino acid condensation into piperazinedione and reduction into pyrazine among other complex degradations. The HTL experiments were run with glucose and soy protein as model compounds

and spirulina in a batch reactor at 300˚C temperature, 20 minutes residence time and 50% mass ratio as centred point, with alpha (α) of 20˚C, 10 minutes and 25% mass ratio.

Keywords: Hydrothermal liquefaction, Maillard reactions, Proline, Piperazinedione, Pyrazine, GC-MS of aqueous samples.

1. Introduction

Hydrothermal liquefaction (HTL) of biomass has the potential to convert non-edible, non-conventional biomass sources like wet biomass and bio-waste into valuable products and renewable energy [1, 2]. This promising waste management method has received special attention as it can process biomass with high moisture and ash content such as algae, municipal waste, and sewage sludge without an energy-intense pre-drying process [1-5]. The product phases and their composition derived from HTL processing heavily depend on reaction conditions, i.e., temperature and residence time, as well as feedstock type and composition [1, 2, 6-9].

Proteins and carbohydrates are two of the major components of all biological organisms and represent a significant portion of biomass and bio-waste [4, 10]. Rich-protein biomass like soy protein produces on average 25% mass yield of water-insoluble bio-crude and around 60% nitrogen recovery in the aqueous phase [8, 10-15]. The HTL conversion of carbohydrates generates high solid yields and acidic aqueous phases with relatively high concentrations of 5-

hydroxymethyl furfural (HMF) and levulinic acid (LA) among other water-soluble intermediates. [3, 11, 12, 14, 16-21]. The Maillard interaction between carbohydrate and protein intermediates might boost the renewable bio-crude yields [2, 5-7, 13]. Despite the Maillard reaction pathway is well known in the food industry, it is scarcely understood throughout the thermochemical conversion of biomass [16, 22-27].

Under HTL conditions, subcritical water turns into a reaction medium and most of the conversion happened within the aqueous phase, even the hydrolysis of insoluble lipids into free fatty acids (FFA) is catalysed by the near critical point water ions [7, 28-30]. However, the HTL aqueous phase has received less attention in the scientific literature to date. The insoluble bio-crude and organic solvent extractions from the aqueous phase are the more commonly investigated products [15, 31-33]. The renewable crude fraction is suggested to be a mixture of medium molecular weight products condensed from the aqueous phase, whilst the solvent-extracted phases are fractions of the aqueous phase with composition depending on the polarity, solubility and efficiency of the solvents and extraction processes used [15, 31]. Gas chromatography coupled to mass spectrometry (GC-MS) is a useful, standard analysis method to elucidate the chemical composition of complex organic mixtures, But direct injection of aqueous samples into a GC-MS analyser is not recommended, and it is typically avoided because of repeatability issues from vacuum fluctuation in the ion source of the mass selective detector and recommendation for durability of the often-used 5% phenyl substituted type GC columns [3, 4, 33-35]. However,

analysis of the aqueous phase provides a wider and better understanding of the reaction mechanism and interactions over the hydrothermal liquefaction of biomass. This has been done with GC-MS with direct injection of aqueous phase and after derivatization [32, 36-39] or using LC-MS.

The amino acids in proteins are known to condensate (cyclo-dimerization) into 2,5-piperazinedione or glycine anhydrite structures with different radicals [25, 36, 40-42]. Depending on the actual amino acid composition share, these compounds follow a reduction into pyrazines. However, this is not the only pathway followed by the proteins; piperidine, pyrrolidone, azocine and imidazole, are among many of the protein degradation products [23, 33, 40, 42, 43]. The most important Maillard reactions are the Strecker degradation, which is an amine group substitution (a α-amino acid into an aldehyde, forming an imine intermediate), and Amadori rearrangement, which is the exchange of an ammonia atom with a saccharide degraded compound forming a keto-amine [4, 8, 10, 32, 44, 45]. Similarly, furfural groups could be converted into pyrrolidone by ammonia replacement under alkaline conditions. However, the scientific literature of the Maillard interactions during hydrothermal conversion is limited to solvent extraction and derivatization processes prior GC-MS, which constrain the analysis due to the solubility and polarity of the solvent extraction procedure [8, 13, 24, 32, 33]. Furthermore, the effects of nitrogen as a heteroatom on the extent of the hydrothermal liquefaction have not been fully clarified [2, 46, 47]. Organic nitrogen heteroatoms in renewable bio-crude and the aqueous phases require a more

complete understanding as nitrogen and high aromatic content are two of the toughest challenges of the renewable bio-crude for the oil industry. While fuel-oil is considered between 0.1 to 1.5% nitrogen content by mass, renewable crudes from the HTL rich-protein biomass might be in the range 6 to 10% nitrogen [2-5, 46].

In the present study, the Maillard reactions from the hydrothermal conversion of glucose and soy protein mixtures are investigated. A Central Composite Design (CCD) is used to determine the influence of reaction temperature, residence time and mass ratio on the product phase yields, boiling point distribution and product composition. GC-MS data from the aqueous phase and ethanol soluble bio-crude are used to identify the major structures formed over the conversion and to suggest a prospective Maillard reaction pathway based on identified compositions. The results obtained with the model compound mixtures are contrasted with similar experiments run with spirulina and a bulk kinetic reaction mechanism for centred composition and circumscribed temperatures. The significance of the present study lies in the consequential understanding of the Maillard reaction as a vital interaction affecting to the hydrothermal conversion, the renewable crude yields, properties, and the nitrogen retention mechanism [4, 14, 16, 46].

2. Method

2.1 Materials and standards

D-glucose anhydrous laboratory reagent (LR) from Chem-Supply and a soy protein natural supplement from Bulk Nutrients (unflavoured) were used as carbohydrate and protein model compounds, respectively. The protein supplement is composed by 13.9 +/- 0.1% Nitrogen content by mass and 89.4 +/-0.5% proteins, according to the Australian National Measurement Institute. This protein isolate also has 0.5% carbohydrates and 700mg/100g of sodium by mass, according to the nutritional information provided by Bulk Nutrients (Australia). Spirulina powder from Bulk Nutrients is a natural source of amino acids with 62% protein and 16% carbohydrate (3% sugars) content.

Ethanol 100% (undenatured), nitrate standards with 50 mg/L as NO_3 and 100 mgN/L, were obtained from Chem-Supply Pty Ltd (Australia). Orion ammonia standard with 100ppm as N was acquired from Thermo Fisher Scientific Australia Pty Ltd.

2.2 Design of Experiments and Reactor system

A circumscribed DOE with three factors and 2 levels is ideal for determining the primary effect and interactions of the three main variables and to obtain the optimal response over the different product phases, properties and the tentatively identify composition. An alpha value of 1.682 for

three factors based on the equation $(2^3)^{1/4}$ generate the star points outside the experiment domain. The CCD parameters are presented in Table. 1.

Table 1. DOE factors, levels, and star points for CCD factorial experiments.

Factors	Units	Centre point	α	Range and levels				
				- 1.682(-α)	-1	0	1	+ 1.682(α)
Temperature (*A*)	°C	300	20	266	280	300	320	334
Time (*B*)	Minutes	20	10	3	10	20	30	37
Mass ratio (*C*)	Glu/SP [%]	50%	25%	8%	25%	50%	75%	92%

A 15ml custom batch reactor made of a 20cm long 316 Swagelok® stainless steel tube, fittings, and ferrules, extended and equipped with a thermocouple probe (type K), a pressure transducer, a pressure relief safety valve, and a ball valve. The system is fully described with a schematic diagram in *Obeid et al. (2019)* [8, 11, 29]. Glucose and soy protein blends were premixed to a 15% (by dry mass) slurry. The reactor was then filled to 50% of its nominal volume capacity, closed, purged, and loaded with nitrogen gas to water saturation pre-pressure [8, 29].

A fluidised bed (Techne SBL-2D) controlled by a temperature and airflow controller system (Techne TC-9D) were used to accomplish and control heating. Cooling was completed in a two-step process, using compressed air until 100°C internal temperature, followed by quenching water bath until room temperature. The reaction counted as started when the internal reactor temperature reached 98% of the nominal desired temperature (3 minutes approx.). The centred point values for temperature and reaction time were defined based on previous studies' results with the same

system, and each experiment was duplicated to quantify the average of product yield reported [29].

2.3 Product recovery and separation

The gaseous product yields were calculated by the weight difference between the pre-charged nitrogen and the total mass of gases released after the reaction was completed and cooled down [11, 12, 29]. Solid and liquid phase products were collected by pouring and pushing the reactor content into separation tubes, centrifuged at 3500 RPM for 10 minutes to separate solid, aqueous, and crude phases, then 1ml of the aqueous phase was pipetted and filtered (0.22µm cellulose acetate) into a 2ml chromatography vial for analysis. Two aqueous samples (50µl each) were taken and diluted 200 and 1000 times in 10 and 50ml volumetric flasks respectively for colorimetric nitrogen tests and non-purgeable organic carbon (NPOC) as total organic carbon (TOC). Subsequently, 10 ml of ethanol was added to rinse the reactor walls and remove trapped products (oil and solids), to maximise product recovery and reduce deviations. After centrifugation of these ethanol rinse samples, 1ml of bio-crude in ethanol was transferred to chromatography vials for analysis [29].

Product separation was accomplished in a two-step filtration process. The recovered products containing aqueous, solid, and crude products were vortexed and filtrated in a Buchner funnel (Whatman's Ashless Grade 42 filter paper) to separate the aqueous (oil-free) phase. Then the

same filter was used to filter the ethanol rinse, to dissolve the renewable bio-crude trapped in the paper by dissolving it in ethanol. The renewable bio-crude in ethanol was then dried in a sample concentrator Techne FSC400D with a dri-block heater Techne DB200/3 set at 79˚C with high purity N_2 gas flow until constant weight (10 ± 2 hours) to determine ethanol soluble bio-crude yield. The filter paper with the solids was dried at 105˚C overnight to compute solid yield. The separation method aimed at maximising product recovery using a fully renewable organic solvent [4, 8, 13, 14].

2.4 Product Analysis

Separation, tentative identification, and semi-quantification of the organic species in the aqueous and renewable crude phases were accomplished via GC-MS on an Agilent 5977B/7890B. Separation was done using a HP-5MS capillary column (30m x 0.25mm x 0.25um) with a flow of 1 ml/min helium carrier gas. A 1µL sample was injected directly into the GC system in split mode (25:1). The oven temperature program started at 50˚C, held for one minute, followed by a 10˚C/minute ramp to 300˚C with a final hold for 9 minutes. The mass spectrometer (5977B MSD) scanned from m/z 40-500. The compounds were tentatively identified with the NIST14 Spectral Library database using ChemStation MS data analysis module (Agilent software) [12, 34].

Elemental analysis (EA) of HTL renewable bio-crude was conducted in a Perkin Elmer 2400 Series II Elemental Analyzer in CHN configuration. The analysis was carried out with a sample

weight of 4±1mg (AD 6000 ultra-microbalance) combusted at 925˚C. Results were calibrated with Acetanilide (C_8H_9NO) analytical standard, which has a known concentration of 71.09%, 6.71% and 10.36% by mass for carbon, hydrogen, and nitrogen, respectively. The measured error between standards was ±0.05%, ±0.13% and ±0.12% for carbon, hydrogen, and nitrogen, respectively. The measured sulphur abundance of the soy protein was 0.88% (CHNS) and considered relatively unchanged and negligible [11].

Total nitrogen in water via persulfate digestion and ammonia via salicylate method were measured in a HACH colorimeter DR/890 using a total nitrogen HR (0 to 150 mgN/L) and ammonia HR (0 to 50 mgN/L) Test 'N Tube HACH kits and the 10072 and 10031 methods for wastewater by Hach, respectively. Calibration was made of three points for total nitrogen and two points for ammonia, using Milli-Q water (zero), two total nitrogen standards (50 and 100 mgN/L) and one ammonia standard (100mgN/L) diluted one in three. Total nitrogen tests were digested on a HACH Digital Reactor Block DRB200 at 105 +/- 1˚C for 30 minutes. Both tests were conducted with samples diluted 200 times in Milli Q water [11]. The total organic carbon (TOC) was analysed by CSIRO (Australia) using a Shimadzu TOC total organic carbon analyser in non-purgeable organic carbon (NPOC) mode (APHA method 5310 B).

Boiling point distributions were measured via thermogravimetric analysis (TGA), performed in a NETZSCH simultaneous thermal analyser (STA) 449 F5 Jupiter. The method started with an isothermal segment for 20 minutes, followed by a ramp from 80 to 600˚C, with a heating rate of

5˚C/min and 50ml/min flow rate of nitrogen gas, finally two isothermal segments at 600˚C for 10 minutes each with nitrogen and air to combust non-volatile matter. Boiling point fractions are calculated by the weight loss over defined temperature ranges of (80-180˚C), (180-300˚C), and (300-600˚C) [8, 11, 14, 29, 48].

2.5 Kinetic modelling

Reaction kinetics were modelled with ordinary differential equations (first-order), solved using *ODE45* function in MATLAB [11, 29]. The reaction mechanism for the product phases aims to foresee the product yields and the equilibrium over the residence time at centred and circunscribed temperatures and compositions. The reaction constants (k) were optimised using the *lsqcurvefit* function by minimizing the squared norm of the residual function [11, 29]. The error bars represent the standard deviation of the experimental data [49].

3. Results and discussion

3.1 Bulk product phase yields and primary impact of factors

The primary impact of the three evaluated factors on renewable bio-crude yield is presented in Fig. 1 (a). The increase in carbohydrate mass ratio reduces the bio-crude yield from approximately 27% to 15% in a carbohydrate mass ratio range of 8% to 92%, with a relatively linear trend response. Residence time seems to be the second most important factor with a decreasing trend

from less than 27% to 18%, and finally the effect of temperature reached the maximum yield near to 300˚C, which is the centre point of this study. The DOE standardised effect of the three factors in a second-order polynomial equation model (Fig. 1 (b)) signifies the influence of the mass ratio, followed by residence time and the combination of these two variables as the third factor to predict the renewable crude yield. Finally, the contour plot (Fig. 1 (c)) for bio-crude yield over residence time and carbohydrate ratio illustrates the region where the two variables may reach the highest renewable crude yield response at centred temperature (see Supplementary Material Table. 1) [10, 24, 25].

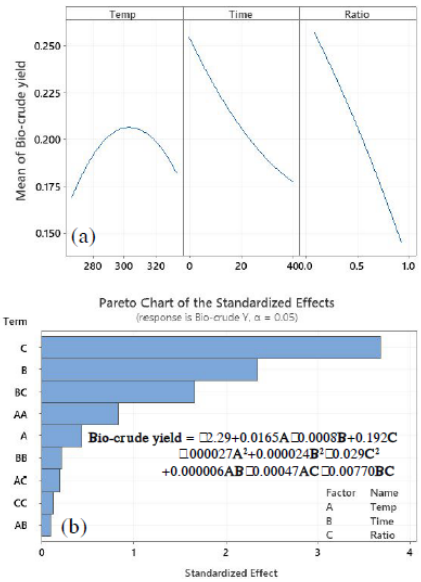

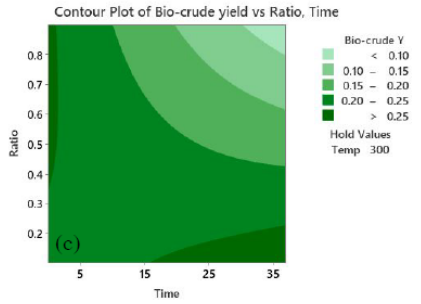

Figure 1. Primary effect of factors on the renewable crude yield (a), Pareto chart of the standardised effect of factor with a quadratic model (b) and a contour plot for renewable crude over time and mas ratio at a holding temperature of 300˚C (c).

The data obtained with the CCD design of the experiments help to understand the major effect of the CCD factors when a third variable, such as the mass ratio, is considered. The influence of residence time and reaction temperature is generally condensed into Arrhenius kinetic models and reaction activation energy [50]. However, as Arrhenius kinetics models chemical reactions, the oversimplified bulk phase kinetic models cannot capture the chemical transformations and the synergetic effect of chemical interactions within the different phases [9, 13, 24, 51, 52]. Some of the latest studies have integrated bulk kinetics with the prominent reaction mechanisms, from biomass key components to product phases based on experimental observations. However, these complex models only apply to the distribution of product phases, not the composition or the changes in composition present in most biomass and bio-waste sources [9-11, 23, 52]. The complexity of including an additional parameter increases the number of experiments

exponentially. For this reason, factorial experiments were selected and developed in the present study [49]. Nonetheless, a bulk phase reaction kinetics model at centre point temperature and mass ratio is presented in Fig. 2. To illustrate the point mentioned above, product phase changes after 5 minutes reaction time are negligible. The circumscribed experiments and the first order ODE system are shown in Supplementary Material Fig. 2 (a-e).

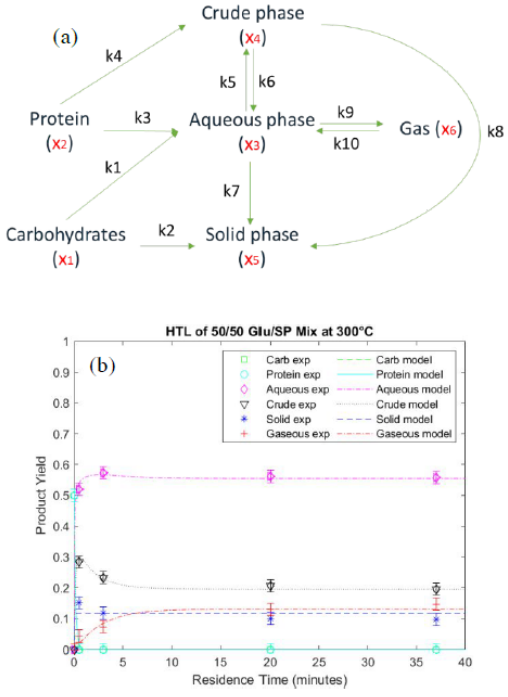

Figure 2. Bulk reaction mechanism model (a) and experimental and modelled product yields fitted to the phase reaction model (b) at 300˚C and 50% mass ratio [11].

It was observed that high carbohydrate mass ratio diminishes the renewable bio-crude yield, while increases the solid (hydrochar) yield, as illustrated in Fig. 3 (a). The significance of mass ratio on

solid product yields is relatively linear, from zero to approximately 24% at 92% glucose ratio [25, 53, 54]. However, including 8% protein by mass significantly reduces the solid yield as the conversion of glucose monosaccharide produced almost 50% solid (hydrochar) yields. The standardised Pareto effect chart (Fig. 3 (b)) shows that carbohydrate mass ratio is over four times the impact of the next factor, which is temperature. Additionally, the contour plot for the solid yield response over reaction temperature and residence time (Fig. 3 (c)), predicts the region where these two variables might promote low hydrochar yields.

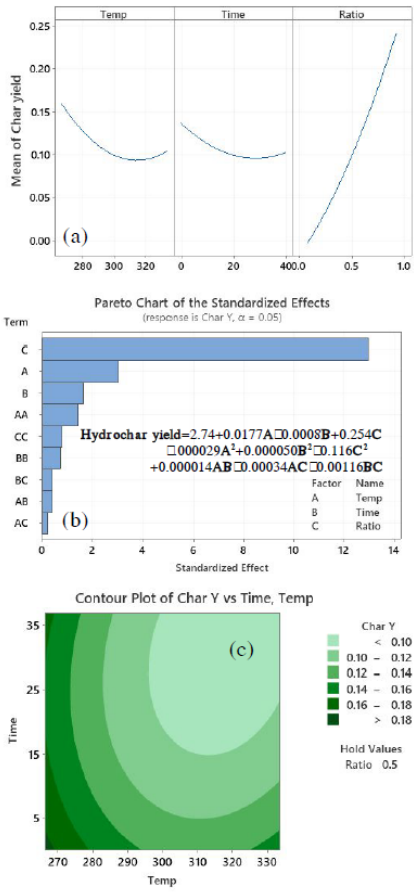

Figure 3. Main effect of factors on the solid (char) yield (a), Pareto chart of the standardised effect of factors with a quadratic model (b) and the contour plot for solid yield over temperature and time with a holding mass ratio of 50% (c).

The significance and impact of the mass ratio of carbohydrates and proteins as two of the most prominent biomass components is shown in the renewable crude and solid yield response over the three factors evaluated [25, 43, 55]. Non-conventional biomass sources like municipal sewage

sludge, algae and bio-waste should be considered as non-homogeneous composition biomass sources, which generate products that vary in composition and properties [56, 57]. However, the bulk product phase fitting and modelling are not enough. The properties and composition of the phases are also crucial to determine the quality of the renewable bio-crude obtained and the transformation further than the phase yield [10, 13, 23, 25, 52].

3.2 Boiling point distribution and elemental composition of the bio-crude.

Boiling point distribution of the renewable bio-crude has been used to estimate the potential fractions over a destructive distillation based on mass loss over a temperature ramp. However, this method has been challenged because of the thermal decomposition through the analysis [48]. Despite the controversy, estimation of volatile and non-volatile fractions from TGA is relatively useful to determine the potential fractionating of the renewable bio-crude and the influence of the evaluated factors [29, 48]. As illustrated in Fig. 4 (a) the effect of mass ratio in volatile matter (80 to 600˚C in a nitrogen atmosphere) is again the most significant factor of the CCD, but this time the maximum point was achieved at approximately 35% carbohydrate mass ratio and the effect of reaction temperature and residence time was limited and relatively lower at near the centred point. However, the volatile fraction could be separated into low (80 to 300˚C) and high (300 to 600˚C) boiling point, providing a better understanding of these two relatively different fractions (see Supplementary Material Table. 3 and Fig. 4 (a and b)). Lower reaction temperature and longer residence time have a positive effect on the desired lower boiling point fraction, while

reducing the high boiling point fraction [29]. Finally, the combustible non-volatile matter (at 600˚C with air) presented a relatively similar trend to the solid phase yields as shown in Fig. 4 (b). Glucose mass ratio had the largest influence, followed by reaction temperature. Using TGA analysis as one-to-one fuel-oil contrasting based on boiling point distribution might not be a correct indicator of renewable crude quality due to thermal decomposition [12, 58]. However, the relevance of the hydrocarbon breaking/fractionation via a reduction in boiling point should be further investigated with more specific analytical methods [54, 58-60].

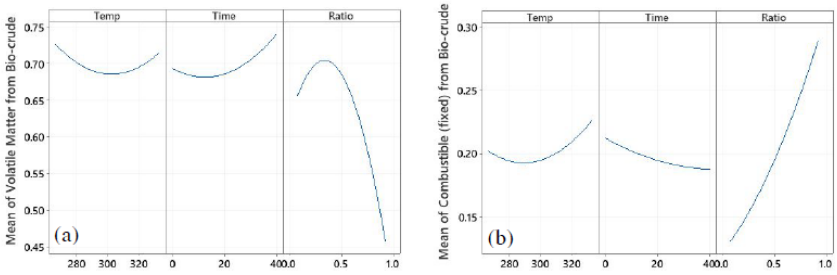

Figure 4. Main effect of factors in the volatile matter fraction (80 to 600˚C) (a) and non-volatile matter fraction (b) of the renewable crude.

Another commonly used thermochemical analysis of bio-crude is elemental composition (CHN/CHNS). The reaction temperature and residence time have a positive effect on carbon content and the high heating value (HHV) via Dulong approximation [13]. However, the effect of biomass composition is usually not included or insufficiently disclosed. The primary effect of the factor on the elemental carbon composition is illustrated in Fig. 5 (a). The carbon content follows a similar effect pattern to the volatile matter and the Dulong approximation HHV

provided in Supplementary Material Fig. 4 (c). Similarly, the elemental hydrogen and nitrogen content drop with the increase in carbohydrate mass ratio as illustrated in Fig. 5 (b and c). The increase in glucose produced a reduction in hydrogen and nitrogen, as well as an increase in oxygen (calculated by difference), which generate a reduction in the theoretical HHV [2, 13, 14, 46].

Boiling point distribution and elemental analysis suggest that changes happen in the renewable bio-crude even after the equilibrium of the bulk phases illustrated in Section 3.1, requiring deeper chemical composition understating. Moreover, two of the most significant drawbacks of the renewable bio-crude from rich protein biomass are the nitrogen heteroatom content and high aromatic content, which require complex chemical analysis to be identified [10, 11, 27, 51]. In this study, GC-MS was selected and used to separate, tentatively identify and semi-quantify the organic species in the aqueous phase and renewable bio-crude species soluble in ethanol [24, 34, 61].

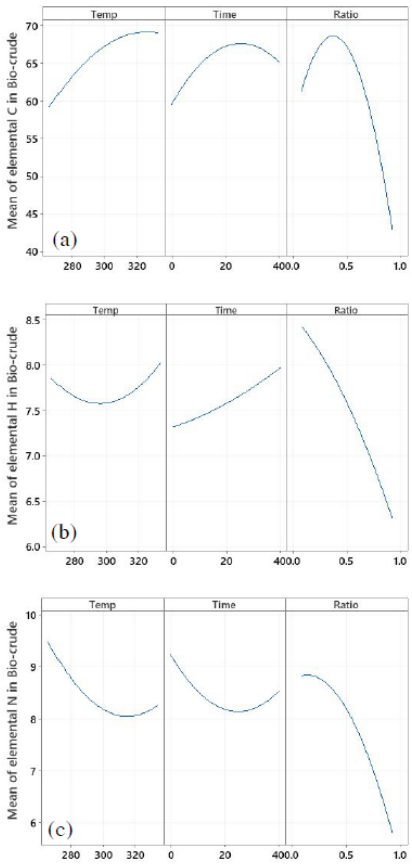

Figure 5. Major effects of factors in the elemental composition of the renewable bio-crude, Carbon (a), Hydrogen (b), and Nitrogen (c).

3.3 Characterisation of the aqueous and renewable bio-crude phases.

Direct injection of aqueous products into a GC-MS is typically avoided because of high-volume expansion and backflash, which can cause fluctuation in the MS vacuum pressure and reduce detector sensitivity [34, 35]. Water may also affect the stationary phase, show beading effect

where water micro-droplets condense on the phase and re-solubilise analysts, changing the retention time, causing doublets or poor peak shape, and increasing bleeding of the column. In the present study, aqueous and ethanol soluble bio-crude samples were analysed and contrasted through the DOE with a direct injection volume of 1µl in (1:25) split mode. Injection of a relatively small volume into a high-volume liner (900µl single taper, ultra-inert liner) in split mode with low injection temperature has been shown to reduce the volume expansion and backflash risks [34, 35]. Experimentally here, the retention time was relatively unchanged, doublets observed were minimal, and the column bleeding was consistent, dependent on the organic content and temperature.

The three primary organic molecular structures identified in the aqueous and ethanol soluble renewable bio-crude phases are presented in Fig. 6. The compounds are heterocyclic nitrogenous molecules known to be formed by the condensation of basic amino acids into piperazinedione compounds, followed by reduction into pyrazines [43, 55, 62].

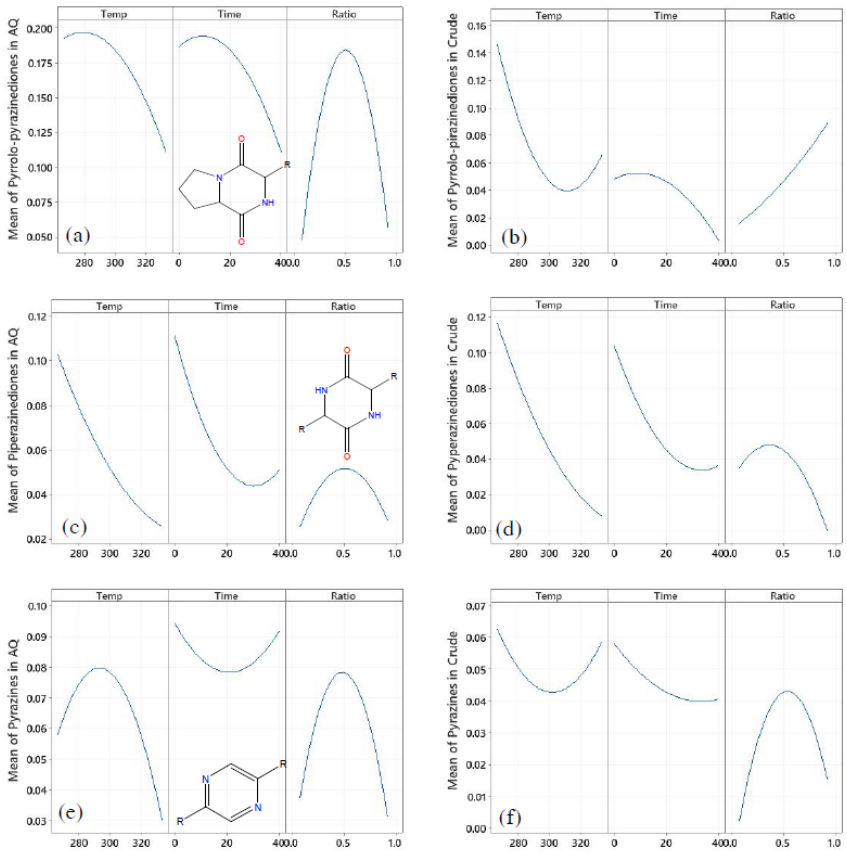

Figure 6. Primary effects of factors in the concentration of pyrrolo-pyrazinediones in aqueous (a) and bio-crude phase (b); piperazinediones in aqueous (c) and bio-crude phase (d); and pyrazines in aqueous (e) and bio- crude phase (f).

These compounds are tentatively identified with the use of the NIST 2017 Mass Spectral Library Database with a Match Factor (SI) threshold of 750 and semi-quantified based on total ion chromatogram (TIC) relative peak area. The pyrrolo[1,2-a]pyrazine-1,4-dione, hexahydro class includes compounds with -3-(2-methylpropyl)-, and -3-(phenylmethyl)- side groups, and 5,10-

Diethoxy-2,3,7,8-tetrahydro-1H,6H-dipyrrolo[1,2-a:1',2'-d]pyrazine as a conjugate. The 2,5-piperazinedione class includes compounds with 3-benzyl-6-isopropyl-, 3-methyl-6-(phenylmethyl)-, 3-(phenylmethyl)-, and 3,6-bis(2-methylpropyl)-, side groups, while cyclic amino acids include Cyclo-(l-leucyl-l-phenylalanyl) and Cyclo-(glycyl-l-leucyl), and finally, the pyrazine class includes compounds with the side groups of methyl-, 2,5-dimethyl-, 2-ethyl-6-methyl-, 2-ethyl-3-methyl-, 3-ethyl-2,5-dimethyl-, 2,6-dimethyl-, 2-ethyl-5-methyl-, 2-Methylpyrazine-5-carboxylic acid, 2,6-diethyl-, and 2-Methoxy-3-hydrazinyl-. A summary table with major structures and semi-quantification is provided in the Supplementary Material Table. 5.

The pyrrolo-pyrazinediones constitute the most notable compound class over the whole DOE. A maximum concentration was reached at 50% mass ratio (centre point), which may be linked to the synergetic optimal Maillard reaction conditions due to the equal mass load of proteins and carbohydrates [23, 27]. Additionally, as an intermediate over the residence time distribution, a concentration close to 20% (by mass of the total organics in the sample) was reached at approximately 10 minutes and a temperature of 280˚C promoting even higher pyrrolo-pyrazinedione concentrations.

For the renewable bio-crude, the concentrations were slightly lower, with differing trends over the three factors as illustrated in Fig. 6. The pyrrolo-pyrazinediones showed a maximum relative concentration of close to 20% by mass (of the organic loading) in the aqueous phase over the

three factors, whilst the renewable bio-crude exhibited a much lower concentration. The piperazinedione showed similar trends and concentrations in the aqueous and renewable, and for the pyrazines, the mass ratio factor showed a similar pattern with double the maximum concentration in the aqueous phase, but for temperature, the trend was the opposite. It is possible that traces of the aqueous phase were extracted with ethanol in the recovery and separation process (section 2.3), as they are completely miscible [47, 63].

Yang et al. (2015) observed some pyrrolo-pyrazinedione and pyrazine structures among other structures by performing GC-MS analysis of the HTL of a mixture (40/60) of polysaccharides and proteins (extracted from algae) at 260˚C [41]. They also found that the interaction between polysaccharides and proteins forming nitrogenous heterocyclic compound, had a positive effect on renewable bio-crude yields at 300˚C, but at lower temperatures (220 and 260˚C) the effect of the mixture interactions was negative [41].

Characterisation of the renewable crude fraction predominantly reported in the scientific literature has been accomplished via GC-MS with an extraction method prior to analysis [13, 32, 64]. However, organic solvent extraction efficiency restricts the tentative identification of organic structures because of the affinity, polarity, and equilibrium degree of the solvent extraction [33-35, 41]. DCM is widely used as a solvent to extract organic products from product phase recovered and it might boost the bio-crude yields as it also retains organics from the aqueous phase. In the present study, as the aqueous phase is recovered and analysed directly, the total area

of the TIC should represent the organic content of the aqueous phase comparatively, as illustrated in Fig. 7(a). The total area of the TIC may serve as an indicator of the total organic content of the aqueous sample, assuming that all water-soluble structures are of the correct molecular weight fraction, size, and polarity for analysis via the GC-MS technique.

The protein mass fraction produces higher concentrations of organics in the aqueous phase while a high carbohydrate ratio produces low retention of organic compounds in the aqueous phase with lower renewable bio-crude and higher solid phase yields [34]. This, in conjunction with the distribution of the top three organic structures presented in Fig. 6, may illustrate the relative concentration based on the distribution of the TIC, or with the NPOC (non-purgeable organic carbon or carbon-free air) to be a more accurate measure of the organic carbon content of the aqueous product phase.

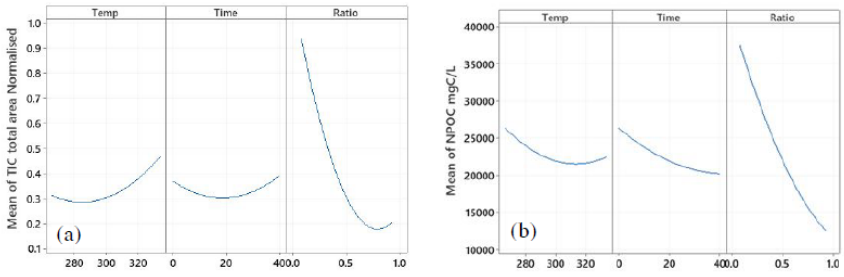

Figure 7. Primary effects of factors in the TIC total area (a), and TOC/NPOC (b) in the aqueous phase.

These chemical analyses of the aqueous phase products cannot be completed without a nitrogen in water test [11, 19]. Total nitrogen and ammonia are illustrated in Fig. 8. As expected, the most significant factor is the protein mass ratio, which is the source of nitrogen in biomass. Residence time increases the ammonia portion, reducing the total organic nitrogen (TON), and the reaction temperature also increases ammonia percentage, but the effect of temperature on the organic nitrogen share seems to reach a minimum value at approximately 310°C. Total nitrogen is a potential environmental pollutant which can harm aquatic flora and fauna, also important for biological nutrient removal (BNR) prior to discharge into bodies of water [65-67]. Ammonia is an essential reagent to interact with the carbohydrate and produce amides and amine via Amadori rearrangement [42, 45, 68].

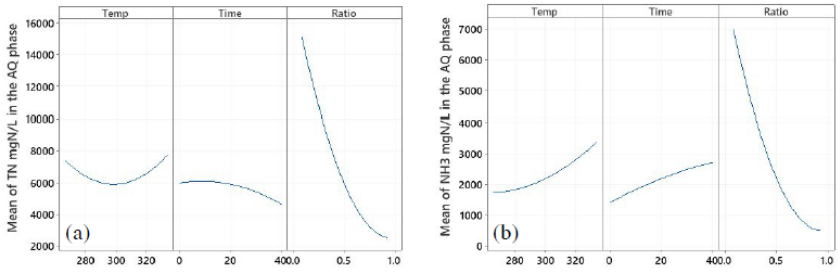

Figure 8. Primary effect of factors on the total nitrogen (a), and ammonia (b) in the aqueous phase.

3.4 Semi-quantification of aromatics, heterocycles, and heteroatoms.

The consolidation of the GC-MS data from the 16 experiments (counting only peaks which represent over 0.5% area or have peak quality higher than 50%) generated 430 different organic

species within the aqueous phase and over 800 from the bio-crude (ethanol soluble) phase, with an average TIC signal recovery of 95%. The phenyl-methyl aromatic (based on a m/z of 91 ± 0.5) is subtracted from the TIC, and the peaks of the m/z-91chromatogram are then contrasted (based on retention time) to the original TIC to sum up and semi-quantify the TIC peak area of the structures containing phenylmethyl ion fragments as illustrated in Fig. 9(a and b). The heterocyclic compounds (non-nitrogenous) and the sum of the most representative nitrogenous structures are also shown in Fig. 9(c to f).

Zhang et al. (2016) have investigated the Maillard reactions by mixing algae (spirulina and nannochloropsis sp.) with model compounds (glucose and soy protein) to determine the effect on product yields and composition [24]. they found that higher protein content had a negative effect on the recovery of the free fatty acids, while the increase in glucose composition enhanced the renewable bio-crude yield and the energy recovery. Finally, they defined 18 main compounds in the bio-crude and estimate the composition of those based on the TIC peak area [24].

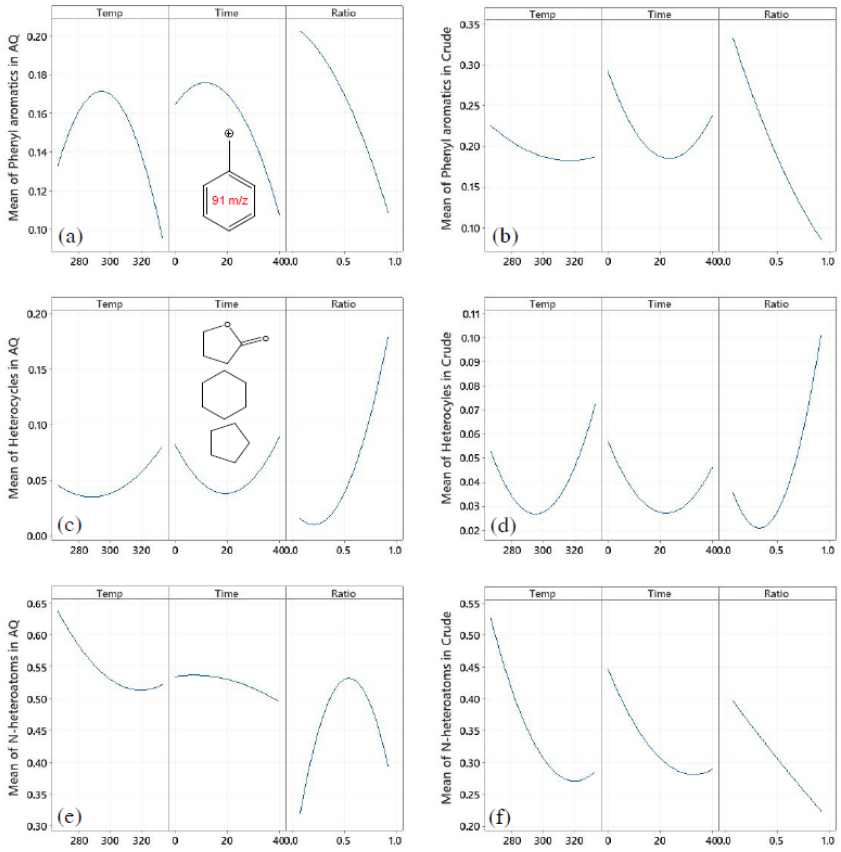

Figure 9. Primary effects of factors in the condensed concentration of phenyl-aromatics in bio-crude (a) and aqueous phase, heterocycle in bio-crude (c) and aqueous phase (d), and nitrogenous organic species in bio-crude (e) and in the aqueous phase (f).

The aromatic amino acids, especially phenylalanine, are highly resistant even to supercritical water conditions [69]. The relative linearity of phenyl aromatic concentration over mass ratio on both the aqueous and renewable bio-crude phases may indicate that the aromatics in the aqueous and ethanol-soluble bio-crude come primarily from the protein, and particularly from the

phenylalanine, which is 5.3% approximately in the soy protein (according to the supplier composition information). The organic heterocycles containing cyclopentane, cyclohexane and lactone structures presented a relatively similar pattern in both the aqueous and bio-crude with higher concentration at high carbohydrate mass ratio and in the aqueous phase [25, 27]. Finally, the nitrogenous organic compounds include the most significant heteroatom organics detected by GC-MS, and the trends showed by the aqueous phase are relatively similar to the TON (see Supplementary Material Table S.4), despite clear differences in the analytical methods [25, 27, 62]. Differences occur in the mass ratio as not all structures are included in Fig. 9(e and f) compounds like 1-(2-Hydroxyethyl) piperidine which were present mostly in high protein ratio experiments as well as some peptides and amino acids were not detected in the GC analysis of nitrogenous organic species.

The analysis of the aqueous phase showed the interactions occurring in the reaction medium phase. However, the composition of the renewable crude phase shares many organic structures identified in the aqueous phase. Differences were observed in the compositions, for example compounds like 2-Methylcyclopent-2-enone which was present in all samples and 4-Isobutyl-1H-imidazole-2-thiol which was present only in experiments two and four (experiments at 280˚C and 75% mass ratio). The above highlight the complexity of the organic nitrogenous compounds, as well as the difficulties in maintaining quality of the peaks based on the mass spectra tentatively identification match [33-35].

3.5 The Maillard reaction pathway under hydrothermal conditions.

Kruse et al. (2005) revealed that the Maillard reactions involve the formation of stable free radicals, which have a scavenging effect on free radical chain reactions responsible for gas formation [22]. Therefore, Maillard interactions reduce the gaseous phase formation while increasing the bio-crude yield. Peterson et al. (2010) have investigated the reaction kinetics of the Maillard reactions of glucose and glycine mixtures under hydrothermal conditions at 250˚C [23]. The results suggest that glucose caused a severe destruction of glycine, and different proportions of glycine affected the conversion of glucose differently [23]. Madsen et al. (2016) and Qiu et al. (2019) studied the Maillard reactions by analysing the products of HTL from model compound mixtures with GC-MS [26, 36]. Lastly, Kristianto et al. (2021) investigated the Amadori rearrangement with glucose and ammonium acetate in a micro-flow reactor, providing a new insight into the Maillard reactions forming nitrogenous species like pyrazine without amino acids as feedstocks [45]. However, the reaction mechanisms involved in the Maillard interactions are still not completely understood.

While the proteins in biomass showed drastic hydrolysis at 190˚C, sugars degrade just above 130˚C. Additionally, over the degradation of amino acids in proteins, the abstraction of the amino group (deamination) competes with the carbonyl functional group (decarboxylation), as a result only one of these reactions can undergo under hydrothermal condition [69]. Based on the results obtained with the GC-MS analysis of the aqueous and renewable crude product phases, and the

structure of the amino acids of the soy protein, the Maillard interactions in the present study may be illustrated in Fig. 10. The condensation of two amino acids (cyclo-dimerization) into heterocyclic organic structures, followed by the reduction and degradation, appears to be most significant pathway for the amino acids from hydrolysis of proteins [23, 25, 33, 43, 55].

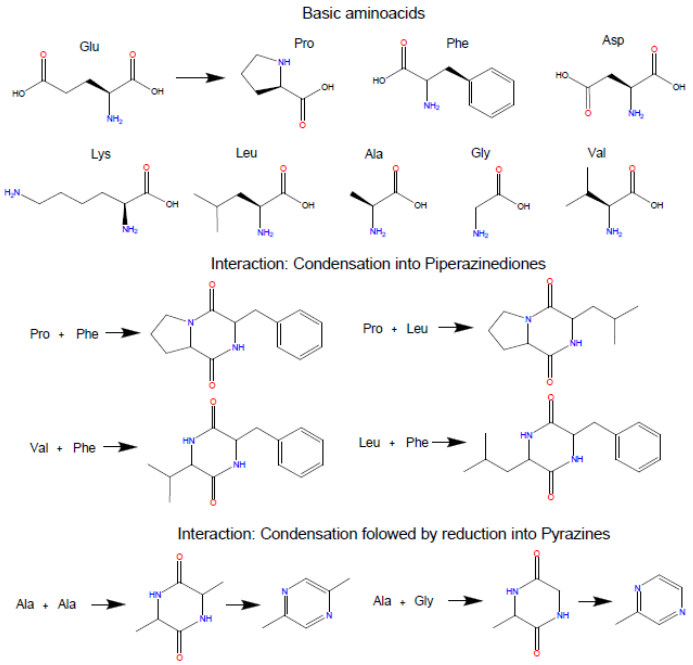

Figure 10. Basic amino acid structures, condensation, and reduction reactions proposed over the HTL of proteins.

The preferred pathway is pyrrolo-pyrazinedione and piperazinedione condensation, followed by reduction into pyrazines. The most common compounds are pyrrolidine (proline), phenyl-methyl (phenylalanine), methyl-isopropyl (leucine), and isopropyl (valine) among others. However, the

proline concentration of the soy protein is approximately 4.2%, so reaching a pyrrolo-pyrazinedione relative concentration close to 20% by mass is not possible directly given the initial concentration. Instead, we propose that glutamic acid is converted into proline. First, the carboxyl group is reduced to an aldehyde, then reacts with the α-amino group, eliminating water (via Schiff base) and finally the Schiff base is reduced, producing proline. Additionally, the production of pyrrolidine (e.g. proline) compounds may also be promoted by the Strecker reaction and Amadori rearrangement of carbohydrates, with release of amino acids and ammonia into the aqueous phase [42, 55, 68, 70].

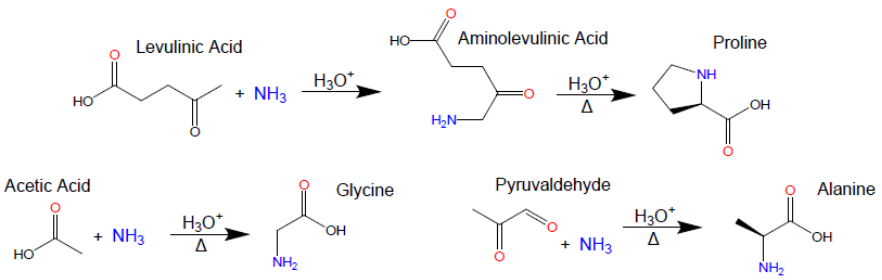

Figure 11. Tentative pathways for the formation of amino acids from glucose degraded products via Amadori rearrangement with ammonia.

Levulinic acid (LA) as one of the most prominent products from glucose degradation, may also produce proline. The formation of levulinic acid as the ring opening of HMF may produce amino-levulinic acid from the addition of the amino group of ammonia under acid autogenous conditions (subcritical water), with subsequent reduction of the ketone to produce a rearrangement and ring

closure of the pyrrolidine to form proline as illustrated in Fig. 11 [70, 71]. These tentative pathways may explain the product profiles observed in Fig. 6(a), though, amino-acid formation via Strecker reaction and Amadori rearrangement will not be limited to these examples. Higher temperatures promote 2-pyrrolidinone formation via oxygen substitution with nitrogen in lactones and furans, while 3-Pyridinol, 6-methyl- may be formed by the rearrangement and closure of some amino acids. Additionally, proline is also known as the precursor of nitrogen-containing humins [42, 68-70].

3.6 Spirulina and soy protein composition profile comparison.

HTL experiments with spirulina and soy protein isolate with CCD centre point temperature of 300˚C and 10 min residence time were performed, and the aqueous phase was analysed using the same GC-MS technique. The normalised organic mass content of the aqueous sample was 71.5% and 65.4% and the summary of the tentative identification is presented In Table. 2. Piperazinedione compounds accounted for 15% of the peak area of detected organic compounds while pyrrolo-pyrazinedione accounted for nearly 8%. The relatively low carbohydrate to protein mass ratio of 25.8% limited the formation of proline and the pyrrolo-pyrazinediones compounds. Soy protein produced more pyrrolo-pyrazinediones because of the high concentration of glutamic acid. However, the piperazinedione was higher, reaching almost 20% of total TIC peak area in the aqueous phase [10, 14, 24].

Table. 2. Summary of the GC-MS tentative identification and semi-quantification of aqueous product phase from the HTL of spirulina and soy protein at 300˚C and 10 min.

	Spirulina		Soy protein isolate	
Compound name	Peak Area [%]	Peak Quality Average [%]	Peak Area [%]	Peak Quality Average [%]
Piperazinediones	15.01%	68.9	19.23%	65.2
Pyrrolo-pyrazinediones	7.92%	86.3	13.39%	67
N-methylene-n-octadecylamine	5.48%	38		
Azocine, octahydro-	5.41%	38		
5,5-Dimethylbarbituric acid	5.34%	30		
Piperidine, 3-methyl-	4.14%	38	0.85%	30
2-methylpiperidine			4.13%	38
Cyclopentanamine, N-ethyl-	4.06%	46		
Pyrazines	2.67%	84.6		
4-Decene, 8-methyl-, (E)-	2.02%	47	6.96%	47

Other components identified in the experiments included: N-methylene-n-octadecylamine was only identified in experiment 3 of the DOE with an organic concentration of 1.2%, Azocine, octahydro- was found in experiments 2, 4, 9, 10, 12, 14 and 15, with an average concentration of 6.6% and a maximum of 12.1% in experiment 12. 5,5-Dimethyl barbituric acid was found in experiments 1 and 5 with a relatively high average concentration of 9.4%. Piperidine, 3-methyl- and 2-methyl piperidine were only found together in experiment 13. 4-Decene, 8-methyl-, (E)- was found in experiment 1, 5 and 15 with an average of 2.3% and a maximum of 4.9%.

Present study aimed to enhance the body of knowledge of the Maillard reactions of biomass key components under hydrothermal conversion conditions by investigating the effect of protein and monosaccharides composition ratio on the aqueous and bio-crude phases via GC-MS whilst vary the mass ratio, temperature, and residence time of the conversion. Proline has appeared as the rational Maillard intermediate candidate from levulinic acid, explaining the concentrations and profiles of pyrrolo-pyrazinediones in both the aqueous and renewable bio-crude phases [27, 33, 34]. However, the modelling of highly complex amino acid interaction requires better understanding to promote the potential application of prediction model for the hydrothermal liquefaction of non-conventional biomass sources with high and variable protein and carbohydrate composition [9, 10].

4. Conclusion

The HTL conversion of model compound protein and monosaccharide mixtures have been studied to provide better understanding of the reaction mechanism involved in the Maillard interactions. The effects of temperature, residence time and carbohydrate/protein mass ratio have been evaluated with a CCD/DOE exemplifying the effect of the mass ratio over various response variables including bio-crude and solid product yields, boiling point distribution and elemental composition of the bio-crude. The potential of GC-MS analysis for aqueous samples and ethanol soluble bio-crude phases via directly injected into the GC has been explained and tested. The

formation of proline via Strecker reaction and Amadori rearrangement of levulinic acid as one of the most prominent intermediates from C6 sugar degradations could explain the higher concentration of pyrrolo-pyrazinediones found at equal protein and carbohydrate mass ratio. However, there are many other amino acids such as alanine which might condensate into piperazinedione before degrading into pyrazine and many other compounds from the Maillard reactions. Other compounds like piperidines, phenyl aromatics and non-nitrogenous heterocycles are also included in the CCD. The value of the present study lies in ambitious scope from statistic evaluation to fundamental reactions exploring the effect of the protein/carbohydrate mass ratio and the GC-MS of aqueous phases via direct injection, which could provide a broader spectrum of the organic compounds formed via the Maillard reaction in the HTL of biomass. Finally, the Maillard reactions are highly complex, and the number of organic compounds produced under HTL conditions is abundant, requiring further investigation. Nonetheless, the present study provides new insight into the interaction of sugar degradation products and amino acids under hydrothermal conversion conditions.

Associated content

Supporting information

Table S.1. CCD factorial experiment conditions and measured product phase yields.

Figure S.2. The differential equations system (Fig. 2 (a) model), experimental and kinetic model data for the circumscribed experiments at (280-320˚C) and (25-75% ratio).

Table S.3. Boiling point fraction and non-volatiles from the thermogravimetric analysis of the renewable bio-crude.

Figure S.4. Primary effect of factors in the low boiling point 80 to 300˚C (a), high boiling point 300 to 600˚C (b) and HHV (c) of the renewable crude.

Table S.5. Relative peak area of common organic species in the aqueous phase.

Author information

Corresponding Author

E-mail: philip.vaneyk@adelaide.edu.au.

ORCID

Andrés Danilo Chacón Parra: 0000-0002-7615-0238

Tony Hall: 0000-0001-8157-9445

David Milton Lewis: 0000-0002-5322-1873

Marianne Glasius: 0000-0002-4404-6989

Philip Joseph van Eyk: 0000-0003-3768-2044

Notes:

The authors declare no competing financial interest

Acknowledgments

The authors acknowledge the financial support of the Australian Research Council's Linkage Project grant (LP150101241) with industry partner Southern Oil Refining.

References

1. Kruse, A., A. Funke, and M.M. Titirici, *Hydrothermal conversion of biomass to fuels and energetic materials.* Curr Opin Chem Biol, 2013. **17**(3): p. 515-21.
2. Biller, P. and A.B. Ross, *17 - Production of biofuels via hydrothermal conversion*, in *Handbook of Biofuels Production (Second Edition)*, R. Luque, et al., Editors. 2016, Woodhead Publishing. p. 509-547.
3. Zhang, Y. and W.T. Chen, *5 - Hydrothermal liquefaction of protein-containing feedstocks*, in *Direct Thermochemical Liquefaction for Energy Applications*, L. Rosendahl, Editor. 2018, Woodhead Publishing. p. 127-168.
4. Leng, L., et al., *Nitrogen in bio-oil produced from hydrothermal liquefaction of biomass: A review.* Chemical Engineering Journal, 2020. **401**.
5. Gollakota, A.R.K., N. Kishore, and S. Gu, *A review on hydrothermal liquefaction of biomass.* Renewable and Sustainable Energy Reviews, 2018. **81**: p. 1378-1392.
6. Kruse, A. and E. Dinjus, *Hot compressed water as reaction medium and reactant.* The Journal of Supercritical Fluids, 2007. **39**(3): p. 362-380.

7. Peterson, A.A., et al., *Thermochemical biofuel production in hydrothermal media: A review of sub- and supercritical water technologies.* Energy & Environmental Science, 2008. **1**(1).

8. Obeid, R., et al., *The elucidation of reaction kinetics for hydrothermal liquefaction of model macromolecules.* Chemical Engineering Journal, 2019. **370**: p. 637-645.

9. Hietala, D.C. and P.E. Savage, *A molecular, elemental, and multiphase kinetic model for the hydrothermal liquefaction of microalgae.* Chemical Engineering Journal, 2021. **407**.

10. Sheehan, J.D. and P.E. Savage, *Products, Pathways, and Kinetics for the Fast Hydrothermal Liquefaction of Soy Protein Isolate.* ACS Sustainable Chemistry & Engineering, 2016. 4(12): p. 6931-6939.

11. Chacón-Parra, A., D. Lewis, and P. van Eyk, *Elemental nitrogen balance, reaction kinetics and the effect of ethanol on the hydrothermal liquefaction of soy protein.* Chemical Engineering Journal, 2021. **425**.

12. Chacón-Parra, A., et al., *A multi-component reaction kinetics model for the hydrothermal liquefaction of carbohydrates and co-liquefaction to produce 5-ethoxymethyl furfural.* Fuel, 2021. **310**(122499).

13. Teri, G., L. Luo, and P.E. Savage, *Hydrothermal Treatment of Protein, Polysaccharide, and Lipids Alone and in Mixtures.* Energy & Fuels, 2014. **28**(12): p. 7501-7509.

14. Luo, L., et al., *Products and Kinetics for Isothermal Hydrothermal Liquefaction of Soy Protein Concentrate.* ACS Sustainable Chemistry & Engineering, 2016. 4(5): p. 2725-2733.

15. Lu, J., et al., *110th Anniversary: Influence of Solvents on Biocrude from Hydrothermal Liquefaction of Soybean Oil, Soy Protein, Cellulose, Xylose, and Lignin, and Their*

Quinary Mixture. Industrial & Engineering Chemistry Research, 2019. **58**(31): p. 13971-13976.

16. Lu, J., et al., *Nitrogen Migration and Transformation during Hydrothermal Liquefaction of Livestock Manures.* ACS Sustainable Chemistry & Engineering, 2018. **6**(10): p. 13570-13578.
17. Sheehan, J.D. and P.E. Savage, *Molecular and Lumped Products from Hydrothermal Liquefaction of Bovine Serum Albumin.* ACS Sustainable Chemistry & Engineering, 2017. **5**(11): p. 10967-10975.
18. Matsumura, Y., S. Yanachi, and T. Yoshida, *Glucose Decomposition Kinetics in Water at 25 MPa in the Temperature Range of 448−673 K.* Industrial & Engineering Chemistry Research, 2006. **45**(6): p. 1875-1879.
19. Martinez-Fernandez, J.S. and S. Chen, *Sequential Hydrothermal Liquefaction characterization and nutrient recovery assessment.* Algal Research, 2017. **25**: p. 274-284.
20. Paksung, N., et al., *Structural Effects of Cellulose on Hydrolysis and Carbonization Behavior during Hydrothermal Treatment.* ACS Omega, 2020. **5**(21): p. 12210-12223.
21. He, Q., et al., *Kinetic Study of the Hydrothermal Carbonization Reaction of Glucose and Its Product Structures.* Industrial & Engineering Chemistry Research, 2021. **60**(12): p. 4552-4561.
22. Kruse, A., et al., *Influence of Proteins on the Hydrothermal Gasification and Liquefaction of Biomass. 1. Comparison of Different Feedstocks.* Industrial & Engineering Chemistry Research, 2005. **44**(9): p. 3013-3020.
23. Peterson, A.A., R.P. Lachance, and J.W. Tester, *Kinetic Evidence of the Maillard Reaction in Hydrothermal Biomass Processing: Glucose−Glycine Interactions in High-*

Temperature, High-Pressure Water. Industrial & Engineering Chemistry Research, 2010. **49**(5): p. 2107-2117.

24. Zhang, C., et al., *Enhancing the performance of Co-hydrothermal liquefaction for mixed algae strains by the Maillard reaction.* Green Chemistry, 2016. **18**(8): p. 2542-2553.

25. Fan, Y., et al., *Hydrothermal liquefaction of protein-containing biomass: study of model compounds for Maillard reactions.* Biomass Conversion and Biorefinery, 2018. **8**(4): p. 909-923.

26. Qiu, Y., et al., *Biocrude Oil Production through the Maillard Reaction between Leucine and Glucose during Hydrothermal Liquefaction.* Energy & Fuels, 2019. **33**(9): p. 8758-8765.

27. Tang, X., C. Zhang, and X. Yang, *Hydrothermal Liquefaction of Model Compounds Protein and Glucose: Effect of Maillard Reaction on Low Lipid Microalgae.* IOP Conference Series: Materials Science and Engineering, 2019. **611**: p. 012026.

28. Biller, P., R. Riley, and A.B. Ross, *Catalytic hydrothermal processing of microalgae: decomposition and upgrading of lipids.* Bioresour Technol, 2011. **102**(7): p. 4841-8.

29. Chacón-Parra, A., D. Lewis, and P. van Eyk, *The effect of ethanol as a homogeneous catalyst on the reaction kinetics of hydrothermal liquefaction of lipids.* Chemical Engineering Journal, 2021. **414**: p. 128832.

30. Tsai, Y.T., H.M. Lin, and M.J. Lee, *Biodiesel production with continuous supercritical process: non-catalytic transesterification and esterification with or without carbon dioxide.* Bioresour Technol, 2013. **145**: p. 362-9.

31. Jiang, J. and P.E. Savage, *Using Solvents To Reduce the Metal Content in Crude Bio-oil from Hydrothermal Liquefaction of Microalgae.* Industrial & Engineering Chemistry Research, 2019. **58**(50): p. 22488-22496.

32. Madsen, R.B. and M. Glasius, *How Do Hydrothermal Liquefaction Conditions and Feedstock Type Influence Product Distribution and Elemental Composition?* Industrial & Engineering Chemistry Research, 2019. **58**(37): p. 17583-17600.

33. Coleman, W.M., III, *A Study of the Behavior of Maillard Reaction Products Analyzed by Solid-Phase Microextraction—Gas Chromatography—Mass Selective Detection.* Journal of Chromatographic Science, 1996. **34**(5): p. 213-218.

34. Aeppli, C., et al., *Simultaneous quantification of polar and non-polar volatile organic compounds in water samples by direct aqueous injection-gas chromatography/mass spectrometry.* J Chromatogr A, 2008. **1181**(1-2): p. 116-24.

35. Yu, B., et al., *Optimizations of large volume-direct aqueous injection-gas chromatography to monitor volatile organic compounds in surface water.* Analytical Methods, 2014. **6**(17).

36. Madsen, R.B., et al., *Predicting the Chemical Composition of Aqueous Phase from Hydrothermal Liquefaction of Model Compounds and Biomasses.* Energy & Fuels, 2016. **30**(12): p. 10470-10483.

37. Madsen, R.B., et al., *Hydrothermal co-liquefaction of biomasses - quantitative analysis of bio-crude and aqueous phase composition.* Sustainable Energy & Fuels, 2017. **1**(4): p. 789-805.

38. Madsen, R.B., et al., *Using design of experiments to optimize derivatization with methyl chloroformate for quantitative analysis of the aqueous phase from hydrothermal liquefaction of biomass.* Analytical and Bioanalytical Chemistry, 2016. **408**(8): p. 2171-2183.

39. Maddi, B., et al., *Quantitative characterization of the aqueous fraction from hydrothermal liquefaction of algae.* Biomass and Bioenergy, 2016. **93**: p. 122-130.

40. Koehler, P.E. and G.V. Odell, *Factors affecting the formation of pyrazine compounds in sugar-amine reactions.* Journal of Agricultural and Food Chemistry, 1970. **18**(5): p. 895-898.

41. Yang, W., et al., *Understanding low-lipid algae hydrothermal liquefaction characteristics and pathways through hydrothermal liquefaction of algal major components: Crude polysaccharides, crude proteins and their binary mixtures.* Bioresource Technology, 2015. **196**: p. 99-108.

42. Nikolov, P.Y. and V.A. Yaylayan, *Reversible and covalent binding of 5-(hydroxymethyl)-2-furaldehyde (HMF) with lysine and selected amino acids.* J Agric Food Chem, 2011. **59**(11): p. 6099-107.

43. Van Lancker, F., A. Adams, and N. De Kimpe, *Formation of Pyrazines in Maillard Model Systems of Lysine-Containing Dipeptides.* Journal of Agricultural and Food Chemistry, 2010. **58**(4): p. 2470-2478.

44. Jazrawi, C., et al., *Two-stage hydrothermal liquefaction of a high-protein microalga.* Algal Research, 2015. **8**: p. 15-22.

45. Kristianto, I., B.S. Haynes, and A. Montoya, *Hydrothermal Decomposition of Glucose in the Presence of Ammonium.* Industrial & Engineering Chemistry Research, 2021.

46. Isa, K.M., T.A.T. Abdullah, and U.F.M. Ali, *Hydrogen donor solvents in liquefaction of biomass: A review.* Renewable and Sustainable Energy Reviews, 2018. **81**: p. 1259-1268.

47. Zhang, J. and Y. Zhang, *Hydrothermal Liquefaction of Microalgae in an Ethanol–Water Co-Solvent To Produce Biocrude Oil.* Energy & Fuels, 2014. **28**(8): p. 5178-5183.

48. Riazi, M.R., *Characterization and Properties of Petroleum Fractions.* 2005: ASTM International.

49. Law, V.J., *Numerical Methods for Chemical Engineers Using Excel, VBA, and MATLAB*. 2013: CRC Press, Taylor & Francis Group.

50. Fogler, H.S., *Elements of Chemical Reaction Engineering*. 2006: Prentice Hall PTR.

51. Valdez, P.J., V.J. Tocco, and P.E. Savage, *A general kinetic model for the hydrothermal liquefaction of microalgae*. Bioresour Technol, 2014. **163**: p. 123-7.

52. Obeid, R., et al., *Reaction Kinetics and Characterization of Species in Renewable Crude from Hydrothermal Liquefaction of Mixtures of Polymer Compounds To Represent Organic Fractions of Biomass Feedstocks*. Energy & Fuels, 2020. **34**(1): p. 419-429.

53. van Zandvoort, I., et al., *Formation, molecular structure, and morphology of humins in biomass conversion: influence of feedstock and processing conditions*. ChemSusChem, 2013. **6**(9): p. 1745-58.

54. Falco, C., N. Baccile, and M.M. Titirici, *Morphological and structural differences between glucose, cellulose and lignocellulosic biomass derived hydrothermal carbons*. Green Chemistry, 2011. **13**(11): p. 3273-3281.

55. Yaylayan, V.A., *Classification of the Maillard reaction: A conceptual approach*. Trends in Food Science & Technology, 1997. **8**(1): p. 13-18.

56. Vardon, D.R., et al., *Chemical properties of biocrude oil from the hydrothermal liquefaction of Spirulina algae, swine manure, and digested anaerobic sludge*. Bioresour Technol, 2011. **102**(17): p. 8295-303.

57. Li, Y., et al., *Quantitative multiphase model for hydrothermal liquefaction of algal biomass*. Green Chemistry, 2017. **19**(4): p. 1163-1174.

58. Ross, A.B., et al., *Investigation of the pyrolysis behaviour of brown algae before and after pre-treatment using PY-GC/MS and TGA*. Journal of Analytical and Applied Pyrolysis, 2009. **85**(1): p. 3-10.

59. Dinjus, E., A. Kruse, and N. Tröger, *Hydrothermal Carbonization - 1. Influence of Lignin in Lignocelluloses.* Chemical Engineering & Technology, 2011. **34**(12): p. 2037-2043.

60. Karayıldırım, T., A. Sınağ, and A. Kruse, *Char and Coke Formation as Unwanted Side Reaction of the Hydrothermal Biomass Gasification.* Chemical Engineering & Technology, 2008. **31**(11): p. 1561-1568.

61. Cheng, S., et al., *Highly Efficient Liquefaction of Woody Biomass in Hot-Compressed Alcohol− Water Co-solvents†.* Energy & Fuels, 2010. **24**(9): p. 4659-4667.

62. Ashoor, S.H. and J.B. Zent, *Maillard Browning of Common Amino Acids and Sugars.* Journal of Food Science, 1984. **49**(4): p. 1206-1207.

63. Tan, K.T., K.T. Lee, and A.R. Mohamed, *Effects of free fatty acids, water content and co-solvent on biodiesel production by supercritical methanol reaction.* The Journal of Supercritical Fluids, 2010. **53**(1-3): p. 88-91.

64. Obeid, R., et al., *Reaction kinetics and characterisation of species in renewable crude from hydrothermal liquefaction of monomers to represent organic fractions of biomass feedstocks.* Chemical Engineering Journal, 2020. **389**.

65. Burton, F.L., et al., *Wastewater Engineering: Treatment and Resource Recovery.* 2013: McGraw-Hill Education.

66. Xu, L., et al., *Assessment of a dry and a wet route for the production of biofuels from microalgae: Energy balance analysis.* Bioresource Technology, 2011. **102**(8): p. 5113-5122.

67. Snoeyink, V.L. and D. Jenkins, *Water chemistry.* 1980: Wiley.

68. Yaylayan, V.A., *Recent Advances in the Chemistry of Strecker Degradation and Amadori Rearrangement: Implications to Aroma and Color Formation.* Food Science and Technology Research, 2003. **9**(1): p. 1-6.

69. Körner, P., *Hydrothermal Degradation of Amino Acids.* ChemSusChem, 2021. 14(22): p. 4947-4957.

70. Cai, R.-F., et al., *Reductive Amination of Biobased Levulinic Acid to Unnatural Chiral γ-Amino Acid Using an Engineered Amine Dehydrogenase.* ACS Sustainable Chemistry & Engineering, 2020. 8(46): p. 17054-17061.

71. Tewari, K.M. and I.M. Eggleston, *Chemical approaches for the enhancement of 5-aminolevulinic acid-based photodynamic therapy and photodiagnosis.* Photochem Photobiol Sci, 2018. 17(11): p. 1553-1572.

Elucidating the Maillard reaction mechanism in the hydrothermal liquefaction of binary model compound mixtures and spirulina

Andrés Chacón-Parra, † Tony Hall, ‡ David Lewis, † Marianne Glasius, ǂ Philip van Eyk†

† School of Chemical Engineering and Advanced Materials,

The University of Adelaide, Adelaide, SA, 5005, Australia

‡ Faculty of Sciences, The University of Adelaide,

Adelaide, South Australia 5005, Australia

ǂ Department of Chemistry, Aarhus University,

8000 Aarhus C, Denmark

*Corresponding author

E-mail address: philip.vaneyk@adelaide.edu.au

Supporting information

Table S.1. CCD factorial experiment conditions and measured product phase yields.

HTL	CCD Conditions			Average HTL Product Yields		
	Temp [°C]	Time [min]	Mass Ratio [glucose/mix]	Bio-crude [%]	Hydrochar [%]	gas [%]
1	280	10	0.26	20.5	5.7	4.5
2	280	10	0.75	17.9	21.3	5.8
3	280	30	0.26	21.3	4.3	12.9
4	280	30	0.75	9.7	21.0	12.0
5	320	10	0.26	22.7	4.7	12.1
6	320	10	0.75	17.5	19.4	15.5
7	320	30	0.26	22.3	2.1	16.5
8	320	30	0.75	11.5	18.1	17.7
9	266	20	0.52	19.3	18.7	6.8
10	334	20	0.52	19.9	9.5	17.6
11	300	3	0.50	23.4	11.9	7.4
12	300	37	0.50	19.6	9.8	14.7
13	300	20	0.10	26.8	2.3	12.7
14	300	20	0.90	18.5	22.1	13.3
15	300	20	0.50	20.7	10.1	13.0
16	300	0	0.52	28.4	15.2	4.4

Figure S.2. The differential equations system (Fig. 2 (a) model), experimental and kinetic model data for the circumscribed experiments at (280-320°C) and (25-75% ratio)

$$\frac{dx_1}{dt} = -(k_1 + k_2)x_1 \quad (1)$$

$$\frac{dx_2}{dt} = -(k_3 + k_4)x_2 \quad (2)$$

$$\frac{dx_3}{dt} = k_1x_1 + k_3x_2 + k_6x_4 + k_{10}x_6 - (k_5 + k_7 + k_9)x_3 \quad (3)$$

$$\frac{dx_4}{dt} = k_4x_2 + k_5x_3 - (k_6 + k_8)x_4 \quad (4)$$

$$\frac{dx_5}{dt} = k_2x_1 + k_7x_3 + k_8x_4 \quad (5)$$

$$\frac{dx_6}{dt} = k_9x_3 - k_{10}x_6 \quad (6)$$

(a)

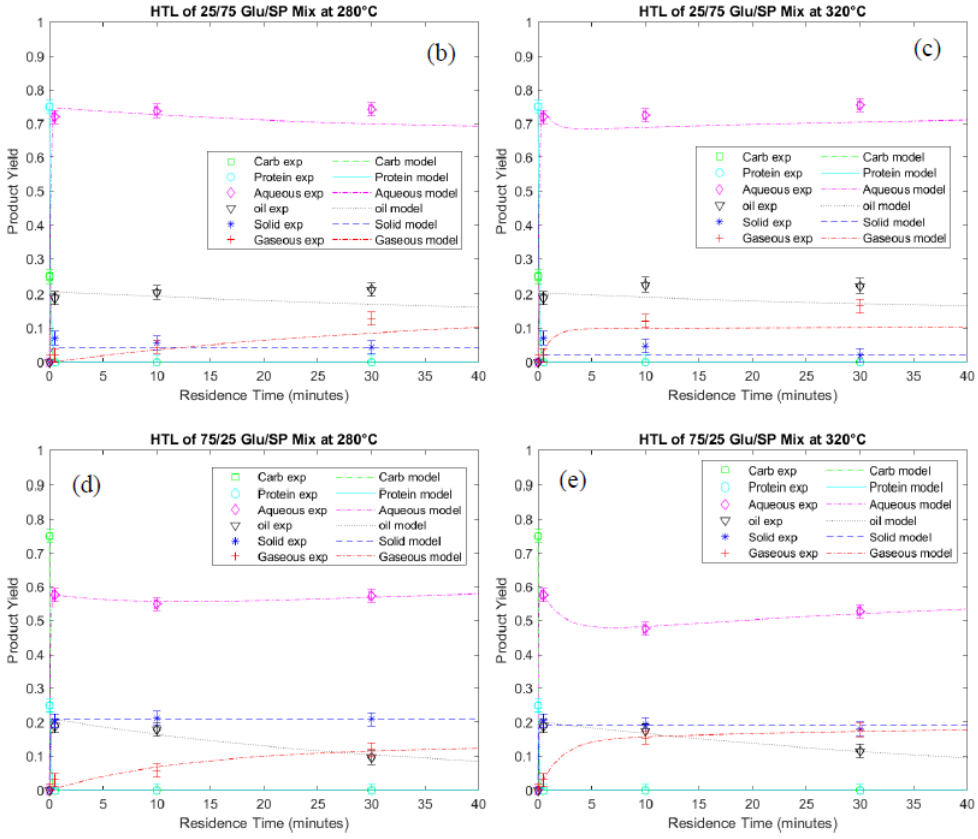

Table S.3. Boiling point fraction and non-volatiles from the thermogravimetric analysis of the renewable bio-crude.

TGA	Volatiles			Non-volatiles	
	80-180°C [%]	180-300°C [%]	300-600°C [%]	Combustible at 600°C [%]	Ash [%]
1	7.1	26.5	36.8	19.7	9.0
2	11.1	25.3	25.5	23.0	13.6
3	11.3	26.5	26.1	17.2	18.5
4	12.5	31.5	23.4	22.9	8.4
5	10.8	28.9	35.6	16.9	7.1
6	0.9	17.4	31.5	39.2	8.5
7	12.3	27.3	30.5	15.5	14.0
8	6.2	28.6	33.4	23.0	7.7
9	14.3	30.9	25.9	20.1	7.8
10	8.8	27.8	31.1	19.7	11.5
11	14.6	27.3	29.3	15.6	12.7
12	10.8	27.0	32.9	21.5	6.8
13	8.2	30.0	33.1	11.8	17.4
14	6.1	12.8	20.5	25.9	33.7
15	7.2	25.2	34.7	19.9	11.9
16	7.2	22.4	34.5	20.8	13.9

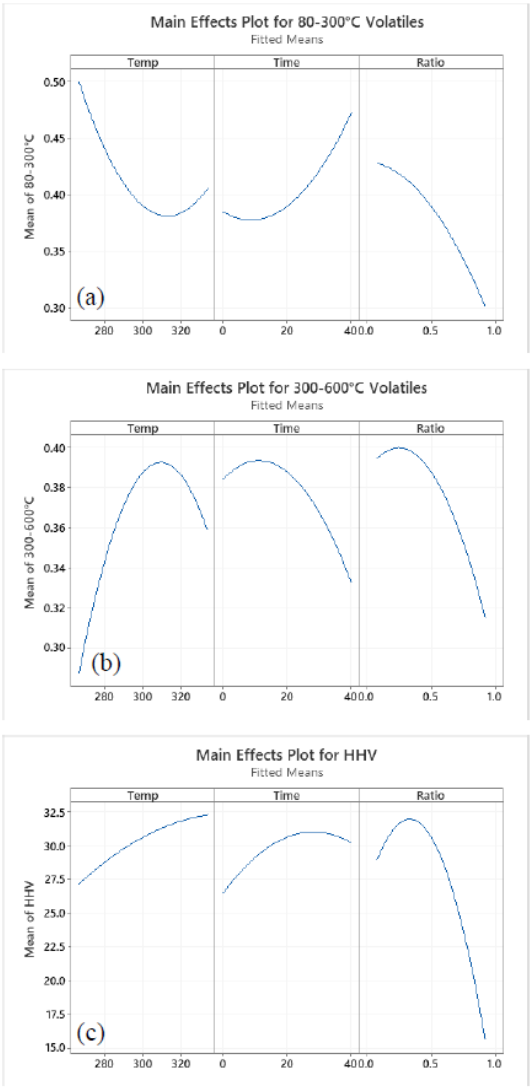

Figure S.4. Primary effect of factors in the low boiling point 80 to 300°C (a), high boiling point 300 to 600°C (b) and HHV (c) of the renewable crude.

Table S.4. Elemental composition of the bio-crude and nitrogen composition of the aqueous phase and the primary effect of factors son TON.

CHN, N and C in water	Elemental composition Bio-crude					Nitrogen in Aqueous phase			TOC
	C [%]	H [%]	N [%]	O [%]	HHV [kJ/kg]	TN mgN/L	NH_3 mgN/L	TON mgN/L	NPOC mgC/L
1	60.7	8.4	10.0	21.0	28.8	11400	3460	7940	36750
2	53.9	7.4	8.0	30.8	23.3	4400	980	3420	20310
3	59.5	8.1	10.0	22.4	27.8	11400	4420	6980	28920
4	54.9	7.1	7.4	30.6	23.3	3400	590	2810	14780
5	63.9	8.4	8.9	18.8	30.3	11600	4790	6810	32120
6	56.9	6.9	7.9	28.3	24.1	4400	1560	2840	16740
7	67.3	8.2	8.6	15.9	31.8	12600	6650	5950	29480
8	62.7	7.5	7.0	22.8	27.9	3800	1200	2600	14800
9	57.7	7.6	9.1	25.7	25.8	6600	1610	4990	26050
10	68.9	8.0	8.0	15.1	32.1	6400	2790	3610	21480
11	57.9	7.6	9.2	25.3	26.0	6400	1680	4720	26390
12	66.1	8.2	8.3	17.4	31.1	3600	2640	960	22170
13	68.3	8.4	8.6	14.7	32.6	13000	6390	6610	35430
14	37.7	6.0	5.7	50.6	12.4	2260	260	2000	13480
15	68.7	7.4	8.1	15.7	31.1	6200	2180	4020	21270
16	61.4	6.7	8.7	23.2	26.2	5400	970	4430	23710

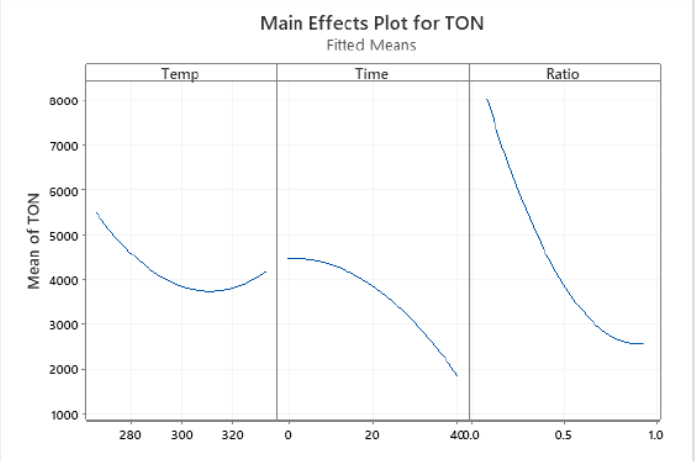

Table S.5. Relative peak area of common organic species in the aqueous phase.

Structure	A1	A2	A3	A4	A5	A6	A7	A8	A9	A10	A11	A12	A13	A14	A15	A16
Pyrrolo-pyrazinediones	15.6%	10.9%	5.9%	15.7%	7.2%	11.9%	8.4%	4.9%	22.9%	12.6%	22.5%	14.0%	10.7%	8.1%	17.3%	18.9%
Pyrazines	4.0%	7.5%	7.5%	2.9%	3.2%	4.6%	5.5%	3.1%	7.0%	3.7%	11.1%	9.8%	5.1%	4.7%	7.0%	8.6%
Piperazinediones	7.9%	3.8%	3.5%	2.9%	3.5%	2.4%	1.1%	1.1%	7.9%	1.9%	7.2%	1.8%	2.1%	2.5%	4.3%	4.8%
Amines (not-heterocycle)	3.0%	3.7%	5.3%	4.0%	3.8%	2.6%	2.0%	2.1%		4.9%	4.0%	2.2%	3.6%	4.5%	2.6%	8.7%
Pyrrolidinones		1.9%		5.0%	1.3%	6.2%	8.3%	9.3%	0.8%	6.1%	2.7%	2.3%	2.2%	5.2%		2.8%
Azocines		10.8%		6.5%					12.1%	4.4%		5.1%		1.9%	5.3%	
Pyridinols		0.8%	0.2%	5.9%	0.8%	4.3%	1.6%	9.1%	2.9%	4.8%	3.2%	0.4%		4.5%		1.0%
Pyrrolidines	1.2%	3.5%	4.9%		4.7%	2.5%	5.3%	2.5%	0.3%	4.3%	0.4%	3.7%	2.2%	0.4%	1.6%	0.5%
Cyclo-leucyl structures	2.9%	1.9%	0.5%	7.4%	2.3%	1.3%	0.5%	1.0%	2.5%	0.4%	2.9%	1.6%	0.4%	0.7%	1.1%	6.6%
Pyrrolidinediones	6.3%	1.1%	1.8%		2.8%	1.4%	6.1%	1.9%	1.8%	2.2%	0.9%	1.5%	3.4%	0.8%	1.5%	
Amides (not-acetamide)	1.6%	4.5%	4.4%	1.7%	2.0%	0.8%	1.9%	0.7%			0.7%	2.0%	2.4%		5.4%	
Acetamides			0.9%		2.5%	0.8%	7.7%	0.6%	1.3%	3.4%		3.2%	2.2%	0.7%	2.9%	
Cyclo-amines			5.9%		4.6%	0.7%	0.3%	1.9%	3.1%		2.6%		2.6%		1.9%	0.3%
Imidazoles		3.6%		4.4%		4.3%	2.8%	2.5%			0.3%		0.6%	2.8%		
Caprolactam		0.9%	0.4%		1.6%		0.7%		5.7%	0.4%			0.9%	0.5%	1.5%	1.3%
Isopropylidenes		5.7%						3.6%								
pyrrolidones						1.8%				0.6%						
Piperazines			0.1%		0.3%	0.8%							1.0%			
Nitrogenous Subtotal [%]	42.6%	60.5%	41.3%	56.3%	40.6%	46.5%	52.2%	44.2%	68.3%	49.6%	58.5%	47.6%	39.5%	37.4%	52.5%	53.5%
Cyclopent		3.6%	2.9%	5.9%	2.2%	7.9%	5.9%	10.8%	1.6%	4.7%	2.1%	4.7%	0.5%	9.9%	2.8%	3.3%
Lactones	3.2%	2.5%		4.1%		3.3%		4.7%	1.5%	0.1%	1.2%	0.6%		4.7%	1.1%	1.6%
Cyclohex		3.3%	0.6%	1.6%		5.3%			2.4%	1.6%	2.8%			1.5%	0.5%	4.5%
Heterocycles Subtotal [%]	3.2%	9.3%	3.5%	11.6%	2.2%	16.5%	5.9%	15.6%	5.4%	6.4%	6.2%	5.3%	0.5%	16.1%	4.4%	9.3%
Decenes	4.7%		7.1%		2.5%	6.7%							12.4%			2.3%
hexanes, heptanes and octanal					0.1%	0.3%						0.7%		4.2%		0.6%
Aliphatics Subtotal [%]	4.7%		7.1%		2.5%	7.0%						0.7%	12.4%	4.2%		3.0%
Total [%]	50.4%	69.8%	51.8%	67.9%	45.3%	70.0%	58.1%	59.8%	73.7%	55.9%	64.7%	53.6%	52.4%	57.7%	56.9%	65.7%

Chapter 7

Conclusions

7.1 Conclusions

This thesis presents advances in the understanding of the reaction mechanism, followed by the biomass key components under hydrothermal liquefaction conditions and links some of the major application drawbacks of the current renewable bio-crude to the undesirable reactions, while investigating a complete renewable co-solvent and homogeneous catalyst system to reduce the impact of those undesirable side reaction and produce higher bio-crude yields. Then, acknowledging the high complexity of the nitrogenous transformation in both the aqueous and bio-crude phases, the Maillard reaction mechanisms are investigated with a central composite design of experiments, considering the effect of temperature, residence time and carbohydrates/proteins mass ratio. The major contribution of the present thesis is the enhancement of the body of knowledge in terms of the reaction mechanisms and kinetic modelling of the main biomass components in non-conventional biomass, whilst the major application drawbacks are addressed in co-liquefaction with an alkylation agent and hydrogen donation system.

7.1.1 The effect of ethanol as a homogeneous catalyst on the reaction kinetics of hydrothermal liquefaction of lipids

This study involved the hydrothermal liquefaction of a lipid model compound to clarify and contrast the major transformations within the renewable bio-crude phase, besides the bulk phase kinetics. Then ethanol under initial acidic conditions is included, as a co-solvent and homogeneous catalyst to promote the in-situ transesterification of triglycerides and the esterification of FFA. The HTL and co-liquefaction approaches are synthesised in a reaction kinetics loop to capture the equilibrium degrees and to define the activation energies. The following conclusions were drawn.

- The hydrolysis and transesterification reactions were identified and quantified with ATR (FT-IR) absorbance analysis of the carbonyl bonds

(acid and esters peaks in the region 1850 to 1550 cm^{-1}) from the renewable bio-crude phase and the data was contrasted with TAN normalised values.

- The reduction in bio-crude boiling point was associated with the hydrolysis of FFA, contrasted with the FT-IR carbonyl bond composition and with the TAN data.
- The Arrhenius activation energy and pre-exponential values obtained for the hydrolysis of lipids were contrasted with the scientific literature, while the activation energies for the alcoholysis were compared with various types of trans-esterification.
- The effect of co-liquefaction conditions promoted the alcoholysis reaction over hydrolysis at lower temperatures. However, higher temperatures hydrolysis surpassed alcoholysis near equilibrium conditions, reducing the amount of FAEE. As a result, ethanol produced the highest impact in reducing the TAN at 300°C, despite at 250°C the amount of FAEE was close to 40% by mass.
- The sensitivity analysis for the ethanol to lipid mass ratio suggested that higher concentrations of ethanol have a negligible effect on producing higher fractions of FAEE, while lower ethanol mass ratio suggested that the equilibrium concentration for the alcoholysis is reached first, then hydrolysis rules the reaction.

7.1.2 Elemental nitrogen balance, reaction kinetics and the effect of ethanol on the hydrothermal liquefaction of soy protein

In this study, the migration and transformations of nitrogen as the most prominent element of rich in protein biomass are investigated. An elemental nitrogen balance is completed and the distribution of nitrogen in the different HTL product phases is condensed in a reaction mechanism and kinetic models. Followed by co-liquefaction conditions to boost the renewable bio-crude yield and promote denitrification via alkylation with a hydrogen donor solvent system. The following conclusions were made.

- The co-liquefaction conditions promoted higher renewable bio-crude yields and higher energy recovery in almost all cases. However, the elemental O/C fractions were higher, generating lower theoretical HHV values.
- The low boiling point fraction (80 to 300°C) was linked to the transformations in the renewable bio-crude phase and the increase in the relative elemental carbon content.
- The migrations and transformations of the nitrogenous species, as well as the equilibrium degrees, were captured and presented in the reaction mechanism and kinetic models for the conditions tested.
- HTL produced high fractions of NH_3, whereas co-liquefaction conditions lowered the ammonia fraction promoting nitrate and organic nitrogen fractions, an observation which coupled with the overall elemental balance, suggests that the missing nitrogen was in the gaseous phase because of the potential denitrification via anammox reaction mechanism.
- Co-liquefaction conditions promoted higher renewable bio-crude yields with lower boiling points, possibly due to the reduction in pH of the aqueous phase. However, the deoxygenation was lower because of the alkylation agent and the synergetic effect of alcohol and water mixtures near the critical point.

7.1.3 A multi-component reaction kinetics model for the hydrothermal liquefaction of carbohydrates and co-liquefaction to produce 5-ethoxymethyl furfural

This study involved the investigation of aqueous and solid transformations of monosaccharides and polysaccharides during HTL. Analysis of these two major product phases was included into a multi-component reaction mechanism, kinetic and a shrinking-core models for cellulose. Additionally, co-liquefaction conditions produced 5-ethoxymethyl furfural and ethyl levulinate, to promising fuel additives and tunable monomers. The following conclusions were drawn.

- The aqueous product phases from the HTL of glucose, fructose and cellulose were identified and quantified with GC-MS and HPLC to determine and synthesise the major organic structures into a multi-component reaction mechanism and kinetic model, providing a new unbiased perception of the HTL products from model carbohydrates.
- The solid products were analysed with derivative TGA (dTG), and the characteristic thermal decompositions were used to semi-quantify the hydrochar and cellulose feedstock in the solid, indispensable to complete the polysaccharide reaction mechanism, including the unreacted cellulose.
- Particle size distribution, glucose concentration and solid characterisation were used to define a shrinking-core reaction model for cellulose based on the hydrolysis of cellulose, the diffusion of glucose on the surface of the particles and hydrochar formation rate, providing a novel vision of the reaction mechanism of cellulose.
- Co-liquefaction conditions reduced the hydrolysis rate and hydrochar formation (from 50% to 32% by mass with cellulose at 250°C), while increases the aqueous phase yield which contains some valuable intermediates.
- The co-liquefaction promoted the esterification of levulinic acid and etherification of 5-HMF, preventing aldol condensation into the solid phase and producing two valuable water-soluble organics with potential application in energy and polymer industries.

7.1.4 Elucidating the Maillard reaction mechanism over the hydrothermal liquefaction of model compound mixtures and spirulina

In this study, the interactions between protein and carbohydrate intermediates are investigated with a central composite design (CCD) to include the effect of mass ratio as an additional variable to reaction temperature and residence time. The effects of the Maillard reactions were evaluated in the product yields, renewable bio-crude elemental composition, and boiling point, as well as the

characterisation of the aqueous phase and ethanol soluble bio-crude with GC-MS. The following conclusions were made.

- The primary effect of protein/carbohydrate mass ratio was identified as the most significant factor which contributes to the renewable bio-crude and hydrochar yields, and second-order polynomial equations based on the three factors are presented for the bio-crude and solid product phases.
- The characterisation and quantification of the organic species in the aqueous and ethanol soluble renewable bio-crude phases showed that the primary structures produced by the Maillard reactions are pyrrolo-pyrazinediones and piperazinediones.
- The carbohydrate mass ratio had a significant effect on reducing the volatile matter (80 to 600°C). However, the maximum volatile fraction was reached at 40% protein/carbohydrates as a synergetic effect of the Maillard reaction on the boiling point distributions.
- The effect of carbohydrates mass ratio on the elemental composition of the renewable bio-crude had a similar pattern to the volatile matter fraction. Similarly, the relative hydrogen and nitrogen dropped with the rise in carbohydrates due to the increase in oxygen content.
- The carbohydrates mass ratio also has a significant effect on the TOC of the aqueous phase, possibly because of the aldol condensation of carbohydrate intermediates into the solid phase.
- The formation of proline as a potential intermediate before ring closure into pyrrolo-pyrazinedione (with up to 20% by mass concentration in the aqueous phase) shall be formed from the glutamic acid ring closure in low carbohydrates conditions and from the Amadori rearrangement and Strecker degradation of levulinic acid with ammonia and amino acids, respectively.

7.2 Recommendations for future work

The present thesis enriches the body of knowledge of the chemical and elemental conversions of the major components in biomass during hydrothermal liquefaction conditions and the Maillard reactions. The main HTL application gaps are linked to some undesirable reactions, and co-liquefaction with a hydrogen donor co-solvent and alkylation agent is assessed to reduce the effect of these drawbacks. Additionally, the main migrations and transformation are condensed in a series of reaction mechanisms and kinetic models, which describe the experimental results and equilibrium degrees. However, further investigation is required to gather a better understanding of the HTL transformations of multiple real biomass sources with natural variations from a fundamental point of view.

- The experiments were limited to a batch micro reactor system, which is ideal for fundamental reaction kinetics (isothermal conditions and Arrhenius model) with an extremely high heating rate. However, it is unrealistic in the real world. Continuous systems at near steady state shall be studied as the best candidate for industrial scale.
- Binary and ternary mixture interactions besides the Maillard reaction must be considered. They may have a negligible effect apart from the changes in pH, according to some of the literature. However, these must be confirmed before considering a biomass component based reaction mechanism and kinetic model.
- Model compounds have been widely used in the literature, making contrast possible. However, these model compounds should be compared with a larger spectrum of biomass compositions to have a wider picture of the hydrothermal transformation of the different biomass types.
- The decomposition and transformation of protein intermediates require more investigation. Out of the three key biomass components, protein holds the highest complexity, as it can produce over 800 different organic structures from one HTL conversion.

- The reaction mechanism and kinetic models require more in-depth research, as they can be quite complex due to a high number of organic structures. However, there should be a balance between the level of detail and the complexity limited by the fitting of the reaction model to the experimental observations.
- In the co-liquefaction technology, ethanol is a renewable resource. However, the recovery of ethanol has to be included, as ethanol is a bio-energy source itself, and the energy recovery from the co-liquefaction must be considered in regards the ethanol consumption.

Chapter 8

References

The following references correspond to citations in chapters 1, 2 and 7. The references in chapter 3 to 6 are included at the end of each chapter as papers and manuscript reference sections.

Aeppli, C., Berg, M., Hofstetter, T. B., Kipfer, R., & Schwarzenbach, R. P. (2008). Simultaneous quantification of polar and non-polar volatile organic compounds in water samples by direct aqueous injection-gas chromatography/mass spectrometry. *J Chromatogr A, 1181*(1-2), 116-124. doi:10.1016/j.chroma.2007.12.043

Alalwan, H. A., Alminshid, A. H., & Aljaafari, H. A. S. (2019). Promising evolution of biofuel generations. Subject review. *Renewable Energy Focus, 28*, 127-139. doi:https://doi.org/10.1016/j.ref.2018.12.006

Alenezi, R., Leeke, G. A., Santos, R. C. D., & Khan, A. R. (2009). Hydrolysis kinetics of sunflower oil under subcritical water conditions. *Chemical Engineering Research and Design, 87*(6), 867-873. doi:10.1016/j.cherd.2008.12.009

Álvarez-Murillo, A., Sabio, E., Ledesma, B., Román, S., & González-García, C. M. (2016). Generation of biofuel from hydrothermal carbonization of cellulose. Kinetics modelling. *Energy, 94*, 600-608. doi:10.1016/j.energy.2015.11.024

Amaya-Farfan, J., & Rodriguez-Amaya, D. B. (2021). Chapter 6 - The Maillard reactions. In D. B. Rodriguez-Amaya & J. Amaya-Farfan (Eds.), *Chemical Changes During Processing and Storage of Foods* (pp. 215-263): Academic Press.

Antal, M. J., Mok, W. S. L., & Richards, G. N. (1990). Mechanism of formation of 5-(hydroxymethyl)-2-furaldehyde from d-fructose and sucrose. *Carbohydrate Research, 199*(1), 91-109. doi:https://doi.org/10.1016/0008-6215(90)84096-D

Arturi, K. R., Kucheryavskiy, S., & Søgaard, E. G. (2016). Performance of hydrothermal liquefaction (HTL) of biomass by multivariate data analysis. *Fuel Processing Technology, 150*, 94-103. doi:https://doi.org/10.1016/j.fuproc.2016.05.007

Ashoor, S. H., & Zent, J. B. (1984). Maillard Browning of Common Amino Acids and Sugars. *Journal of Food Science, 49*(4), 1206-1207. doi:https://doi.org/10.1111/j.1365-2621.1984.tb10432.x

Baccile, N., Laurent, G., Babonneau, F., Fayon, F., Titirici, M.-M., & Antonietti, M. (2009). Structural Characterization of Hydrothermal Carbon Spheres by Advanced Solid-State MAS 13C NMR Investigations. *The Journal of Physical Chemistry C, 113*(22), 9644-9654. doi:10.1021/jp901582x

Baccile, N., Weber, J., Falco, C., & Titirici, M.-M. (2013). Characterization of Hydrothermal Carbonization Materials. In *Sustainable Carbon Materials from Hydrothermal Processes* (pp. 151-211).

Becker, E. W. (1994). *Microalgae: Biotechnology and Microbiology*: Cambridge University Press.

Bergius, F. (1913). Production of hydrogen from water and coal from cellulose at high temperatures and pressures. *Journal of the Society of Chemical Industry, 32*(9), 462-467. doi:https://doi.org/10.1002/jctb.5000320904

Berrios, M., Siles, J., Martin, M., & Martin, A. (2007). A kinetic study of the esterification of free fatty acids (FFA) in sunflower oil. *Fuel, 86*(15), 2383-2388. doi:10.1016/j.fuel.2007.02.002

Biller, P., Riley, R., & Ross, A. B. (2011). Catalytic hydrothermal processing of microalgae: decomposition and upgrading of lipids. *Bioresour Technol, 102*(7), 4841-4848. doi:10.1016/j.biortech.2010.12.113

Biller, P., & Ross, A. B. (2011). Potential yields and properties of oil from the hydrothermal liquefaction of microalgae with different biochemical content. *Bioresour Technol, 102*(1), 215-225. doi:10.1016/j.biortech.2010.06.028

Biller, P., & Ross, A. B. (2016). 17 - Production of biofuels via hydrothermal conversion. In R. Luque, C. S. K. Lin, K. Wilson, & J. Clark (Eds.), *Handbook of Biofuels Production (Second Edition)* (pp. 509-547): Woodhead Publishing.

Bobleter, O., & Pape, G. (1968). Der hydrothermale abbau von glucose. *Monatshefte für Chemie/Chemical Monthly, 99*(4), 1560-1567.

Burnham, A. K., Zhou, X., & Broadbelt, L. J. (2015). Critical Review of the Global Chemical Kinetics of Cellulose Thermal Decomposition. *Energy & Fuels, 29*(5), 2906-2918. doi:10.1021/acs.energyfuels.5b00350

Burton, F. L., Tchobanoglous, G., Tsuchihashi, R., Stensel, H. D., Metcalf, & Eddy, I. (2013). *Wastewater Engineering: Treatment and Resource Recovery*: McGraw-Hill Education.

Chacón-Parra, A., & van Eyk, P. (2022). Reaction kinetics for the hydrothermal carbonisation of cellulose in a two-phase pathway. *Fuel, 309*, 122169. doi:https://doi.org/10.1016/j.fuel.2021.122169

Chen, W.-T. (2017). Hydrothermal liquefaction of protein-containing feedstocks. In.

Chen, W.-T., Qian, W., Zhang, Y., Mazur, Z., Kuo, C.-T., Scheppe, K., . . . Sharma, B. K. (2017). Effect of ash on hydrothermal liquefaction of high-ash content algal biomass. *Algal Research, 25*, 297-306. doi:https://doi.org/10.1016/j.algal.2017.05.010

Cheng, S., D'cruz, I., Wang, M., Leitch, M., & Xu, C. (2010). Highly Efficient Liquefaction of Woody Biomass in Hot-Compressed Alcohol−Water Co-solvents†. *Energy & Fuels, 24*(9), 4659-4667. doi:10.1021/ef901218w

Chuntanapum, A., & Matsumura, Y. (2009). Formation of Tarry Material from 5-HMF in Subcritical and Supercritical Water. *Industrial & Engineering Chemistry Research, 48*(22), 9837-9846. doi:10.1021/ie900423g

Chuntanapum, A., & Matsumura, Y. (2010). Char Formation Mechanism in Supercritical Water Gasification Process: A Study of Model Compounds. *Industrial & Engineering Chemistry Research, 49*(9), 4055-4062. doi:10.1021/ie901346h

Coleman, W. M., III. (1996). A Study of the Behavior of Maillard Reaction Products Analyzed by Solid-Phase Microextraction—Gas Chromatography—Mass Selective Detection. *Journal of Chromatographic Science, 34*(5), 213-218. doi:10.1093/chromsci/34.5.213

da Silva, V. T., & Sousa, L. A. (2013). Chapter 3 - Catalytic Upgrading of Fats and Vegetable Oils for the Production of Fuels. In K. S. Triantafyllidis, A. A. Lappas, & M. Stöcker (Eds.), *The Role of Catalysis for the Sustainable Production of Bio-fuels and Bio-chemicals* (pp. 67-92). Amsterdam: Elsevier.

Dinjus, E., Kruse, A., & Tröger, N. (2011). Hydrothermal Carbonization - 1. Influence of Lignin in Lignocelluloses. *Chemical Engineering & Technology, 34*(12), 2037-2043. doi:10.1002/ceat.201100487

dos Santos, K. C., Hamerski, F., Pedersen Voll, F. A., & Corazza, M. L. (2018). Experimental and kinetic modeling of acid oil (trans)esterification in supercritical ethanol. *Fuel, 224*, 489-498. doi:10.1016/j.fuel.2018.03.102

Duan, P., & Savage, P. E. (2011). Hydrothermal Liquefaction of a Microalga with Heterogeneous Catalysts. *Industrial & Engineering Chemistry Research, 50*(1), 52-61. doi:10.1021/ie100758s

Falco, C., Baccile, N., & Titirici, M. M. (2011). Morphological and structural differences between glucose, cellulose and lignocellulosic biomass derived hydrothermal carbons. *Green Chemistry, 13*(11), 3273-3281. doi:10.1039/c1gc15742f

Fan, Y., Hornung, U., Dahmen, N., & Kruse, A. (2018). Hydrothermal liquefaction of protein-containing biomass: study of model compounds for Maillard reactions. *Biomass Conversion and Biorefinery, 8*(4), 909-923. doi:10.1007/s13399-018-0340-8

Galadima, A., & Muraza, O. (2018). Hydrothermal liquefaction of algae and bio-oil upgrading into liquid fuels: Role of heterogeneous catalysts. *Renewable and Sustainable Energy Reviews, 81*, 1037-1048. doi:https://doi.org/10.1016/j.rser.2017.07.034

Galgano, A., & Blasi, C. D. (2003). Modeling Wood Degradation by the Unreacted-Core-Shrinking Approximation. *Industrial & Engineering Chemistry Research, 42*(10), 2101-2111. doi:10.1021/ie020939o

García-Bordejé, E., Pires, E., & Fraile, J. M. (2017). Parametric study of the hydrothermal carbonization of cellulose and effect of acidic conditions. *Carbon, 123*, 421-432. doi:https://doi.org/10.1016/j.carbon.2017.07.085

Go, A. W., Sutanto, S., Ong, L. K., Tran-Nguyen, P. L., Ismadji, S., & Ju, Y.-H. (2016). Developments in in-situ (trans) esterification for biodiesel production: A critical review. *Renewable and Sustainable Energy Reviews, 60*, 284-305. doi:10.1016/j.rser.2016.01.070

Gollakota, A. R. K., Kishore, N., & Gu, S. (2018). A review on hydrothermal liquefaction of biomass. *Renewable and Sustainable Energy Reviews, 81*, 1378-1392. doi:10.1016/j.rser.2017.05.178

Hayes, D. J. M. (2013). Chapter 2 - Biomass Composition and Its Relevance to Biorefining. In K. S. Triantafyllidis, A. A. Lappas, & M. Stöcker (Eds.), *The Role of Catalysis for the Sustainable Production of Bio-fuels and Bio-chemicals* (pp. 27-65). Amsterdam: Elsevier.

He, Q., Yu, Y., Wang, J., Suo, X., & Liu, Y. (2021). Kinetic Study of the Hydrothermal Carbonization Reaction of Glucose and Its Product Structures. *Industrial & Engineering Chemistry Research, 60*(12), 4552-4561. doi:10.1021/acs.iecr.0c06280

Hietala, D. C., & Savage, P. E. (2021). A molecular, elemental, and multiphase kinetic model for the hydrothermal liquefaction of microalgae. *Chemical Engineering Journal, 407*. doi:10.1016/j.cej.2020.127007

Huang, H.-j., & Yuan, X.-z. (2015). Recent progress in the direct liquefaction of typical biomass. *Progress in Energy and Combustion Science, 49*, 59-80. doi:https://doi.org/10.1016/j.pecs.2015.01.003

Isa, K. M., Abdullah, T. A. T., & Ali, U. F. M. (2018). Hydrogen donor solvents in liquefaction of biomass: A review. *Renewable and Sustainable Energy Reviews, 81*, 1259-1268. doi:10.1016/j.rser.2017.04.006

Jatzwauck, M., & Schumpe, A. (2015). Kinetics of hydrothermal carbonization (HTC) of soft rush. *Biomass & Bioenergy, 75*, 94-100. doi:10.1016/j.biombioe.2015.02.006

Jatzwauck, M. S. (2015). *Kinetik der Hydrothermalen Karbonisierung von Modellsubstanzen und Biomassen.*

Jayathilake, M., Rudra, S., & Rosendahl, L. A. (2020). Hydrothermal liquefaction of wood using a modified multistage shrinking-core model. *Fuel, 280*, 118616. doi:https://doi.org/10.1016/j.fuel.2020.118616

Jung, D., Zimmermann, M., & Kruse, A. (2018). Hydrothermal Carbonization of Fructose: Growth Mechanism and Kinetic Model. *ACS Sustainable Chemistry & Engineering, 6*(11), 13877-13887. doi:10.1021/acssuschemeng.8b02118

Kambo, H. S., & Dutta, A. (2015). A comparative review of biochar and hydrochar in terms of production, physico-chemical properties and applications. *Renewable and Sustainable Energy Reviews, 45*, 359-378. doi:10.1016/j.rser.2015.01.050

Karagöz, S., Bhaskar, T., Muto, A., Sakata, Y., Oshiki, T., & Kishimoto, T. (2005). Low-temperature catalytic hydrothermal treatment of wood biomass: analysis of liquid products. *Chemical Engineering Journal, 108*(1), 127-137. doi:https://doi.org/10.1016/j.cej.2005.01.007

Karayıldırım, T., Sınağ, A., & Kruse, A. (2008). Char and Coke Formation as Unwanted Side Reaction of the Hydrothermal Biomass Gasification. *Chemical Engineering & Technology, 31*(11), 1561-1568. doi:https://doi.org/10.1002/ceat.200800278

Khan, T. A., Saud, A. S., Jamari, S. S., Rahim, M. H. A., Park, J.-W., & Kim, H.-J. (2019). Hydrothermal carbonization of lignocellulosic biomass for carbon rich material preparation: A review. *Biomass and Bioenergy, 130*, 105384. doi:https://doi.org/10.1016/j.biombioe.2019.105384

Kim, S., Kramer, R. W., & Hatcher, P. G. (2003). Graphical Method for Analysis of Ultrahigh-Resolution Broadband Mass Spectra of Natural Organic Matter, the Van Krevelen Diagram. *Analytical Chemistry, 75*(20), 5336-5344. doi:10.1021/ac034415p

Knežević, D., van Swaaij, W. P. M., & Kersten, S. R. A. (2009). Hydrothermal Conversion of Biomass: I, Glucose Conversion in Hot Compressed Water. *Industrial & Engineering Chemistry Research, 48*(10), 4731-4743. doi:10.1021/ie801387v

Körner, P., Jung, D., & Kruse, A. (2018). The effect of different Brønsted acids on the hydrothermal conversion of fructose to HMF. *Green Chemistry, 20*(10), 2231-2241. doi:10.1039/C8GC00435H

Kruse, A., & Dinjus, E. (2007). Hot compressed water as reaction medium and reactant. *The Journal of Supercritical Fluids, 39*(3), 362-380. doi:10.1016/j.supflu.2006.03.016

Kruse, A., Funke, A., & Titirici, M. M. (2013). Hydrothermal conversion of biomass to fuels and energetic materials. *Curr Opin Chem Biol, 17*(3), 515-521. doi:10.1016/j.cbpa.2013.05.004

Kruse, A., Krupka, A., Schwarzkopf, V., Gamard, C., & Henningsen, T. (2005). Influence of Proteins on the Hydrothermal Gasification and Liquefaction of Biomass. 1. Comparison of Different Feedstocks. *Industrial & Engineering Chemistry Research, 44*(9), 3013-3020. doi:10.1021/ie049129y

Kumar, M., Olajire Oyedun, A., & Kumar, A. (2018). A review on the current status of various hydrothermal technologies on biomass feedstock. *Renewable and Sustainable Energy Reviews, 81*, 1742-1770. doi:https://doi.org/10.1016/j.rser.2017.05.270

Lascaray, L. (1949). Mechanism of Fat Splitting. *Industrial & Engineering Chemistry, 41*(4), 786-790. doi:10.1021/ie50472a025

Leng, L., Zhang, W., Peng, H., Li, H., Jiang, S., & Huang, H. (2020). Nitrogen in bio-oil produced from hydrothermal liquefaction of biomass: A review. *Chemical Engineering Journal, 401*. doi:10.1016/j.cej.2020.126030

Li, Y., Leow, S., Fedders, A. C., Sharma, B. K., Guest, J. S., & Strathmann, T. J. (2017). Quantitative multiphase model for hydrothermal liquefaction of algal biomass. *Green Chemistry, 19*(4), 1163-1174. doi:10.1039/c6gc03294j

Liu, H., Chen, Y., Yang, H., Gentili, F. G., Söderlind, U., Wang, X., . . . Chen, H. (2020). Conversion of high-ash microalgae through hydrothermal liquefaction. *Sustainable Energy & Fuels, 4*(6), 2782-2791. doi:10.1039/C9SE01114E

Lu, J., Li, H., Zhang, Y., & Liu, Z. (2018). Nitrogen Migration and Transformation during Hydrothermal Liquefaction of Livestock Manures. *ACS Sustainable Chemistry & Engineering, 6*(10), 13570-13578. doi:10.1021/acssuschemeng.8b03810

Lu, J., Liu, Z., Zhang, Y., & Savage, P. E. (2019). 110th Anniversary: Influence of Solvents on Biocrude from Hydrothermal Liquefaction of Soybean Oil, Soy Protein, Cellulose, Xylose, and Lignin, and Their Quinary Mixture.

Industrial & Engineering Chemistry Research, 58(31), 13971-13976. doi:10.1021/acs.iecr.9b02442

Lucian, M., Volpe, M., & Fiori, L. (2019). Hydrothermal Carbonization Kinetics of Lignocellulosic Agro-Wastes: Experimental Data and Modeling. *Energies, 12*(3), 516. Retrieved from https://www.mdpi.com/1996-1073/12/3/516

Luijkx, G. C. A., van Rantwijk, F., & van Bekkum, H. (1993). Hydrothermal formation of 1,2,4-benzenetriol from 5-hydroxymethyl-2-furaldehyde and d-fructose. *Carbohydrate Research, 242*, 131-139. doi:https://doi.org/10.1016/0008-6215(93)80027-C

Luo, L., Sheehan, J. D., Dai, L., & Savage, P. E. (2016). Products and Kinetics for Isothermal Hydrothermal Liquefaction of Soy Protein Concentrate. *ACS Sustainable Chemistry & Engineering, 4*(5), 2725-2733. doi:10.1021/acssuschemeng.6b00226

Mackie, D. M., Jahnke, J. P., Benyamin, M. S., & Sumner, J. J. (2016). Simple, fast, and accurate methodology for quantitative analysis using Fourier transform infrared spectroscopy, with bio-hybrid fuel cell examples. *MethodsX, 3*, 128-138. doi:10.1016/j.mex.2016.02.002

Maddi, B., Panisko, E., Wietsma, T., Lemmon, T., Swita, M., Albrecht, K., & Howe, D. (2016). Quantitative characterization of the aqueous fraction from hydrothermal liquefaction of algae. *Biomass and Bioenergy, 93*, 122-130. doi:https://doi.org/10.1016/j.biombioe.2016.07.010

Madsen, R. B., Biller, P., Jensen, M. M., Becker, J., Iversen, B. B., & Glasius, M. (2016). Predicting the Chemical Composition of Aqueous Phase from Hydrothermal Liquefaction of Model Compounds and Biomasses. *Energy & Fuels, 30*(12), 10470-10483. doi:10.1021/acs.energyfuels.6b02007

Madsen, R. B., & Glasius, M. (2019). How Do Hydrothermal Liquefaction Conditions and Feedstock Type Influence Product Distribution and Elemental Composition? *Industrial & Engineering Chemistry Research, 58*(37), 17583-17600. doi:10.1021/acs.iecr.9b02337

Madsen, R. B., Jensen, M. M., Morup, A. J., Houlberg, K., Christensen, P. S., Klemmer, M., . . . Glasius, M. (2016). Using design of experiments to optimize derivatization with methyl chloroformate for quantitative analysis

of the aqueous phase from hydrothermal liquefaction of biomass. *Anal Bioanal Chem, 408*(8), 2171-2183. doi:10.1007/s00216-016-9321-6

Mann, B. F., Chen, H., Herndon, E. M., Chu, R. K., Tolic, N., Portier, E. F., . . . Gu, B. (2015). Indexing Permafrost Soil Organic Matter Degradation Using High-Resolution Mass Spectrometry. *PLOS ONE, 10*(6), e0130557. doi:10.1371/journal.pone.0130557

Martinez-Fernandez, J. S., & Chen, S. (2017). Sequential Hydrothermal Liquefaction characterization and nutrient recovery assessment. *Algal Research, 25*, 274-284. doi:https://doi.org/10.1016/j.algal.2017.05.022

Matsumura, Y., Yanachi, S., & Yoshida, T. (2006). Glucose Decomposition Kinetics in Water at 25 MPa in the Temperature Range of 448−673 K. *Industrial & Engineering Chemistry Research, 45*(6), 1875-1879. doi:10.1021/ie050830r

Minowa, T., Inoue, S., Hanaoka, T., & Matsumura, Y. (2004). Hydrothermal Reaction of Glucose and Glycine as Model Compounds of Biomass. *Journal of the Japan Institute of Energy, 83*(10), 794-798. doi:10.3775/jie.83.794

Mohamed, M. A., Jaafar, J., Ismail, A. F., Othman, M. H. D., & Rahman, M. A. (2017). Chapter 1 - Fourier Transform Infrared (FTIR) Spectroscopy. In N. Hilal, A. F. Ismail, T. Matsuura, & D. Oatley-Radcliffe (Eds.), *Membrane Characterization* (pp. 3-29): Elsevier.

Moquin, P. H. L., & Temelli, F. (2008). Kinetic modeling of hydrolysis of canola oil in supercritical media. *The Journal of Supercritical Fluids, 45*(1), 94-101. doi:10.1016/j.supflu.2007.11.018

Morales, G., Melero, J. A., Paniagua, M., Iglesias, J., Hernández, B., & Sanz, M. (2014). Sulfonic acid heterogeneous catalysts for dehydration of C6-monosaccharides to 5-hydroxymethylfurfural in dimethyl sulfoxide. *Chinese Journal of Catalysis, 35*(5), 644-655. doi:10.1016/s1872-2067(14)60020-6

Obeid, R., Lewis, D., Smith, N., & van Eyk, P. (2019). The elucidation of reaction kinetics for hydrothermal liquefaction of model macromolecules.

Chemical Engineering Journal, 370, 637-645. doi:10.1016/j.cej.2019.03.240

Obeid, R., Lewis, D. M., Smith, N., Hall, T., & van Eyk, P. (2020a). Reaction kinetics and characterisation of species in renewable crude from hydrothermal liquefaction of monomers to represent organic fractions of biomass feedstocks. *Chemical Engineering Journal, 389*. doi:10.1016/j.cej.2020.124397

Obeid, R., Lewis, D. M., Smith, N., Hall, T., & van Eyk, P. (2020b). Reaction Kinetics and Characterization of Species in Renewable Crude from Hydrothermal Liquefaction of Mixtures of Polymer Compounds To Represent Organic Fractions of Biomass Feedstocks. *Energy & Fuels, 34*(1), 419-429. doi:10.1021/acs.energyfuels.9b02936

Obeid, R., Smith, N., Lewis, D. M., Hall, T., & van Eyk, P. (2022). A kinetic model for the hydrothermal liquefaction of microalgae, sewage sludge and pine wood with product characterisation of renewable crude. *Chemical Engineering Journal, 428*, 131228. doi:https://doi.org/10.1016/j.cej.2021.131228

Paksung, N., Pfersich, J., Arauzo, P. J., Jung, D., & Kruse, A. (2020). Structural Effects of Cellulose on Hydrolysis and Carbonization Behavior during Hydrothermal Treatment. *ACS Omega, 5*(21), 12210-12223. doi:10.1021/acsomega.0c00737

Patil, S. K. R., Heltzel, J., & Lund, C. R. F. (2012). Comparison of Structural Features of Humins Formed Catalytically from Glucose, Fructose, and 5-Hydroxymethylfurfuraldehyde. *Energy & Fuels, 26*(8), 5281-5293. doi:10.1021/ef3007454

Patil, S. K. R., & Lund, C. R. F. (2011). Formation and Growth of Humins via Aldol Addition and Condensation during Acid-Catalyzed Conversion of 5-Hydroxymethylfurfural. *Energy & Fuels, 25*(10), 4745-4755. doi:10.1021/ef2010157

Peterson, A. A., Lachance, R. P., & Tester, J. W. (2010). Kinetic Evidence of the Maillard Reaction in Hydrothermal Biomass Processing: Glucose−Glycine Interactions in High-Temperature, High-Pressure

Water. *Industrial & Engineering Chemistry Research, 49*(5), 2107-2117. doi:10.1021/ie9014809

Peterson, A. A., Vogel, F., Lachance, R. P., Fröling, M., Antal, J. M. J., & Tester, J. W. (2008). Thermochemical biofuel production in hydrothermal media: A review of sub- and supercritical water technologies. *Energy & Environmental Science, 1*(1). doi:10.1039/b810100k

Pinnarat, T., & Savage, P. E. (2010). Noncatalytic esterification of oleic acid in ethanol. *The Journal of Supercritical Fluids, 53*(1-3), 53-59. doi:10.1016/j.supflu.2010.02.008

Poerschmann, J., Weiner, B., Koehler, R., & Kopinke, F.-D. (2017). Hydrothermal Carbonization of Glucose, Fructose, and Xylose—Identification of Organic Products with Medium Molecular Masses. *ACS Sustainable Chemistry & Engineering, 5*(8), 6420-6428. doi:10.1021/acssuschemeng.7b00276

Poiana, M.-A., Alexa, E., Munteanu, M.-F., Gligor, R., Moigradean, D., & Mateescu, C. (2015). Use of ATR-FTIR spectroscopy to detect the changes in extra virgin olive oil by adulteration with soybean oil and high temperature heat treatment. *Open Chemistry, 13*(1). doi:doi:10.1515/chem-2015-0110

Promdej, C., & Matsumura, Y. (2011). Temperature Effect on Hydrothermal Decomposition of Glucose in Sub- And Supercritical Water. *Industrial & Engineering Chemistry Research, 50*(14), 8492-8497. doi:10.1021/ie200298c

Qi, L., Mui, Y. F., Lo, S. W., Lui, M. Y., Akien, G. R., & Horváth, I. T. (2014). Catalytic Conversion of Fructose, Glucose, and Sucrose to 5-(Hydroxymethyl)furfural and Levulinic and Formic Acids in γ-Valerolactone As a Green Solvent. *ACS Catalysis, 4*(5), 1470-1477. doi:10.1021/cs401160y

Qiu, Y., Aierzhati, A., Cheng, J., Guo, H., Yang, W., & Zhang, Y. (2019). Biocrude Oil Production through the Maillard Reaction between Leucine and Glucose during Hydrothermal Liquefaction. *Energy & Fuels, 33*(9), 8758-8765. doi:10.1021/acs.energyfuels.9b01875

Rasmussen, H., Sorensen, H. R., & Meyer, A. S. (2014). Formation of degradation compounds from lignocellulosic biomass in the biorefinery: sugar reaction mechanisms. *Carbohydr Res, 385*, 45-57. doi:10.1016/j.carres.2013.08.029

Reyero, I., Arzamendi, G., Zabala, S., & Gandía, L. M. (2015). Kinetics of the NaOH-catalyzed transesterification of sunflower oil with ethanol to produce biodiesel. *Fuel Processing Technology, 129*, 147-155. doi:10.1016/j.fuproc.2014.09.008

Reza, M. T., Yan, W., Uddin, M. H., Lynam, J. G., Hoekman, S. K., Coronella, C. J., & Vasquez, V. R. (2013). Reaction kinetics of hydrothermal carbonization of loblolly pine. *Bioresour Technol, 139*, 161-169. doi:10.1016/j.biortech.2013.04.028

Riazi, M. R. (2005). *Characterization and Properties of Petroleum Fractions*: ASTM International.

Ross, A. B., Anastasakis, K., Kubacki, M., & Jones, J. M. (2009). Investigation of the pyrolysis behaviour of brown algae before and after pre-treatment using PY-GC/MS and TGA. *Journal of Analytical and Applied Pyrolysis, 85*(1), 3-10. doi:https://doi.org/10.1016/j.jaap.2008.11.004

Ross, A. B., Biller, P., Kubacki, M. L., Li, H., Lea-Langton, A., & Jones, J. M. (2010). Hydrothermal processing of microalgae using alkali and organic acids. *Fuel, 89*(9), 2234-2243. doi:https://doi.org/10.1016/j.fuel.2010.01.025

Saber, M., Golzary, A., Hosseinpour, M., Takahashi, F., & Yoshikawa, K. (2016). Catalytic hydrothermal liquefaction of microalgae using nanocatalyst. *Applied Energy, 183*, 566-576. doi:https://doi.org/10.1016/j.apenergy.2016.09.017

Sasaki, M., Adschiri, T., & Arai, K. (2004). Kinetics of cellulose conversion at 25 MPa in sub- and supercritical water. *AIChE Journal, 50*(1), 192-202. doi:10.1002/aic.10018

Sevilla, M., & Fuertes, A. B. (2009a). Chemical and structural properties of carbonaceous products obtained by hydrothermal carbonization of

saccharides. *Chemistry, 15*(16), 4195-4203. doi:10.1002/chem.200802097

Sevilla, M., & Fuertes, A. B. (2009b). The production of carbon materials by hydrothermal carbonization of cellulose. *Carbon, 47*(9), 2281-2289. doi:https://doi.org/10.1016/j.carbon.2009.04.026

Sheehan, J. D., & Savage, P. E. (2016). Products, Pathways, and Kinetics for the Fast Hydrothermal Liquefaction of Soy Protein Isolate. *ACS Sustainable Chemistry & Engineering, 4*(12), 6931-6939. doi:10.1021/acssuschemeng.6b01857

Socrates, G. (2004). *Infrared and Raman Characteristic Group Frequencies: Tables and Charts*: Wiley.

Soler-Jofra, A., Perez, J., & van Loosdrecht, M. C. M. (2020). Hydroxylamine and the nitrogen cycle: A review. *Water Res, 190*, 116723. doi:10.1016/j.watres.2020.116723

Teri, G., Luo, L., & Savage, P. E. (2014). Hydrothermal Treatment of Protein, Polysaccharide, and Lipids Alone and in Mixtures. *Energy & Fuels, 28*(12), 7501-7509. doi:10.1021/ef501760d

Titirici, M.-M., Antonietti, M., & Baccile, N. (2008). Hydrothermal carbon from biomass: a comparison of the local structure from poly- to monosaccharides and pentoses/hexoses. *Green Chemistry, 10*(11), 1204-1212. doi:10.1039/B807009A

Titirici, M.-M., White, R. J., Falco, C., & Sevilla, M. (2012). Black perspectives for a green future: hydrothermal carbons for environment protection and energy storage. *Energy & Environmental Science, 5*(5), 6796-6822. doi:10.1039/C2EE21166A

Toor, S. S., Rosendahl, L., & Rudolf, A. (2011). Hydrothermal liquefaction of biomass: A review of subcritical water technologies. *Energy, 36*(5), 2328-2342. doi:https://doi.org/10.1016/j.energy.2011.03.013

Torri, C., Garcia Alba, L., Samorì, C., Fabbri, D., & Brilman, D. W. F. (2012). Hydrothermal Treatment (HTT) of Microalgae: Detailed Molecular Characterization of HTT Oil in View of HTT Mechanism Elucidation. *Energy & Fuels, 26*(1), 658-671. doi:10.1021/ef201417e

Tsilomelekis, G., Orella, M. J., Lin, Z., Cheng, Z., Zheng, W., Nikolakis, V., & Vlachos, D. G. (2016). Molecular structure, morphology and growth mechanisms and rates of 5-hydroxymethyl furfural (HMF) derived humins. *Green Chemistry, 18*(7), 1983-1993. doi:10.1039/C5GC01938A

Valdez, P. J., & Savage, P. E. (2013). A reaction network for the hydrothermal liquefaction of Nannochloropsis sp. *Algal Research, 2*(4), 416-425. doi:https://doi.org/10.1016/j.algal.2013.08.002

Valdez, P. J., Tocco, V. J., & Savage, P. E. (2014). A general kinetic model for the hydrothermal liquefaction of microalgae. *Bioresour Technol, 163*, 123-127. doi:10.1016/j.biortech.2014.04.013

Van Gerpen, J., & Knothe, G. (2010). Biodiesel Production (4). In G. Knothe, J. Krahl, & J. Van Gerpen (Eds.), *The Biodiesel Handbook (Second Edition)* (pp. 31-96): AOCS Press.

van Zandvoort, I., Wang, Y., Rasrendra, C. B., van Eck, E. R., Bruijnincx, P. C., Heeres, H. J., & Weckhuysen, B. M. (2013). Formation, molecular structure, and morphology of humins in biomass conversion: influence of feedstock and processing conditions. *ChemSusChem, 6*(9), 1745-1758. doi:10.1002/cssc.201300332

Vardon, D. R., Sharma, B. K., Scott, J., Yu, G., Wang, Z., Schideman, L., . . . Strathmann, T. J. (2011). Chemical properties of biocrude oil from the hydrothermal liquefaction of Spirulina algae, swine manure, and digested anaerobic sludge. *Bioresour Technol, 102*(17), 8295-8303. doi:10.1016/j.biortech.2011.06.041

Vardon, D. R., Sharma, B. K., Scott, J., Yu, G., Wang, Z., Schideman, L., . . . Strathmann, T. J. (2011). Chemical properties of biocrude oil from the hydrothermal liquefaction of Spirulina algae, swine manure, and digested anaerobic sludge. *Bioresource Technology, 102*(17), 8295-8303. doi:https://doi.org/10.1016/j.biortech.2011.06.041

Vassilev, S. V., Baxter, D., Andersen, L. K., & Vassileva, C. G. (2010). An overview of the chemical composition of biomass. *Fuel, 89*(5), 913-933. doi:https://doi.org/10.1016/j.fuel.2009.10.022

Velez, A., Soto, G., Hegel, P., Mabe, G., & Pereda, S. (2012). Continuous production of fatty acid ethyl esters from sunflower oil using supercritical ethanol. *Fuel, 97*, 703-709. doi:10.1016/j.fuel.2012.02.024

Wu, Z., Rodgers, R. P., & Marshall, A. G. (2004). Two- and Three-Dimensional van Krevelen Diagrams: A Graphical Analysis Complementary to the Kendrick Mass Plot for Sorting Elemental Compositions of Complex Organic Mixtures Based on Ultrahigh-Resolution Broadband Fourier Transform Ion Cyclotron Resonance Mass Measurements. *Analytical Chemistry, 76*(9), 2511-2516. doi:10.1021/ac0355449

Yakubu, O., Gto, O., & Daniel, U. (2019). A review of impact of recurrent bush burning on the climate change paradigm: The Nigerian experience. *4*, 92-101.

Yang, J., He, Q., Niu, H., Corscadden, K., & Astatkie, T. (2018). Hydrothermal liquefaction of biomass model components for product yield prediction and reaction pathways exploration. *Applied Energy, 228*, 1618-1628. doi:https://doi.org/10.1016/j.apenergy.2018.06.142

Yang, W., Li, X., Li, Z., Tong, C., & Feng, L. (2015). Understanding low-lipid algae hydrothermal liquefaction characteristics and pathways through hydrothermal liquefaction of algal major components: Crude polysaccharides, crude proteins and their binary mixtures. *Bioresource Technology, 196*, 99-108. doi:https://doi.org/10.1016/j.biortech.2015.07.020

Yin, S., & Tan, Z. (2012). Hydrothermal liquefaction of cellulose to bio-oil under acidic, neutral and alkaline conditions. *Applied Energy, 92*, 234-239. doi:https://doi.org/10.1016/j.apenergy.2011.10.041

Yu, B., Song, Y., Yu, H., Han, L., & Liu, H. (2014). Optimizations of large volume-direct aqueous injection-gas chromatography to monitor volatile organic compounds in surface water. *Analytical Methods, 6*(17). doi:10.1039/c4ay00266k

Zhang, C., Tang, X., Sheng, L., & Yang, X. (2016). Enhancing the performance of Co-hydrothermal liquefaction for mixed algae strains by the Maillard reaction. *Green Chemistry, 18*(8), 2542-2553. doi:10.1039/C5GC02953H

Zhang, J., & Zhang, Y. (2014). Hydrothermal Liquefaction of Microalgae in an Ethanol–Water Co-Solvent To Produce Biocrude Oil. *Energy & Fuels, 28*(8), 5178-5183. doi:10.1021/ef501040j

Zhang, M., Yang, H., Liu, Y., Sun, X., Zhang, D., & Xue, D. (2012). First identification of primary nanoparticles in the aggregation of HMF. *Nanoscale Research Letters, 7*(1), 38. doi:10.1186/1556-276X-7-38

Zhang, Y., & Chen, W. T. (2018). 5 - Hydrothermal liquefaction of protein-containing feedstocks. In L. Rosendahl (Ed.), *Direct Thermochemical Liquefaction for Energy Applications* (pp. 127-168): Woodhead Publishing.

Zhu, C., Wang, H., Liu, Q., Wang, C., Xu, Y., Zhang, Q., & Ma, L. (2020). Chapter 3 - 5-Hydroxymethylfurfural—a C6 precursor for fuels and chemicals. In S. Saravanamurugan, A. Pandey, H. Li, & A. Riisager (Eds.), *Biomass, Biofuels, Biochemicals* (pp. 61-94): Elsevier.